Chemically-Reactive Polymeric Multilayer Coatings for Tailoring Durable Liquid Wettabilities

A thesis submitted by

Dibyangana Parbat
Roll No. 156122001

to

Indian Institute of Technology Guwahati

for

the award of the degree

of

Doctor of Philosophy

Department of Chemistry

Indian Institute of Technology Guwahati

Guwahati- 781039, Assam

India

26th June 2020

Dedicated to My Parents……

Indian Institute of Technology

Guwahati

Department of Chemistry

STATEMENT

I hereby proclaim that the work presented in the thesis entitled **"Chemically-Reactive Polymeric Multilayer Coatings for Tailoring Durable Liquid Wettabilities"** is the result of investigations of research work accomplished by me in the Department of Chemistry, under the supervision of Dr. Uttam Manna, Associate Professor, Department of Chemistry, Indian Institute of Technology Guwahati, Assam, India.

Research works used in this thesis from any other source has been fully cited and acknowledged. This work is original and has not been submitted elsewhere for the award of any degree.

Dibyangana Parbat

26th June, 2020

IIT Guwahati

Dibyangana Parbat

Indian Institute of Technology

Guwahati

Department of Chemistry

CERTIFICATE

This is to certify that the work introduced in this thesis entitled **"Chemically-Reactive Polymeric Multilayer Coatings for Tailoring Durable Liquid Wettabilities"** by **Dibyangana Parbat**, a Ph.D. student of Department of Chemistry, Indian Institute of Technology Guwahati, for the degree of Doctor of Philosophy has been carried out under my supervision and this work has not been submitted elsewhere for the award of any degree.

Dr. Uttam Manna

Associate Professor

Department of Chemistry

Indian Institute of Technology Guwahati Guwahati–781039

Assam, India

26th June, 2020

Sincere gratitude is hereby extended to the following who never ceased in helping throughout this journey.

I cannot thank enough my supervisor, Dr. Uttam Manna for his unwavering guidance through thick and thin. He provides me with the flexibility to follow my research interests but concurrently he was always there with me at every step to direct me in the right way. I will remain grateful to him for his constant support, motivation, ceaseless efforts to inculcate great values in me and being a great teacher I can always look up to.

The members of the doctoral committee, Prof. Biplab Mondal (Chairperson), Dr. Kalyan Raidongia and Dr. A. S. Achalkumar for sparing their precious time and giving positive insights to improve the analysis and interpretation of the data. Their invaluable advice and fruitful discussions always inspired me to improve my knowledge. A special thanks to Dr. Devasish Chowdhury, Associate Professor at Institute of Advanced Study in Science & Technology (IASST), for his extremely valuable help in resolving some basic data of my work.

I am grateful to all the faculty members of Department of Chemistry, IIT Guwahati for their ingenious advice and encouragement and also all the non-teaching staffs for technical help. I am also thankful to Central Instruments Facility (CIF), IIT Guwahati for the instrumental facilities. I gratefully acknowledge Indian Institute of Technology, Guwahati for funding without which my Ph.D. work would not have been possible.

Thanks are due to all my lovable labmates and project students for creating an environment which felt like a home away from home. Their assistance helped me a lot in completing projects in time. Staffs, students and fellows at Indian Institute of Technology, Guwahati have helped a lot in many ways and also make my tenure really memorable. My heartiest thanks to all my friends and all my teachers for being extremely supportive which makes my five years of journey truly enjoyable.

I would like to take this opportunity to thank each one of my family especially my parents Mr. Gautam Parbat and Mrs. Mala Parbat and my husband Mr. Nirban Jana for their unwavering moral, emotional and financial support whenever required.

Above all, utmost appreciation to the Almighty God for the divine intervention in academic endeavour.

Various bio-inspired extremes of liquid wettabilities, including superhydrophobicity, underwater superoleophobicity/superoleophilicity, and so on are of enormous potential for diverse applications, including oil-transportation, oil-water separation, fabrication of robotic devices, anti-biofouling coatings, microfluidics and so forth. In the past decades, such liquid wettabilities have been designed following various top-down and bottom-up approaches. The appropriate co-optimization of hierarchical topography and surface chemistry is the primary requisite for adopting desired and extreme liquid wettabilities. A low surface energy coating is mainly required for designing superhydrophobic or underwater superoleophilic surface, whereas high surface energy coating is needed for achieving underwater superoleophobic surface. In the past, distinct synthetic approaches were followed for preparing different bio-inspired (e.g., fish scale-inspired coating, lotus leaf-inspired coating etc.) coatings. Moreover, synthesis of physically/chemically durable biomimicked wettability is highly important for various prospective applications at practically relevant scenarios. Thus, a common and facile synthetic approach is essential for adopting durable and different extremes of liquid wettabilities, where a simple and robust chemistry would be allowed to tailor diverse liquid wettabilities. In this synopsis report, I have summarized a facile and common chemical approach for achieving various durable bio-mimicked wettabilities, where 1,4-conjugate addition reaction between amine and acrylate groups was successfully extended for constructing covalently cross-linked and chemically-reactive multilayer coatings. This synopsis report with a title of '**Chemically-Reactive Polymeric Multilayer Coatings for Tailoring Durable Liquid Wettabilities'** is segregated into six chapters. **Chapter 1** includes an introduction to the fundamentals of various biomimicked liquid wettabilities and a brief overview on conventional techniques for achieving such biomimicked wattability. The existing challenges related to the bio-inspired liquid wettabilities have also been also discussed in this chapter. In the **Chapter 2**, chemically-reactive polymeric nanocomplex (NC) was integrated into a multilayer coating (20-bilayers) through subsequent deposition of BPEI and NC following a covalent layer-by-layer (LbL) deposition process. The post-covalent modification of the multilayer coating with glucamine through facile and robust 1,4-conjugate addition reaction allowed to adopt a bulk underwater superoleophobicity. The underwater superoleophobic coating remained highly durable towards both harsh physical abrasions (including adhesive tape peeling test, sandpaper abrasion test, etc.) and various complex chemical exposures like extremes of pH (pH 1, pH 12), artificial sea-water, river water, etc. Next, in the **Chapter 3**, this abrasion-tolerant underwater superoleophobic coating was successfully deposited on a stretchable and fibrous matrix for developing a deformable and durable underwater superoleophobic membrane for gravity-driven and environmentally-friendly separation of various oil-water mixtures under practically relevant severe

settings. However, this synthesized multilayer coating failed to display superhydrophobicity even after post-covalent modification with alkylamine having a long hydrocarbon tail. **Chapter 4** accounts a salt (NaCl)-assisted and high throughput synthesis of chemically-reactive multilayer (9 bilayers) coating with optimum topography to display both underwater superoleophobicity and superhydrophobicity. A controlled and selective post-covalent modification of this chemically-reactive multilayer coating allowed tailoring of various liquid wettabilities. In general, a continuous trapped air layer present in superhydrophobic interfaces is considered as the primary basis for achieving another super liquid wettability—i.e., underwater superoleophilicity. **Chapter 5** includes a detailed investigation on the essential requirements for fabricating a durable underwater superoleophilic interface. This study validated that a hydrophobic multilayer coating (consisting of 20 bilayers, octadecylamine-modified) with discontinuous trapped air was also capable of displaying durable underwater super-oil-affinity. Moreover, the stability of this extreme oil-wettability was superior over superhydrophobic multilayer coating (consisting of 9 bilayers, octadecylamine-modified). The hydrophobic multilayer coating (20 bilayers) remained highly selective to oil phase under water as observed in superhydrophobic coating. Further, this durable underwater superoleophilicity was extended to develop a super-oil-absorbent for comprehensive oil/water separation under practically relevant severe settings. In the **Chapter 6**, a brief overview of the thesis work has been presented along with the prospective applications of this chemically-reactive multilayer coatings that will be explored in future.

Chapter 1: Introduction

Nature is full of wonders; every tiny and single thing is a standing mystery which always endows the curiosity to get to the bottom of its secret. Starting from the invention of aeroplane to velcro, submarine to bullet train— mostly these important and highly relevant discoveries were materialized through the contemplation of mother nature. In addition to that, several biomimicked liquid wettabilities have emerged to be a potential tool for developing smart materials. Lotus leaf inspired extreme water repellence, is widely and formally recognized as superhydrophobicity in the literature.[4] The micro and nano features (recognized as hierarchical interface) of the lotus leaf were decorated

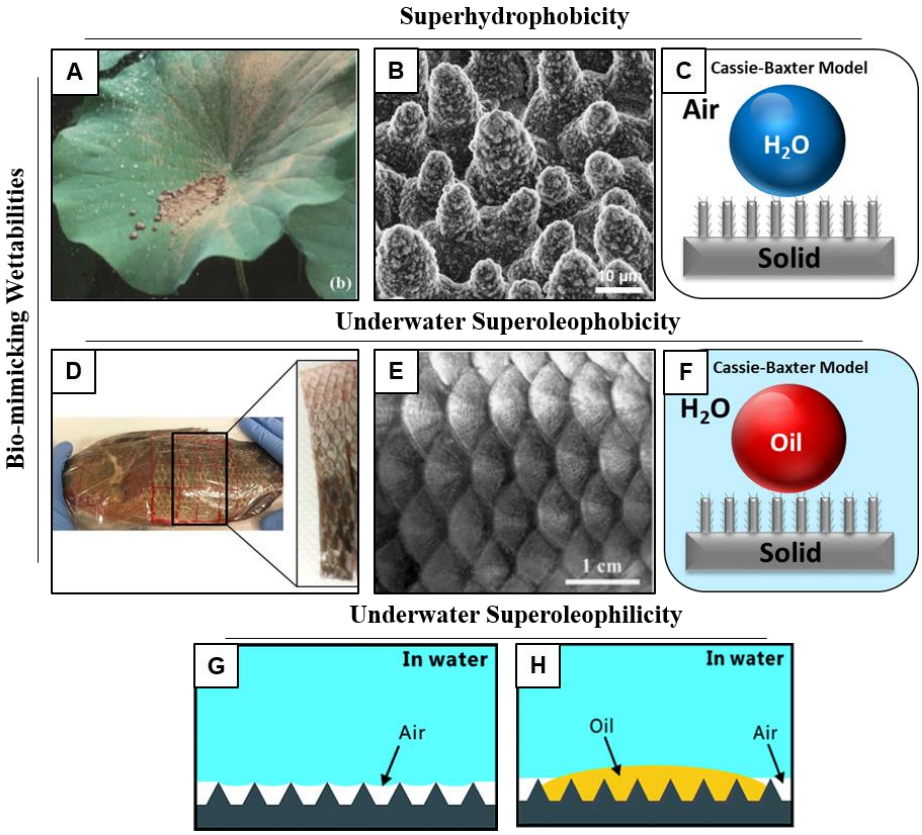

Figure 1: Digital photographs (A,D) and FESEM images (B, E) of superhydrophobic lotus-leaf (A-B) and underwater superoleophobic fish-scales (D-E). (C-F) Schematic illustration of two biomimicked extreme liquid wettabilities both in air (C) and underwater (F) which can be explained by Cassie-Baxter model of heterogeneous wettability. (G-H) Schematic representation of underwater superoleophilic interface. (A) Reprinted with permission from **(***Bionanosci.*, 2011, **1**, 63**)**, Copyright 2011, Springer; (B) Reprinted with permission from **(***Beilstein Journal of Nanotechnology*, 2011, **2**,152**)**, Copyright 2011, Beilstein; (D) Reprinted with permission from *(Sci. Reports*, 2015, **4**, 7454*)*, Copyright 2015, Science; (E) Reprinted with permission from **(***Adv. Mater.*, 2009, **21**, 665**)**, Copyright 2009, Wiley-VCH; (G-H) Reprinted with permission from (*J. Mater. Chem. A*, 2017, **5**, 25249**)**, Copyright 2017, Royal Society of Chemistry.

with long-chain hydrophobic waxy material.[5] Eventually, such physical and chemical co-optimization is the primary basis for achieving superhydrophobicity (Fig. 1A-B). On the other side, fish-scales are extremely unaffected by any kind of oil/oily-contaminations under water due to the inherent existence of underwater superoleophobicity (Fig. 1D-E) on the scales. Both these bio-inspired (lotus leaf and

fish-scale) extreme liquid (water and oil) wettabilities have been theoretically explained following the Cassie-Baxter wettability model. This heterogeneous wettability model explains the high contact angle of the beaded liquid droplets on the solid surface, where external third phase trapped between solid and liquid (probe) phases minimizes the contact of the respective beaded liquid on a bio-inspired solid surface. The entrapped third phase in between the hierarchical topography is air for lotus leaf-inspired superhydrophobic interface (Fig. 1C), whereas the confined aqueous-phase is the external third phase for the fish-scale-mimicked underwater superoleophobic interface (Fig. 1F). Both the essential topography and appropriate chemistry are required for achieving superhydrophobicity (in air) and superoleophobicity (under water). Interestingly, the superhydrophobic interface inherently displays another extreme liquid wettability—that is underwater superoleophilicity (Fig. 1G-H). Generally, the presence of continuous trapped air layer is considered as the primary basis for achieving underwater superoleophilicity.

In general, two distinct approaches were adopted for synthesizing artificial superhydrophobic

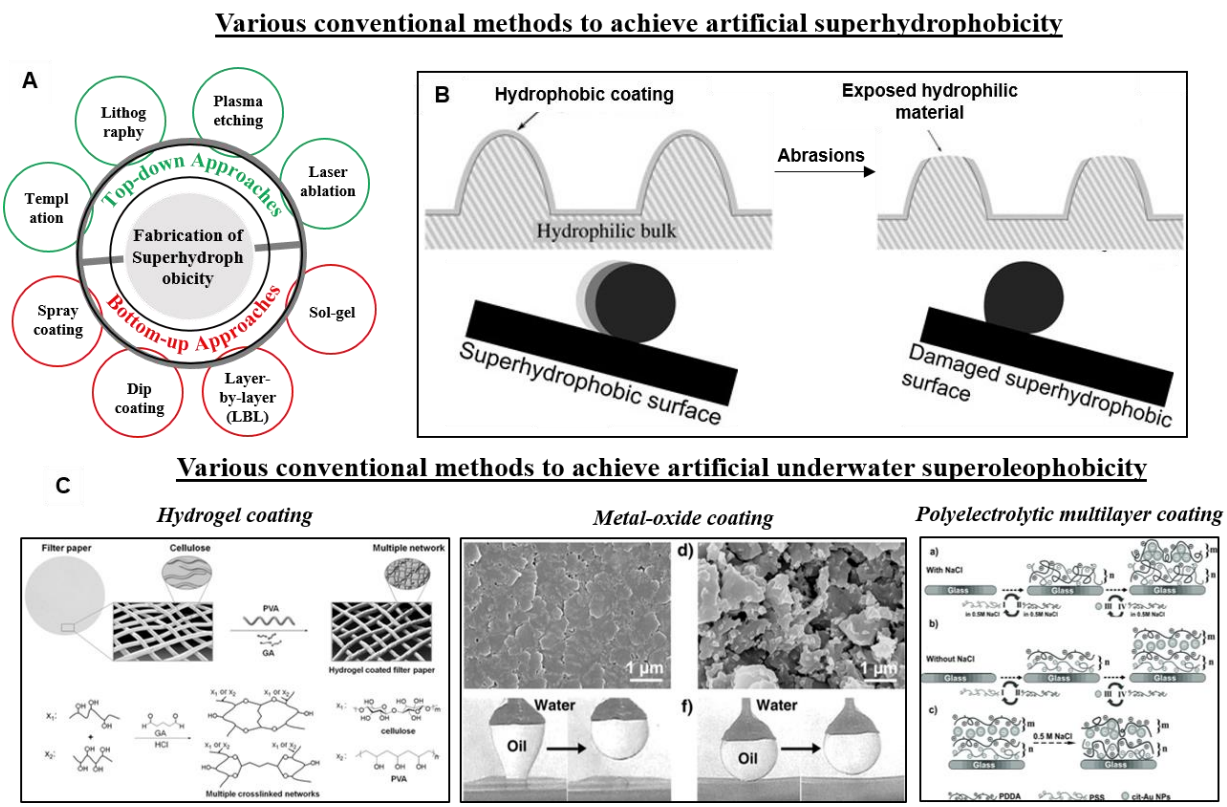

Figure 2: (A-B) Schematic accounting various top-down and bottom-up approaches (A) and the conventional design (B) for achieving the superhydrophobic interface and its limitations.[21] (C) Conventional methods for artificial underwater superoleophobic interfaces that were prepared by depositing hydrogel, metal-oxide and electrostatic multilayers. (B) Reprinted with permission from (*Adv. Mater.*, 2011, **23**, 673) Copyright 2011, Wiley-VCH; (C) Reprinted with permission from (*Adv. Funct. Mater.*, 2015, **25**, 5368) Copyright 2015, (*Adv. Mater.*, 2012, **24**, 3401) Copyright 2012 and (*Adv. mater.*, 2013, **25**, 606) Copyright 2013, Wiley-VCH.

and underwater superoleophobic interfaces. In the past, various top-down and bottom up methods,

including chemical etching, electrochemical deposition, template-based coating, electrostatic/hydrogen bonded LbL assembly, sol-gel method, dip coating, spray coating and so on were introduced for achieving appropriate hierarchical topography (Fig. 2A). Generally, the top surface of such hierarchical topography was modified with essential low surface energy molecules following weak chemistries and interactions, including silane or thiol chemistry, metal-ion interactions etc. for achieving superhydrophobicity. In such widely accepted synthetic approaches, the essential co-optimization of chemistry and topography was mostly maintained over a few nanometres. Thus, any minor physical abrasion is likely to compromise the artificial embedded superhydrophobicity (Fig. 2B). Further, the weak chemistries that were used in optimization of low surface energy coating on the hierarchical topography are likely to fall apart easily under practically relevant chemically complex environments like high salinity, extremes of pH, UV exposure etc. On the other hand, underwater superoleophobic coatings were mostly achieved by depositing highly hydrophilic ingredients, including polymeric hydrogels metal oxides and electrostatic multilayers (Fig. 2C). However, easily deformable hydrogels, fragile/brittle metal-oxides are highly susceptible to lose the essential topography under harsh physical and chemical environments. In another alternative approach, the electrostatic multilayer coatings that were used for preparing underwater superoleophobic interfaces, are also likely to disintegrate in high salinity and other extreme chemical conditions. Thus, the lack of durability is a common existing challenge for both the artificial biomimicked wettabilities—superhydrophobicity and underwater superoleophobicity.

In this thesis work, a simple and common chemical approach is introduced for achieving durable and different bio-inspired wettabilities. Two distinct chemically-'reactive' polymeric multi-layered coatings were developed through the strategic use of 1,4-conjugate addition reaction, and appropriate post-covalent modifications of these multi-layered coatings yielded abrasion-tolerant and highly durable superhydrophobicity and underwater superoleophobicity. Further, this chemical approach allowed us to develop a highly stable underwater superoleophilic coating, without having continuous trapped air-layer. Such extremely durable super-liquid wettabilites were also successfully extended for environmentally-friendly and energy-efficient cleaning of oil spillages at practically relevant severe and diverse settings.

Chapter 2: Synthesis of Chemically 'Reactive' Polymeric Multilayer coating.

Fish-scale mimicked underwater superoleophobicity has emerged as a prospective tool for addressing practically relevant different severe challenges related to healthcare, environment, energy, etc. However, the reported materials with this bio-inspired liquid wettability developed using polymeric

hydrogels, metal-oxide coating and electrostatic multilayer, are inappropriate to perform in practical scenarios as discussed in the earlier section. In the Chapter 2, a facile 1,4-conjugate addition reaction between amines and acrylates (Fig. 3A) was used to develop an 'amine-reactive' polymeric multilayer coating of nanocomplexes (NC, Fig. 3C). At first, a chemically reactive NC was synthesized by mixing the selected reactants (which are BPEI and dipentaerythritol pentaacrylate (5Acl); Fig. 3B) through same 1,4-conjugate addition reaction as shown in Fig. 3B.

This reactive NC was covalently and consecutively deposited in combination with BPEI following a simple LbL deposition technique as shown in Fig. 3E. After 20 bilayers (each layer was denoted as sequential deposition of reactive NC and BPEI) deposition, a chemically reactive and underwater oleophilic multilayer coating was formed (Fig. 3F). Moreover, the residual acrylates in the polymeric multilayer provided a simple basis for appropriate chemical modification (high surface

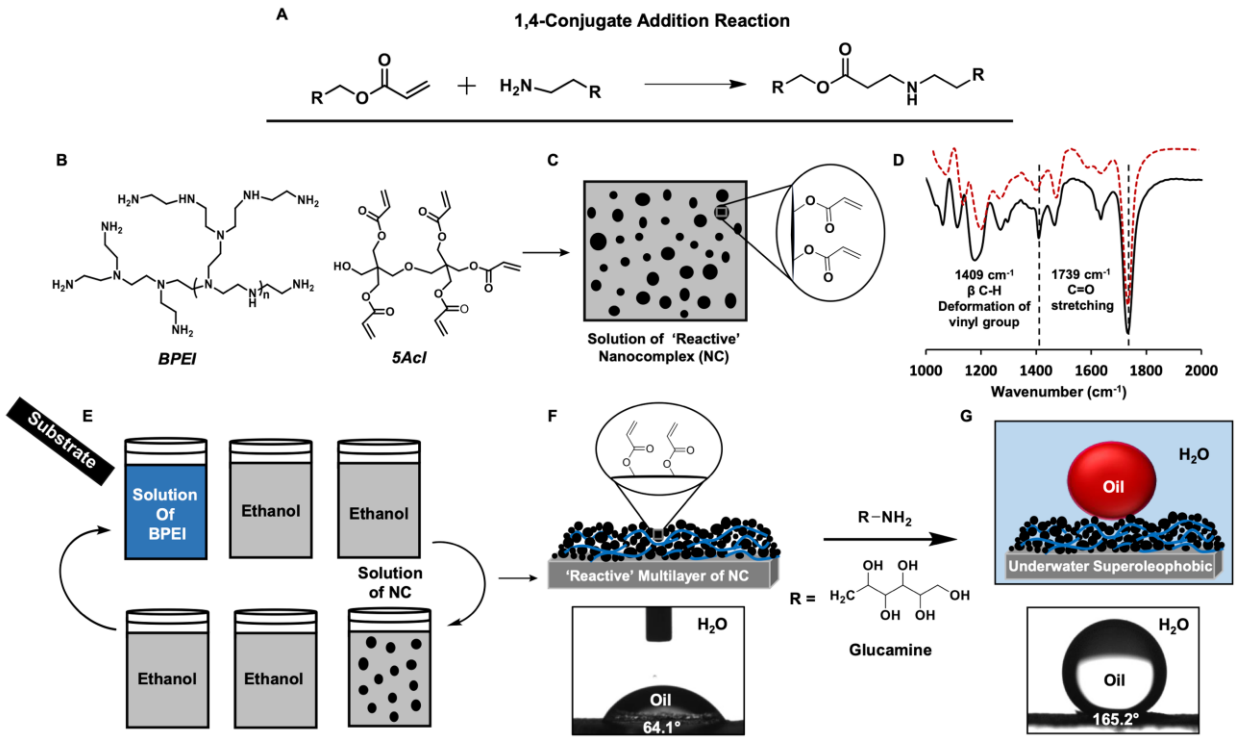

Figure 3: (A-C) 1,4-conjugate addition reaction (A) between the amine group of BPEI (B) and acrylate group of 5Acl (B) to develop a stable dispersion of 'reactive' NC (C). (D) FTIR analysis illustrating the reactivity of the NC before (black curve) and after (red curve) post-covalent modification with primary amine-containing small molecule. (E-G) Schematic representation of the LbL deposition (E) of both the NC and BPEI for developing a 'reactive'-multilayer coating (F). The post-chemical modification of multilayer coating with glucamine provided underwater superoleophobicity (G).

energy). The post-covalent reaction of the synthesized multilayer coating with glucamine through 1,4-conjugate addition reaction yielded an extremely oil repellent coating (Fig. 3G) under water. The

covalent optimization of essential chemistry in the porous polymeric coating provided underwater superoleophobicity with impeccable physical and chemical durability as shown in Fig. 4. The essential topography and chemistry that conferred underwater superoleophobicity, remained appropriately co-optimized beyond the surface of the coating. Thus, the polymeric coating sustained severe physical

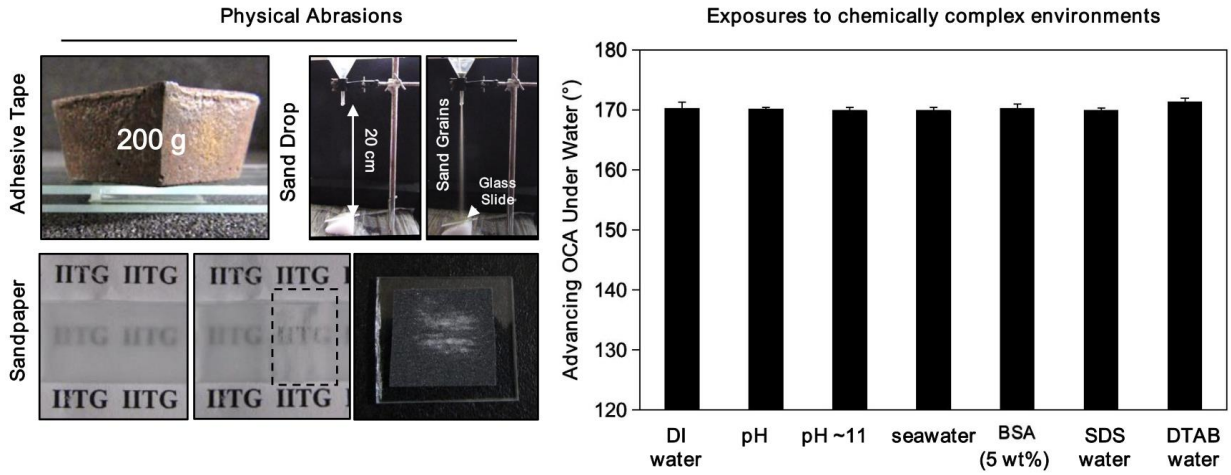

Figure 4: (A) Digital images of various physical challenges on the underwater superoleophobic multilayer coating including adhesive tape test, sand drop test and sandpaper abrasion. (B) Bar graph accounting the impeccable chemical durability of the underwater superoleophobicity, even after exposing the multilayer coating to harsh chemical environments including extremes of pH, saline water and surfactant/protein contaminated water.

abrasions including adhesive tape test, sandpaper test and sand drop test (Fig. 4A). Further, the synthesized coating was capable of withstanding severe chemical insults like exposures to extremes of pH, saline water, surfactant/protein-contaminated aqueous environments as shown in Fig. 4B. Moreover, this current coating approach was successfully extended to coat various objects. It is believed that this contemporary study will make a worthwhile contribution for developing multifunctional materials.

Chapter 3: Synthesis of Stretchable and Durable Underwater Superoleophobic Membrane for Filtration-based Oil/Water Separation.

Synthesis of a stretchable and durable fish-scale inspired—extreme oil-repellent interface, is even more challenging. In the Chapter 3, a stretchable fibrous substrate was successfully coated with chemically reactive multilayer coating that displayed abrasion-tolerant and deformable superoleophobicity under water (Fig. 5A-H). The as-prepared ‘reactive’ multilayer coating on the stretchable fibrous substrate completely soaked the beaded oil droplet under water as shown in Fig. 5C-D. However, the post-covalent modification of the residual acrylate groups in the multilayer coating (Fig. B, E) with a hydrophilic amine-containing small molecule, i.e. glucamine (denoted as

Glu) provided underwater superoleophobicity as shown in Fig. 5F-G. This synthesized biomimicked wettability remained unaltered under a high tensile strain of up to 150% as shown in Fig. 5H. However, the extreme oil repellency of the modified fabric was slightly compromised on further increasing in

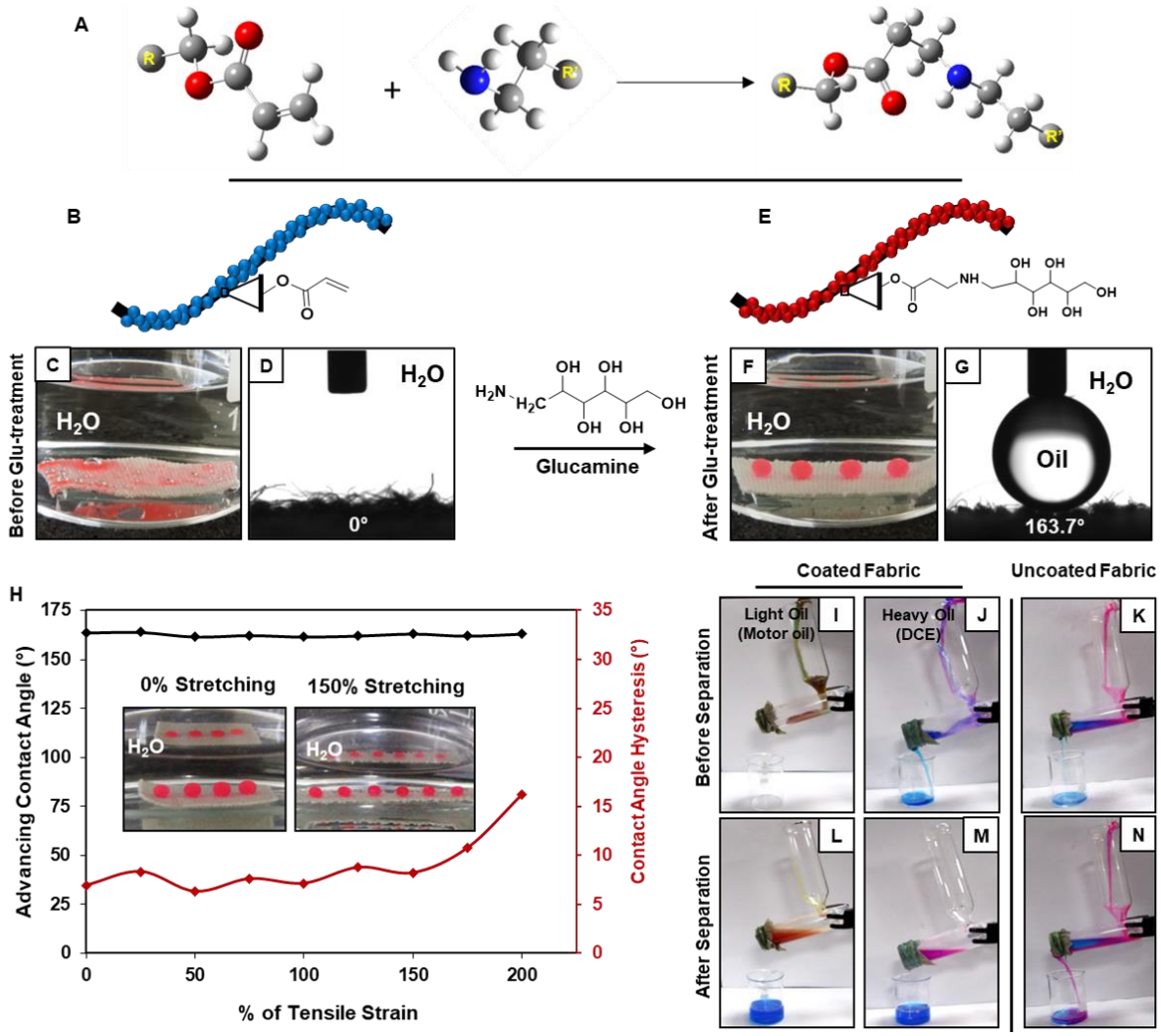

Figure 5: (A) The strategic immobilization of 'reactive' multilayer of NC developed by 1,4-conjugate addition reaction between amines and acrylates, on the stretchable fibrous substrate. (B-G) Schematic presentation (B,E), digital photographs (C,F) and contact angle images (D,G) of the multilayer-coated fabric before (B) and after (E) modification with glucamine molecules. (H) Graphical representation illustrating the change in wettability of the glucamine-modified coating on stretchable matrix where contact angles (advancing contact angles: black curve, contact angle hysteresis: red curve) were recorded with increasing percentage (%) of the tensile strain (inset: digital images of glucamine-modified fabric with 0% and 150% stretching). (I-N) Digital images of bulk oil-water separation with coated (I-J, L-M; post-modified with glucamine) and uncoated (K,N) fibrous substrate for both heavy (dichloromethane) and light (motor oil) oils.

the tensile strain from 150% to 175%. Moreover, an adhesive underwater superoleophobic behaviour was observed with contact angle hysteresis above 15º after applying 200% of tensile strain on the coated membrane as shown in Fig. 5H (red curve). In addition to that, this underwater superoleophobic interface was capable of withstanding various harsh physical and chemical settings—including

successive (1000 times) tensile deformations, different physical abrasive tests, prolonged exposure of (30 days) UV irradiation, extremes of temperatures (100°C and 10°C) and severe complex aqueous phases. Thereafter, the synthesized underwater superoleophobic membrane was successfully extended for gravity-driven and eco-friendly separation of oil/water mixtures (Fig. 5I-N) even under practically relevant various and severe physical/chemical conditions (e.g. extremes of temperatures, tensile strain, pH, sea water, river water, etc.) with separation efficiency more than 95%.

Chapter 4: A Single Multilayer Coating for Controlled Tailoring of Different Liquid Wettabilities.

The chemically 'reactive' multilayer coating (consisting of 20 bilayers) discussed in the Chapter 2, was capable of displaying underwater superoleophobicity with appropriate post-covalent modification.

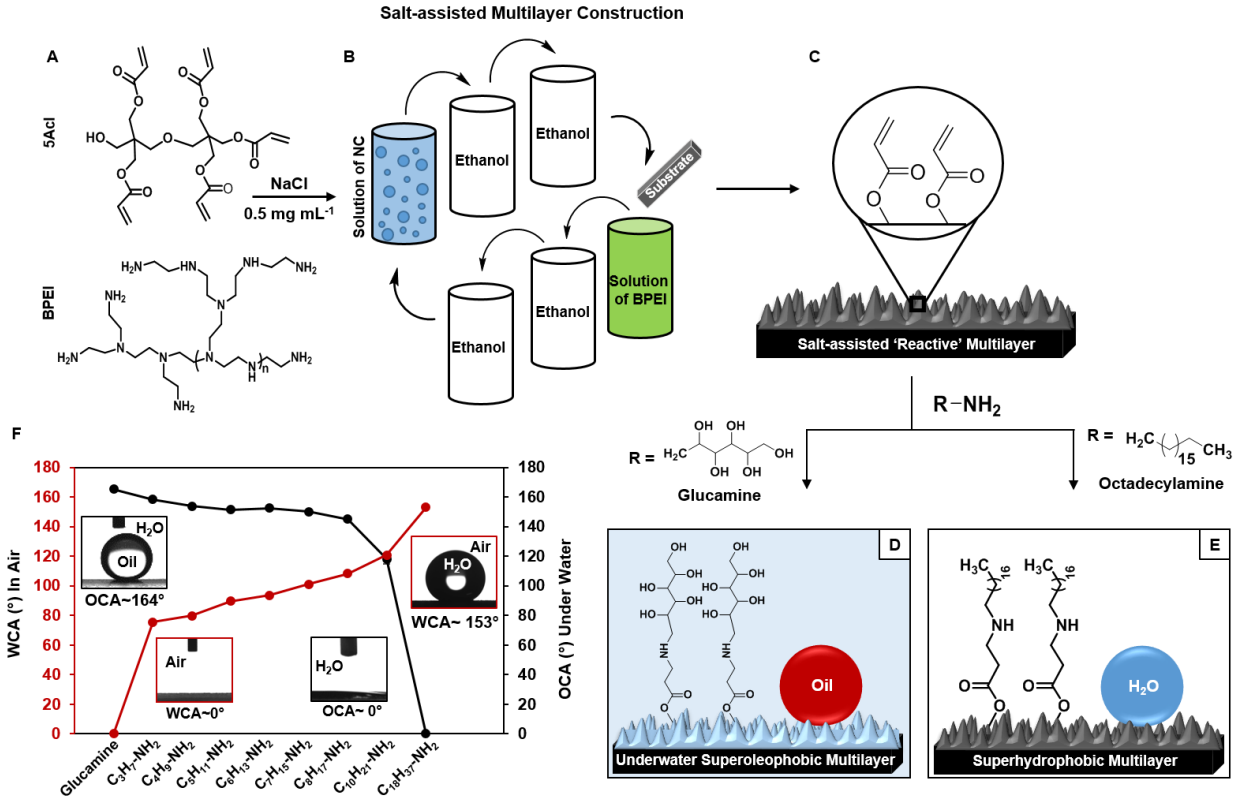

Figure 6: (A) Chemical structures of BPEI and 5Acl. (B-C) Schematic illustration for the fabrication of chemically-'reactive' polymeric multilayer (associating with 9 bilayers) of nanocomplexes (C) (prepared by mixing of BPEI and 5Acl) in presence of salt (NaCl) through LbL deposition (B) approach. (D-E) Schematic of selective post-chemical modifications of the reactive-multilayers with appropriate small molecules (ODA and glucamine), which provided extremes of liquid wettabilities both in air (superhydrophobicity, (E)) and under water (superoleophobicity, (D)). (F) The plot illustrating the controlled and extreme change in both the water contact angle (WCA; red line) in air and the oil contact angle (OCA; black line) under water by regulating the post-chemical modification with selected primary amine containing small molecules. (Inset: extremes of both water wettability in air and oil wettability underwater after post-modification with ODA (red boxes) and glucamine molecules (black boxes)).

However, this reactive polymeric coating remained inappropriate to display superhydrophobicity, even after post-covalent modification with low surface energy molecule (i.e. octdecylamine having a long hydrocarbon tail). The lack of essential topography in the multilayer coating might be the reason behind the failure in displaying extreme water wettability. In the recent past, Rather et al. prepared a polymeric gel by reaction between BPEI and 5Acl in ethanol, and the rate of sol-gel conversion was accelerated by addition of sodium chloride in the reaction mixture. Inspired by this result, In the Chapter 4, a salt-assisted LbL deposition of reactive NC was introduced for accelerated growth of chemically reactive polymeric coating (Fig. 6A-B). The LbL deposition cycle was repeated for only 9 times to achieve the appropriate multilayer (9 bilayers) coating—which was capable of displaying both superhydrophobicity and underwater superoleophobicity, depending on the selection of appropriate post-covalent modifications as shown in Fig. 6C-E. Along with extremes of liquid (water and oil) wettability, this same multilayer construction also provided a basis to adopt various other liquid wettabilities both in air and under water as shown in Fig. 6F. The bio-inspired super liquid wettabilities remained intact even after exposure to various severe physical and chemical insults, including adhesive tape test, sand drop test, and exposures to extremes of pH, salinity, surfactant-contaminated aqueous media, etc. Moreover, such a facile and simple LbL fabrication strategy also allowed to decorate various flexible and rigid substrates (including wood, Al-foil, synthetic fabric, etc.) with desired bio-inspired wettability. This current design allows independent investigation of the essential physical and chemical parameters that confer the heterogeneous wettability for beaded water and oil droplets on respective solid surface.

Chapter 5: A Facile Approach for Stabilizing Underwater Superoleophilicity.

In the literature, continuous trapped air layer, present in superhydrophobic interface, is considered as the primary requirement for achieving underwater superoleophilicity. This selective and extreme oil affinity could be useful for selective collection of oil/oily phase from aqueous phase. However, the stability of this entrapped metastable continuous air layer, present in superhydrophobic interface is poor under water. The inherently embedded extreme oil-affinity in the superhydrophobic interface under water is compromised within a few hours under water. In the Chapter 5, two distinct chemically reactive multilayer coatings that were prepared in the presence (introduced in the Chapter 4) and absence (already discussed in the Chapter 2) of NaCl, were post-modified with ODA to compare the durability of underwater superoleophilicity. After the same post-covalent modification (Fig. 7A) with ODA, the multilayer coating that was prepared in the absence of salt displayed hydrophobicity, whereas the salt-assisted multilayer coating exhibited superhydrophobicity as shown in Fig. 7B. These

two different multilayer coatings consisted of distinct topography—but with identical post-covalent modification (Fig. 7C-D). However, both the multilayer coatings with discontinuous (hydrophobic multilayer) and continuous (superhydrophobic multilayer) trapped air layer displayed selective and

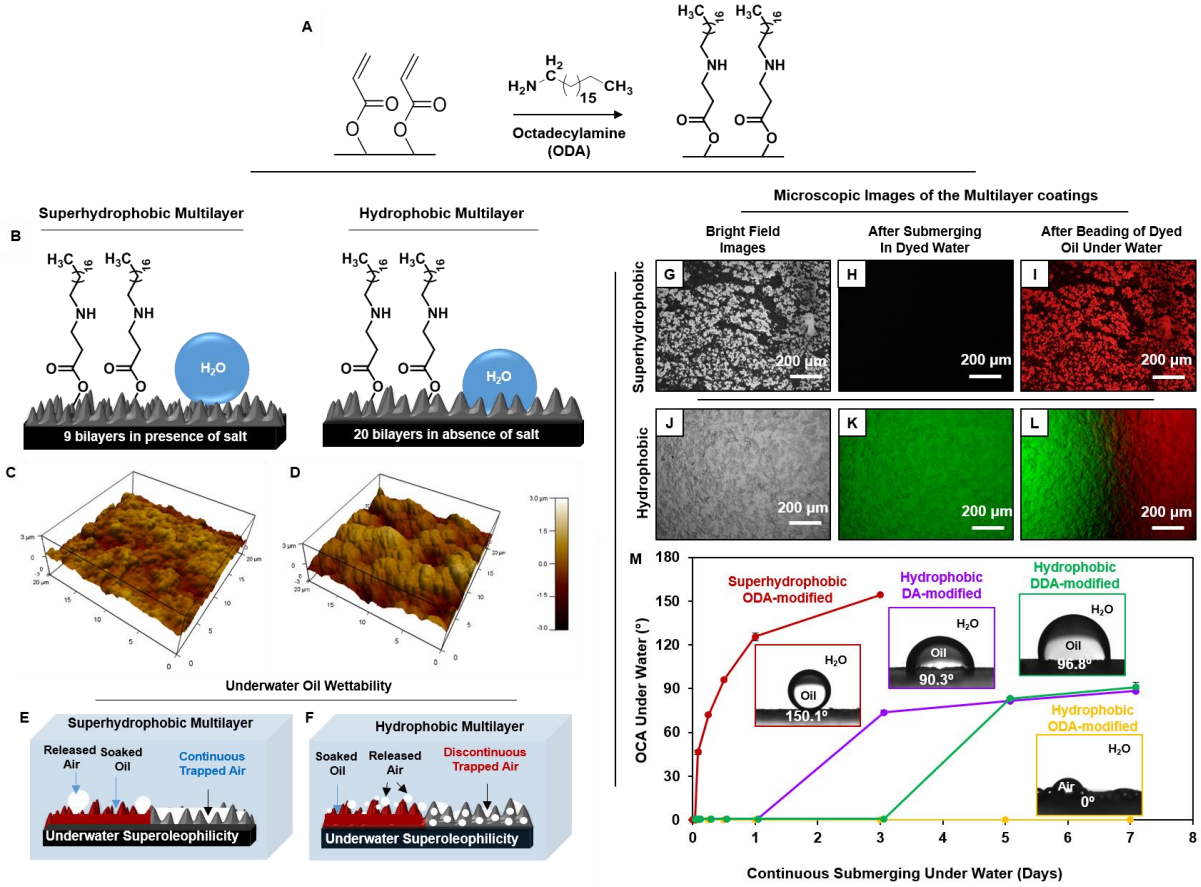

Figure 7: (A) Schematic for the post-chemical modification (A) of the chemically-reactive polymeric multilayer prepared in presence (superhydrophobic multilayer) and absence (hydrophobic multilayer) of salt (NaCl) through 1,4-conjugate addition reaction between residual acrylates of the multilayer and amine moieties of ODA molecules. (C-D) Atomic force microscope (AFM) images of hydrophobic (C) and superhydrophobic (D) multilayer depicting the difference in roughness of the respective multilayer. (E-F) Schematic representing the extreme oil-affinity by hydrophobic (E, having discontinuous trapped air phase) and superhydrophobic (F, having continuous trapped air phase) multilayer coatings. (G-L) Fluorescence microscopic images (scale bar 200 µm) of superhydrophobic (G-I) and hydrophobic (J-L) multilayers after submerging in the fluorescein dye-added aqueous phase (H, K) followed by underwater exposure to Nile red-added silicone oil (I, L). (M) Graphical representation of the change in water contact angles of the superhydrophobic (ODA (red curve) -treated) and hydrophobic (decylamine (DA, violet curve), dodecylamine (DDA, green curve), and octadecylamine (ODA, yellow curve) -treated) multilayer over time after continuous immersion in water. Kindly put space in between number and unit in the Figure.

super-oil-affinity under water as shown in Fig. 7E-L. The hydrophobic multilayer coating selectively absorbed the oil phase (nile red aided microscopic imaging) even after impregnation of water phase (water soluble green fluorescent dye aided microscopic characterization) in the multilayer which was evident from the microscopic images in Fig. 7K-L. Interestingly, the multilayer coating that was prepared in the absence of salt and post-modified with ODA, displayed the most stable underwater

superoleophilicity. On the other hand, superhydrophobic multilayer with continuous trapped air layer displayed the least stable underwater superoleophilicity. Moreover, the hydrophobic multilayer coatings having discontinuous entrapped air were with superior underwater superoleophilicity over superhydrophobic multilayer coating, even at elevated temperature.

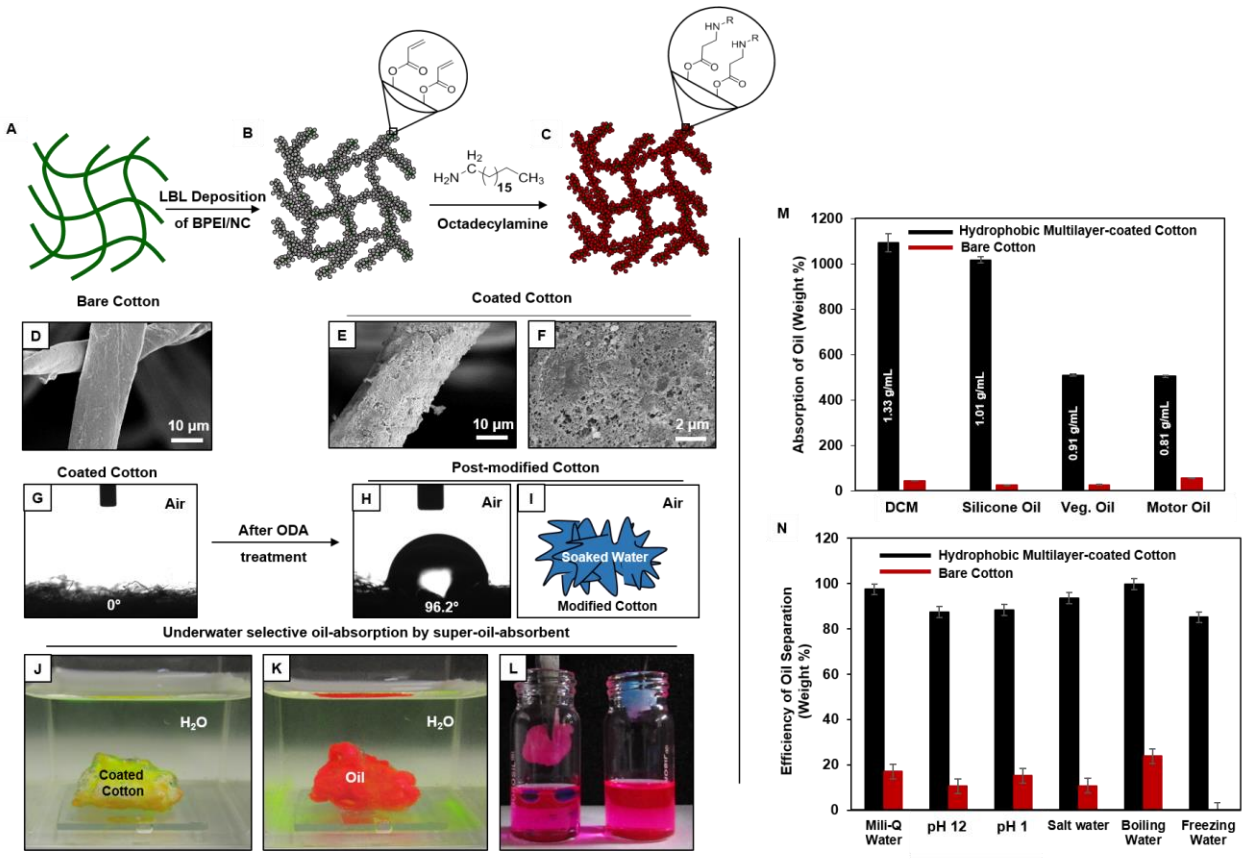

Figure 8: (A-C) Schematic illustration for the fabrication of super-oil-absorbent (A) by depositing hydrophobic multilayer (consisting of 20 bilayers) on a naturally-abundant cotton (A). (D-F) FESEM images of the pristine (D) and hydrophobic multilayer-coated cotton (E-F) in low (E) and high (F) magnifications. (G-I) Contact angle images unambiguously exhibiting the hydrophobicity (H) with an WCA of ~96º in the coated cotton (G) after post-covalent modification (H) with ODA molecules. (I) Schematic of the hydrophobic multilayer-coated cotton soaked with aqueous phase in air. (J-K) Digital images displaying the underwater selective oil (dyed with Nile red having red fluorescence)-absorption (K) under water by hydrophobic multilayer-coated cotton by ejecting the impregnated aqueous phase (dyed with fluorescein having green fluorescence; J) from the material. (L) Digital image illustrating selective oil-absorption performance of the hydrophobic super-oil-absorbent (coated cotton) in comparison with the bare (uncoated) cotton. (M-N) Plots accounting oil-absorption capacity (M) for various oil-phases (M) and oil/water separation performance of the super-oil absorbent cotton, under diverse chemically complex environments (N).

Further, the hydrophobic multilayer coating was deposited on a naturally abundant and fibrous substrate (Fig. 8A-I, i.e., cotton fibres) to examine the ability for comprehensive oil/water separation following the principle of selective absorption of oil/oily phase. The synthesized fibrous cotton-based super-oil-absorbent was capable of absorbing both oil and water phases in air as shown in Fig. 8I. However, the as-synthesized material, soaked with water (green dyed aqueous phase for fluorescence

imaging and visual investigation) in air, was capable of absorbing both heavy and light oils under water. At the same time, the impregnated metastable aqueous phase was spontaneously and selectively ejected out from the hydrophobic oil-absorbent (Fig. 8K). This unprecedented super-oil-absorption property remained intact in diverse scenarios, including extremes of temperature (100°C and 10°C), pressure (184.7 mbar), and prolonged (7 days) exposure to extremes of pH (1/12), surfactants (DTAB/SDS, 1 mM)-contaminated water, artificial sea water, etc. Moreover, this hydrophobic

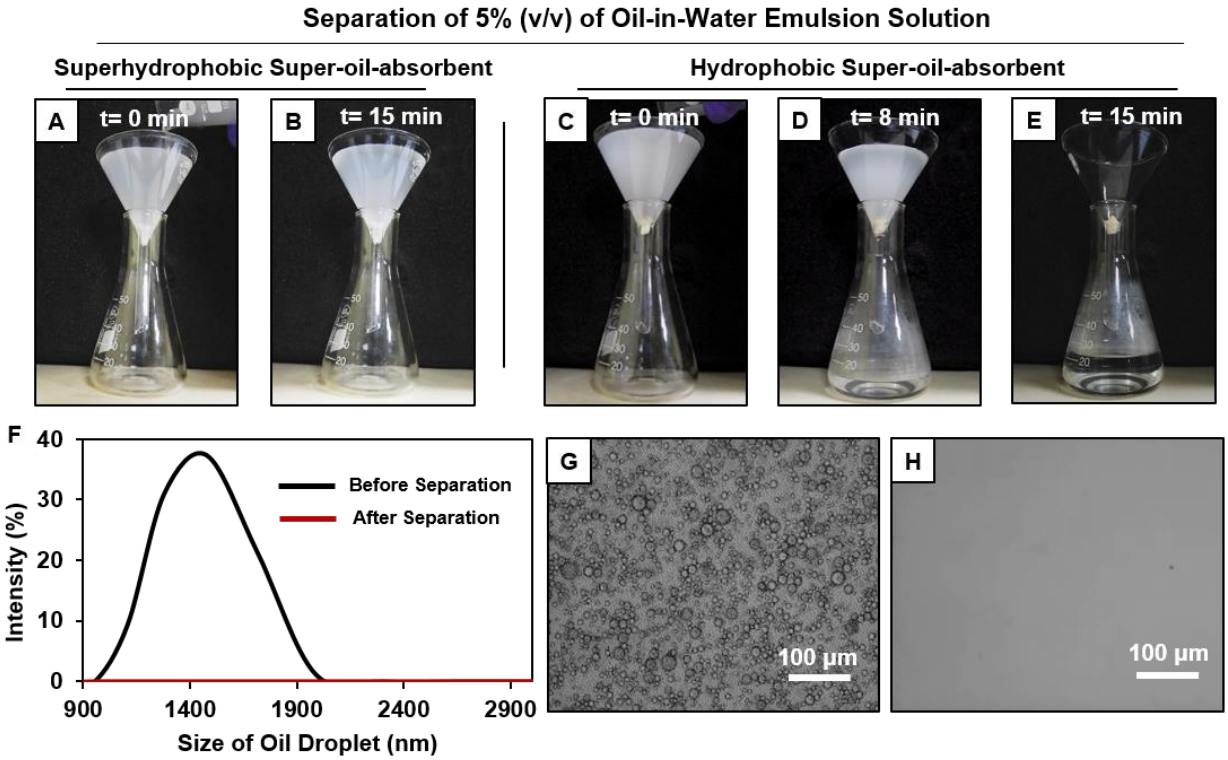

Figure 9: (A-E) Digital images accounting the performances for oil-in-water emulsion (5% (v/v) DCE in water) separation by both superhydrophobic (A-B) and hydrophobic (C-E) multilayer-coated cottons. (F-H) Dynamic light scattering (DLS) plot (F) and bright field microscopic images (G-H) accounting the oil-in-water emulsions before (F: black curve, G) and after (F: red curve, H) performing oil/water separation with hydrophobic multilayer-coated cotton; scale bar: 100 µm.

multilayer coating that displayed an unusual and unperturbed underwater superoleophilicity even at a highly elevated temperature (90°C), was further explored for the comprehensive separation of various forms of oil/water mixtures including both bulk-oil spills (Fig. 8M-N) and oil-in-water emulsions (Fig. 9) following eco-friendly and energy-efficient absorption/filtration principles. Such dual-mode operations with a single interface were practically challenging to achieve with any existing biomimicked approaches.

Interestingly, unlike the superhydrophobic cotton (Fig. 9A-B), the as-synthesized hydrophobic super-oil-absorbent remained very efficient in separating oil-in-water emulsion as shown in Fig. 9C-

E. Due to the presence of continuous metastable trapped air, the superhydrophobic interfaces inherently restricted the passage of oil-in-water emulsion where tiny oil droplets with the diameter of hundreds/thousands of nanometers were dispersed in the bulk water phase. Eventually, no oil/water separation was observed as shown in Fig. 9A-B. On the other hand, hydrophobic cotton having the discontinuous trapped air, readily and selectively allowed the passage of bulk aqueous phase from oil-in-water emulsion under gravity, and the embedded underwater superoleophilicity in the hydrophobic multilayer coating helped in selective absorption of the oil droplets (Fig. 9C-E) from oil-in-water emulsion. Consequently, the oil-in water emulsion was separated under gravitational force which was further confirmed by DLS (Fig. 9F) and microscopic (Fig. 9G-H) studies. Thus, the hydrophobic super-oil-absorbent was capable of cleaning up different forms of oil spillages including oil-in-water emulsions and bulk oil/water mixtures following both the selective absorption and filtration processes; such demonstration of comprehensive oil/water separation is rare in the literature.

Chapter 6: Conclusion and Future Direction

In conclusion, I have introduced a common and facile synthetic approach for adopting durable and various extreme liquid wettabilities, where the LbL deposition process allowed to adopt appropriate topography and 1,4-conjugate addition reaction provided a simple basis for tailoring the essential chemistry. The underwater superoleophobic coating was successfully extended for gravity-driven and eco-friendly separation of various forms of oil-water mixtures in practically relevant diverse and harsh conditions. Further, a salt-assisted multilayer coating was introduced for achieving both underwater superolephobicity and superhydrophobicity, depending on the selection of appropriate post-covalent modifications. Finally, these multilayer coatings were extended to study another super liquid wettability—that is underwater superoleophilicity. The detailed study validated that a moderately hydrophobic multilayer coating had superior ability to clean-up of oil-spills under diverse complex scenarios, in comparison to superhydrophobic multilayer coatings.

In the past, such underwater superoleophobicity and superhydrophobicity were explored for anti-platelet adhesion and prevention of biofilm formation etc. In that context, I strongly believe that the as-synthesized chemically reactive multilayer coatings that capable of displaying various liquid wettabilies would be highly useful for developing different biologically relevant interfaces. In the future, this covalently cross-linked durable coating would be exploited for controlled prevention andpromotion of platelet adhesion on biologically relevant interfaces.

Table of Content

Introduction

1.1. Evolution of Biomimetic Research

Nature has the potential to design its living organisms to adapt to their environment through a process of evolution. As a result, every living being is special—endowed with unique and fascinating features. Various smart developments gradually evolve and thrive with time, mostly inspired by nature's pattern. For instance, bullet trains had been invented by studying the pointed-beak design of the kingfisher bird to reduce the friction with air and noise during travelling.[1] Another great invention is sonar system, originated from the echolocation of bats and dolphins, which is invariably used by ships to find the depth of the sea, detect any incoming torpedo, pipeline inspection, etc.[2] Apart from that, several other smart inventions like painless needle, aeroplane, velcro, etc. were also inspired by mother nature.[3-5] Such inventions have been emerging through continuous learning from Nature and ceaseless efforts to mimic those designs to make our daily life simpler and facilitate our pursuit to know the unknown.

In that context, biomimetics was introduced as a common and versatile platform to address complex human problems by imitating the models, elements and systems of nature. Thus, the research on biomimetics has largely contributed in developing various smart and advanced materials through the exact replication of nature. Consequently, several astounding properties of naturally existing living species are also achievable in an artificial design. On that note, extremely water-repellent lotus leaf[6] (in air) and oil-repellent fish scale[7] (under water) have attracted considerable attention due to their exemplary properties which have enormous prospective applications in a variety of fields like energy, architecture, transportation, medicine, agriculture and so on. Several successful methodologies were adopted and subsequently modified over time for designing even a better version of this property which acts as a silver bullet in resolving various practical issues. An elaborate discussion on the evolution and growth of such properties are assembled in the following sections.

1.2. Progress in Different Liquid Wettabilities

Bio-inspired wettability is one of the most useful multi-functional properties which has emerged to be a potential tool in developing smart materials to address severe practical issues. The evolution of different bio-inspired wettability is mainly based on two well-known forces of attraction that are adhesive force and cohesive force. The adhesive force is defined as the attraction between unlike molecules which is very relevant in explaining a complete spreading of the liquid droplet on a solid surface. On the contrary, the cohesive force is mainly the attraction force among the like molecules that results in lowering the contact between the solid and the liquid phases. The extent of spreading or the complete bouncing of a liquid droplet on a solid surface is mainly determined by these two forces of attraction. The moment these two forces of attraction come into equilibrium, the liquid droplet stops spreading on the solid/air interface. The tangential angle of contact made by the liquid

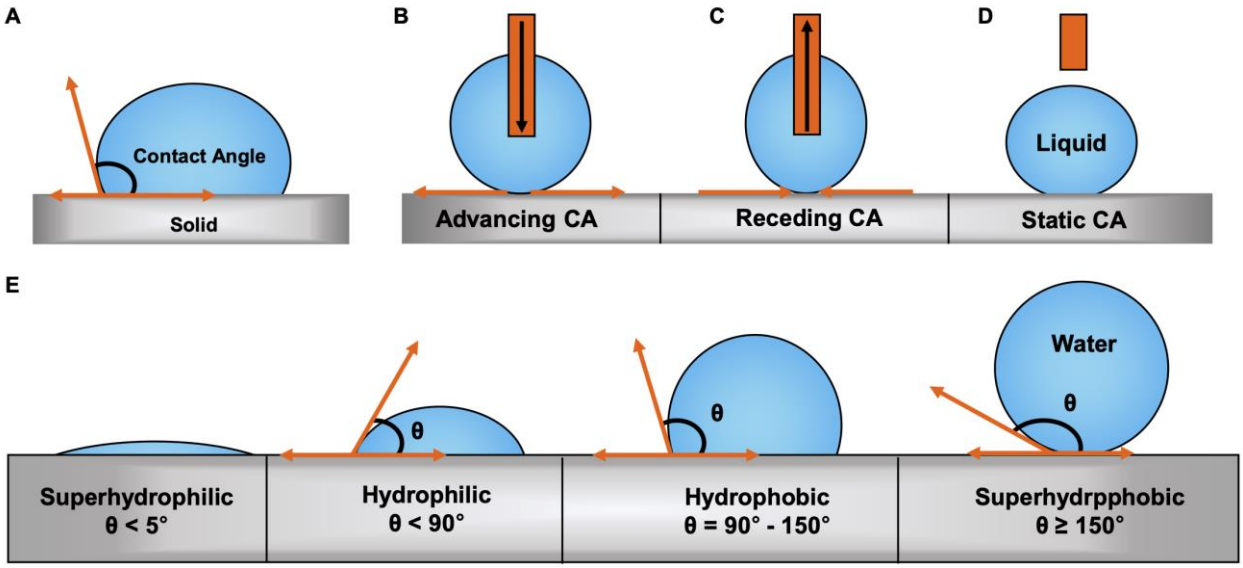

Figure 1.1: (A) Schematics for contact angle (θ) which defines as the tangential angle between the liquid and the solid phases at three phases contact point. (B-D) Schematic representation of advancing (B), receding (C) and static (D) contact angles. (E) Representation of various wettabilities of beaded water droplet on solid surfaces based on the contact angles and those are superhydrophilic ($\theta \leq 5^o$), hydrophilic ($\theta < 90^o$), hydrophobic ($\theta = 90^o$ - 150^o) and superhydrophobic ($\theta \geq 150^o$).

droplet on the solid surface at solid/air interface is defined as the contact angle (CA) as shown in Fig. 1.1A. Contact angles are broadly categorized as dynamic and static CAs. The dynamic CAs can again be of two types— advancing CA and receding CA (Fig. 1.1B-C).[8-10] Advancing CA is defined as the tangential angle between the solid and liquid phases just when a growing liquid droplet touches the solid surface (Fig. 1.1B). This angle is the maximum angle created by the liquid droplet with the solid surface.[10] The liquid droplet is further allowed to grow a bit more on the solid surface by infusing more liquid into it and then the liquid is made to recede to the dispensing needle. The CA just before the

droplet detaches from the surface or breaks is known as receding angle (Fig. 1.1C). The difference between these two dynamic contact angles is termed as contact angle hysteresis[9] which is in a way the measure of adhesive interaction between the probe liquid phase and the solid surface. Now, based on these contact angles of the liquid phase on a solid surface, the surfaces are broadly categorized in hydrophilic and hydrophobic surfaces when the liquid phase is water (Fig. 1.1E).[11] Hydrophilic surfaces allow the spontaneous spreading of aqueous phase on a solid surface and possess a water contact angle (WCA) of <90º.[11] Whereas, surfaces having WCA of >90º are denoted as hydrophobic surfaces that can demonstrate the partial/complete non-wetting behaviour of a surface by the aqueous phase.[11] To achieve an extremely liquid-repellent interface, the design of heterogeneous interface is essential, where the external trapped third phase between solid and liquid phases minimizes the contact area between the solid and liquid droplet to a significant extent which results in immediate bouncing of the liquid droplet when hit such solid surfaces. The surfaces that extremely repel aqueous phase in air are termed as superhydrophobic[11, 6] surfaces (Fig. 1.1E) and on the other hand surfaces repelling oil phase under water are named as underwater superoleophobic surfaces[7]. Such extremely liquid (oil/water) repelling surfaces possess an advancing liquid contact angle of ≥150º and liquid contact angle hysteresis of ≤10º.

On the contrary, the other extreme of liquid wettability is the complete soaking of a liquid (water/oil) phase by solid surface both in air and under water with liquid contact angles of ≤5º (Fig. 1.1E).[11-12] Depending on the absorbing phase, the solid surfaces are termed as superhydrophilic when the aqueous phase is absorbed in air and underwater superoleophilic when oil phase is absorbed under water.

1.2.1. Wettability models

1.2.1.1. Young's model:

The importance of wettability was realized way back in the 18th century because of its enormous potential in revolutionizing surface science. Thomas Young was the first to propose a model (Fig. 1.2A) in 1805[13] which was the first-ever model efficiently capable of explaining the contact angle of a liquid droplet (oil/water) on a smooth and featureless surface. In that context, when a liquid droplet is placed on a smooth and featureless substrate, this model plays a pivotal role in determining the accurate contact angle measurement of the beaded liquid droplet on the solid surface. The solid surfaces are broadly referred to as 'hydrophilic' in nature when the contact angle of water droplet on such kind of solid surfaces is limited to ≤ 90º which can be calculated by resolving the following Young's equation (eqn 1.1):

$$\cos\theta_Y = \frac{\gamma_{SG} - \gamma_{LS}}{\gamma_{LG}} \quad \ldots\ldots\ldots\ldots\ldots\ldots\ldots\ldots (1.1)$$

where, θ_Y is the equilibrium contact angle of a beaded liquid droplet on featureless solid surface, which is also referred as Young's contact angle, whereas, γ_{SG}, γ_{LS} and γ_{LG} are the surface free energy of solid, interfacial tension of solid/liquid and surface tension of liquid phase, respectively.

1.2.1.2 Wenzel model:

In reality, most of the commonly used solid surfaces have certain features and roughness. Consequently, the contact angle of beaded liquid droplet on rough surfaces consisting of either micro or nano features cannot be accurately determined following Young's model. This anomaly was addressed when Wenzel[14] proposed another wettability model (Fig. 1.2B) incorporating the roughness factor which is capable of quantitatively and accurately analysing the liquid contact angle of beaded liquid droplet on a featured/rough solid surface. Wenzel's equation (eqn 1.2) which is used to evaluate the liquid CAs on a rough solid surface (micro or nano), is as follows:

$$\cos\theta_W = r\cos\theta_Y \quad \ldots\ldots\ldots\ldots\ldots\ldots\ldots\ldots\ldots\ldots (1.2)$$

where, θ_W and θ_Y are denoted as Wenzel's and Young's contact angle, respectively. The roughness

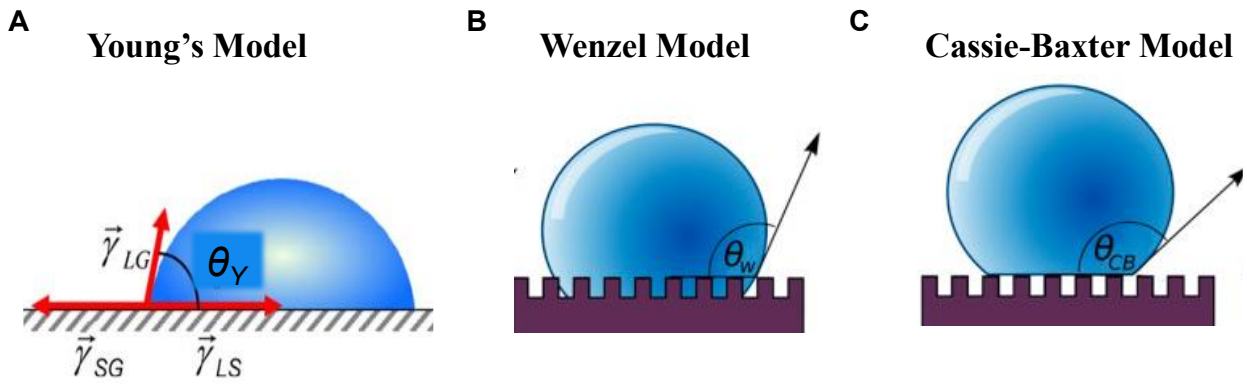

Figure 1.2: (A-C) Schematic interpretation of Young's model (A), Wenzel model (B) for homogeneous wetting and Cassie-Baxter model (C) for heterogeneous wetting. (A) Reprinted with permission from Ref. 15 Copyright 2007, Springer. (B-C) Reprinted with permission from Ref. 16 Copyright 2016, Elsevier.

factor (r) is defined as the ratio of the actual area to the projected area of the solid surface.

1.2.1.3. Cassie-Baxter model:

Nevertheless, the contact angles beyond a certain limit (>150º) cannot be justified by any of these two models (i.e. Young's model and Wenzel model) of homogeneous wetting discussed earlier. In that regard, Cassie and Baxter proposed a wettability model (Fig. 1.2C) based on heterogeneous

wetting that can efficiently describe the higher contact angles (≥150º) of the beaded liquid phases on a solid surface.[17] The hierarchical surfaces can trap a sufficient amount of external third phase into the micro/nano grooves of the bio-inspired interfaces which play a pivotal role in minimizing the contact between the solid and the liquid phase and maintaining a discontinuous tri-phase (solid-external third phase-liquid) interface. On decreasing the fraction of contact area (f_1) between solid and beaded liquid phase, an extremely liquid-repellent interface can be developed, where the beaded liquid phase rolled off the tilted (≤10º) surfaces with an advancing liquid contact angle of ≥150º. The equation (eqn 1.3) below is widely recognized as Cassie-Baxter equation and is capable of accounting for the heterogeneous wettability of beaded liquid droplet on solid surfaces:

$$\cos \theta_{CB} = f_1 \cos \theta_1 + f_2 \cos \theta_2 \quad \text{..... (1.3)}$$

where, θ_{CB} is the Cassie-Baxter angle, f_1, f_2, are the fraction of contact areas for solid/liquid and liquid/air interfaces, respectively, and θ_1, θ_2 are the contact angles of the liquid droplet on solid and air phases, respectively. As the total fraction of contact area i.e. $f_1 + f_2$ equals to 1 and the ideal contact angle of liquid droplet in air is considered to be 180º, the Cassie-Baxter equation can be simplified and rewritten as following equation (eqn 1.4):

$$\cos \theta_{CB} = f_1 (\cos \theta_1 + 1) - 1 \quad \text{..... (1.4)}$$

This Cassie-Baxter model explains the superhydrophobicity that was first discovered in 1997[6] where the role of trapped air layer in micro/nano featured[18] lotus-leaf surface was held to be responsible for such extreme water-repellent property (in air). The same model has been successfully extended to understand another bio-inspired wettability—that is underwater superoleophobicity.[7] This property was first discovered on the fish scales'.[7]

1.3. Prerequisites for Artificial Designing of Nature-inspired Extreme Liquid Wettabilities

1.3.1. Naturally existing anti-liquid wettabilities

To adopt the survival strategies in harsh environments, natural organisms have developed various functional properties through million years of evolution in terms of structural development and chemical modifications which enhanced their performance to a greater extent. Similarly, the evolution of diverse wettabilities spreads into different plants and animals that exist in nature, e.g. fog-basking by Namib desert beetles[19], prey-trapping mechanism of nepenthes pitcher plants,[20] etc. Plenty of biological organisms with different non-wetting properties—especially superhydrophobic and underwater superoleophobic instigated the innovations of designing various smart and advanced

materials which are inevitable for significant contribution in our daily life. However, the development started in 1997, when two German Botanists, Neinhuis and Barthlott[6] first discovered the extreme water-repellency of the lotus leaf (Fig. 1.3A) and provided a successful explanation behind the self-cleaning property of that leaf. The bumpy features of the lotus leaf consist of both micro/nano papillae as shown in Fig. 1.3F and an epicuticular wax coating which had been validated to be the backbone of the water-repellent property—superhydrophobicity and displays a water contact angle of >150º with roll-off angle of <5º.[21]

The available literature[22] conspicuously shows that superhydrophobicity is one of the most explored among all the wettabilities— lots of bio-organisms have evolved over the years with embedded superhydrophobicity in their very skin which helps them in survival under severe environments with additional advantages like, (a) controlled and guided sliding of water droplet on the superhydrophobic rice leaf with anisotropic microstructures[23] (Fig. 1.3B,G), (b) directional adhesion of water droplet on orientation-tunable microstructures containing butterfly wings[24] (Fig. 1.3C,H), (c) superhydrophobic water strider's leg composed of microsetae with fine nano grooves covered with secreted wax for effortless walking in water/air interface[25] (Fig. 1.3D,I), (d) combination of hexagonally non-close-packed nano-nipples and close-packed micro-hemispheres responsible for the anti-fogging properties in mosquitoes eyes[26] (Fig. 1.3E,J), etc.

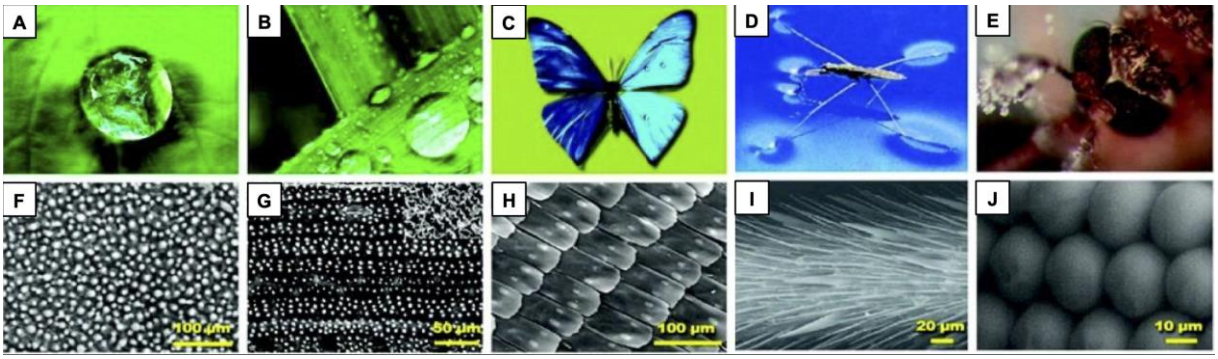

Figure 1.3: (A-J) Digital images (A-E) and scanning electron microscope (SEM) images (F-J) of various naturally existing superhydrophobic surfaces including lotus leaf (A,F), rice leaf (B,G), butterfly wings (C,H), water strider's leg (D,I) and mosquito's eye (E,J). Reprinted with permission from Ref. 27 Copyright 2011, American Chemical Society.

On the other hand, Jiang et al. first explored the possible internal mechanism of the extreme oil-repelling ability of fish scales as shown in Fig. 1.4A.[7] Fish scales are made up of hydrophilic hierarchical building blocks (consisting of calcium phosphate, protein) and a thin layer of mucus which helps in trapping a large amount of water in its micro/nano grooves as shown in Fig. 1.4B and eventually lowering the oil adhesion under water.

Different other examples exist in nature whose specific body parts are decorated with such anti-oil wettability property that exists in fish-scale, i.e. underwater superoleophobicity property. Later, a salt-tolerant underwater superoleophobicity of seaweed (Fig. 1.4C-D) was investigated by Cai et al. which is mainly due to its high content of polysaccharide including carrageenan, agar, and alginate

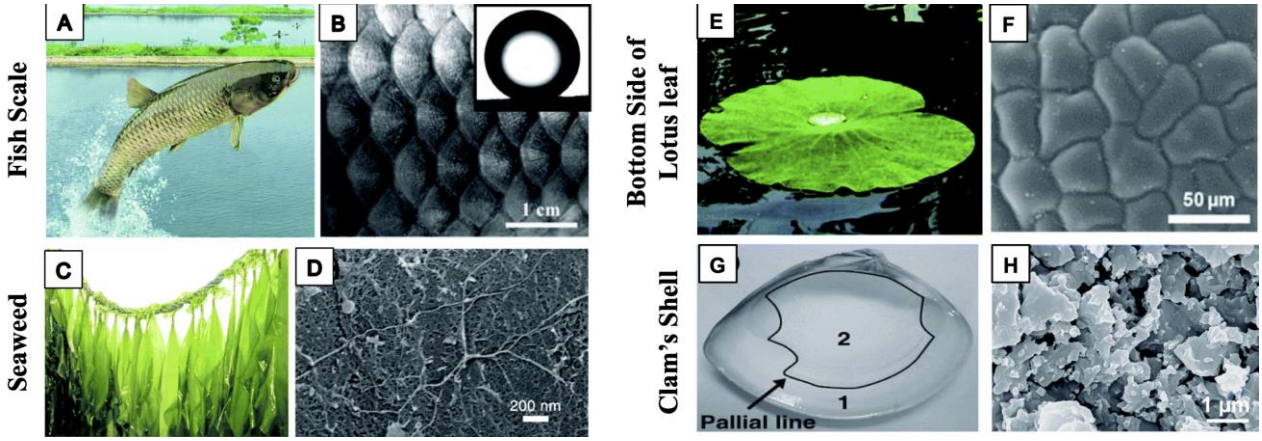

Figure 1.4: (A-H) Digital (A,C,E,G) and SEM (B,D,F,H) images of naturally existing underwater superoleophobic surfaces including fish scales (A-B), seaweed (C-D), the bottom side of lotus leaf (E-F) and clam's shell (G-H). Reprinted with permission from Ref. 28, Copyright 2011, Royal Society of Chemistry.

(Saccharina japonica).[29] Moreover, the bottom side of the lotus leaf is also displaying such underwater extreme oil-repellency which is contrasting to the upper side of the lotus leaf (Fig. 1.4E). Cheng et al[30] validated that the tabular and slightly convex papillae were designed with nano-grooves of around 4 µm height present on the bottom side (Fig. 1.4F) following environmental scanning electron microscopic (ESEM) imaging. The secretion of some hydrophilic molecule like ferns from the epidermal glands provided essential surface energy to confer a low adhesive superoleophobicity in the bottom side of the lotus leaf.[30] The transparent petal of *Diphylleia grayi* comprises numerous air-filled lacunae and colourless cytolymphs. However, the trapped air present in intercellular spaces are completely replaced by water, in the rain and transforms the air–liquid cytolymph interface to liquid water–liquid cytolymph interface. Due to the comparable refractive index of water and liquid cytolymph, it exhibits complete transparency with underwater oil-repulsion.[31] Besides, Liu et al. explained the complete oil-repelling property of pallium-covered region of a short clam's shell underwater as shown in Fig. 1.4G. They claimed that such unique underwater property of the clam's shell mainly originated from its hierarchical distribution of micro/nano structures (Fig. 1.4H) along with the high energy inorganic composition of $CaCO_3$.[32]

Interestingly, the superhydrophobic interface which extremely repels the aqueous phase inherently displays another extreme liquid wettability[11-12,33]—that is refereed as underwater superoleophilicity (Fig. 1.5D), which allowed a rapid and selective soaking of oil phase on solid surface under water with

contact angle 0°. Generally, the presence of continuous trapped air layer (Fig. 1.5B-C) is considered as the primary basis for achieving underwater superoleophilicity. Later on, the basics of superoleophilicity property underwater come out with a concept of tri-phase contact line (TPCL)

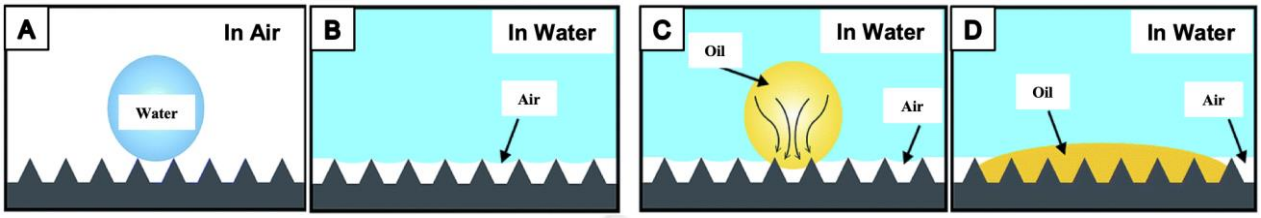

Figure 1.5: (A-D) Schematic illustrating the complete soaking and spreading beaded oil droplet on the superhydrophobic surfaces under water. Reprinted with permission from Ref. 33 Copyright 2017, Royal Society of Chemistry.

among two liquids with different polarity and the solid surface.[12] The existence of continuous trapped air layer is considered as an essential factor to achieve such extreme affinity for oil phase under water.

1.3.2. Essential criteria for artificial designing of extreme liquid wettability

Later on, naturally existing extremely super-water-repellent lotus leaf[6] or underwater extreme oil-repellent fish-scales[7] were studied in detail to find out essential and optimum parameters that conferred super-liquid-repellences. In a close investigation into the prerequisite for artificially achieving these extreme liquid wettability properties, researchers have turned to two essential criteria[18,28,34-37]- i) micro/nano features and ii) desired surface energy coating. In that context, this super liquid (water or oil) wettabilities are obtained by exploring different three-phase systems which are complementing and correlating in a way to each other. The artificial super-liquid repellent interfaces were initially developed by mimicking the naturally existing extreme liquid-repellent surfaces.[7,18]

Barthlott et al.[6] first observed that the lotus leaves are mainly covered with the micro-meter sized cuticles of about 1–5 µm height which are composed of soluble lipids embedded in a polyester matrix. The presence of lipids makes the cuticles hydrophobic and further acts as an interfacial barrier between the plants and the environment. Whereas, the addition of an epicuticular waxy layer provides superhydrophobicity in the lotus leaf. However, there was some ambiguity regarding the topography of the lotus leaf. Further, Feng and his co-workers[35] confirmed the presence of both micro and nano structures as shown in Fig. 1.6A-B where the nano structures (Fig. 1.6B) were a key component of topography of the lotus leaf, having a very high water contact angle of 161.0º ± 2.7º and a very low sliding angle of 2º. So by mimicking/replicating the lotus leaf features on different other substrates like aligned carbon nanotube (ACNT) films (Fig. 1.6C), Silicon (Si)- surface (Fig. 1.6D-E), etc., the same anti-wettability was achieved artificially. Any destruction of the nano structures drastically

changes the contact angles of the lotus leaf (Fig. 1.6F) and further the equally important role of both micro and nano structures on serving the superhydrophobicity in lotus leaf was confirmed by Koch et. al.[18]

In 2009, Liu and his co-workers[7] revealed the key components of the fish scale that conferred underwater superoleophobicity. SEM images (Fig. 1.7A) have confirmed that the micropapillae with 100–300 μm in length and 30–40 μm in width, on the fish scales were randomly oriented in the radial

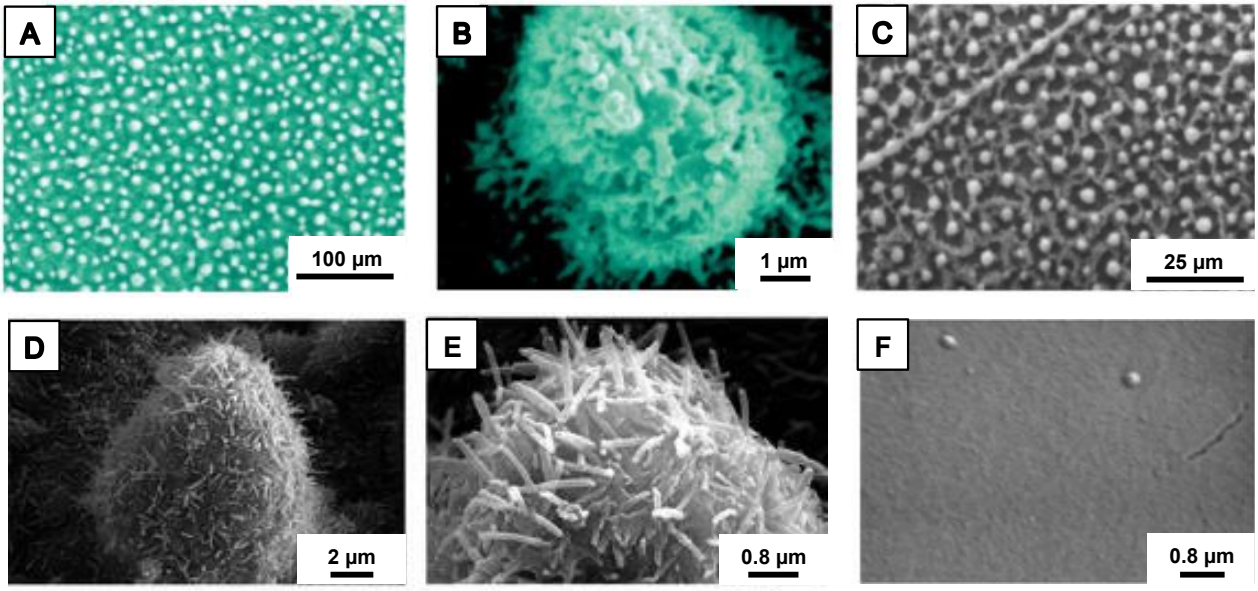

Figure 1.6: (A-B) SEM images of the lotus leaf consisting of micro/nano papillae with a dense layer of epicuticular wax layer. (C-F) SEM images of the artificially synthesized superhydrophobic interface that made out of aligned carbon nanotube (ACNT) film (C) and micropatterned Si replicas (D-F). Reprinted with permission from ref. 35 Copyright 2002, Wiley-VCH (A-C). Reprinted with permission from Ref. 18 Copyright 2009, Royal Society of Chemistry (D-F).

direction. Due to the presence of hierarchical structures made out of hydrophilic components with an additional mucus layer atop, fish scales are believed to have a high affinity towards aqueous phase in air (Fig. 1.7B), and as a result, the scales display the super-oil repellency under water with a very high OCA of 156.4º ± 3º as shown in Fig. 1.7C. Then, the fish scales[7] was used as a template to mimic the topography on a hydrogel matrix. The same topography that is present in the fish-scale (Fig. 1.7D) was achieved on polyacrylamide (PAM) hydrogel[7] which displayed the oil contact angle of 162.6º ± 1.8º as shown in Fig. 1.7D (inset), even higher than that of the fish scales. However, their investigation on fish scales was not sufficient in supporting the role of mucus towards this superoleophobic behaviour and the wettability reversion in air and under water. Bhushan and his co-workers[38-39] thoroughly studied the effect of mucus layer on the water wettability in air, where both fish scale (Oncorthynchus mykiss; Fig. 1.7E) and shark skin (Insurus oxyrinchus) used selected as model substrates for their study. Their study supported the fact that the removal of mucus layer from fish

scales altered its wettability to a great extent and the static contact angle in air for water changed from 10° to 58° as shown in Fig. 1.7E. It is also well established that due to the presence of the mucus layer, fishes can easily overcome the drag that helps them to swim with less friction under water.[39-41] Further, Waghmare et al.[42] revalidated the impact of mucus layer on the liquid wettability of the fish scales of *Oreochromis niloticus* both in air and under water, where the water contact angle was found to shift significantly from 85.7° ± 4.7° to 34.1° ± 2.7° in air and the oil contact angle also changed from 178.4° ± 1.3º to 148.9° ± 5.5° under water, after the removal of mucus layer from the fish scales as shown in Fig. 1.7F.

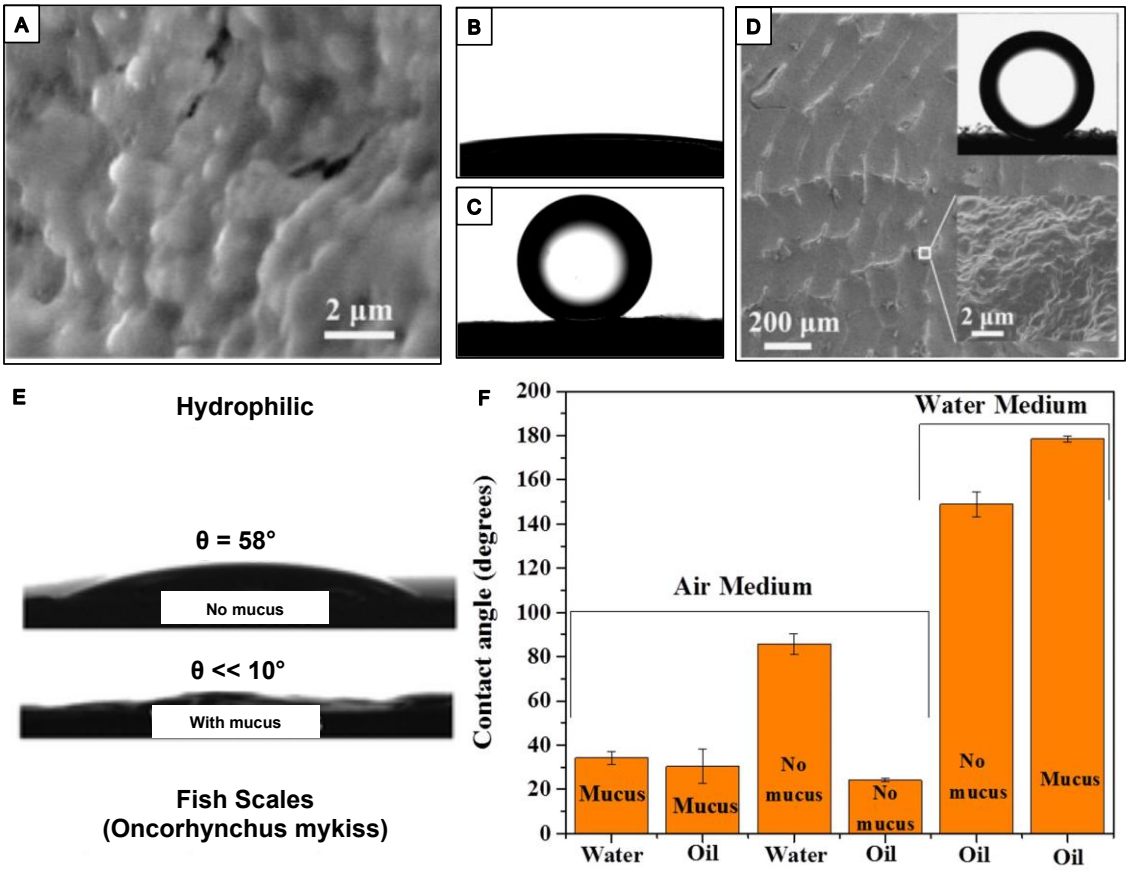

Figure 1.7: (A) SEM images of the nanostructures of the papillae present in fish scales. (B-C) OCAs on fish scales in air (B) and under water (C). (D) Underwater superoleophobic Poly acrylamide hydrogel (PAM) film having exact Fish scale structures, developed by templation method. (E) Variation in OCAs of fish scales in presence and absence of natural mucus layer. (F) Change in WCA and OCAs on fish scale depending on the presence and absence of mucus layer for both in air and under water. Reprinted with permission from Ref. 7 Copyright 2009, Wiley-VCH (A-D). Reprinted with permission from Ref. 39 Copyright 2012, Royal Society of Chemistry (E). Reprinted with permission from Ref. 42 Copyright 2015, Nature.

In the recent past, the wettability of liquids was thoroughly investigated on differently featured (micro or nano or both) or featureless substrates as shown in Fig. 1.8.[34] Considering the homogeneous wettability models, the wetting of beaded liquid on both featured and featureless substrates can be explained following Young's state[13] and Wenzel's state[14], whereas Cassie-Baxter

model described the super-liquid-wettability on solid surface following the principle of heterogeneous wettability, where trapped external third phase minimized the contact between the beaded liquid droplet and solid surface.[34] The topography of solid surface played an important role in stabilizing the external trapped phase in the solid interface. The entrapped third phase would like to be easily replaced

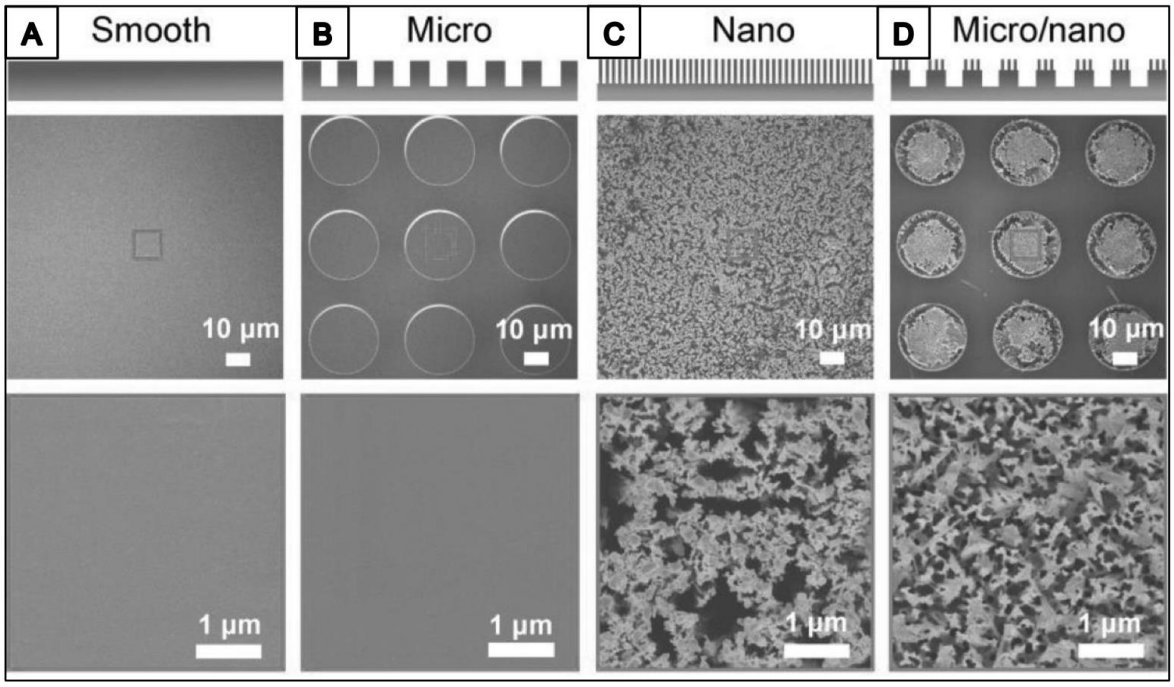

Figure 1.8: (A-D) Schematic illustration and scanning electron microscopic (SEM) images of: smooth (A), micro (B), nano (C), and hierarchically (micro/nano; D) structured interfaces. Reprinted with permission from Ref. 34 Copyright 2015, Wiley-VCH.

by the probe liquid due to the unstable nature of the trapped phase in the grooves of micro features Fig. 1.8B. On the other hand, the entrapped third phase is significantly stable in the nano-featured asperities due to its clogged environment as shown in Fig. 1.8C, yet the presence of trapped phase is very low in such cases as well. Being compelled to achieve super anti-wettability is strongly necessitating such substrate, featuring significant hierarchy.[35] The hierarchical features (Fig. 1.8D) can entrap appropriate external third phase inside the asperities, depending on the selection of top surface chemistry and conferred either superhydrophobicity in air[6] or superoleophobicity underwater.[7]

1.4. Conventional Methods to Achieve Bio-inspired Extreme Liquid Wettabilities

Myriads of research have been acknowledged that are continuously evolved to mimic wettability of both lotus leaf[6] (anti-water repellence) and fish-scales[7] (anti-oil repellence underwater) for the practical applications of these embedded extreme liquid wettability. Artificially designed biomimicked surfaces possessing hierarchical micro and nano structures are prepared by adopting

several methodologies following different protocols. Some of the commonly and widely adopted approaches for preparing super-liquid repellent interfaces are discussed in the following sections:

1.4.1. Superhydrophobic surfaces

The fabrication processes for hierarchical interfaces that display artificial superhydrophobic property are broadly categorised as (i) top-down[18,43-49] and (ii) bottom-up[11,50-58] approaches. The top-approaches are involved with template-based techniques,[18,43,59-60] lithography,[47,49] plasma treatment,[44-46] etc. On the other hand, some examples of bottom-up approaches are chemical vapour deposition (CVD),[52-53,61] layer-by-layer (LbL) deposition,[51,53] electrospinning method,[11,62-63] spray coating,[56-58] etc. In that regard, various approaches for developing artificial superhydrophobic surfaces (denoted as SHS) are briefly discussed in the following sections:

1.4.1.1. Top-down approaches:

Top-down approaches[18,43-49,59-60] involve preparation of the hierarchical features which is one of the essentials for achieving the superhydrophobicity by mechanical/manual itching of the bulk material with different tools or lasers. Some of the examples of top-down approaches like, template-based coating, lithography are discussed in the following section:

1.4.1.1.1. Template-based technique:

The template-based technique[64-65] is the oldest technique to develop the micro/nano structures on a bulk material, where a hierarchical substrate was used as a template.[18,43,59-60] The replica of the hierarchical template can be achieved on selective substrates by simply moulding followed by lifting off[66-68] or dissolving[69-70] or sublimation[71-72] of the template. On account of developing these hierarchical features to achieve superhydrophobicity, Koch et al. used the superhydrophobic lotus-leaf as a template and replicated the topography by using polydimethylsiloxane (PDMS). Later, various other substrates were also used as a template in tailoring the micro/nano features.[18,68,70] Xiong et al.[68] used the featured non-woven fabric as a template for mimicking the plant roots holding soil behaviour on a (polyvinylidene difluoride) PVDF membrane followed by TiO_2 coating as shown in Fig. 1.9A. The SEM images (Fig. 1.9B-G) confirmed that the unique interface of as-synthesized material possessed large quantities of cilia-like micro/nano-fibrils embedded with superhydrophobicity with the contact angle of ~154° even after applying 0.2MPa hydraulic pressure as shown in Fig. 1.9I.

Hoshian et al.[70] used HCl-etched aluminium wafer as a template for developing a hybrid exoskeleton-like elastomer covered with robust and photoactive metal-oxide (titania) for developing UV-responsive superhydrophobic PDMS/titania hybrid elastomer (Fig. 1.9J). The superhydrophobicity of PDMS/titania elastomer with atomic layer deposition (ALD) titania (25 nm

thickness) displayed an advancing WCA of about 163º and receding WCA of ~161º with extremely small CA hysteresis.

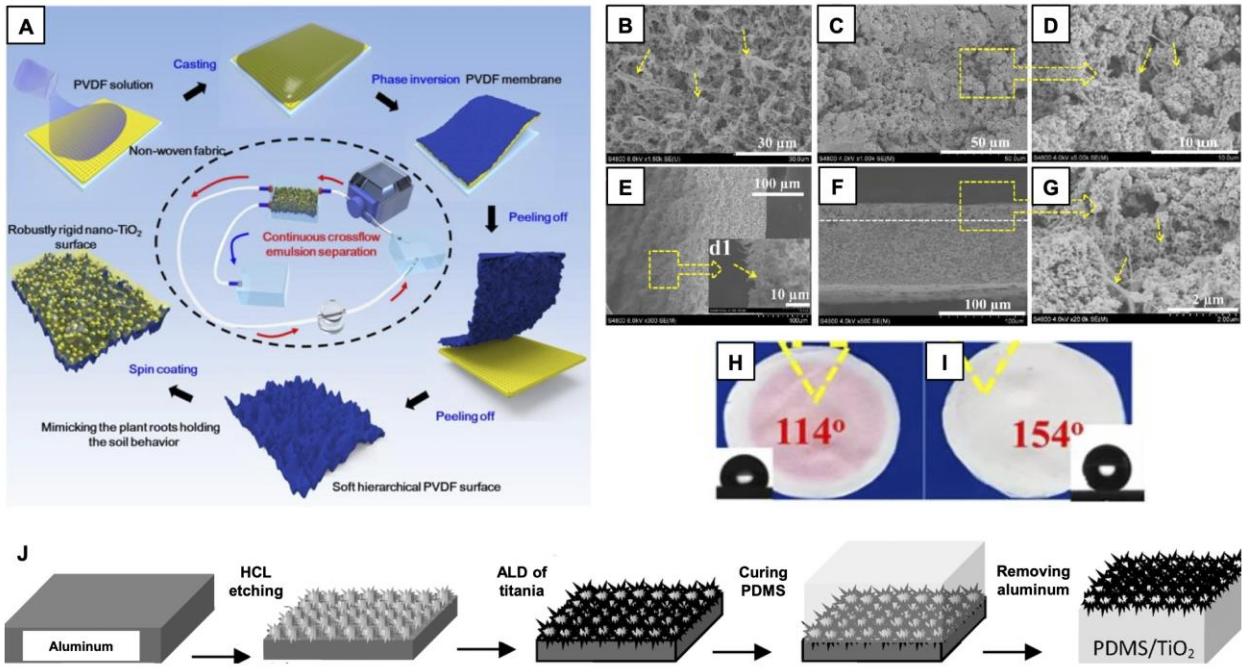

Figure 1.9: (A) Schematic illustrating the preparation of superhydrophobic membrane of polyvinylidene difluoride (PVDF)/titania (TiO_2) through template-based process. (B-D) SEM images of the surface (B), cross-sectional view (C) and enlarged cross-sectional view (D) of pristine PVDF membrane. (E-G) SEM images of the surface (E), cross-section (F) and enlarged cross-sectional (G) view of nano-TiO_2 incorporated membrane. (H-I) Water contact angles (WCAs) of beaded water droplet on soft PVDF membrane and rigid PVDF membrane after applying 1 h hydraulic pressure. (J) Fabrication process of hybrid elastomer using atomic layer deposition (ALD) film of titania. Reprinted with permission from Ref. 68 Copyright 2017, Nature (A-I). Reprinted with permission from Ref. 70 Copyright 2016, Royal Society of Chemistry (J).

1.4.1.1.2. Lithography Technique:

In general, the term lithography refers to the process of writing on hard surfaces like stones and metals.[73-75] Earlier, the process of printing using a polar/non-polar ink on a hydrophilic master plate was considered as lithography.[76-77] Nevertheless, this principle was extended later in developing organized topography in the micro/nano scales.[78-80] Lithographic methods provide good control over surface structuring and patterning for preparing artificial SHS. Rough surfaces patterned with various shapes (e.g., circular, square, star, etc.) of pillars with different dimensions, have been developed by adopting this technique.[81-82]

In 2016,[83] Kim et al. used this lithographic technique for fabricating a triboelectric sponge made of PDMS using 3D soft lithography (Fig. 1.10A). Sugar particles of 300, 500, and 1500 micrometre sizes were used to make sugar templates for PDMS sponges with various pore sizes as shown in Fig. 1.10C. After the curing between PDMS prepolymer and curing agent, the sugar

templates were dissolved and washed away. The sponge, made from the smallest sugar cube, displayed high water repellency with a contact angle of 151.2°. Later, Milionis et al.[84] fabricated a fully organic, bioinspired superhydrophobic material composed of degradable and green constituents, similar to the ones found in superhydrophobic leaves in nature. Cellulose micropillars (Fig. 1.10D) were developed

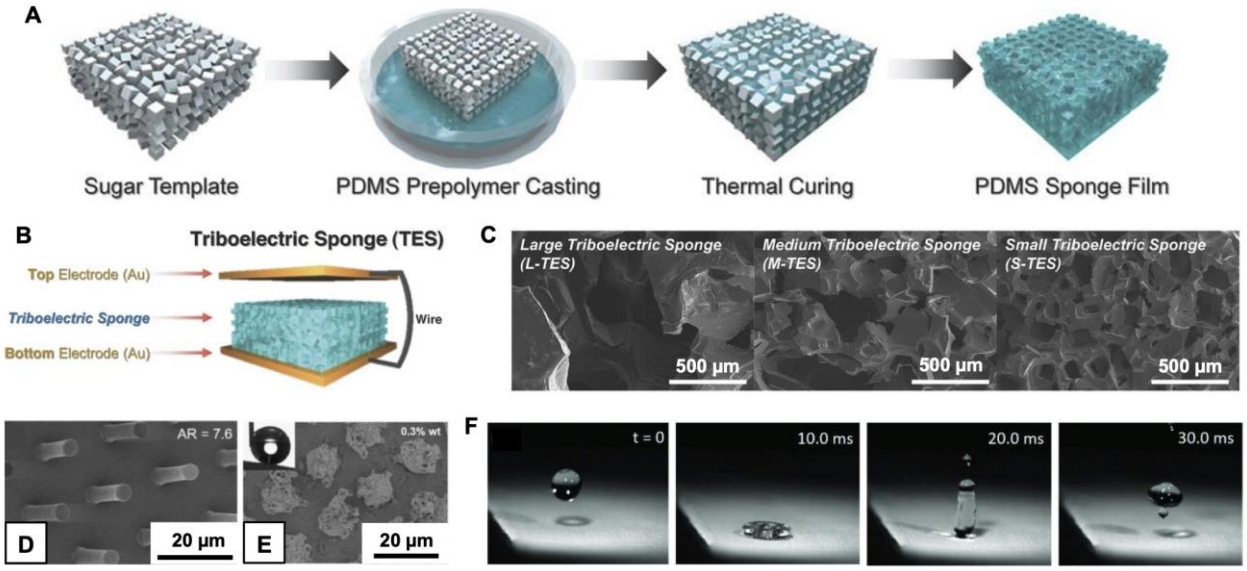

Figure 1.10: (A) Schematics for the preparation of porous polydimethylsiloxane (PDMS) sponge using sugar particles through 3D soft lithography. (B) Illusrating the triboelectric sponge (TES) with an embedded generator. (C) SEM images of TESs of three types: small, medium and large. Scale bar: 500 µm. (D-E) SEM images of the cellulose micropillars with maximum aspect ratio of 7.5 before (D) and after (E) spray coating with solution (0.3 wt%) of carnauba wax in chloroform. (F) Digital images depicting bouncing of water droplet on superhydrophobic interface after 1000 impacts. Reprinted with permission from Ref. 83 Copyright 2016, Wiley-VCH (A-C). Reprinted with permission from Ref. 84 Copyright 2019, Wiley-VCH (D-F).

with a high aspect ratio of 7.5 following a soft moulding procedure of a cellulose solution on prefabricated Si masters to replicate the negative structure of the silicon wafer microholes. Since cellulose is a hygroscopic material and tends to absorb water, superhydrophobicity on this material was achieved by a physical deposition of carnauba wax (Fig. 1.10E-F), a natural wax obtained by Brazilian Copernicia prunifera palm trees. The wax is intended to act in a similar manner to the wax structures covering the Lotus leaf and other natural superhydrophobic plant surfaces, which are responsible for their self-cleaning properties.

1.4.1.2. Bottom-up approaches:

In contrast to the top-down approaches, bottom-up[11,50-58] approaches mainly refer to the development of hierarchical topography by strategic integration and accumulation of micro/nano-scaled features on the surface of various substrates. The methods involved in bottom-up approach are briefly discussed in the following sections:

1.4.1.2.1. LbL technique:

The Layer-by-Layer (LbL) deposition terchnique[51,53,85] is an easy and versatile approach for designing superhydrophobicity, where this facile deposition process provided a simple basis to control both the topography and thickness of the coatings.[86-88] Decher and coworkers[87] introduced a seminal report on electrostatic multilayer coating in 1991.[86] This method involves electrolytic deposition of

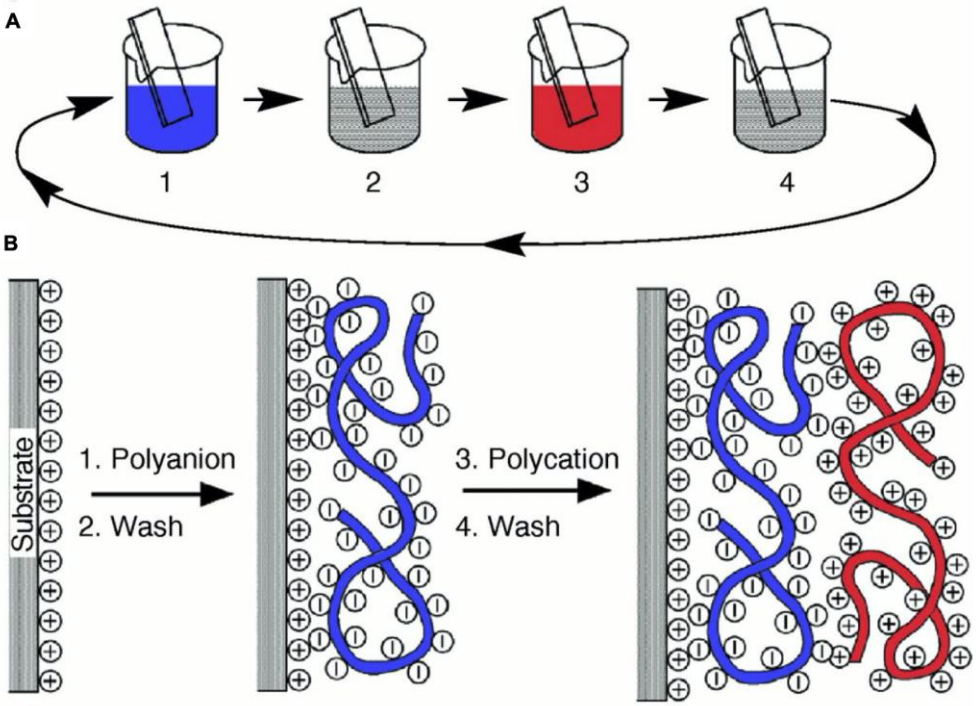

Figure 1.11: (A) Schematic representation of Layer-by-Layer (LbL) deposition process. (B) Illustrating electrostatic interaction between polycation and polyanion. Reprinted with permission from Ref. 88 Copyright 1997, Science.

multilayers by simple adsorption of a polyanion and polycation, respectively (Fig. 1.11), and the washing steps allowed to remove loosely bound polyelectrolytes during multilayer construction.[87-88] Leem et. al.[89] reported a porous multilayer coating for water oxidation. The assembly consisted of a cationic polystyrene-based Ru polychromophore (PS-Ru) and a [Ru(tpy)(2-pyridyl-N-methylbenzimidazole)(OH_2)]$^{2+}$ (Mebim-py = 2-pyridyl-N-methylbenzimidazole) (RuC) water oxidation catalyst, co-deposited with poly(acrylic acid) (PAA) as an oppositely charged polyelectrolyte (Fig. 1.12A-B). Planar indium tin oxide substrates were used for electrochemical characterization, and mesoporous substrate (a SnO_2/TiO_2 core/shell structure atop fluorine-doped tin oxide (FTO)) was coated for light-driven water oxidation (Fig. 1.12C). The LbL deposition allowed facile control over the amount of chromophore and catalyst immobilized on the substrate, variation of the chromophore-catalyst ratio, and for future studies, incorporation of different chromophore or catalyst layers for altering reaction kinetics or the catalytic pathway.

In another report, reversible photoisomerization of a photoreversibly tunable superhydrophobic surfaces was prepared (Fig. 1.12D) by Lim et al.[90] using LbL deposition (10 cycles)

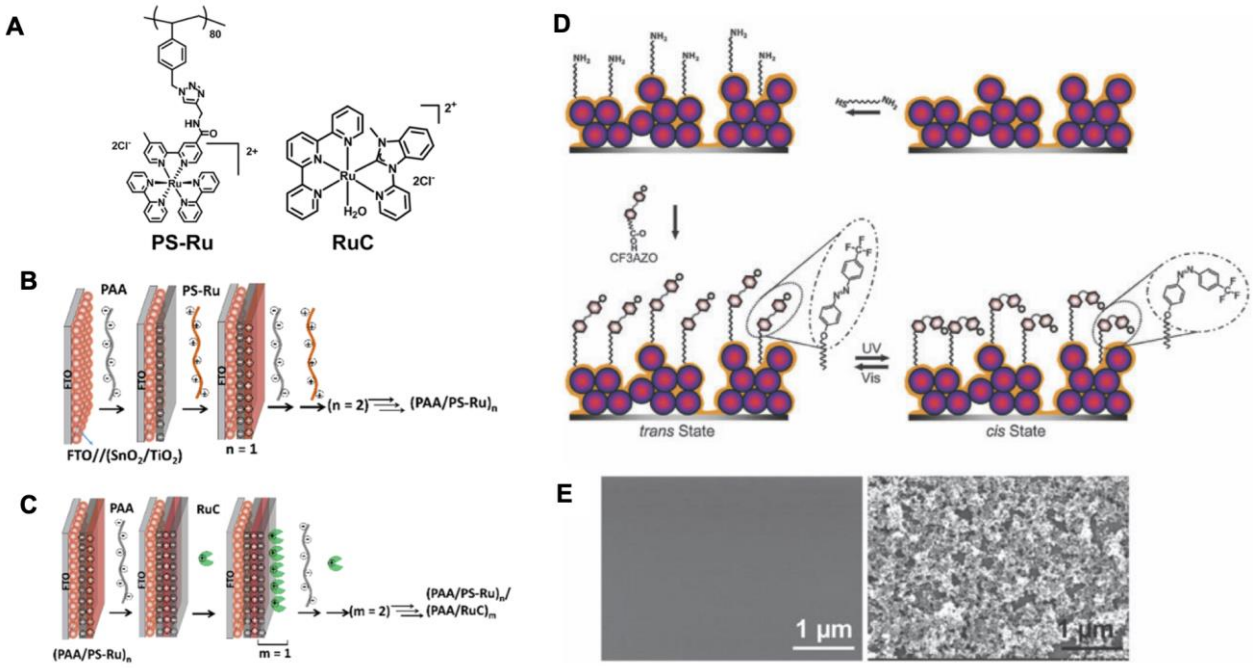

Figure 1.12: (A) Molecular structures of polystyrene-based Ru polychromophore (PS-Ru) and Ru(tpy)(2-pyridyl-N-methylbenzimidazole) $(OH2)]^{2+}$ (RuC). (B-C) Schematic illustration for fabrication of porous multilayers coatings of fluorine-doped tin oxide (FTO)// tin oxide (SnO_2) /titanium dioxide (TiO_2)// poly(acrylic acid) $(PAA/PS\text{-}Ru)_n$ (B) and $FTO//(SnO_2/TiO_2)//(PAA/PS\text{-}Ru)_n/(PAA/RuC)_m$ (C). (D) Schematic illustration of the fabrication and reversible photoisomerization of a photo-responsive superhydrophobic surface. (E) SEM images of a smooth (left) surface and a rough (right) multilayer coating. Reprinted with permission from Ref. 89 Copyright 2016, American Chemical Society (A-C). Reprinted with permission from Ref. 90 Copyright 2010, Royal Society of Chemistry (D-E).

of two oppositely charged polyelectrolytes— poly(allylamine hydrochloride) (PAH) and silica (SiO_2) nanoparticles. The highly porous micro/nano structures developed (Fig. 1.12E) on the substrate were mainly formed by the complicated interconnections between silica nanoparticles. Finally, the post-treatment with azobenzene molecules to the substrate produced the surface covered with string-like fluorinated azobenzene derivatives on the topmost layer of the nanostructured substrate and switchable superhydrophobicity was obtained on this highly textured multilayer.

1.4.1.2.2. Electrospinning method:

Electrospinning is a very simple and cost-effective technique for the fabrication of polymeric nanofibers with well-defined topology. A high voltage is applied between the metallic collector and a syringe containing the polymer solution which will be spun. Once the critical value of voltage is reached, the electrostatic attractive force overcomes the surface tension of the solution and the solution is dragged towards the collector from the needle/spinneret (Fig. 1.13A).[11] Solvent from the extruded

polymer fibre evaporates rapidly resulting in the formation of a long thread with a diameter as small as several nanometres to tens of micrometres.[11,91,92] The fibre diameter, the porosity of nanofiber mats, etc. can be easily adjusted by controlling the process parameters like electric potential, flow rate, polymer concentration, the distance between the capillary and collection screen, temperature, humidity, and air velocity in the electrospinning chamber.[11,93-95] In 2016, Arslan et al.[96] developed an

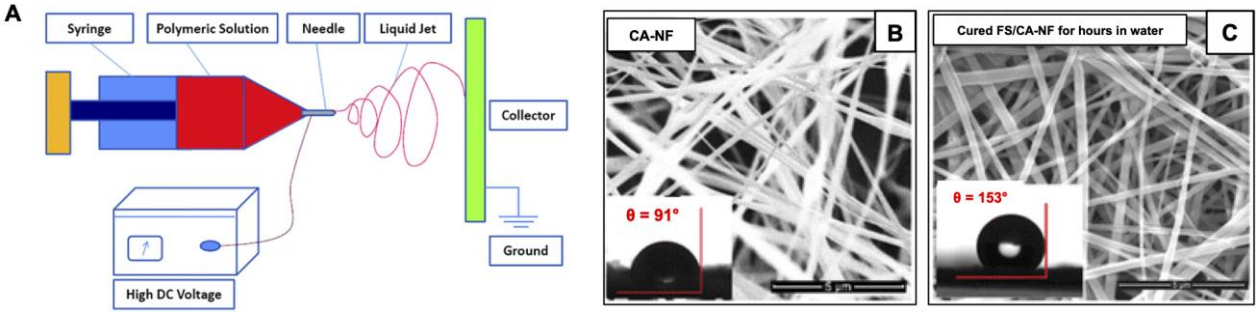

Figure 1.13: (A) Schematic for standard electrospinning procedure. (B-C) SEM images of electrospun cellulose acetate nanofibrous (CA-NF) mat and cured superhydrophobic 1H,1H,2H,2H Perfluorooctyltriethoxysilane (FS)/CA-NF mat after 24 hours in water (inset: WCA angle measurement). Reprinted with permission from Ref. 11 Copyright 2013, Royal Society of Chemistry (A). Reprinted with permission from Ref. 96 Copyright 2016, American Chemical Society (B-C).

elctrospun nanofibrous mat (Fig. 1.13C) from cellulose acetate (CA) and made it superhydrophobic by functionalizing the mat with 1H,1H,2H,2H Perfluorooctyltriethoxysilane (FS) via hydrolysis and condensation reactions. In 2019,[97] a fibrous membrane (Fig. 1.14B) was developed by electrospinning of poly(styrene-butadiene-styrene) (SBS) and by subsequent hydrophobization with a fluoroalkyl

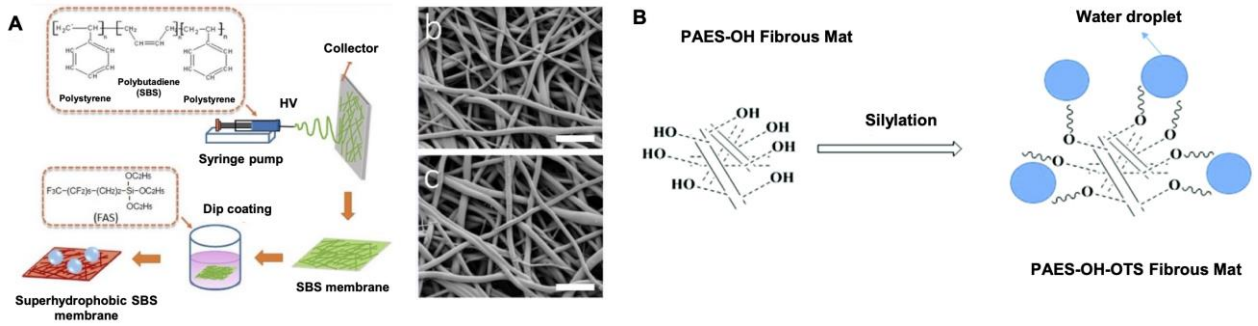

Figure 1.14: (A) Fabrication procedure of superhydrophobic fibrous membrane. (B-C) SEM images of (B) electrospun poly(styrene-butadiene-styrene) (SBS) fibers and (C) fluoroalkyl silane (FAS)-modified SBS fibers (scale bar: 10 μm). (D) The fabrication of electrospun fibrous membrane using poly(arylene ether sulfone) containing hydroxyl groups (PAES-OH) grafted with octadecyltrichlorosilane (OTS). Reprinted with permission from Ref. 97 Copyright 2015, Nature (A). Reprinted with permission from Ref. 98 Copyright 2019, Royal Society of Chemistry (B).

silane (FAS) (Fig. 1.14A). The FAS-modified membrane (Fig. 1.14C) had preternatural ability to display superhydrophobicity even after being exposed to a large strain (1500% for uniaxial stretching and 700% for biaxial stretching). Its extreme water repellency was intact even after 1,000 cycles of stretching to uniaxial strain as high as 1500% or biaxial strain of 700%. In another report, Zhang et

al.[98] synthesized poly(arylene ether sulfone) containing hydroxy units (PAES-OH) and that was electrospun into a highly porous nonwoven membrane, followed by the grafting of octadecyltrichlorosilane (OTS) on this membrane (Fig. 1.14D). This OTS-modified fibrous membrane displayed a CA of 159.2°. The existence of chemical bonding interactions between the hydroxyl group and silane were responsible for the stability and durability of the superhydrophobic membrane.

Needle-based processes are very slow because one fibre is produced at a time and therefore it takes hours to spin even one gram of polymer solution. To overcome this problem associated with throughput, different needleless techniques were developed which are very efficient for bulk production for practical applications.[99]

1.4.2. Underwater superoleophobic surfaces

Based on the reported designs, the synthesis approaches for underwater superoleophobic coatings are categorized in the following three parts: i) Hydrogel-based coating[7,29,37,100-102] ii) metal oxide-based coating[32,103-105] and iii) electrostatic multilayer based coating.[106-107] All these processes are widely used in the preparation of fish-scale mimicked underwater superoleophobic interface.

1.4.2.1. Hydrogel-based coating:

The basic study behind this concept is to develop hierarchically featured interface that made out of hydrophilic (high surface energy) constituents. In fact, hydrogel-based material that provided

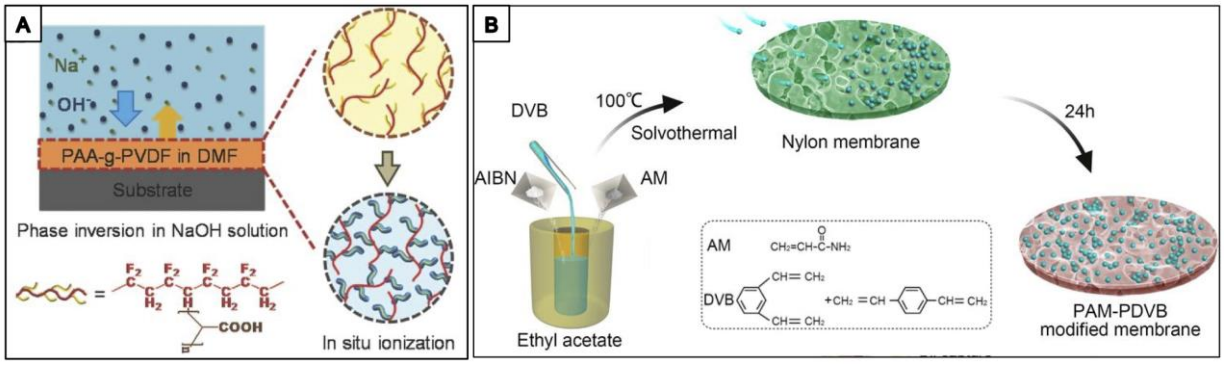

Figure 1.15: (A) Schematic for the fabrication of underwater superoleophobic coating using sodium polyacrylate-grafted poly(vinylidene fluoride) (PAAS-g-PVDF) hydrogel in dimethylformamide (DMF). (B) Fabrication of underwater superoleophobic membrane through deposition of polyacrylamide-polydimethylbezene (PAM-PDVB) hydrogel in presence of azobisisobutyronitrile (AIBN) on nylon membrane. (A) Reprinted with permission from Ref. 108 Copyright 2016, Wiley-VCH. (B) Reprinted with permission from Ref. 109 Copyright 2016, American Chemical Society.

hierarchical topography yielded a highly water-repellent interface under water.[7] Various approaches are reported in the literature based on the hydrogel coating protocol to achieve artificial underwater superoleophobicity. Here, some of the hydrogel-derived underwater superoleophobic interfaces are presented:

Gao et al.[108] explored a polyionized hydrogel polymer (sodium polyacrylate-grafted poly(vinylidene fluoride) (PAAS-g-PVDF)) in the fabrication of underwater superoleophobic coating via a one-step alkaline-induced phase inversion process as shown in Fig. 1.15A. An outstanding anti-oil fouling behaviour of the coating was observed for different oils like silicone oil, heavy diesel oil, light crude oil, and even heavy crude oil under aqueous environment and exhibited underwater OCAs all above 165° with nearly zero underwater oil adhesion. In another report, Zhang et al. introduced a polyacrylamide-polydimethylbezene (PAM-PDVB) polymer to decorate a nylon microfiltration membrane via a facile solvothermal route,[109] where polyacrylamide (PAM) was used as the main component, while the PDVB plays the role of a cross-linker to improve the interaction between the polymer and the substrate (Fig. 1.15B). Due to the combination of the superhydrophilic and underwater superoleophobic wettability of the PAM polymer with the appropriate pore size of the membrane, the modified membrane was highly efficient in separating highly stabilized oil/water emulsions (containing cationic, anionic and non-ionic surfactants). Various other hydrogels like polyvinyl alcohol (PVA) hydrogel, [7,110] alginate hydrogel,[111] composite hydrogels[100] etc. were also used in fabricating underwater superoleophobic interfaces.

1.4.2.2. Metal oxide coating:

Another widely used approach to adopt underwater superoleophobicity is the preparation of hierarchically featured metal oxide coating of nickel (Ni),[112] copper (Cu),[32,105] zinc (Zn),[113] titanium (Ti),[114], aluminium[115] etc. In that context, Zhang et al.[116] reported an underwater superoleophobic Ni/nickel oxide (NiO) surface which was based on an electro-deposition technique in combination with post-annealing process. A piece of stainless steel cathode, platinum (Pt) counter electrode plate and an electrolytic solution of nickel chloride and ammonium chloride were used in the electro-deposition process. Based on the microstructures, the wettability of the surface can be tuned from high adhesion (Wenzel state) to low adhesion (Cassie state) of oil under water as evidenced from Fig. 1.16C.

In another report, hierarchically porous NiTi/hydrogel nanocomposites were fabricated by combining the electrochemical dealloying technique at room-temperature with in-situ photopolymerization.[117] A TiO_2 nanolayer (TiNL) was directly developed on NiTi sheets which led to the growth of micro/nano featured surface during the electrochemical dealloying process which was considered as first network (Fig. 1.16E). Then, PVA was incorporated as a second network to improve the elastic modulus (about 0.2 MPa) of the composite material. The porous NiTi hydrogels nanocomposites (PNH NCs) displayed the OCA of 167.2° ± 5.6° for 1,2-dichloroethane underwater as shown in Fig. 1.16F.

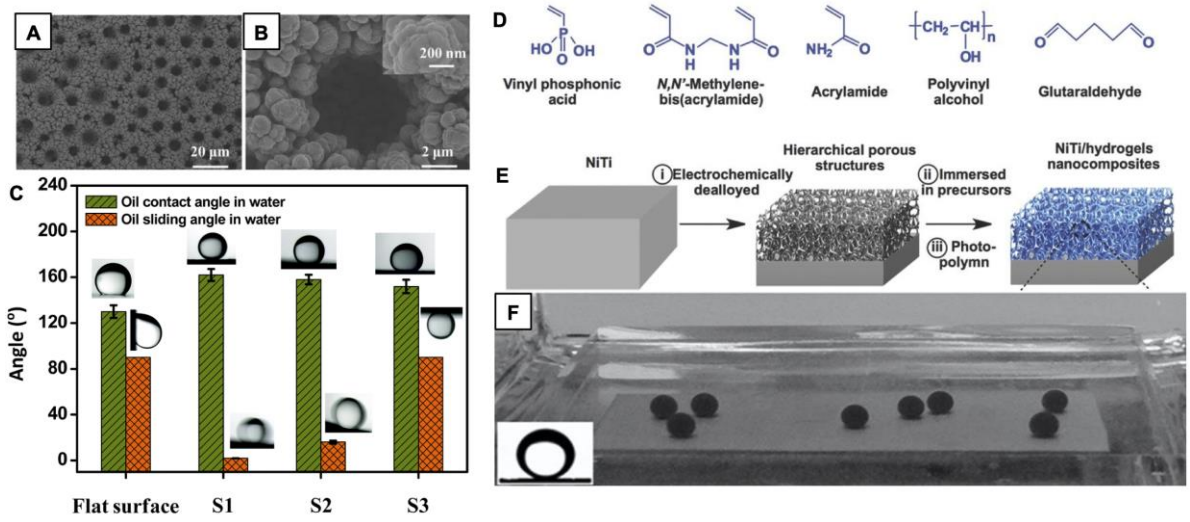

Figure 1.16: (A-B) SEM images of Ni/ nickel oxide (NiO) interface after annealed at different temperatures at: (A) 500 °C; (B) 900 °C, respectively. (C) Plot depicting underwater OCAs and sliding angle measurements on different surfaces. (D) Chemical structures of the precursors for fabricating porous nickel titanium (NiTi)/hydrogels nanocomposites (PNHNCs). (E-F) Fabrication procedure of the micro/nano features on the NiTi sheet by electrochemical dealloying technique which was further decorated with hydrogels to acheive underwater superoleophobicity (F; CA images in the inset). Reprinted with permission from Ref. 116 Copyright 2009, Royal Society of Chemistry (A-C). Reprinted with permission from Ref. 117 Copyright 2017, Wiley-VCH (D-F).

1.4.2.3. Electrostatic multilayer:

Polyelectrolyte multilayers (PEMs), which can be fabricated via the LbL assembly technique on a large variety of substrates, including polymers,[118-119] oxides,[119] and metals,[119-120] of different sizes and shapes, have emerged among others as promising coatings for surface wettability manipulation. This is a very simple and versatile approach with easy execution protocol that is very much adequate to tune the desired thickness and functionalities of the coating.

An organic/inorganic hybrid salt-added (gold nanoparticles/ poly(diallyldimethyl-ammonium chloride)) ($(AuNPs/PDDA)_{7\text{-salt}}$) film (7 bilayers) was fabricated by Xu et al.[118] on a model glass substrate by LbL deposition of the substrate into poly(diallyldimethyl-ammonium chloride) (PDDA) (with NaCl) and poly(4-styrenesulfonic acid) (PSS) (with NaCl) solution for four times followed by additional seven bilayers deposition of citrate-capped Au nanoparticle (abbreviated as cit-AuNPs) and PDDA (Fig. 1.17A). In their experimental design, the presence of 0.5 M NaCl in the polyelectrolyte solutions helped to achieve the adequate high-ion-strength very close to seawater. Therefore, the $(AuNPs/PDDA)_{7\text{-salt}}$ film displayed superoleophobicity underwater with an OCA of 168.3° ± 0.6°. However, a very similar multilayer coating prepared in the absence of salt failed to display such extreme oil-repellence under water.

Similarly, Zhang et al[119] fabricated an LbL assembly of silicate/TiO_2 composite coatings on stainless steel mesh which was conducted automatically by a programmable dipping robot at room

temperature. The assembly of silicate and TiO_2 was repeated until the desired cycle number was reached. The LbL assembled silicate/TiO_2 coatings with 20 cycle deposition exhibited extreme oil-

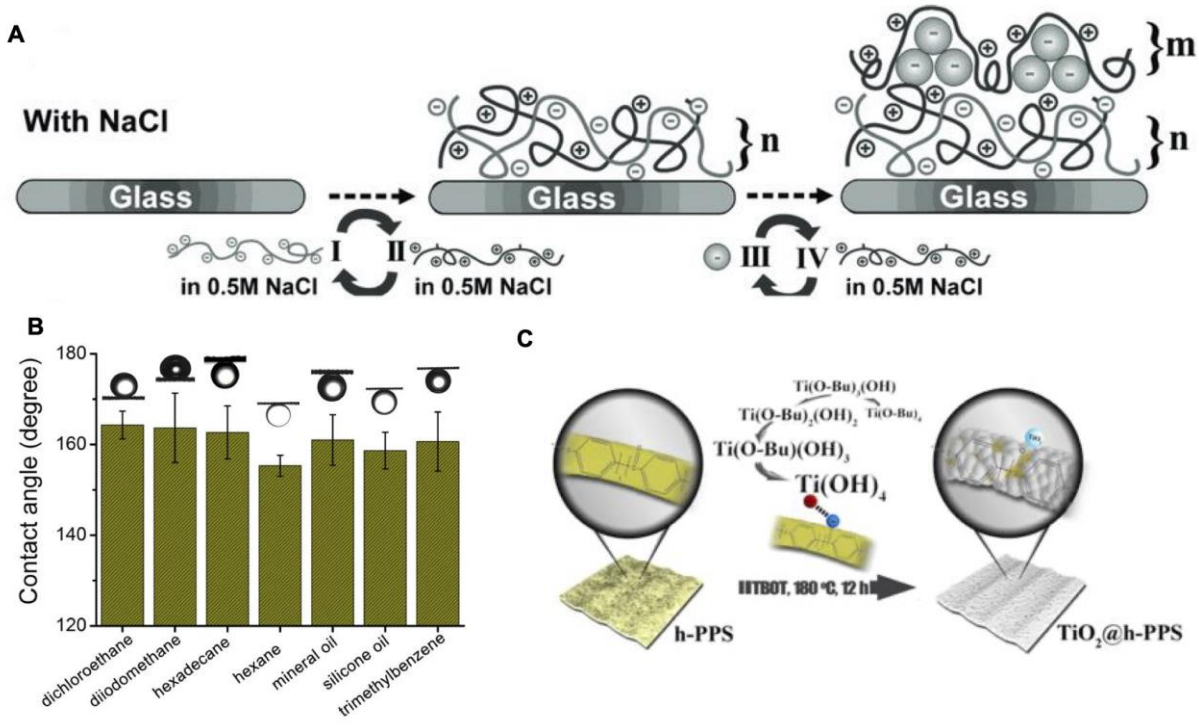

Figure 1.17: (A) Schematic representing the preparation of multilayer coatings (7 bilayers) of gold nanoparticles (AuNPs)/ poly(diallyldimethyl-ammonium chloride) (PDDA) in presence of sodium chloride (NaCl) salt. (B) Bar graph accounting the OCAs of various oil droplets on the multilayer (20 bilayers) coating of sodium silicate/TiO_2 nanoparticles on stainless steel mesh. (C) Schematic illustrating the fabrication of the titanium dioxide-(poly(phenylene sulfide) (TiO_2@h-PPS) membrane. Reprinted with permission from Ref. 118 Copyright 2013, Wiley-VCH (A). Reprinted with permission from Ref. 119 Copyright 2013, Nature (B). Reprinted with permission from Ref. 119 Copyright 2019, American Chemical Society (C).

repellency for a wide range of oils under water as shown in Fig. 1.17B. Han et al.[120] constructed a TiO_2-to-h-PPS-toTiO_2 sandwich structure using the in-situ growth of highly rough TiO_2 layers on the surfaces of hydrophilic poly(phenylene sulfide) (h-PPS) membrane that was prepared through electrostatic interaction between the sulfoxide bond on the membrane surface and the TiO_2 precursor. The rough superhydrophilic TiO_2 layer effectively reduced the contact of the h-PPS membrane with oil droplets and therefore, underwater superoleophobicity was achieved with OCA above 150°.

1.5. Applications

Plenty of research attempts have been made and are still being made on these two extreme liquid repellency properties (i.e. superhydrophobicity and underwater superoleophobicity) because of their numerous potential applications in various fields (Fig. 1.18). Realizing the self-cleaning phenomenon of lotus leaf was the beginning of this journey.[6] Cleaning of deposited dust and dirt on

lotus leaves by rolling water droplets helps these superhydrophobic leaves to stay spotless even in murky ponds. Inspiration from this property of lotus leaf led to many studies to fabricate materials with self-cleaning performance.[121-122] For instance, Lu et al.[123] prepared a superhydrophobic paint by mixing two different size ranges of TiO_2 nanoparticles (~60 to 200 nm and ~21 nm) in an ethanolic solution containing perfluorooctyltriethoxysilane, and the coated substrates were able to display self-cleaning performance in air as well as in oil. Superhydrophobicity has many other applications as well.

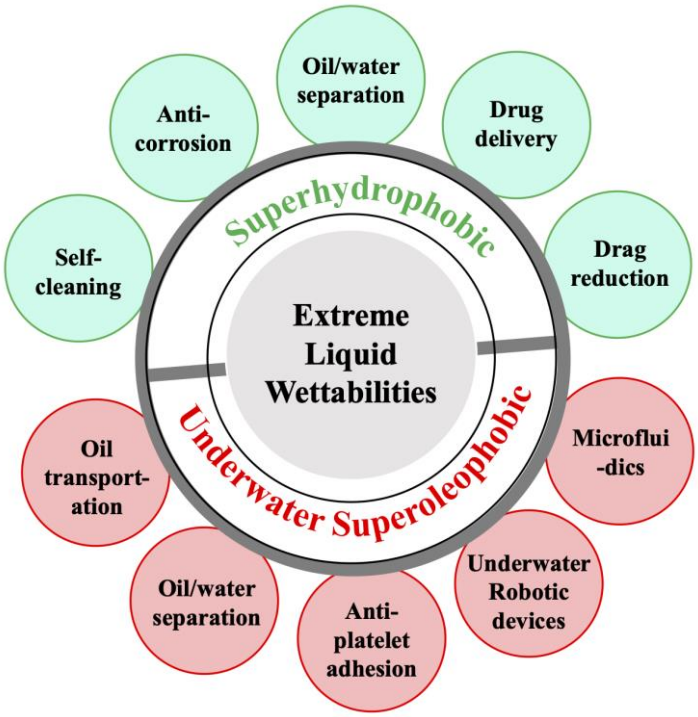

Figure 1.18: Accounting various applications of both superhydrophobic (in air) and superoleophobic (under water) properties.

For example, Zhang et al.[124] decorated a porous anodic alumina/aluminum substrate with laurate-intercalated films of ZnAl layered double hydroxide to achieve superhydrophobicity for the successful demonstration of promising anti-corrosion performance which may address the massive economic losses due to corrosion of metals and metal alloys every year. Later, many other research groups have extended this approach for addressing the corrosion-related challenges. Yohe et al.[125] prepared 3D superhydrophobic mesh by electrospinning technique and showed that superhydrophobic materials may be ideal for extended drug delivery applications in which slow release of an active agent is required. The entrapped air in the 3D mesh acted as a removable barrier against the aqueous phase and therefore slow release of the loaded molecule of interest. But, the superhydrophobicity is not only restricted to these applications, but it can also influence any phenomenon occurring at the solid-liquid interface. Drag reduction is one such example which is very important due to its benefits such as an increase in fuel efficiency, speed of marine vehicles, etc. The trapped air serves the role of a lubricating

layer and reduces the drag. Shirtcliffe et al.[126] displayed that superhydrophobic Cu tube had enhanced flow rates and reduced drag as compared to non-superhydrophobic one.

The other property I am interested in is underwater superoleophobicity and it is no less than superhydrophobicity as far practical applications are concerned. Research on underwater superoleophobicity property started in 2009[7] and therefore, its full potential is yet to be realized. I will discuss some of the applications reported in the literature. Designing blood-compatible devices and materials are very important for implantation and many other medical uses because most implanted material surfaces adsorb blood proteins, after which platelet activation and adhesion occur resulting in blood coagulation and thrombosis. Among the many crucial factors (Charge, flexibility, surface composition, etc.), wettability is one of the most important parameters affecting the aforesaid process of blood coagulation. In 2009, Chen et al.[127] constructed nanoscale topography on poly(N-isopropylacrylamide) (PNIPAAm) surface by introducing Si nanowire arrays. The surface displayed significantly reduced activation and adhesion of platelets (as compared to the Si, SiNWA, and Si-PNIPAAm surfaces) both below and above the lower critical solution temperature of PNIPAAm LCST. The results of contact angle and adhesive force measurements in water confirmed that the nanoscale topography helped to maintain a relatively high ratio of water content on the PNIPAAm surface and played a key role in significantly reducing the adhesion of platelets.

Underwater superoleophobicity provided a simple basis for manipulating water droplets for open microfluidic application, which is another important topic of research. Precise manipulation of individual microdroplets can offer lower cost, higher flexibility and less reagent consumption for biochemical reactions, protein crystallization, miniature reaction systems, etc. Su et al.[128] prepared an underwater superoleophobic tweezer using superhydrophilic materials and successfully demonstrated arbitrary manipulation and on-demand transportation of oil droplets in water. Marine biofouling on ships, oceanographic sensors, leisure vessels has been a great concern for ages. Underwater superoleophobicity comes with immense prospects to address various relevant problems. However, the synthesis of durable underwater superoleophobic interface is important for prospective applications. In this context, Chen at al.[129] fabricated a self-healing underwater oil-repellent and biofouling-resistant coating via self-assembly of hydrophilic polymeric chains grafted hierarchical hybrid microgel spheres. The durability of bio-inspired wettability was demonstrated in the presence of highly acidic, alkaline, and salty environments. Later, inspired by seaweeds, Cai et al.[29] introduced a salt-tolerant underwater superoleophobicity, where a salt-tolerant coating was developed using calcium alginate. The performance of this coating in resisting fouling by various types of oil during 30-day immersion in artificial seawater was promising.

Application of this property has even expanded for development of smart aquatic devices which are able to move in oil/water system without any kind of oil contamination which may hamper its function. Such an approach can also be adopted by underwater vent devices, underwater oil-cleaning

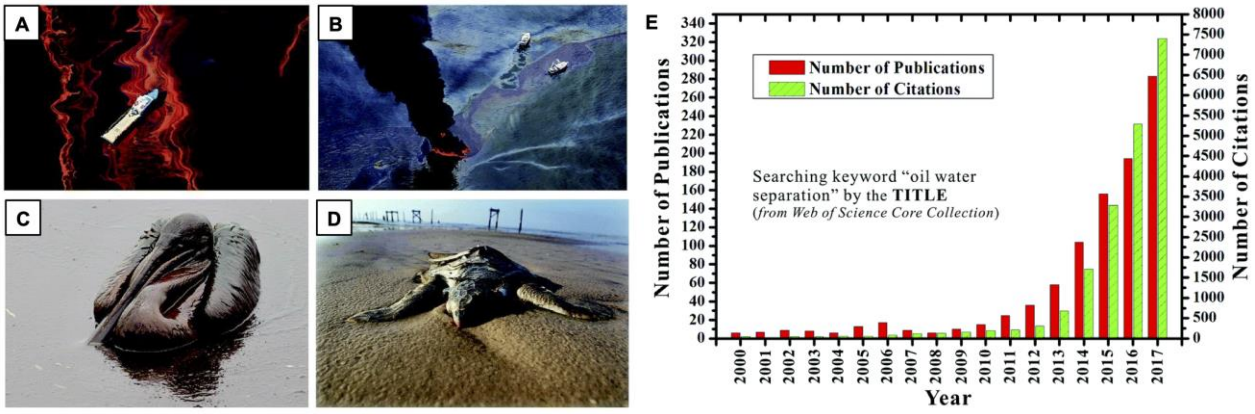

Figure 1.19: (A-D) Images of the crude oil spillages on the ocean surface after oil spill accident in the Gulf of Mexico which destroyed the aqua-eco system of ocean and coastal area. (E) Plot displaying the number of papers published on oil-water separation. Reprinted with permission from Ref. 138 Copyright 2018, Royal Society of Chemistry.

devices for better performance or efficiency. Liu et al.[130] developed an 'oil strider' whose legs were made of underwater superoleophobic copper wires. The copper wires were coated with micro/nano hierarchical structured copper oxide by a base-corrosion process.

The continual progress of science and technology has made our life much easier, but this progress is also associated with many environmental and energy issues. As the global demand for energy continues to grow, oil-spill accidents and industrial wastewater with oily contaminants discharges become very frequent.[131-136] For example, the Exxon Valdez oil tanker accidentally spilt 11 million gallons of oil into Alaska's Prince William Sound in 1989.[137] In 2002, the tanker Prestige encountered a storm and split up at sea and resulted in spreading of 20 million gallons of heavy fuel oil onto Spanish coasts.[138] Few years after that, oil spill in the Gulf of Mexico released 200 million gallons of crude oil into the sea (Fig. 1.19A-D).[139] These oil spills had disastrous effect on most animals and plants living near the incident areas, natural resources, coastal zones, aquaculture activities, etc. (Fig. 1.19C-D). Apart from these huge spills, many smaller spills (of less than 7 ton) happen frequently contributing to 80% (by number) of all recorded spills, but most of the time remain unnoticed and unreported. [140] On the other side, wastewater having oily contaminants is released into various water reservoirs from many industries every day, such as biopharmaceuticals, mining, textiles, metal smelting, petrochemicals, and foods.[141] Such oily sewage has already become a common source of pollutants across the globe and poses a great threat to the environment. The frequency of oil spills in enormous quantities and the oily sewages are not only causing ecological problems but also cause huge

economic losses. To resolve the above-mentioned problem, researchers have developed many technologies and materials for effective oil/water separation, but oil/water separation remains an exciting research topic to protect the environment and reduce its impact on the economy. An exponential growth of published research articles on oil/water separation can be seen in recent years as shown in Fig. 1.19E.

Conventional measures, including chemical dispersants, in-situ burning, skimming, etc.[142-143] are mostly associated for removing the oil spills, however, such approaches are associated with low

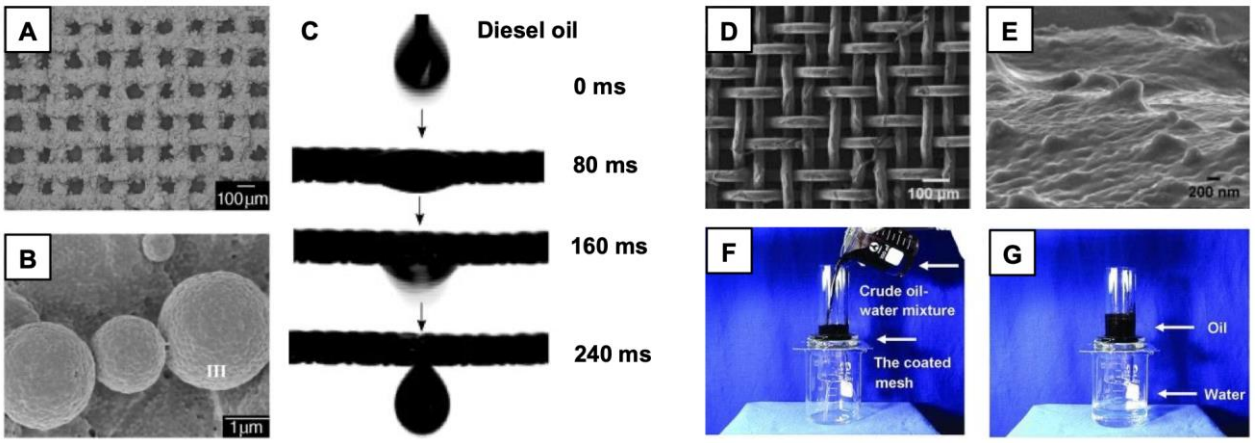

Figure 1.20: (A-B) SEM images of the superhydrophobic polytetrafluoroethylene (PTFE)-coated mesh film. (C) Demonstration of oil/water separation by using the superhydrophobic film. (D-E) SEM images of polyacrylamide (PAM) hydrogel-coated mesh. (F-G) Oil-water separation performance of the underwater superoleophobic mesh. Reprinted with permission from Ref. 144 Copyright 2004, Wiley-VCH (A-C). Reprinted with permission from Ref. 147 Copyright 2011, Wiley-VCH (D-G).

efficiency, secondary pollutions or involve highly energy consuming process. Therefore, the development of an eco-friendly and energy-efficient approach for separating the oil/water mixture is the need of the hour in the current context. The lotus leaf-inspired superhydrophobicity and fish scale-inspired underwater superoleophobicity can be employed to resolve the existing issues in an environment-friendly way. Superhydrophobic interfaces are inherently superoleophilic and allow the spread of oil and oily liquids instantly and selectively. In 2004, Feng et al.[144] exploited this principle for the very first time in gravity-driven selective filtration of oil from oil/water mixture by using a stainless steel mesh that was decorated with lotus leaf-inspired superhydrophobicity (Fig. 1.20A-C). The water droplet beaded on the superhydrophobic mesh with WCA of ~156º, while oil passed immediately through the membrane as shown in Fig. 1.20C. This principle was successfully used for gravity-driven filtration-based separation of oil/oily contaminants from oil/water mixture. Later, this bio-inspired superhydrophobicity was extended for selective absorption-based oil/water separation, where porous superhydrophobic materials were used to collect the spilt oil, selectively, from aqueous phase.[145-146] However, the demonstration of oil/water separation using this strategy in the practically

relevant severe settings is rare in the literature, likely due to the poor durability of artificial superhydrophobicity in challenging scenarios. Xue et al.[147] utilized underwater superoleophobicity unprecedentedly for oil/water separation. An underwater superoleophobic hydrogel-coated mesh, which consists of rough nanostructured hydrogel coatings and microscale porous metal substrate (Fig. 1.20D-E), was able to separate water from various oil/water mixtures (such as vegetable oil, gasoline, diesel, and even crude oil/water mixtures) selectively and effectively (> 99%) without any external intervention as shown in Fig. 1.20F-G. A lot of other research articles were published later where underwater superoleophobicity was used for efficient oil/water separation.[148-151]

These two properties are especially advantageous over the conventional methods because the purity of the separated phase meets the requirements for reuse and such approaches do not have any adverse effect on the environment. I intend to develop materials with durable and extreme anti-wettability properties keeping the practical application of oil/water separation in mind because of its huge impact on the environment.

1.6. Limitations of Conventional Methods

Most of the approaches which were sought to prepare smart materials with biomimicked wettability properties with the afore-mentioned properties are not suitable for practical applications owing to various durability issues. Demerits of the conventional designs for achieving extreme liquid wettabilities both in air and under water are discussed below.

1.6.1. Superhydrophobic surfaces

Since the discovery, several top-down and bottom-up synthetic approaches have been developed to achieve the prerequisites: 1) hierarchical topography generally using hydrophilic elements, and 2) a thin layer of low surface energy coatings on top by mostly chemical vapour deposition of fluorinated inert molecules.[152-153] This general procedure has been widely adopted and modified to develop superhydrophobic materials, and some of them are used in demonstration of its

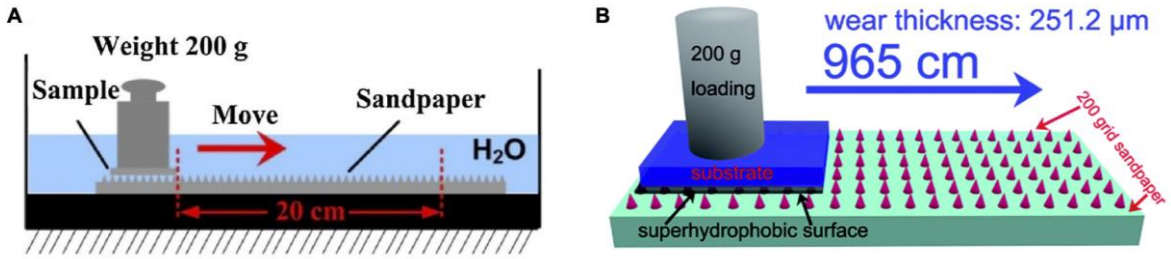

Figure 1.21: (A-B) Sandpaper abrasion test performed on superoleophobic surface under water (A) and superhydrophobic surface in air (B). Reprinted with permission from Ref. 181 Copyright 2018, Elesvier (A). Reprinted with permission from Ref. 182 Copyright 2016, Royal Society of Chemistry (B).

several prospective applications, however, the use of such materials is drastically restricted at practical scenarios where exposure to different physical (scratching, creasing, etc.) and chemical (high salt, acidic and alkaline conditions) insults are very common. Appropriate hierarchical (micro-/nano-

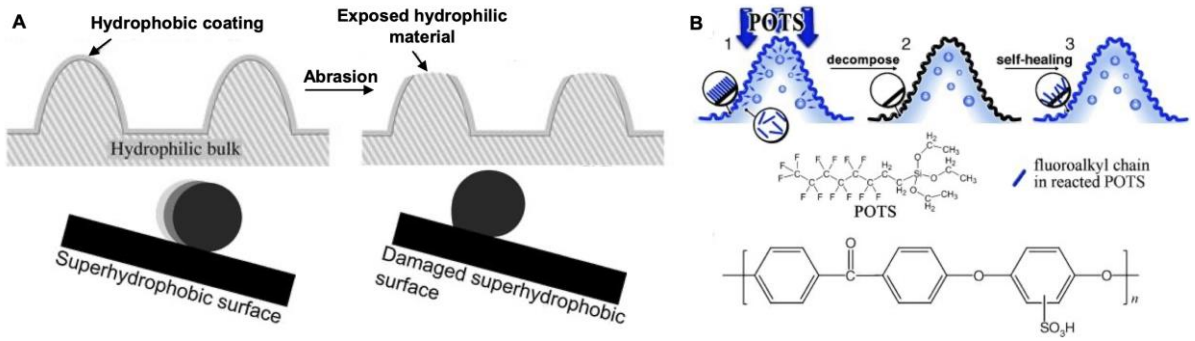

Figure 1.22: (A) Illustrating the loss of superhyphobicity upon physical abrasion which causes removal of top surface and exposes the hydrophilic bulk. (B) Schematic representation of self-healing superhydrophobic coatings that sustained physical abrasions for few healing cycles through migration of 1H,1H,2H,2H-Perfluorooctyltriethoxysilane (POTS) to the abraded top surface. Reprinted with permission from Ref. 154 Copyright 2011, Wiley-VCH. Reprinted with permission from Ref. 161 Copyright 2010, Wiley-VCH.

scaled) topography and essential chemistry are likely to be perturbed even when a small amount of force is applied to the material. The damaged interface under mechanical stresses exposed hydrophilic interior as shown in Fig. 1.22A, and thus, the superhydrophobicity was compromised.[154] Often, the essential low surface energy is optimized on top of the hierarchical features by depositing a thin (in nm scale) layer of low surface energy molecules through weak covalent bonds (e.g. metal-sulfur chemistry[155-156]) or ionic interactions[157-158] which is likely to fail under chemically complex and harsh environments like extremes of pH or salt. Silane chemistry[159-160] has also been widely employed to achieve this extreme water-repelling property, but this approach has downsides as well, which is mainly its inability to sustain prolonged UV exposure. These kinds of functionalization failed to maintain low surface energy upon exposure to various chemical environments. By and large, it can be inferred that physical and chemical insults lead to compromise of the anti-wetting property of the artificial superhydrophobic materials. To overcome these limitations, self-healing (Fig. 1.22B) and post-repairing approaches were introduced with improved durability. However, the performance of such designs under harsh settings are limited for few cycles and such approaches also demand external intervention to cure the damaged wettability.[161-162] Thus, the development of the chemically and physically durable superhydrophobic interface remained an exciting research topic.

1.6.2. Underwater superoleophobic surfaces

The two prerequisites (i.e. hierarchical topography and high surface energy) to achieve underwater superoleophobic surfaces are mostly fulfilled by the following approaches - (i) Hydrogel-

based approach[7,110-111], (ii) metal oxide-based coating[112,116-117] and (iii) Electrostatic multilayers[118-120]. These approaches have been discussed earlier. A large number of reported underwater superoleophobic surfaces, fabricated by the aforementioned methods one or the other, are available in the literature, but

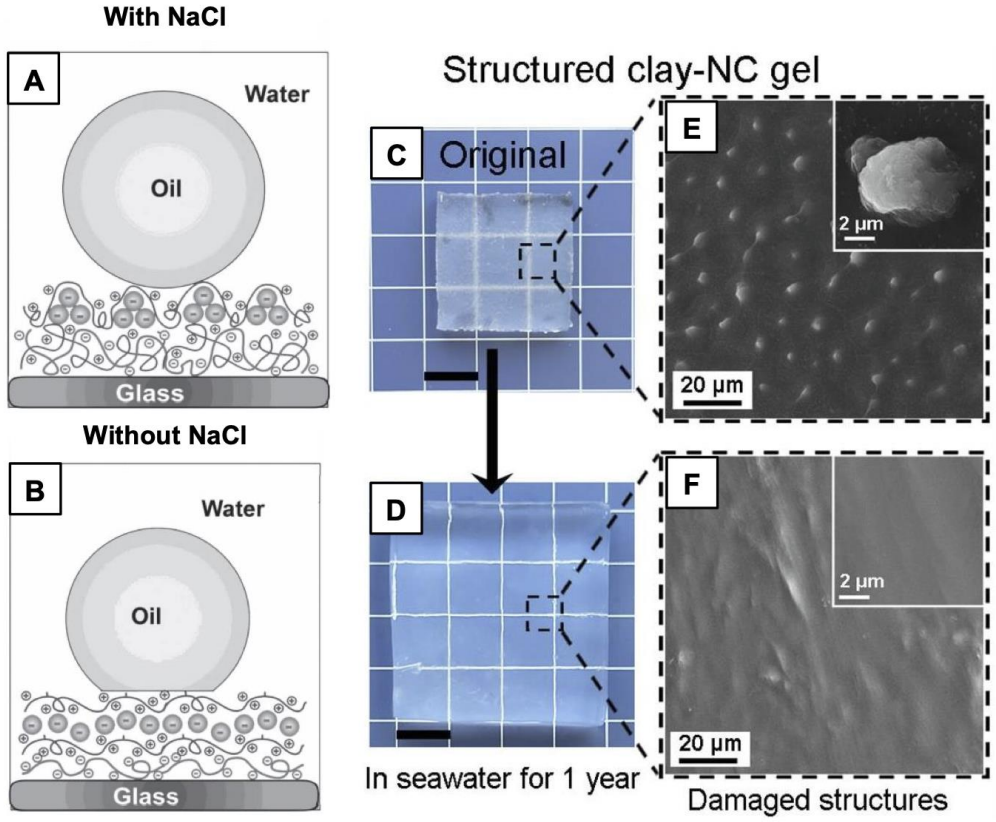

Figure 1.23: (A-B) Schematic illustration of the underwater oil wetting state on gold nanoparticle (AuNPs)/ poly(diallyldimethyl-ammonium chloride) (PDDA) film consisting of 7 bilayers in presence (A) and absence (B) of salt. Presence of ions effects roughness through coiling of polyelectrolyte chains and the ratio of water content, and thereby changes the underwater superolephobicity (C-F) Swelling of clay-nanocomposite (NC) gel before (C,E) and after (D,F) their immersion in seawater for one year which affected the topography of the gel material (E-F). Reprinted with permission from Ref. 118 Copyright 2013, Wiley-VCH (A-B). Reprinted with permission from Ref. 164 Copyright 2019, Elsevier (B)

there are many disadvantages associated with these methods restricting their practical application. For the hydrogel-based approach, the issue is the delicate nature (Fig. 1.23C-F) of the hydrogels whenever exposed to aqueous phase[163-164], thereby unable to withstand any mechanical stresses (Fig. 1.21A) which are inevitable during transportation, packing or intended use. In comparison to that, metal oxides are much more rigid and tough. However, due to the reactive nature, such hydrophilic metal oxide coatings are highly prone to disintegrate in practically relevant severe chemical environments like extremes of pH, saline water, etc. and as a consequence, the bio-inspired wettability of the coating is eventually compromised. On the other hand, the weak electrostatic interaction between the oppositely charged polymers/nanoparticles in electrostatic multilayer coating that tightly holds the special orientation of each polymer in the multilayer coating, easily gets compromised on various harsh

physical as well as chemically complex exposures.[118,165] For instance, Xu et al.[118] prepared an electrostatic multilayer using gold nanoparticle (anionic in nature) and a cationic polymer which changes its wettability depending on the salt concentration of the medium (Fig. 1.23A-B), and therefore it cannot be used for real-life application. In short, the underwater superoleophobic interfaces that are designed following these approaches are not suitable as far as practical applications are concerned.

Therefore, it is very evident that the practical implementation of both the properties is highly challenging due to the poor durability of the materials against physical and chemical manipulations. Further, a common synthetic approach for adopting two different biomimicked wettability properties, i.e. superhydrophobicity and underwater superoleophobicity by appropriate optimization of chemistry and topography could be useful for various applied and fundamental contexts.

1.7. Use of Chemically Reactive Interfaces in Developing Bio-inspired Wettability

Various covalently crosslinking chemistries like thiol-ene click chemistry, epoxy ring-opening reactions, Michael addition reaction, azlactone-amine reactions, etc.[166-175] are well established for developing smart materials. Among these chemistries, Michael addition reaction (Fig. 1.24) stands out

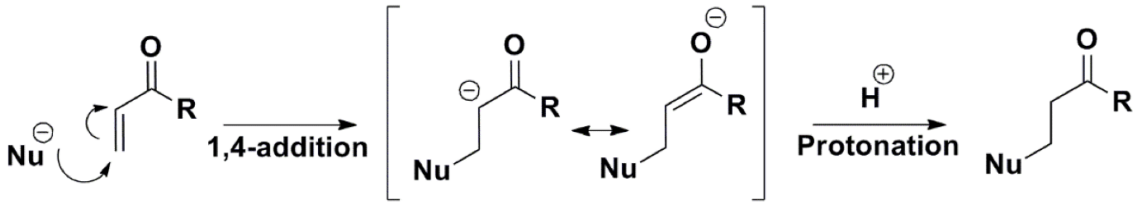

Figure 1.24: Schematic representation of 1,4-conjugate addition reaction (Michael Addition).

owing to the advantages it possesses—(a) facile, (b) catalyst-free, (c) mild condition and (d) flexibility to react in liquid or solid phases.[169-172] In general, Michael Addition reaction refers to the nucleophilic addition of a nucleophile (mostly carbanion) to an α,β-unsaturated carbonyl compound, and this group of reactions is very useful for carbon-carbon bond formation in mild condition (Fig. 1.24). During the reaction, a resonance stabilized enolate intermediate is formed leading to the formation of a thermodynamically stable 1,4-conjugate addition product. Nucleophiles based on amines, thiol and phosphine groups can also participate in Michael addition because of considerable electron density to serve as donors and therefore, C-O, C-N, C-S, C-P bonds can also be formed with the help of this reaction.[169-172]

In the recent past, Ford et al. [173] developed a covalently cross-linked polymeric coating with various nano-structures through Michael addition reaction, where branched poly(ethyleneimine) (PEI) and small multifunctional acrylate (Fig. 1.25A) were consecutively deposited by adopting LbL

deposition process. Later, Bechler et al.[174] extended this covalent LbL deposition of BPEI and dipentaerythritol pentaacrylate (5Acl) for 80 cycles to achieve a porous 'chemically reactive'

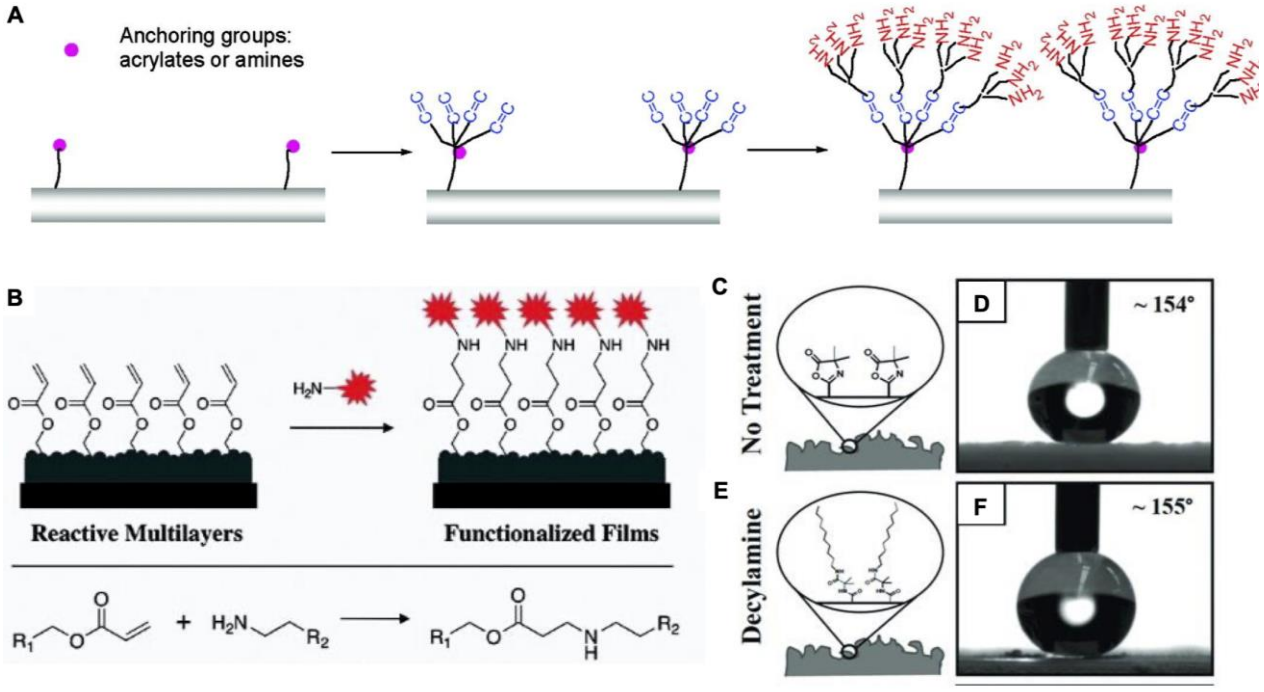

Figure 1.25: (A) Schematic illustration of the fabrication and growth of hyperbranched poly(ester amine) through 1,4-conjugate addition reaction on photo-crosslinked surfaces. (B) Schematic for the construction of reactive branched poly(ethyleneimine) (PEI)/ dipentaerythritol pentaacrylate (5Acl) films consisting of 80 bilayers on silicon substrates through Michael addition reaction. (C-F) Schematics (C,E) and WCA (D,F) images of the reactive PEI/ poly(2-vinyl-4,4-dimethylazlactone) (PVDMA) films (C-D) before (E-F) after modification with decylamine. Reprinted with permission from Ref. 173 Copyright 2009, American Chemical Society (A). Reprinted with permission from Ref. 174 Copyright 2012, American Chemical Society (B). Reprinted with permission from Ref. 175 Copyright 2013 Wiley-VCH (C-F).

polymeric multilayer with thickness of 750 nm as shown in Fig. 1.25B. The developed multilayer was decorated with residual acrylate functionalities that allowed post-modification with amine-containing small molecules. After hydrophobization with decylamine, the multilayer became hydrophobic with a contact angle of 138º, but remained inefficient to display superhydrophobicity. In the past, Manna et al.[175] used azlactone-amine reaction to develop a bulk (80 µm thick) superhydrophobic coating through LbL deposition of poly(2-vinyl-4,4-dimethylazlactone) (PVDMA) and BPEI for 100 cycles, which involves subsequent dipping of substrate in respective polymeric solutions and washing solution for 600 times. Hence, this approach is very laborious and time-consuming. Later, Rather et al.[176] extended 1,4-conjugate addition reaction for achieving a polymeric monolith with durable superhydrophobicity through the formation of 'reactive' nanocomplex. This 'reactive' nanocomplex, prepared by spontaneous reaction between amine groups of BPEI and acrylate groups of 5Acl through 1,4-conjugate addition reaction (Fig. 1.26A-B), was randomly aggregated to form the gel matrix (Fig.

1.26C) which exhibited superhydrophobic property after post-covalent modification with selected alkyl amine. Owing to the covalent cross-linking of the polymeric matrix, the superhydrophobic gel material can retain its property under physically and chemically harsh environments which would be of great potential interest in practical use.

Besides, Manna et al.[178] explored the mutual reaction between azlactone and amine for fabricating fish-scale inspired underwater superoleophobic interface (Fig. 1.27A-D), where residual azlactone groups in multilayer coating of BPEI/PVDMA allowed to adopt essential chemistry that conferred underwater superoleophobicity as shown in Fig. 1.27A. This chemically crosslinked

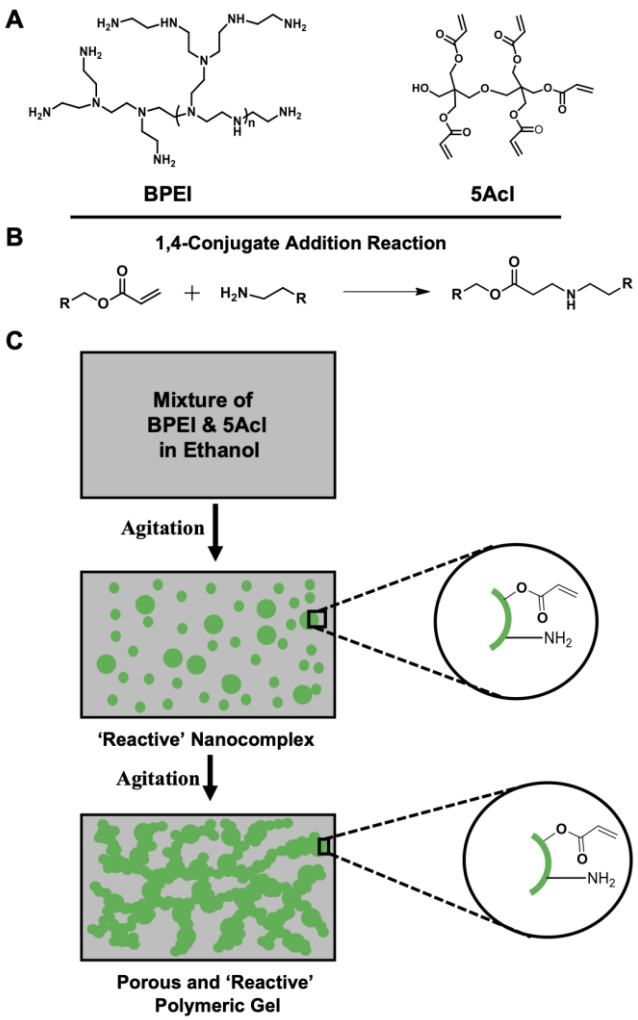

Figure 1.26: (A) Chemical structures of branched poly(ethyleneimine) (BPEI) and dipentaerythritol pentaacrylate (5Acl) molecules. (B) 1,4-conjugate addition reaction between primary amine and acrylate groups. (C) Schematic illustrating the formation of reactive polymeric gel from BPEI/5Acl mixture via the formation of reactive nanocomplex intermediate. Reprinted with permission from Ref. 176 Copyright 2016, American Chemical Society.

multilayer coating, having chemically stable amide/amide linkages exhibited robust underwater superoleophobicity with tolerance to a broad range of physical, chemical, and environmental

challenges, after modification with hydrophilic D-glucamine molecules (Fig. 1.27B-D). Therefore,

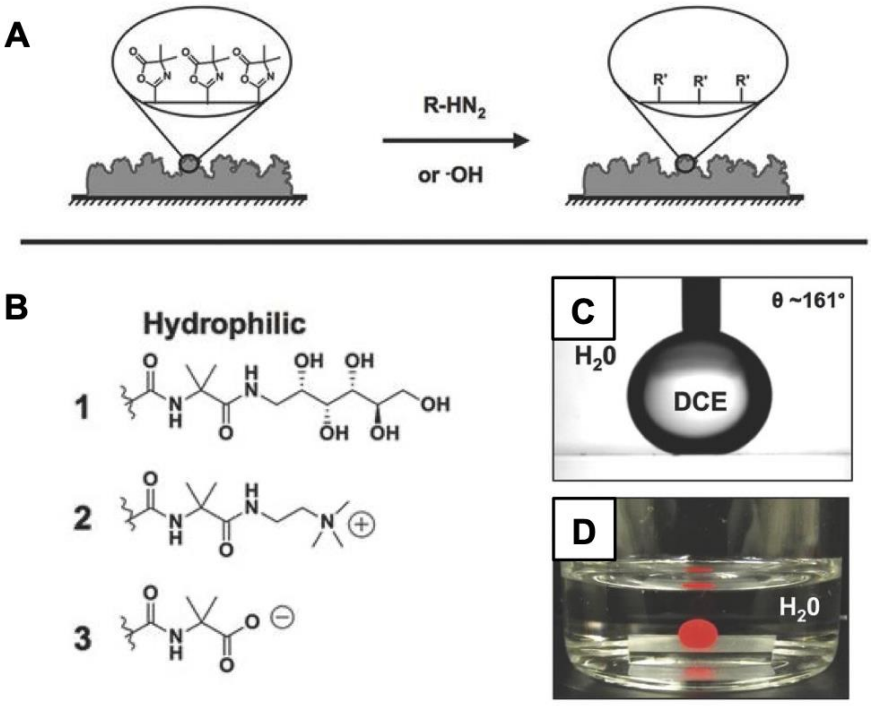

Figure 1.27: (A-B) Schematic representation of the modification of reactive azlactone-functionalized multilayer with hydrophilic (1, 2, 3) small molecules. (C-D) Underwater OCA (C) and digital image (D) of the post-modified multilayer with hydrophilic glucamine. Reprinted with permission from Ref. 178 Copyright 2015, Wiley-VCH.

chemically reactive porous interface has a lot of potential for synthesizing various advanced materials with durable anti-wetting properties.

1.8. Motivation and Objectives

It can be inferred from the discussions so far that in order to develop the essential hierarchical topography and chemistry, 1,4-conjugate addition (Michael addition)[169-172] reaction can be rationally used for designing various functional materials. In the past, 1,4-addition reaction between suitable reactants provided an avenue to synthesize polymeric coatings with various complex nanostructures[173-174] and modification of three dimensional objects[179] through dendritic amplification of branched functional groups.[180] On the other side, the LbL deposition process provides facile control over thickness and topography. Thus, the strategic association of 1,4-conjugate addition reaction with LbL deposition process is likely to provide a common avenue to achieve various and durable bio-inspired interfaces. Here, I assume that the LbL deposition of appropriate constituent would allow a rapid and simple control over the topography of the coating. Further, the residual chemical reactivity of the LbL coating would be available for facile modifications with various molecules of interest to tune various bio-inspired wettability.

In this thesis work, the LbL deposition technique and 1,4-conjugate addition reaction are adopted for achieving different durable bio-inspired wettabilities. Two distinct chemically-'reactive' polymeric multilayer coatings were developed through the strategic use of 1,4-conjugate addition reaction, and the appropriate post-covalent modifications of these multilayer coatings yielded abrasion-tolerant and highly durable extreme liquid (oil/water) wettabilities. Such extremely durable super-liquid wettabilites are believed to be invaluable weapons in the arsenal of methods to fight against the adverse repercussions of oil spillages on the environment in an energy-efficient way in practically relevant severe and diverse settings. Performance of these multilayer coatings was found to be excellent in separating various forms of oil/water mixture. Thereby, we envision that this promising single chemical avenue to design both the physical and chemical abrasion-tolerant biomimicked wettability properties (superhydrophobicity and underwater superoleophobicity) would be useful for different practical applications in the near future.

1.9. References

(1) K. Verbrugge, *Harvard Review*, 2011, 16.

(2) M. N. Hill, and A. R. Robinson. *Harvard University Press.* 1962, 498.

(3) H. Izumia, M. Suzukia, S. Aoyagia and T. Kanzaki, *Sensor Actuat. A Phys*., 2011, **165**, 115.

(4) Wilbur and Orville Wright U.S. Patent 821393A, 1906.

(5) Mestral, G. D. U. S. Patent 2717437A, 1955.

(6) W. Barthlott and C. Neinhuis, *Planta*, 1997, **202**, 1.

(7) M. J. Liu, S. T. Wang, Z. X. Wei, Y. L. Song, L. Jiang, *Adv. Mater.*, 2009, **21**, 665.

(8) Y. Wei, H. Qi, X. Gong, and S. Zhao, *Adv. Mater. Interfaces*, 2018, **5**, 1800576.

(9) S. Li, J. Huang, Z. Chen, G. Chen and Y. Lai, *J. Mater. Chem. A*, 2017, **5**, 31.

(10) J. T. Korhonen, T. Huhtamäki, O. Ikkala, and R. H. A. Ras, *Langmuir*, 2013, **29**, 12, 3858.

(11) N. Nuraje, W. S. Khan, Y. Lei, M. Ceylan and R. Asmatulu, *J. Mater. Chem. A*, 2013, **1**, 1929.

(12) M. Jin, S. Li, J. Wang, Z. Xue, M. Liao and S. Wang, *Chem. Commun*., 2012, **48**, 11745.

(13) T. Young, *Phil. Trans. R. Soc. Lond.*, 1805, **95**, 65.

(14) R. N. Wenzel, *Ind. Eng. Chem*., 1936, **28**, 988.

(15) Verplanck et al. *Nanoscale Res Lett*., 2007, **2**, 577.

(16) Khojasteh et al., *J. Ind. Eng. Chem.*, 2016, **42**, 1.

(17) A. B. D. Cassie and S. Baxter, *Trans. Faraday Soc.*, 1944, **40**, 546.

(18) K. Koch, B. Bhushan, Y. C. Jung and W. Barthlott, *Soft Matter*, 2009, **5**, 1386.

(19) A. R. Parker, C.R. Lawrence, *Nature*, 2001, **414**, 33.

(20) H. F. Bohn, and W. Federle, *Proc. Natl Acad. Sci. USA*, 2004, **101**, 14138.

(21) V. Zorba, E. Stratakis, M. Barberoglou, E. Spanakis, P. Tzanetakis, S. H. Anastasiadis and C. Fotakis, *Adv. Mater*., 2008, **20**, 4049.

(22) W. Barthlott, M. Mail and C. Neinhuis, Phil. Trans. R. Soc. A, 2016, **374**, 191.

(23) D. Wu, J.-N. Wang, S.-Z. Wu, Q.-D. Chen, S. Zhao, H. Zhang, H.-B. Sun, L. Jiang, *Adv. Funct. Mater*., 2011, **21**, 2927.

(24) Y. Zheng, X. Gao and L. Jiang, *Soft Matter*, 2007, **3**, 178.

(25) X. Gao and L. Jiang, *Nature*, 2004, **432**, 36.

(26) X. Gao, X. Yan, X. Yao, L. Xu, K. Zhang, J. Zhang, B. Yang and L. Jiang, *Adv. Mater.*, 2007, **19**, 2213.

(27) K. Liu and L. Jiang, *ACS Nano*, 2011, **5**, 6786.

(28) J. Yong, F. Chen, Q. Yang, J. Huo and X. Hou, *Chem. Soc. Rev.*, 2017, **46**, 4168.

(29) Y. Cai, Q. Lu, X. Guo, S. Wang, J. Qiao and L. Jiang, *Adv. Mater.*, 2015, **27**, 4162.

(30) Q. Cheng, M. Li, Y. Zheng, B. Su, S. Wang and L. Jiang, *Soft Matter*, 2011, **7**, 5948.

(31) J. L. Yong, F. Chen, Q. Yang, G. Du, C. Shan, H. Bian, U. Farooq and X. Hou, *J. Mater. Chem. A*, 2015, **3**, 9379.

(32) X. Liu, J. Zhou, Z. Xue, J. Gao, J. Meng, S. Wang and L. Jiang, *Adv. Mater.*, 2012, **24**, 3401.

(33) J. Yong, F. Chen, M. Li, Q. Yang, Y. Fang, J. Huo and X. Hou, *J. Mater. Chem. A*, 2017, **5**, 25249.

(34) P. Zhang, S. Wang, S. Wang and L. Jiang, *Small*, 2015, **11**, 16, 1939.

(35) L. Feng, S. H. Li, Y. S. Li, H. J. Li, L. J. Zhang, J. Zhai, Y. L. Song, B. Q. Liu, L. Jiang and D. B. Zhu, *Adv. Mater.*, 2002, **14**, 1857.

(36) U. Manna, M. C. D. Carter and D. M. Lynn, *Adv. Mater.*, 2013, **25**, 3085.

(37) A. Giacomello, L. Schimmele, S. Dietrichbc and M. Tasinkevych, *Soft Matter*, 2016, **12**, 8927.

(38) B. Dean and B. Bhushan, *Philos. Trans. R. Soc. A*, 2010, **368**, 4775.

(39) G. D. Bixler and B. Bhushan, *Soft Matter*, 2012, **8**, 11271.

(40) S. Wainwright, F. Vosburgh, and J. Herbrank, *Science*, 1978, **202**, 747.

(41) G. D. Bixler and B. Bhushan, *Philos. Trans. R. Soc. London*, Ser. A, 2012, **370**, 2381.

(42) P. R. Waghmare, N. S. K. Gunda and S. K. Mitra, *Sci. Rep.*, 2015, **4**, 7454.

(43) J. Li, J. Fu, Y. Cong, Y. Wu, L. J. Xue and Y. C. Han, *Appl. Surf. Sci.*, 2006, **252**, 2229.

(44) J. Fresnais, L. Benyahia and F. P. Epaillard, *Surf. Interface Anal*., 2006, **38**,144.

(45) J. Ryu, K. Kim, J. Y. Park, B. G. Hwang, Y. ChulKo, H. J. Kim, J. S. Han, E. R. Seo, Y. J. Park and S. J. Lee, *Scientific Reports*, 2017, **7**, 1981.

(46) W.-K. Lee, C. J. Engel, M. D. Huntington, J. Hu and T. W. Odom, *Nano Lett.*,2015, **15**, 5624.

(47) C. Frankiewicz and D. Attinger, *Nanoscale*, 2016, **8**, 3982.

(48) T. Liu and C.-J. Kim, *Science*, 2014, **346**, 1096.

(49) M. Im , H. Im , J.-H. Lee , J.-B. Yoon and Y.-K. Choi, *Soft Matter*, 2010, **6**, 1401.

(50) A. Gao, Q. Wu, D. Wang, Y. Ha, Z. Chen and P. Yang, *Adv. Mater*., 2016, **28**, 579.

(51) T. Soeno , K. Inokuchi , S. Shiratori , *Trans. Mater. Res. Soc. Jpn*., 2003 , **28** , 1207.

(52) M. M. Aljumaily, M. A. Alsaadi, R. Das, S. B. A. Hamid, N. A. Hashim, M. K. AlOmar, H. M. Alayan, M. Novikov, Q. F. Alsalhy and M. A. Hashim, *Sci. Rep.*, 2018, **8**, 2778.

(53) X.-J. Guo, C.-H. Xue, S. Sathasivam, K. Page, G. He, J. Guo, P. Promdet, F. L. Heale, C. J.

Carmalt and I. P. Parkin, *J. Mater. Chem. A*, 2019, **7**, 17604.

(54) A. Das, J. Deka, A. M. Rather, B. K. Bhunia, P. P. Saikia, B. B. Mandal, K. Raidongia, and U. Manna, *ACS Appl. Mater. Interfaces*, 2017, **9**, 48, 42354.

(55) A. M. Rather and U. Manna, *ACS Appl. Mater. Interfaces*, 2018, **10**, 28, 23451.

(56) K. Maji and U. Manna, *J. Mater. Chem. A*, 2018, **6**, 6642.

(57) N. Jana, D. Parbat, B. Mondal, S. Das, and U. Manna, Journal of Materials Chemistry A., *J. Mater. Chem. A*, 2019,**7**, 9120.

(58) B. Chen, J. Qiu, E. Sakai, N. Kanazawa, R. Liang, and H. Feng, *ACS Appl. Mater. Interfaces*, 2016, **8**, 27, 17659.

(59) Y. Lee, S. H. Park, K. B. Kim and J. K. Lee, *Adv. Mater.*, 2007, **19**, 2330.

(60) L. Feng, S. Li, H. Li, J. Zhai, Y. Song, L. Jiang and D. Zhu, *Angew. Chem. Int. Ed.*, 2002, **41** , 1221.

(61) A. Tombesi, S. Li, S. Sathasivam, K. Page, F. L Heale, C. Pettinari, C. J. Carmalt, I. P. Parkin, *Sci. Rep*., 2019, **9**, 7549.

(62) D. Han and A. J. Steckl, *Langmuir*, 2009, **25**, 9454.

(63) H. Zhou, H. Wang, H. Niu & T. Lin, *Sci. Rep.*, 2015, **5**, 15863.

(64) W. Li, J. Liu & D. Zhao, *Nat. Rev. Mater.*, 2016, **1**, 16023.

(65) J. Hu, C. F. Sun, E. Gillette, Z. Gui, Y. H. Wang and S. B. Lee, *Nanoscale*, 2016, **8**, 12958.

(66) K. Y. Suh and S. Jon, *Langmuir*, 2005, **21**, 6836.

(67) B. He, N. A. Patankar and J. Lee, *Langmuir*, 2003, **19**, 4999.

(68) Z. Xiong, H. Lin, F. Liu, P. Xiao, Z. Wu, T. Li and D. Li, *Sci. Rep.*, 2017, **7**, 14099.

(69) M. H. Jin, X. J. Feng, L. Feng, T. L. Sun, J. Zhai, T. J. Li and L. Jiang, *Adv. Mater.*, 2005,**17**, 1977.

(70) S. Hoshian, V. Jokinena and S. Franssila, *Soft Matter*, 2016, **12**, 6526.

(71) A. Nakajima, K. Abe, K. Hashimoto and T. Watanabe, *Thin Solid Films*, 2000, **376**, 140.D. S. Kim, A. Honglawan, S. Yang and D. K. Yoon, *ACS Appl. Mater. Interfaces*, 2017, **9**, 7787.

(72) D. S. Kim, A. Honglawan, S. Yang and D. K. Yoon, *ACS Appl. Mater. Interfaces*, 2017, **9**, 7787.

(73) G. Tallents, E. Wagenaars and G. Pert, *Nature Photonics*, 2010, **4**, 809.

(74) H Guckel, US Patent US5190637A, 1993.

(75) T. E. Lewis, M. T. Nowak, US Patent 5249525A, 1993.

(76) J. W. Vanderhoff, ACS Symposium Series, 25, 1976, 162.

(77) N. Cordeiro, A. Blayo, N. M. Belgacem, A. Gandini, C. Pascoal Neto and J.-F L. Nest, *Industrial Crops and Products*, 2000, **11**, 63.

(78) S. Y. Chou, P. R. Krauss, W. Zhang, L. G. Guo, L. V. Zhuang, *J. Sci. Technol. B*, 1997, **15**, 2897.

(79) M. Callies, Y. Chen, F. Marty, A. Pepin and D. Quere, *Microelectron Eng.*, 2005, **78**, 100.

(80) J. Fresnais, L. Benyahia, F. E. Poncin, *Surf. Interface Anal*., 2006, **38**, 144.

(81) S.Y. Chou, C. Keimel, J. Gu, *Nature*, 2002, **417**, 835.

(82) L. Zhu, Y. Feng, X. Ye and Z. Zhou, *Sens. Actuators A*, 2006, **130**, 595.

(83) D. Kim, S.-J. Park, S.-B. Jeon, M.-L. Seol, Y.-K. Choi, *Adv. Electron. Mater.*, 2016, **2**,

1500331.

(84) A. Milionis, C. S. Sharma, R. Hopf, M. Uggowitzer, I. S. Bayer and D. Poulikakos, *Adv. Mater. Interfaces*, 2019, **6**, 1801202.

(85) M. Keeney, X. Y. Jiang, M. Yamane, M. Lee, S. Goodman and F. Yang, *J. Mater. Chem. B*, 2015, **3**, 8757.

(86) N. Joseph, P. Ahmadiannamini, R. Hoogenboom and Ivo. F. J. Vankelecom, *Polym. Chem.*, 2014, **5**, 1817.

(87) G. Decher and J.-D. Hong, *Macromol. Chem., Macromol. Symp*., 1991, **46**,321

(88) Gero Decher, *Science*, 1997, **277**, 1232.

(89) G. Leem, B. D. Sherman, A. J. Burnett, Z. A. Morseth, K.-R. Wee, J. M. Papanikolas, T. J. Meyer and K. S. Schanze, *ACS Energy Lett.*, 2016, **1**, 339.

(90) H. S. Lim, W. H. Lee, S. G. Lee, D. Lee, S. Jeon and Kilwon Cho, *Chem. Commun*., 2010, **46**, 4336.

(91) M. Yasuhiro, D. Bin and S. Seimei, *Nanotechnology*, 2006, **17**, 5151.

(92) Y. Li, C. Li, S. O. Cho, G. Duan and W. Cai, *Langmuir*, 2007, **23**, 9802.

(93) I. Sas, R. E. Gorga, J. A. Joines and K. A. Thoney, *J. Polym. Sci., Part B: Polym. Phys*., 2012, **50**, 824.

(94) A. K. Haghi and M. Akbari, *Phys. Status Solidi A*, 2007, **204**, 1830.

(95) V. E. Kalayci, P. K. Patra, A. Buer, S. C. Ugbolue, Y. K. Kim and S. B. Warner, *J. Adv. Mater.*, 2004, **36**, 43.

(96) O. Arslan, Z. Aytac, and T. Uyar, *ACS Appl. Mater. Interfaces*, 2016, **8**, 19747.

(97) H. Zhou, H. Wang, H. Niu and T. Lin, *Sci. Rep.*, 2015, **5**, 15863.

(98) G. Zhang, S. Yuan, S. Cao, G. Yan, X. Wang, J. Yang and B. V. D. Bruggen, *Nanoscale*, 2019, **11**, 7166.

(99) H. S. SalehHudin, E. N. Mohamad, W. N. L. Mahadi and A. M. Afifi, *Mater. Manuf. Process.*, 2017, **33**, 479.

(100) C. Teng, D. Xie, J. Wang, Y. Zhu and L. Jiang, *J. Mater. Chem. A*, 2016, **4**, 12884.

(101) Y. Cai, L. Lin, Z. Xue, M. Liu, S. Wang and L. Jiang, *Adv. Funct. Mater.*, 2014, **24**, 809.

(102) X. Meng, M. Wang, L. Heng and L. Jiang, *Adv. Mater*., 2018, **30**, 1706634.

(103) Q. Wang, B. Xu, Q. Hao, D. Wang, H. Liu and Lei Jiang, *Nat. Commun.*, 2019, **10**, 1212.

(104) W. Liu, M. Cui, Y. Shen, P. Mu, Yaoxia Yanga and Jian Li, *New J. Chem*., 2020, **44**, 2705.

(105) S. Xu, R. Sheng, Y. Cao and J. Yan, *Sci. Rep.*, 2019, **9**, 12486.

(106) H. Jin, W. Wang, Z. Yu, Y. Shen, K. Li, H. Chang, Y. Ge, and J. Gong, *ACS Appl. Polym. Mater*., 2019, 10, 2582.

(107) L. Ping, X. Jing, Z. Bin, S. Xueli, L. Jitao, P. Yibiao, L. Hongliang, L. Gao, Y. LeiJiang, Y. Wen, X. Zhang and S. Wang, *Adv. Mater.*, 2012, **25**, 606.

(108) S. Gao, J. Sun, P. Liu, F. Zhang, W. Zhang, S. Yuan, J. Li and J. Jin, *Adv. Mater.*, 2016, **28**, 5307.

(109) W. Zhang, N. Liu, Y. Cao, Y. Chen, Q. Zhang, X. Lin, R. Qu, H. Li and Lin Feng, *ACS Appl. Mater. Interfaces*, 2016, **8**, 21816.

(110) J.-B. Fan, Y. Song, S. Wang, J. Meng, G. Yang, X. Guo, L. Feng and L. Jiang, *Adv. Funct.*

Mater., 2015, **25**, 5368.

(111) L. P. Xu, D. Han, X. Wu, Q. Zhang, X. Zhang and S. Wang, *Sci. Rep.*, 2016, **6**, 38016.

(112) Z. Yu, Frank F. Yun, Z. Gong, Q. Yao, S. Dou, K. Liu, L. Jiang and X. Wang, *J. Mater. Chem. A*, 2017, **5**, 10821.

(113) P. Raturi, K. Yadav, and J. P. Singh, *ACS Appl. Mater. Interfaces*, 2017, **9**, 6007.

(114) X. Zheng, Z. Guo, D. Tian, X. Zhang, W. Li and L. Jiang, *ACS Appl. Mater. Interfaces*, 2015, **7**, 4336.

(115) J. Song, L. Huang, Y. Lu, X. Liu, X. Deng, X. Yang, S. Huang, J. Sun, Z. Jin and I. P. Parkin, *Scientific Reports*, 2016, **6**, 31818.

(116) E. Zhang, Z. Cheng, T. Lv, L. Li and Y. Liu, *Nanoscale*, 2015, **7**, 19293.

(117) D. Zang, H. Yi, Z. Gu, L. Chen, D. Han, X. Guo, S. Wang, M. Liu and L. Jiang, Adv. *Mater.*, 2017, **29**, 1602869.

(118) L.-P. Xu, J. Zhao, B. Su, X. Liu, J. Peng, Y. Liu, H. Liu, G. Yang, L. Jiang, Y. Wen, X. Zhang and S. Wang, *Adv. Mater.*, 2013, **25**, 606.

(119) L. Zhang, Y. Zhong, D. Cha and P. Wang, *Sci. Rep.*, 2013, **3**, 2326.

(120) N. Han, C. Yang, Z. Zhang, W. Wang, W. Zhang, C. Han, Z. Cui, W. Li and X. Zhang, *ACS Appl. Mater. Interfaces*, 2019, **11**, 35479.

(121) P. Wang, M. Chen, H. Han, X. Fan, Q. Liu and J. Wang, *J. Mater. Chem. A*, 2013, **4**, 7869.

(122) R. Fürstner, W. Barthlott, C. Neinhuis and P. Walzel, *Langmuir*, 2005, **21**, 956.

(123) Y. Lu, S. Sathasivam, J. Song, C. R. Crick, C. J. Carmalt and I. P. Parkin, *Science*, 2015, **347**, 1132.

(124) F. Zhang, L. Zhao, H. Chen, S. Xu, D. G. Evans, X. Duan, *Angew. Chem. Int. Ed.*, 2008, **47**, 2466.

(125) S. T. Yohe, Y. L. Colson and M. W. Grinstaff, *J. Am. Chem. Soc.*, 2012, **134**, 2016.

(126) N. J. Shirtcliffe, G. McHale, M. I. Newton and Y. Zhang, ACS *Appl. Mater. Interfaces*, 2009, **1**, 1316.

(127) L. Chen, M. Liu, H. Bai, P. Chen, F. Xia, Dong Han, and Lei Jiang, *J. Am. Chem. Soc.*, 2009, 131, **30**, 10467.

(128) B. Su, S. Wang, Y. Song and L. Jiang, *Soft Matter*, 2011, **7**, 5144.

(129) K. Chen, S. Zhou and L. Wu, *ACS Nano*, 2016, **10**, 1386.

(130) X. Liu, J. Gao, Z. Xue, L. Chen, L. Lin, L. Jiang and S. Wang, *ACS Nano*, 2012, **6**, 5614.

(131) Z. Xue, Y.Cao, N.Liu, L.Feng and L. Jiang, *J. Mater. Chem. A*, 2014, **2**, 2445.

(132) B. Wang, W. Liang, Z. Guo and W. Liu, *Chem. Soc. Rev.*, 2015, **44**, 336.

(133) Z. Chu, Y. Feng and S. Seeger, *Angew. Chem. Int. Ed.*, 2015, **54**, 2328.

(134) R. K. Gupta, G. J. Dunderdale, M. W. England and A. Hozumi, *J. Mater. Chem. A*, 2017, **5**, 16025.

(135) E. Stokstad, *Science.*, 2010, **328**, 1618.

(136) J. L. Schnoor, *Environ. Sci. Technol.*, 2010, 44, 13, 4833

(137) C. H. Peterson, S. D. Rice, J. W. Short, D. Esler, J. L. Bodkin, B. E. Ballachey and D. B. Irons, *Science*, 2003, **302**, 2082.

(138) J. Yong, J. Huo, F. Chen, Q. Yang and X. Hou, *Phys. Chem. Chem. Phys.*, 2018, **20**, 25140.

(139) T. J. Crone and M. Tolstoy, *Science*, 2010, **330**, 634.

(140) C. P. D. Brussaard, L. Peperzak, S. Beggah, L. Y. Wick, B. Wuerz, J. Weber, J. S. Arey, B. Burg, A. Jonas, J. Huisman and J. R. Meer, *Nat. Commun.*, 2016, **7**, 11206.

(141) R. K. Gupta, G. J. Dunderdale, M. W. England and A. Hozumi, *J. Mater. Chem. A*, 2017, **5**, 16025.

(142) S. Kleindienst, J. H. Paul and S. B. Joye, *Nat. Rev. Micro.*, 2015, **13**, 388.

(143) J. F. Rasmussen, S.Wegeberg and K. Gustavson, *Water Air Soil Pollut.*, 2015, **226**, 329.

(144) L. Feng, Z. Y. Zhang, Z. H. Mai, Y. M. Ma, B. Q. Liu, L. Jiang and D. B. Zhu, *Angew. Chem. Int. Ed.*, 2004, **43**, 2012.

(145) X. Gui, J. Wei, K. Wang, A. Cao, H. Zhu, Y. Jia, Q. Shu and D. Wu, *Adv. Mater.*, 2010, **22**, 617.

(146) B. Li, L. Li, L. Wu, J. Zhang and A. Wang, *Chem. Plus Chem.*, 2014, **79**, 850.

(147) Z. Xue, S. Wang, L. Lin, L. Chen, M. Liu, L. Feng and L. Jiang, *Adv. Mater.*, 2011, **23**, 4270.

(148) Z. Chu, Y. Feng and S. Seeger, *Angew. Chem. Int. Ed.*, 2015, **54**, 2328.

(149) Z. Shi, W. Zhang, F. Zhang, X. Liu, D. Wang, J. Jin and L. Jiang, *Adv. Mater.*, 2013, **25**, 2422.

(150) D. Li, A. Wu, G. Xu, H. Lai, Z. Cheng and Y. Liu, *Langmuir*, 2016, **32**, 13493.

(151) Z. Wang, X. Jiang, X. Cheng, C. H. Lau and L. Shao, *ACS Appl. Mater. Interfaces*, 2015, **7**, 9534.

(152) D. J. C. Gomes, N. C. de Souza and J. R. Silva, *Measurement*, 2013, **46**, 3623.

(153) S. S. Latthe, C. Terashima, K. Nakata and A. Fujishima, *Molecules*, 2014, **19**, 4256.

(154) T. Verho, C. Bower, P. Andrew, S. Franssila, O. Ikkala and R. H. A. Ras, *Adv. Mater.*, 2011, **23**, 673.

(155) B. Wang and Z. G. Guo, *Chem. Commun.*, 2013, **49**, 9416,

(156) J. Osicka, M. Ilcikova, A. Popelka, J. Filip, T. Bertok, J. Tkac and P. Kasak, *Langmuir*, **2016**, **32**, 5491.

(157) Z. Han, B. Li, Z. Mu, S. Niu, J. Zhang and L. Ren, *Small*, 2017, **13**, 1701121.

(158) C. Zhou, Z. Chen, H. Yang, K. Hou, X. Zeng, Y. Zheng and J. Cheng, *ACS Appl. Mater. Interfaces*, 2017, **9**, 9184.

(159) C. R. Crick, J. A. Gibbons and I. P. Parkin, *J. Mater. Chem. A*, 2013, **1**, 5943.

(160) Z. Wang, Y. Wang and G. Liu, *Angew. Chem., Int. Ed.*, 2016, **55**, 1291.

(161) Y. Li, Long Li, J. Sun, *Angew. Chem. Int. Ed*., 2010, **49**, 6129–6133

(162) X. Zhu, Z. Zhang, X. Men, J. Yang, K. Wang, X. Xu, X. Zhou and Q. Xue, *J. Mater. Chem.*, 2011, **21**, 15793.

(163) H. Kamata, Y. Akagi, Y. K. Kariya, U. Chung, T. Sakai, *Science*, 2014, **343**, 873.

(164) F. Li, G. Zhang, Z. Wang, H. Jiang, X. Feng, S. Yan, L. Zhang, H. Li, T. Zhao and M. Liu, *Chem. Eng. J.*, 2019, **375**, 122047.

(165) H. Jin, W. Wang, Z. Yu, Y. Shen, K. Li, H. Chang, Y. Ge and J. Gong, *ACS Appl. Polym. Mater.*, 2019, **1**, 2582.

(166) J. Li, L. Li, X. Du, W. Feng, A. Welle, O. Trapp, M. Grunze, M. Hirtz and Pavel A. Levkin, *Nano Lett.*, 2015, **15**, 675.

(167) H.-C. Yang, K.-J. Liao, H. Huang, Q.-Y. Wu, L.-S. Wana and Zhi-Kang Xu, *J. Mater. Chem. A*, 2014, **2**, 10225.

(168) S. Amigoni, E. T. Givenchy, M. Dufa, and F. Guittard, *Langmuir*, 2009, **25**, 18, 11073.

(169) D. P. Nair, M. Podgorski, S. Chatani,T. Gong, W. Xi, C. R. Fenoli and C. N. Bowman, *Chem. Mater.* 2014, **26**, 724.

(170) C. F. Nising and S. Brase, *Chem. Soc. Rev.*, 2008, **37**, 1218.

(171) J. L. Vicario, D. Badia and L. Carrillo, *Synthesis*, 2007, **14**, 2065.

(172) J. Ford, S. R. Marder and S. Yang, *Chem. Mater.*, 2009, **21**, 476.

(173) S. L. Bechler and D. M. Lynn, *Biomacromolecules*, 2012, **13**,1523.

(174) U. Manna and D. M. Lynn, *Adv. Mater.*, 2013, **25**, 5104.

(175) A. M. Rather and U. Manna, *Chem. Mater.*, 2016, **28**, 8689.

(176) M. E. Buck, J. Zhang, D. M. Lynn, *Adv. Mater.*, 2007, **19**, 3951.

(177) U. Manna and D. M. Lynn, *Adv. Funct. Mater.*, 2015, **25**, 1672.

(178) R. A. Farrer, C. N. LaFratta, L. Li, J. Praino, M. J. Naughton, B. E. A. Saleh, M. C. Teich, and J. T. Fourkas, *J. Am. Chem. Soc.*, 2006, **128**, 1796.

(179) G. Wang, Y. Fang, P. Kim, A. Hayek, M. R. Weatherspoon, J. W. Perry, K. H. Sandhage, S. R. Marder and S. C. Jones, *Adv. Funct. Mater.*, 2009, **19**, 2768.

(180) H. Yu, Z. Lian, J. Xu, Y. Wan, Z. Wang, Y. Lia, Z. Yu, and Z. Weng, *Appl. Sur. Sci.*, 2018, **437**, 400.

(181) N. Wang, Y. Lu, D. Xiong, C. J. Carmalt and I. P. Parkin, *J. Mater. Chem. A*, 2016, **4**, 4107.

Title: Synthesis of Chemically-Reactive Polymeric Multilayer Coating*

An 'amine-reactive' polymeric multilayer of nanocomplex (NC) were developed by taking advantage of 1, 4-conjugate addition reaction between acrylate and amine to fabricate bulk underwater superoleophobic coatings with impeccable physical/chemical durability. The acrylate groups of dipentaerythritol penta-acrylate (5Acl) and amine groups of branched poly(ethylenimine) (BPEI) readily reacted to form a 'chemically-reactive' NC. This polymeric NC was further extended for developing 'reactive' multilayer by following a simple layer-by-layer deposition process. The residual acrylate moiety in the synthesized multilayer coating allowed covalent post-modification with amine-containing hydrophilic molecule (i.e. glucamine (Glu)). Eventually, the multilayer coating displayed abrasion-tolerant under-water superoleophobicity. The post-modified multilayer was with appropriate topography and chemistry that conferred superoleophobicity underwater— throughout the multilayer coating including the top interface and the interior of the polymeric coating. Thus, the superoleophobicity of the material remained intact even after various severe physical damages, extremes of temperatures and continuous exposure to artificial marine environment (for more than 80 days), surfactant-contaminated water, extremes of pH. Such highly physically/chemically durable multilayer coating would be appropriate for various applications in practically relevant severe settings.

*D. Parbat and U. Manna, *Chem. Sci.*, 2017, **8**, 6092

2.1. Introduction

Underwater superoleophobic materials can extremely repel liquid oil (with advancing oil CA > 150° and CA hysteresis < 5°) droplets under water, though such interfaces are with extreme liquid (oil and water) affinity (superoleophilicity and superhydrophilicity, respectively) in air.[1-3] Synthesis of underwater superoleophobic coating, inspired by fish-scale features,[4] is of great importance owing to the potential of this property in various fundamental and applied contexts such as synthesis of efficient organic field-effect transistors, marine anti-fouling coatings, rapid oil/water separation, etc.[2,5-10] The general requirements to develop such coatings are significantly different from the conventional fluorine-based superoleophobicity property that displays extreme oil-repellency mostly in air.[11-12] The underwater anti-oil-wetting property is often explained using the Cassie-Baxter model, where the trapped liquid water layer within the material is solely responsible for the heterogeneous and extreme wettability under water.[4,13] So, the fabrication of hierarchical surface topography—made out of high surface energy materials, is hypothesized to achieve desired under-water superoleophoibicity property. Jiang and coworkers first mimicked the fish-scale topography using polyacrylamide (PAM) hydrogel and achieved the artificial underwater superoleophobicity.[4] Thereafter, various materials have been developed to achieve such underwater superoleophobicity property[4,8-9,14-19]—mostly based on polymeric hydrogels[4,8-9,18-20] and metal oxide[14,21-23] coatings. However, such reported interfaces are highly susceptible to loss of this extreme wettability in harsh physical/chemical environments (including extremes of pH, salt etc.)[24]. However, such approaches are well recognized and widely practiced in literature as it paved the way to reveal both the fundamentals and prospective applications of this anti-wetting property. Examples of durable coatings with the capability to withstand severe chemical/physical treatments are still rare in the literature. [10, 24] Thus, further development is essential to synthesize highly robust underwater superoleophobic coatings.

The work presented in this chapter is primarily motivated from the past demonstrations, where several functional materials were fabricated by employing the robust Michael addition reaction[25-29] between primary amine group and acrylate at ambient conditions including 1) synthesis of polymeric coatings with various complex nanostructures,[27,29] 2) dendritic amplification of desired functional groups,[28] 3) selective and three-dimensional (3D) functionalization of polymer microstructures.[25] The appropriate use of this facile chemical approach would allowed to tailor both the essential chemistry and topography that conferred superoleophobicity under water.[25-29] In this chapter, I have introduced an amine-'reactive' multilayer of polymeric NC exploiting the 1,4-conjugate addition reaction between amine and acrylate groups of BPEI (polymer) and 5Acl, respectively, to synthesize a) covalently cross-linked, b)

thick, c) chemically/physically durable and d) substrate-independent polymeric coating having durable underwater superoleophobicity property. This current design is further explored in revealing the fundamentals of the extremes of anti-oil wettability under water in detail. In my present design, we have developed a heterogeneous three-phase (solid/water/oil) system for achieving superoleophobicity by adopting the appropriate chemistry in the multilayer coating through strategic and facile post-chemical modification with selected small molecule. Further, such bio-inspired coating has been exploited in the demonstration of gravity driven and 'No-loss' transport of oil droplet under water.

2.2. Experimental Section

2.2.1. Materials

Branched poly(ethyleneimine) (BPEI, MW~ 25, 000 Da), Dipentaerythritol penta-acrylate (5Acl, MW~ 524.21 g mol^{-1}), propylamine, bovine serum albumin (BSA), sodium dodecyl sulphate (SDS), Nile red (Technical grade, Sigma-N3013) and dodecyltrimethylammonium bromide (DTAB) were purchased from Sigma Aldrich, Bangalore, India. 1-octadecylamine was obtained from Alfa Aesar and n-heptane was bought from Spectrochem Pvt. Ltd., Mumbai, India. HCl and dimethyl sulfoxide (DMSO) were purchased from Fischer Scientific, Mumbai, India. Sodium hydroxide (NaOH), sodium chloride (NaCl), magnesium sulfate ($MgSO_4$), calcium chloride ($CaCl_2$) and toluene were bought from Merck Specialties Private, Ltd. Ethyl alcohol was purchased from TEDIA Company (United States of America). Tetrahydrofuran (THF) and chloroform were acquired from RANKEM, Maharashtra (India). Sandpaper (grit no. 400) was obtained from Million International, India. Microscopic glass slides were purchased from Jain Scientific Glass Works (JSGW), India. Aluminium foil (Al-foil) (Parekh Aluminex Ltd., India), adhesive tape (Jonson tape Ltd. India) and plastic sheets were obtained from local sources. Dichloromethane (DCM), dichloroethane (DCE) and ethyl acetate were acquired from Merck Life Science Pvt. Ltd., New Delhi, India. D-glucamine (>95%) was purchased from TCI (Tokyo Chemical Industry). n-hexane and n-heptane were purchased from Central Drug House Pvt. Ltd. (CDH), Mumbai, India. Sand and wood were collected from a construction site of IIT Guwahati, Assam.

2.2.2. General characterization

The glass dipping vials were washed thoroughly with ethyl alcohol and then by acetone before preparing the LbL dipping solutions, and compressed air was used to dry the synthesized multilayer of the polymeric NC. CAs were measured at five different locations on each sample using the KRUSS Drop

Shape Analyzer-DSA25 instrument with an automatic liquid dispenser at ambient temperature. A dynamic light scattering (DLS) study was performed using a Zetasizer Nano ZS90 instrument with model no. ZEN3690. All the samples were coated with a thin layer of gold using a gold sputterer prior to capturing scanning electron microscopic images (SEM) of the multilayer using a Carl Zeiss field emission scanning electron microscope (FESEM). Fourier transform infrared (FTIR) spectra were recorded using a Perkin-Elmer FTIR spectrophotometer instrument at ambient temperature, where the digital images captured using a Canon Power Shot SX420 IS digital camera. The thickness of the coatings was estimated using a Veeco Dektak 150 surface profilometer.

2.2.3. Preparation of the 'reactive' layer by layer (LbL) coating

The solutions of 5Acl (265 mg mL^{-1}) and BPEI (50 mg mL^{-1}) in ethanol were prepared first in two separate glass vials. Then, a solution (500 mL) of BPEI was mixed with another solution (5 mL) of 5Acl in ethanol and the mixture was kept with continuous agitation for 20 minutes to initiate the formation of the 'reactive' polymeric NC. Then, a clean glass slide (5.5 cm x 1 cm) was taken as a model substrate, where the layer-by-layer (LbL) deposition of 'reactive' NC was achieved with the help of another dipping solution—that is the solution of BPEI in ethanol. The detailed LbL deposition process was as follows; (a) glass substrates were placed in a solution of BPEI for 10 seconds; (b) the substrates were removed and washed initially in an ethanol bath for 10 seconds followed by a second ethanol bath for another 10 seconds; (c) the substrates were then placed in a stable dispersion of 'reactive' NC in ethanol for 10 seconds; and (d) substrates were removed from the 'reactive' NC solution and washed again, following the process described in step (b). This cycle was repeated 20 times to fabricate a porous polymeric multilayer consisting of 20 BPEI/NC layer pairs, where subsequent deposition of BPEI and NC in single cycle was referred as 'bilayer'. Following similar protocol, another multilayer that consisting of BPEI/5Acl was developed, where the 'reactive' NC solution was replaced with solution of 5Acl (265 mg mL^{-1}) in ethanol. During the whole LbL deposition process, the concentrations of the polymer (or NC) solutions were maintained by the addition of ethanol as needed after regular intervals to compensate the solvent evaporation.

2.2.4. Post-modification of the multilayer

The 'reactive' multilayer (20 bilayers) coating consisting of BPEI/NC was chemically post-functionalized with hydrophilic amine containing small molecule i.e. glucamine (2.5 mg ml^{-1}, in DMSO) following a previously reported procedures.[30] After exposing the multilayer to the solutions of glucamine

for overnight, the multilayer coating was thoroughly washed with ethyl alcohol/THF and exposed to compressed air to dry, prior to further essential characterization or other relevant proof-of-concept demonstrations. This post-modification of multilayer coating of NC with glucamine is denoted as 'Glu-treated' multilayer of NC for rest of the discussion in the chapter.

2.2.5. Physical and chemical durability of the underwater superoleophobicity property

2.2.5.1. Sand drop test: The 'Glu-treated' multilayer of NC on glass slide (1 cm x 1 cm) was immobilized on a microscope glass slide using adhesive tape, where the multilayer coating was exposed to air. The whole system was tilted at 45° prior to pouring a continuous stream of sand grains (100 g) from a height of 20 cm using a funnel. The anti-wetting property of the material was examined by acquiring CAs and digital images of beaded oil droplets under water, before and after performing the sand drop test on the 'Glu-treated' multilayer of NC.

2.2.5.2. Sandpaper abrasion test: An abrasive sandpaper (size of 2 cm x 2 cm; grit no. 400) and a 'Glu-treated' multilayer of NC on a glass slide (1 cm x 1 cm) were immobilized on two separate bare microscope glass slides using double-sided adhesive tape, where both the abrasive sandpaper surface and the multilayer coating were exposed to air. Next, the abrasive sandpaper was manually rubbed over the 'Glu-treated' multilayer of NC under a 200 g load. Afterwards, the anti-oil wetting property of the material was examined via CA measurements and digital imaging using colored DCM.

2.2.5.3. Adhesive tape test: Double-sided adhesive tape (1 cm x 1 cm) was first attached onto a microscope glass slide prior to bringing the adhesive surface into contact with 'Glu-treated' multilayer of NC, and an external load of 200 g was applied on the system to facilitate better and uniform contact of the polymeric coating against the adhesive surface. After 30 min, the polymeric multilayer-coated glass slide was manually peeled off from the adhesive tape surface, and the morphology of the coating and the oil-wettability of the multilayer coatings were examined by FESEM study and CA instruments, respectively.

2.2.5.4. Effect of freezing on the anti-oil wetting property: Deionized water (DI) was first degassed under high vacuum in an inert atmosphere (argon gas was used) prior to submerging 'Glu-treated' multilayer of NC on glass slide (0.6 cm x 0.6 cm). Then, a red coloured (due to the added Nile red dye for improved visual inspection) DCM droplet was gently placed on the flat piece of the coated glass slide and kept in a freezer for 2 hours at -20°C. Afterwards, the glass vial was removed from the freezer and the wettability of the model oil droplets was further characterized by acquiring digital images and measuring the CAs,

where the whole frozen system manually tilted at different angles including 0°, 90° and 180°. Furthermore, the whole system was allowed to thaw at room temperature, and the anti-wetting property was examined by measuring the CA of the beaded oil droplets.

2.2.5.5. Effect of heating on the anti-wetting property: The multilayer (that consists of 20 bilayers of BPEI/NC) coated glass slide that was post-functionalized with glucamine was submerged in DI water (20 ml) in a glass beaker, which was later placed in a water bath (borosil; 450 mm x 150 mm, having 450 ml of tap water). This was again placed on a hot plate, and a mercury thermometer was used for continuous monitoring of the temperature of the system. Next a droplet (8 ml) of red coloured DCM was gently placed on the 'Glu-treated' multilayer of NC, and the temperature of the system was gradually increased up to 100°C. The effect of this gradual heating of the aqueous phase on the underwater oil wettability was examined by visual inspections and CA measurements.

2.2.5.6. Effect of water-steam on the anti-oil wetting property: The underwater superoleophobic multilayer of NC was further exposed to steam for 2 hours using a tweezer which was again fixed with a clamp and stand. The steam was generated by boiling tap water (450 ml) at above 100°C. The effect of this treatment was further investigated by measuring the CA of the beaded oil droplets.

2.2.5.7. Chemical durability test: The chemical durability of underwater superoleophobicity was examined by exposing the glucamine-treated multilayer of NC to different harsh and chemically complex conditions including alkaline solution (0.1 M NH_3; pH 11.13), acidic solution (0.1 M HCl; pH 1), SDS solution (1 mM), DTAB solution (1 mM), BSA solution (5 weight% (wt%)) and artificial seawater. The artificial seawater was prepared by mixing $MgCl_2$ (0.226 g), $MgSO_4$ (0.325 g), NaCl (2.673 g) and $CaCl_2$ (0.112 g) in 100 ml of DI water in a volumetric flask.

2.2.6. Coating on various substrates

Initially, the underwater oil wettability on various bare substrates (like plastic—made of polyester, wood, sandpaper and Al-foil was examined to ensure that none of the selected substrates were capable of displaying underwater superoleophobicity property. Next, all the above mentioned substrates were submerged in solutions of BPEI in ethanol overnight, prior to introducing the consecutive LBL deposition of BPEI and NC following the earlier described procedure. The underwater superoleophobicity was characterized after the post-chemical modification of the 'reactive' multilayer of NC with glucamine. Moreover, the interior of a glass tube was also successfully coated with this multilayer of NC to achieve

the desired underwater superoleophobicity, and this material was further exploited in the demonstration of guided 'No-loss' transport of tiny oil-droplet, which was not possible to achieve with the bare glass tube.

2.3. Results and Discussions

2.3.1. Synthesis and characterizations of reactive and covalent multilayer

In the recent past,[30] the fabrication of an amine-'reactive' polymeric gel was reported by mixing an appropriate composition of BPEI/5Acl in ethanol under ambient conditions, where the branched polymeric amine (BPEI; Fig. 2.1B) and the multifunctional cross-linker (5Acl; Fig. 2.1C) readily reacted

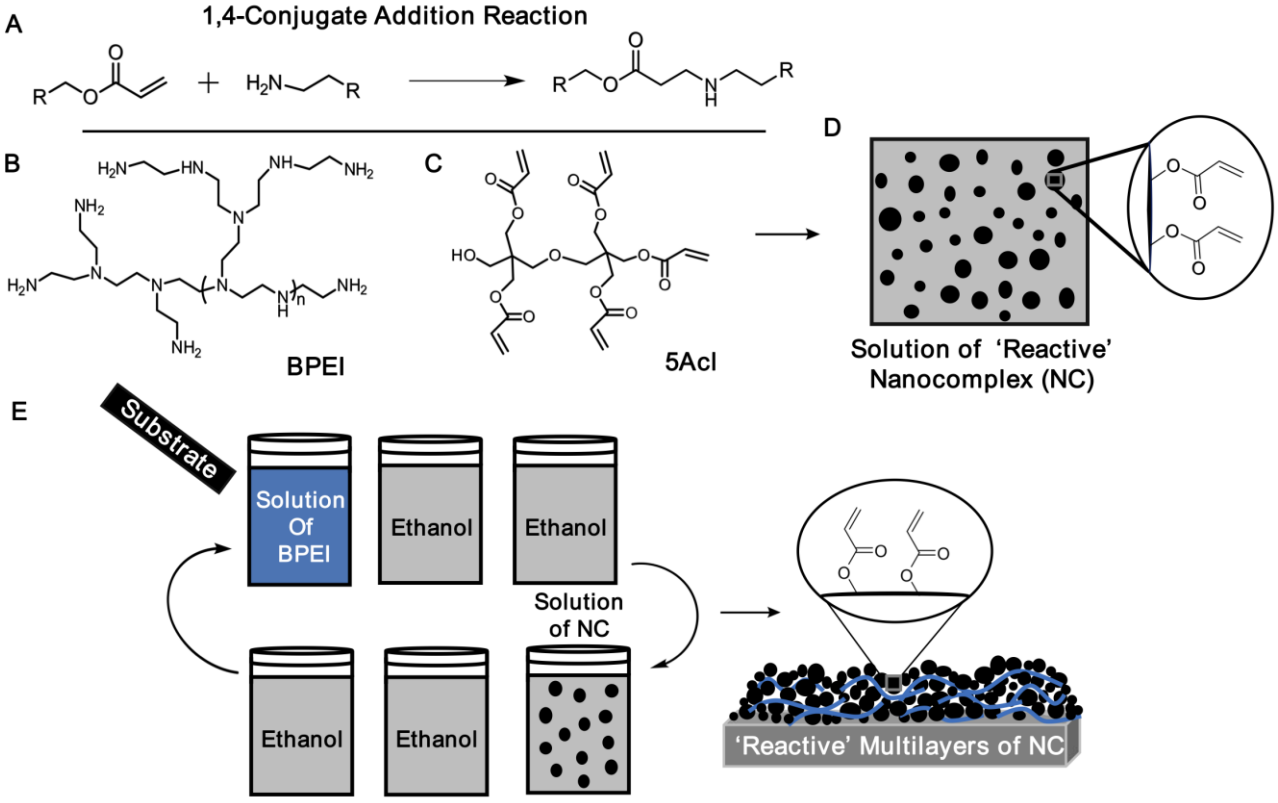

Figure 2.1: (A) Illustrating 1,4-conjugate addition reaction between primary amine and acrylate groups. (B-C) Chemical structures of poly(ethylenimine) (BPEI: B) and dipentaerythritol penta-acrylate (5Acl: C). (D) Formation of the stable dispersion of reactive nanocomplex (NC) by appropriate mixing of BPEI and 5Acl in ethanol. (E) Schematic representation depicting the formation of reactive multilayer of NC through LBL deposition of BPEI and the reactive NC.

through a 1,4-conjugate addition reaction (Fig. 2.1A) to form a 'reactive' NC. Eventually, this polymeric NC aggregated to form a polymeric gel matrix which further allowed development of a self-standing

superhydrophobic monolith. By taking advantage of the same facile 1,4-conjugate addition chemistry (Fig. 2.1A) , I have developed a thick and porous polymeric multilayer through layer-by-layer (LBL) deposition

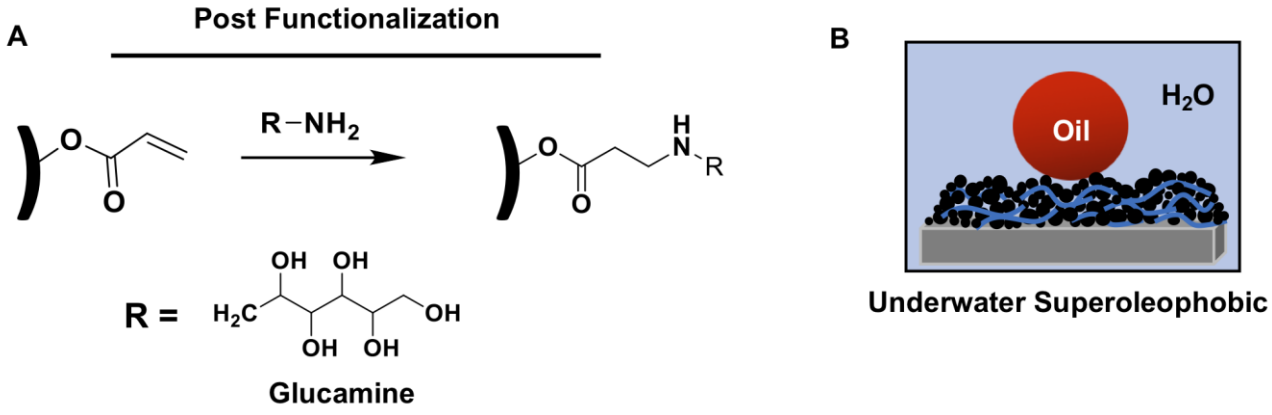

Figure 2.2: (A) Schematic representing the post-chemical modification of the multilayer of NC with glucamine, a hydrophilic amine. (B) Schematic illustration of underwater superoleophobic multilayer after modification of multilayer of NC with glucamine.

of BPEI and 'reactive' NC as shown in Fig. 2.1E. Further, this polymeric multilayer of NC having residual acrylate group was post-modified with hydrophilic amine-containing small molecules (Fig. 2.2A) for achieving underwater superoleophobicity (Fig. 2.2B). At first, a composition of BPEI/5Acl (Fig. 2.1B) in

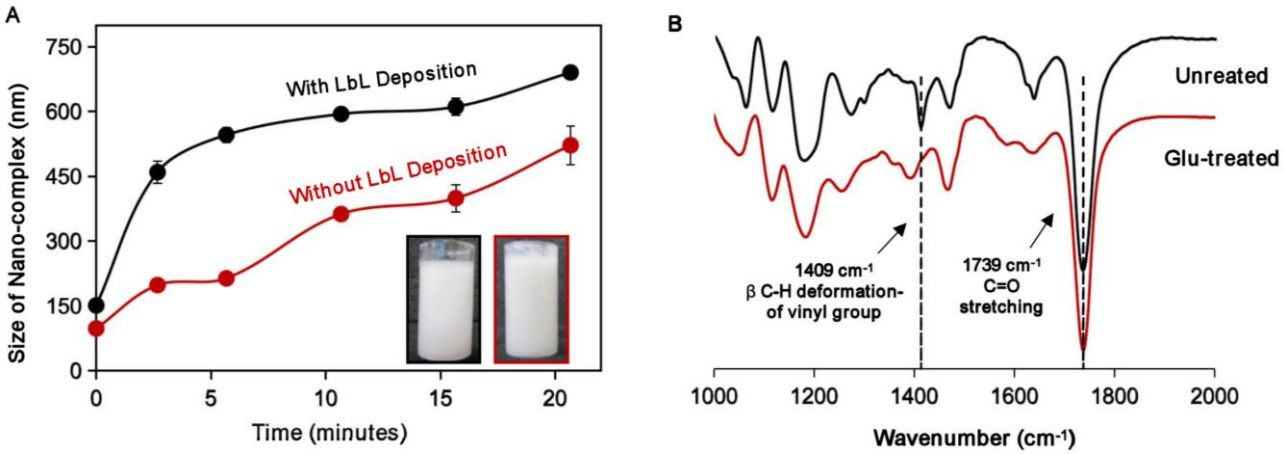

Figure 2.3: (A) Graphical depiction comparing the growth of NC with (Black) and without (red) LBL deposition process. Inset images depicting the stable dispersion of NC solutions with (right-side vial) and without (left-side vial) LbL deposition process. (B) FTIR spectra for reactive NC before (black) and after (red) treatment with glucamine (denoted as 'Glu-treated').

ethanol was optimized to obtain a stable dispersion of NC solution (Fig. 2.1D). However, the size of the NC was further grown during the course of LBL deposition process. Both the formation of NC and the

growth of the NC were investigated by visual inspection and a DLS study as shown in Fig. 2.3A. A faint turbid solution of the NC with the size of ~151 nm rapidly transformed to a highly opaque and milky

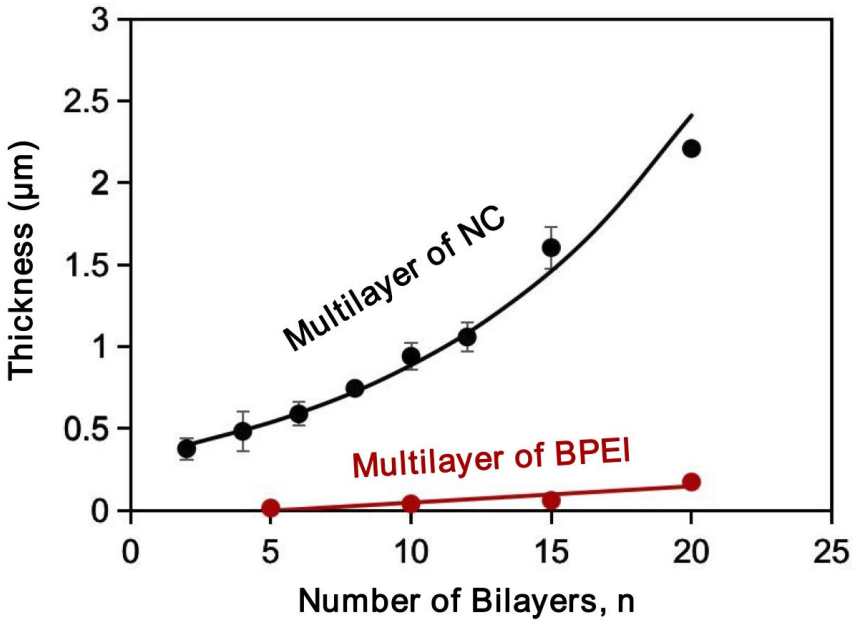

Figure 2.4: The plot accounting the thickness of both the multilayer of NC (black line) and multilayer of BPEI (red line) with increasing the number of respective bilayers depositions.

solution (size ~459 nm) in a span of ~3 min during the LBL deposition process, and the size of the NC was observed to grow further with time without any sedimentation even after 21 min (size ~690 nm) (Fig. 2.3A: black curve). The same composition of BPEI/5Acl, which was not used in successive LbL deposition process, was also capable of forming NC, however, the growth of the NC was slow as in Fig. 2.3A: red curve. The accelerated growth of the NC in the BPEI/5Acl mixture during LbL deposition was likely due to the gradual and the additional transfer of the BPEI solution to the amine-'reactive' NC solution (mixture of BPEI/5Acl) through consecutive dipping of the substrates in the respective dipping solutions (Fig. 2.1E). Then, this dispersion of the NCs was thoroughly washed with ethanol prior to examination by FTIR spectroscopy. Two characteristic IR signatures at 1739 cm^{-1} and 1409 cm^{-1} (Fig. 2.3B; black curve) were noticed due to the carbonyl stretching and the symmetric deformation of the C–H bond for the β-carbon of the vinyl groups, respectively. This IR study revealed the presence of residual acrylate groups in the polymeric NCs. Furthermore, the depletion of the characteristic peak intensity at 1409 cm^{-1} (Fig. 2.3B; red curve) for the residual acrylate moieties upon treatment with primary amine-containing small molecules (i.e. glucamine) unambiguously suggested the existence of residual chemical

reactivity (Fig. 2.3B) in the synthesized NC. The chemically reactive residual acrylate group in the polymeric NC provided an opportunity to develop a covalently cross-linked multilayer of NC in combination with the multiple amine-containing BPEI polymer through consecutive 1,4-Michael addition reactions (Fig. 2.1A). During LBL deposition process, no sedimentation of the NC solution was observed, rather a rapid growth of multilayer of NC was observed at ambient conditions. The thickness of the

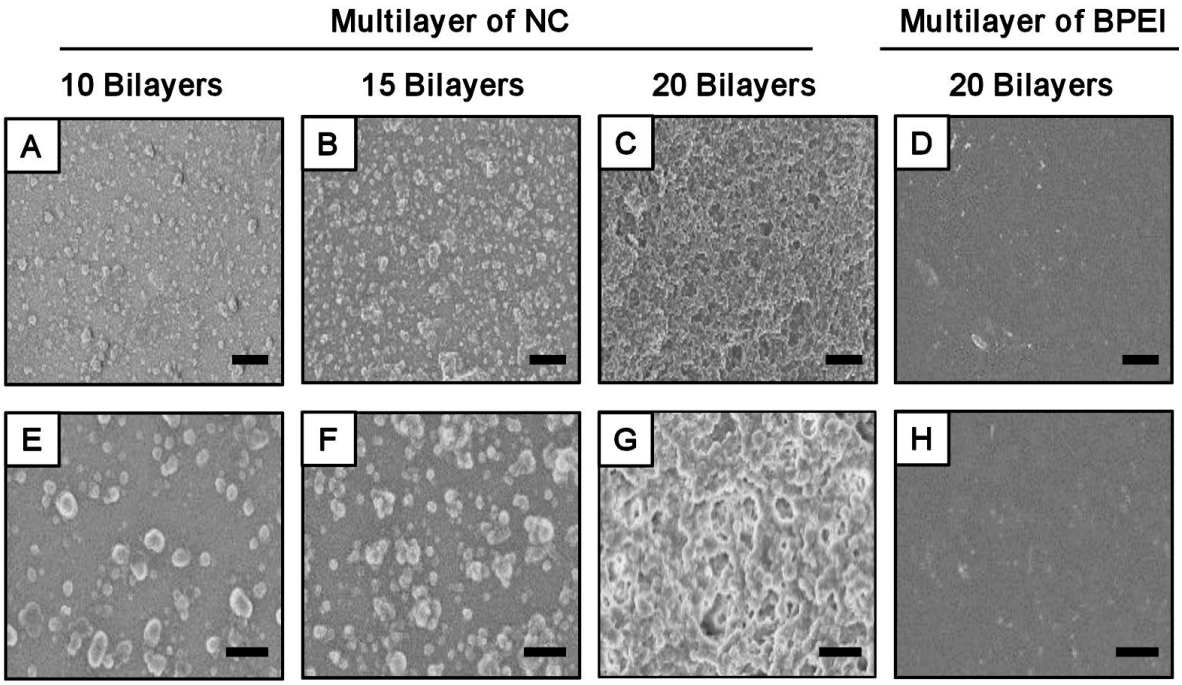

Figure 2.5: (A-C, E-G) FESEM images of the reactive multilayer of NC in low magnification (A-C; scale bar = 10 μm) and high magnification (E-G; scale bar = 3 μm), after depositions of 10 bilayers (A, E), 15 bilayers (B,F) and 20 bilayers (C,G), where each bilayer consisted of sequential deposition of BPEI and NC. D,H) The FESEM images of multilayer of BPEI in both low (D; scale bar = 10 μm) and high (H; scale bar = 3 μm) magnifications, after 20 bilayers deposition of BPEI/5Acl.

multilayer increased exponentially with increasing the deposition cycles (Fig. 2.4; black curve). The thickness of the multilayer (20 bilayers) of NC was measured to be 2.2 μm (Fig. 2.4; black curve). In comparison to that, the LbL growth for the multilayer of BEPI, which was constructed by replacing the NC solution mixture with 5Acl solution, was observed to be significantly sluggish. The thickness of the multilayer was only 174.09 nm, even after 20 cycles of LbL depositions (Fig. 2.4; red curve), where at each cycle, each bilayer was referred to the sequential deposition of BPEI and 5Acl. This observation supported that the deposition of branched polymeric amine (BPEI) through covalent cross-linking with small molecules (5Acl) was much slower than the multilayer of NC. Furthermore, the topography of both the multilayer of NC and multilayer of BPEI was examined by FESEM imaging (Fig. 2.5A-H). After

deposition of 20 bilayers of NC, an arbitrary hierarchical and porous topography was observed under FESEM (Fig. 2.5C,G). Whereas, the topography of the multilayer of BPEI was noticed to be featureless and smooth (Fig. 2.5D,H), even after repeating deposition cycles for 20 times. The gradual change in the morphology in the multilayer of NC was exploited later in revealing the role of surface topography behind the underwater oil-wettability property.

2.3.1. Characterization of super-oil-wettability under water

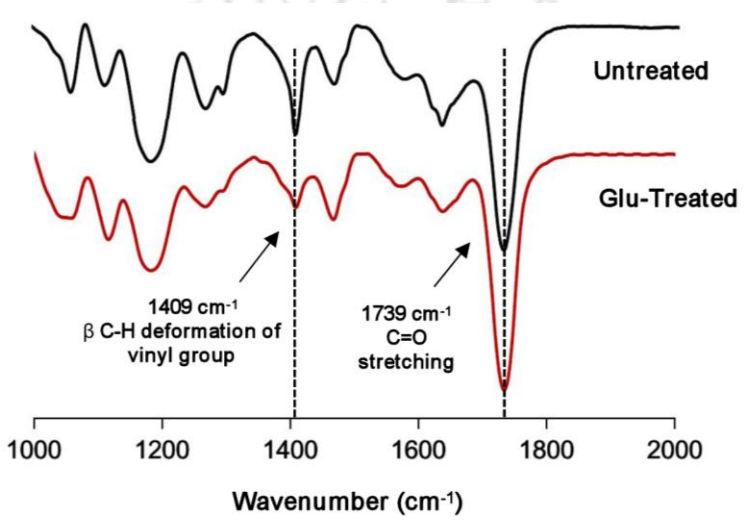

Figure 2.6: The FTIR spectra of reactive multilayer of NC before (black) and after (red) glucamine treatment.

Furthermore, the appearance of two characteristic peaks at 1739 cm^{-1} and 1409 cm^{-1} (for carbonyl stretching and symmetric deformation of the C–H bond for the β carbon of the vinyl groups, respectively) in the FTIR spectrum of the multilayer (20 bilayers) revealed the existence of residual acrylate moieties, even after successive deposition of NC on a glass substrate (Fig. 2.6; black curve) through LbL method. However, the peak at 1409 cm^{-1} was significantly depleted after successful covalent modification of multilayer of NC with amine-containing small molecule (glucamine; Fig. 2.6; red curve). Besides, oil and water wettabilities were thoroughly examined on both the amine-'reactive' multilayer (20 bilayers) of NC and multilayer of BPEI (20 bilayers) in air as well as under water. The hydrophilic (with a water CA of 72.1°; Fig. 2.7A) and superoleophilic (with an oil CA of 0°; Fig. 2.7C) multilayer of NC were found to be inherently oleophilic under water with an oil CA of 64.1° (Fig. 2.7E), likely due to the preferable interaction of the beaded oil droplet with the hydrophobic residual acrylate groups present in that multilayer. However, the post-chemical modification of the multilayer (20 bilayers) of NC with

strategically selected glucamine molecule through 1,4-conjugate addition reaction provided underwater superoleophobicity with an advancing oil contact angle (OCA) of 170.8° (Fig. 2.7F). This post-chemical modification is referred as 'Glu-treated' in rest of the discussion. In comparison to that, after same post-

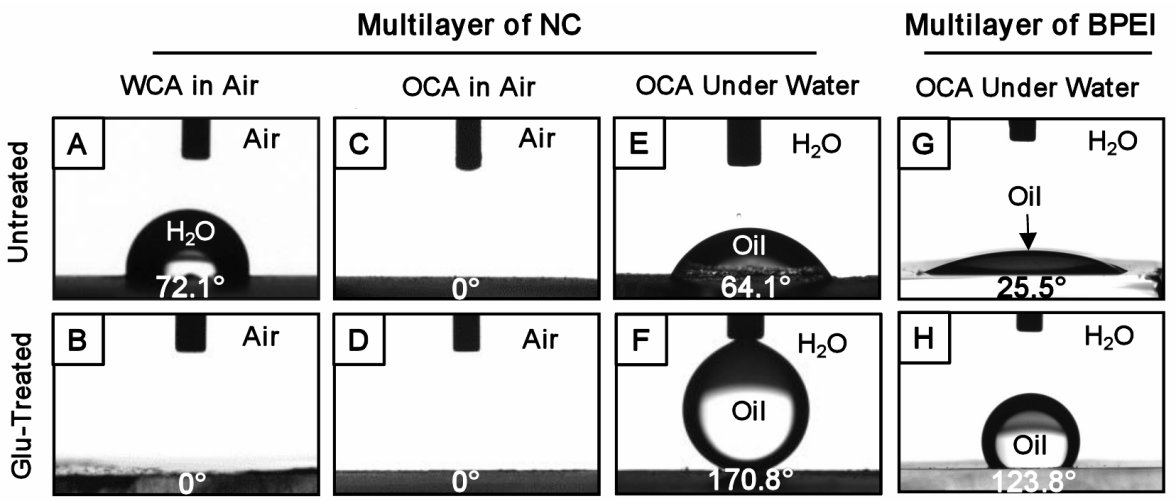

Figure 2.7: (A-F) The CA images of beaded water (A-B) and oil (C-F) droplets on multilayer of NC (A-F) in air (A-D) and under water (E-F), before (A,C,E) and after (B,D,F) post modification with glucamine. (G-H) CA images of beaded oil droplet on untreated (G) and glucamine treated multilayer (H) of BPEI under water.

chemical modification (with glucamine) of multilayer (20 bilayers) of BPEI, the featureless (Fig. 2.5D,H) and inherently underwater oleophilic (OCA of 25.5°; Fig. 2.7G) coating became underwater oleophobic

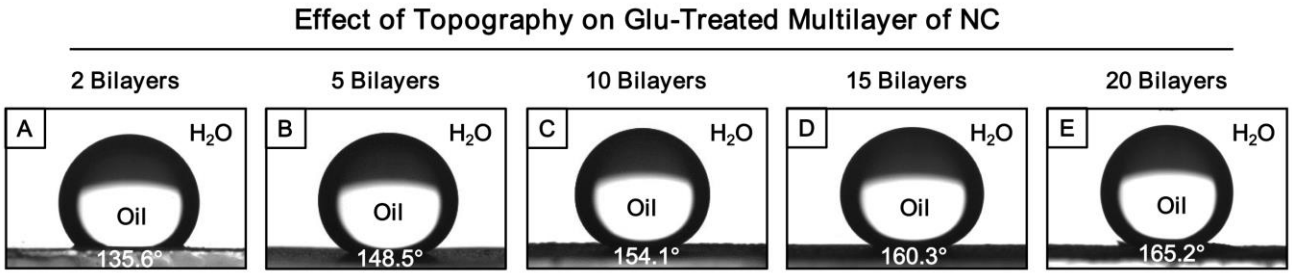

Figure 2.8: CA images showing the change in static OCA of beaded oil droplets on post-modified (A-E: glucamine) multilayer of NC with increasing the LbL deposition cycles.

with an OCA of 123.8° as shown in Fig. 2.7H. Thus, this study further revealed the need for a porous hierarchical topography to achieve underwater superoleophobicity. Moreover, it was noticed that the underwater oil-wettability of the 'Glu-treated' multilayer of NC was varied by increasing the number of bilayer depositions. The underwater static OCA gradually increased from 135.6° (2 bilayers; Fig. 2.8A) to 165.2° (20 bilayers' Fig. 2.8E) for the 'Glu-treated' multilayer of NC on increasing the number of

bilayer depositions (Fig. 2.8) from 2 to 20. Thus, this current study confirmed the need for appropriate chemical (hydrophilic/hydrophobic) and physical (surface topography) optimizations to achieve the

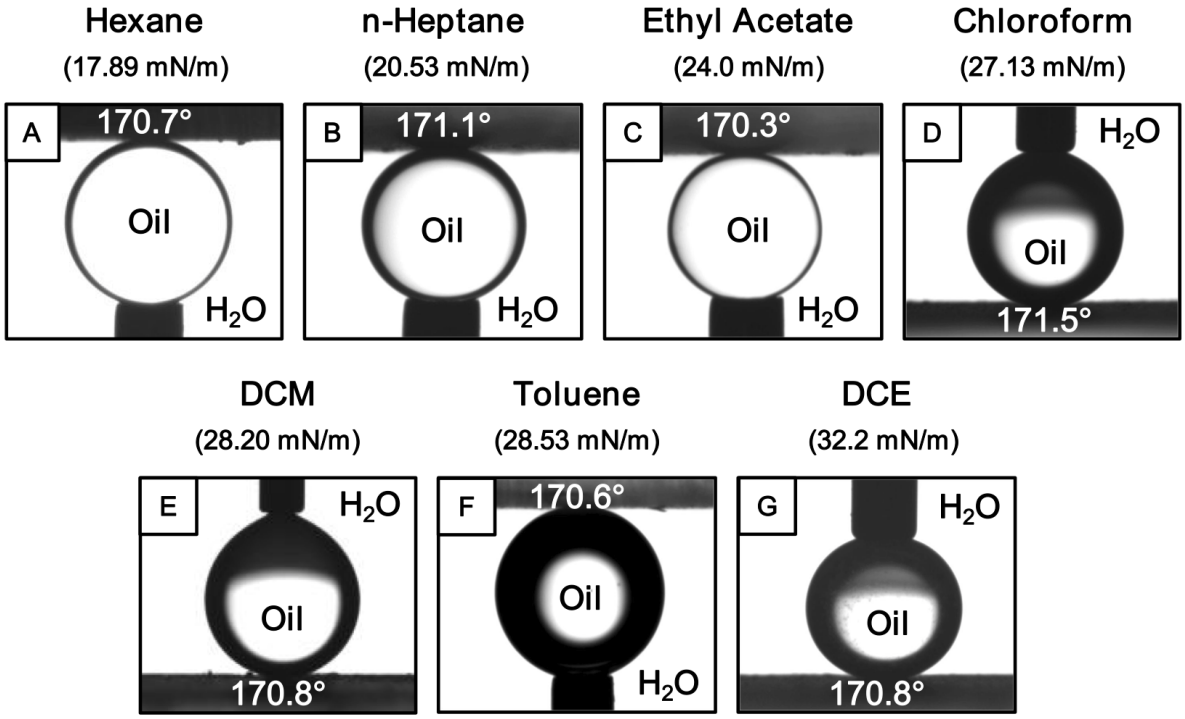

Figure 2.9: A-G) CA images of various water immiscible organic solvents that were beaded on the post-functionalized (glucamine) multilayer of NC. The surface tensions of the selected model oils, varied from 17.89 mN m^{-1} (hexane) to 32.2 mN m^{-1} (DCE).

desired underwater anti oil-wettability. Moreover, these 'Glu-treated' multilayer of NC were capable of displaying underwater super oil repellency with a wide range (in terms of surface tension) of water immiscible model oils (Fig. 2.9) starting from hexane (17.89 mN m^{-1}; Fig. 2.9A) to DCE (32.2 mN m^{-1};

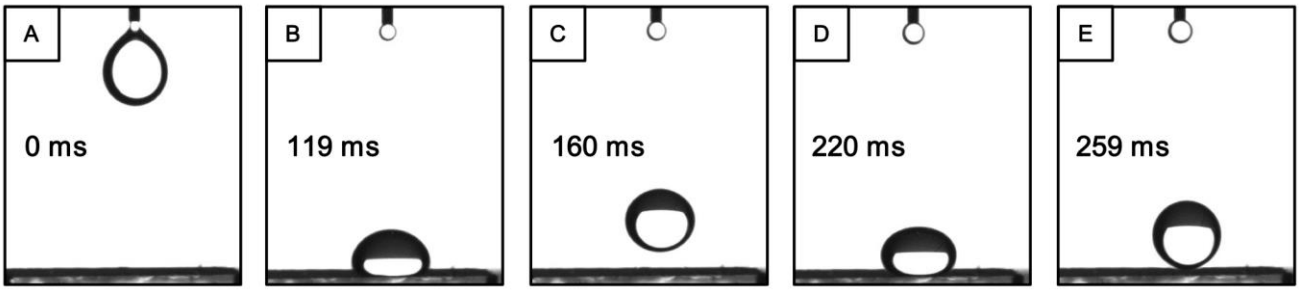

Figure 2.10: (A-E) CA images accounting bouncing of DCM (model oil) droplet (11 µl of DCM) on 'Glu-treated' multilayer (20 bilayers) of NC.

Fig. 2.9G). On dropping of a model oil (DCM) droplet (11 mL) on to the 'Glu-treated' multilayer (20

bilayers) of NC from a height of 12.5 mm, it was noted that the oil droplet bounced (Fig. 2.10) multiple times before eventually settling on the multilayer with an OCA of 165° (Fig. 2.10E). On the other hand, beaded oil droplet readily rolled off (Fig. 2.11) when the surface was tilted at 3°. This extreme oil-repellency under water is often explained using the Cassie–Baxter model,[4] where the heterogeneous

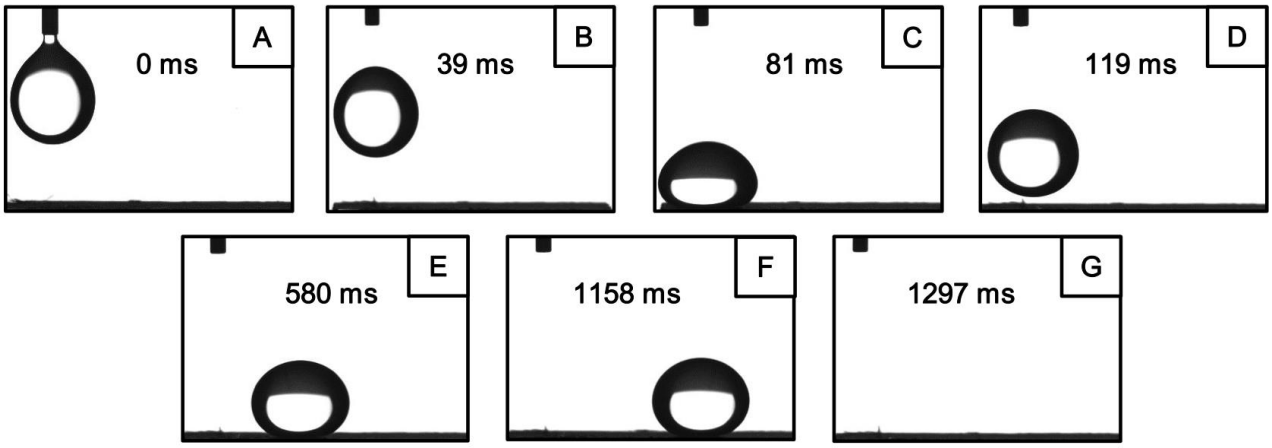

Figure 2.11: CA images illustrating the rolling of 11 µl DCM droplet at tilting angle of 3°, where DCM droplet was dispensed from a height of 0.7 cm.

wetting of oil on a multilayer of NC is due to the impregnation and confinement of aqueous phase within the hierarchically featured surface. The confined water layer within the 'Glu-treated' porous NC multilayer reduced the contact area between the beaded oil droplet and 'Glu-treated' multilayer of NC. Furthermore, the fractional area of contact between the liquid droplet (model oil DCM droplet) and the 'Glu-treated' multilayer of NC was estimated using eqn (2.1) and eqn (2.2),

$$\cos\theta_{CB} = f_1 \cos\theta_1 + f_2 \cos\theta_2 \quad \text{..... (2.1)}$$

$$f_1 + f_2 = 1 \quad \text{..... (2.2)}$$

where, θ_1 and θ_{CB} are the oil CAs on the multilayer (20 bilayers) of BPEI (smooth surface, glu-treated:123.8°) and NC (porous, glu-treated: 165.2°), respectively. The fraction of contact areas of the beaded oil droplet with both the 'Glu-treated' multilayer of NC and trapped aqueous phase were labelled as f_1 and f_2, respectively. The estimated fraction of the contact area of the beaded oil droplet on the 'Glu-treated' NC multilayer (20 bilayers) was 0.075, whereas the values were 0.621 and 0.86 for the 15- and 10-bilayers coatings (where each coating was 'Glu-treated'), respectively. The increase in fraction of contact area between the beaded oil droplet and the solid NC multilayer induced more adhesive interaction between the liquid and solid phases. This was mostly because of the difference in the surface topography

of the multilayer as confirmed by the FESEM study (Fig. 2.5). The topography of multilayer coatings plays a critical role in controlling the adhesive interaction of the beaded liquid droplet on the solid interfaces,[31] and the appropriate hierarchical topography is essential for minimizing (Cassie state) the contact area between the beaded oil droplet and the solid interface. After 20 bilayers of NC depositions (Fig. 2.5C,G), the multilayer of NC was inherently decorated with an essential hierarchical topography, and as a result, such interface displayed non-adhesive superoleophobicity under water. However, a less prominent microdomains in the multilayer of NC having 10 (Fig. 2.5A,E) and 15 (Fig. 2.5B,F) bilayers of depositions were attributed to the higher contact area between the beaded oil droplet and the NC multilayer, and eventually the multilayer adopted a Cassie–Wenzel transition state.[31]

2.3.2. Physical/chemical durability of underwater superoleophobicity property

Next, this covalently cross-linked multilayer of NC was exposed to various complex and harsh physical/chemical settings to investigate the durability of the embedded underwater superoleophobicity. First, this 'Glu-treated' multilayer of NC was exposed to hot water steam (Fig. 2.12A-B) and hot water (100°C; Fig. 2.12C-D), however, there was no apparent change in the underwater anti-oil wetting property before (Fig. 2.12A,C) and after the treatments (Fig. 2.12B,D). Next, an oil droplet (Fig. 2.12E, Advancing OCA ~ 172°) was placed on the 'Glu-treated' multilayer of NC that was submerged underwater and kept at -20 °C. Over a duration of 2 hours, the liquid water phase was frozen into ice, however, the shape of the beaded oil droplet remained intact after the freezing process (Fig. 2.12G), which indicated that the underwater anti oil-fouling property of the material remained unaltered during the whole process. The property remained unchanged, even after thawing the frozen ice with Advancing OCA ~172° (Fig. 2.12F). Additionally, a droplet of DCM (model oil) was beaded on 'Glu-treated' multilayer of NC, and it was exposed to elevated temperature. The size of the beaded model-oil droplet on the multilayer-coated substrate was observed to shrink on increasing the temperature of the aqueous phase, (Fig. 2.12H–K) due to gradual evaporation of DCM at the elevated temperature. The droplet eventually disappeared at prolonged exposure to 100 °C (Fig. 2.12K), however, the underwater superoleophobicity of the material remained intact during the course of the experiment (Fig. 2.12H-K). Next, some standard physical abrasion tests including sandpaper abrasion test, adhesive tape peeling test, and sand drop test were adopted to investigate the physical durability of the underwater superoleophobicity. First, a sandpaper (2 cm x 2 cm) was manually rubbed back and forth on the polymeric-material (1 cm x 1 cm) five times with an applied load of 200 g leading to in substantial formation of white powdery material (that adhered on the abrasive

sandpaper) as shown in Fig. 2.13A-D, however, the 'Glu-treated' multilayer of NC displayed extreme oil-repelling property (Fig. 2.13E-F) without considerable changes in the OCA underwater, even after removal of the top surface of the coating. Thus, the current study revealed the existence of 'bulk' underwater superoleophobicity property in the NC multilayer. Such robust materials are rare in the

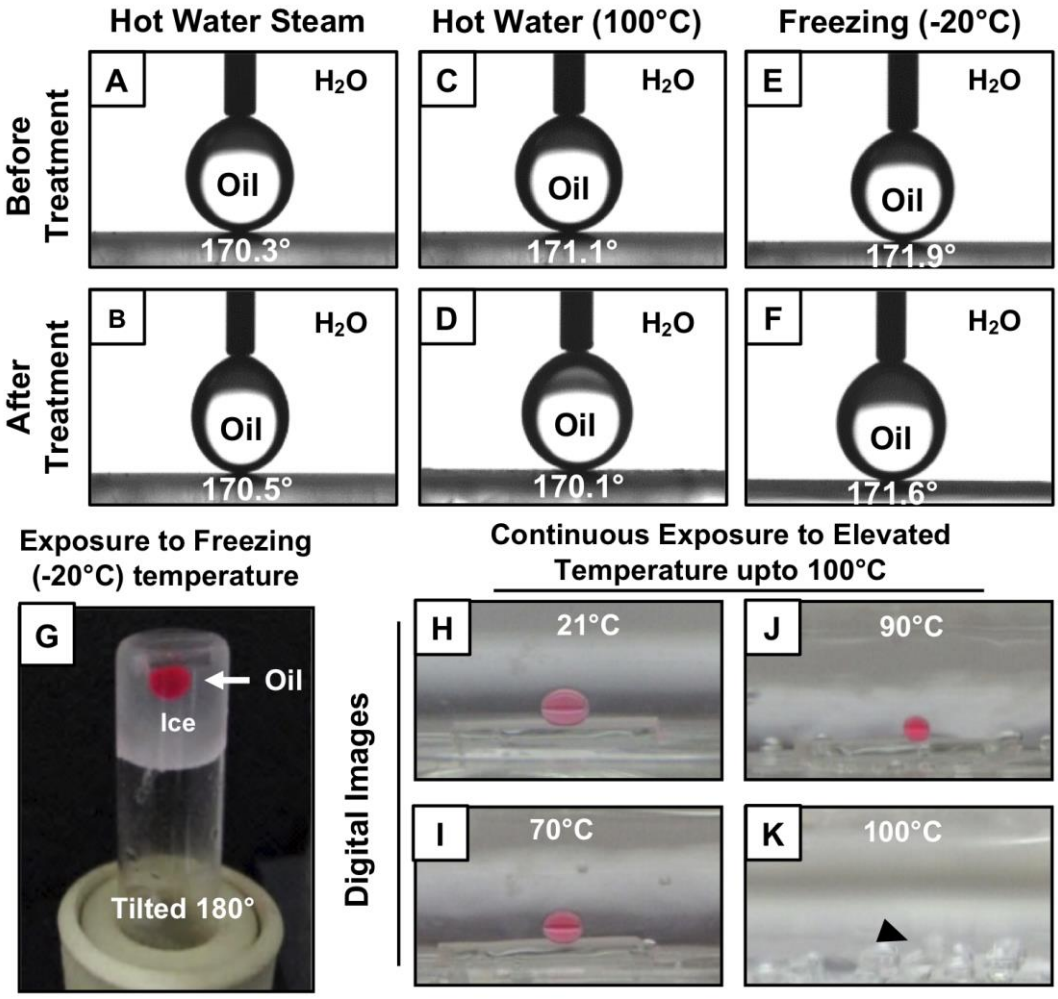

Figure 2.12: Advancing CA images (A-F) of beaded oil droplet on the 'Glu-treated' multilayer of NC before (A, C, E) and after (B, D, F) different and harsh exposures of hot water steam, hot water (100°C) and freezing (-20°C) condition. (G-J) Digital images illustrating the impact of with increasing temperature (up to 100°C) on the beaded DCM droplet on 'Glu-treated' multilayer of NC under water. (K) Digital image of beaded oil droplet at freezing (-20°C) condition, where the vial was kept inverted.

literature. Furthermore, the FESEM image of the abraded multilayer revealed that the topography of the material (Fig. 2.14A) was significantly different from the native coating (Fig. 2.5F), however, this physically-damaged coating had appropriate hierarchical structures to display underwater anti oil-fouling property (Fig. 2.13E-F). Further, an adhesive tape test was performed on underwater superoleophobic

coating, however, any delamination of the polymeric coating from the substrate was not noticed after performing the adhesive tape test. Moreover, a very porous morphology with arbitrary arrangement of

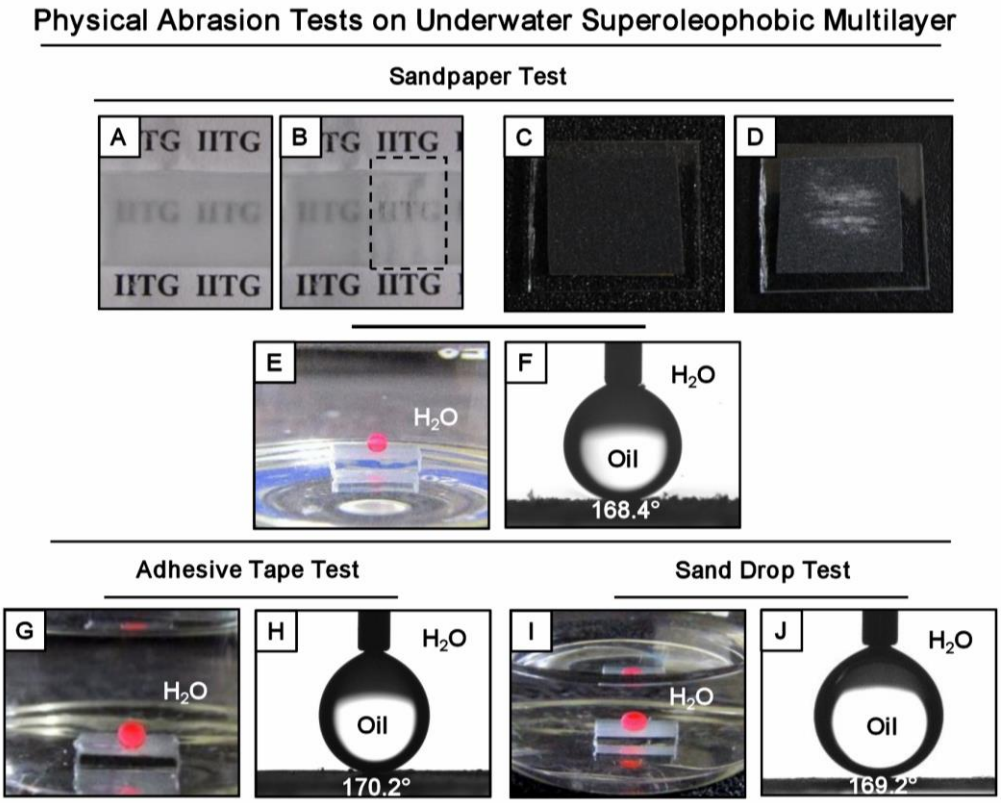

Figure 2.13: (A-D) Digital of superoleophobic coating (A-B) and abrasive sandpaper (C-D) before (A,C) and after (B,D) performing the sandpaper abrasion test. E-F) Digital (E) and CA image (F) of beaded oil droplet on physically abraded multilayer of NC. G-J) Digital images (G, I) and CA image (H, J) of beaded oil droplet on the underwater superoleophobicity interface after conducting the adhesive tape peeling test (G-H) and sand drop test (I-J).

granular domains, which is similar to untreated material, was observed under FESEM study (Fig. 2.14B). As expected, the anti-oil wetting property remained unaffected even after the adhesive tape test (Fig.

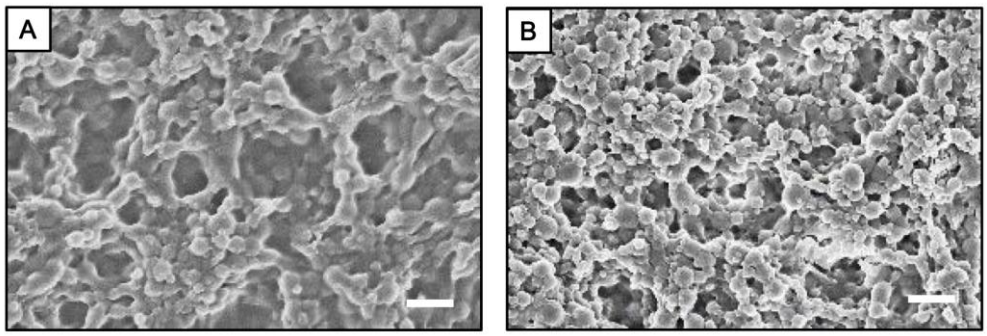

Figure 2.14: (A-B) FESEM images of multilayer of NC after performing (A) sandpaper and (B) adhesive tape tests, respectively (scale bar = 1 μm).

2.13G-H). Lastly, the impact of sand grain (100 g) on the material from a distance of 20 cm was tested following standard protocol and the anti-wetting property was found to be remained intact (Fig. 2.13I-J), without causing any noticeable physical damage to the polymeric coating. Thus, the synthesized

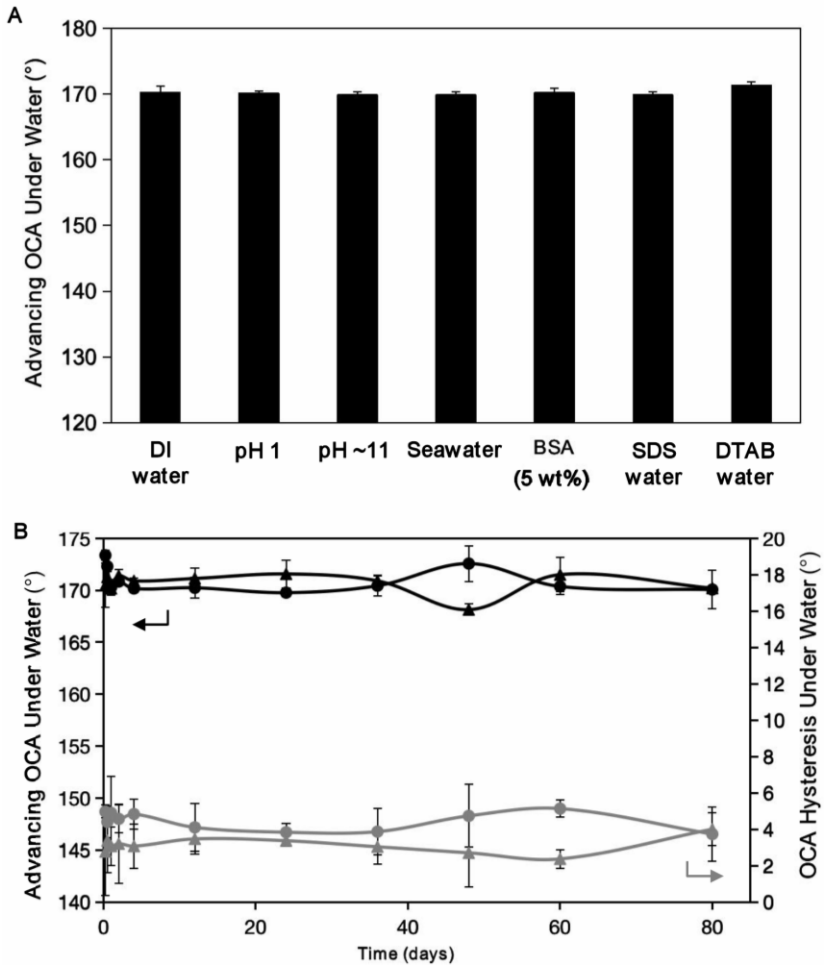

Figure 2.15: (A) Bar chart representation of advancing CA of beaded oil droplet on the Glu-treated multilayer after exposure to various aqueous phase, including DI-water, alkaline solution (pH 11.13), acidic solution (pH 1), saline water, BSA solution (5 wt %) and surfactant solutions (SDS, DTAB; concentration = 1 mM each). (B) Graphical depiction of advancing CA (black) and CA hysteresis (grey) of beaded oil droplet on 'Glu-treated' multilayer after continuous submersion in milli-Q water (▲) and salt water (●) for 80 days.

underwater superoleophobic coating displayed extraordinary tolerance to various physical insults including physical damage that eroded the top surface of the polymeric coating. Moreover, the underwater superoleophobic property remained intact with Advancing OCA >165° (Fig. 2.15A), even after exposure of this Glu-treated multilayer of NC to various harsh and complex aqueous systems including extremes of pH (pH 1 and pH 11.13), surfactants (DTAB, SDS; 1 mM each), and BSA protein (5 wt%)-contaminated

aqueous phases for 10 days. Furthermore, the multilayer of NC was separately submerged in DI water and artificial seawater for continuous and prolonged (80 days) exposure, however, this material continued to display robust underwater anti oil-fouling property with Advancing OCA of >165° and OCA hysteresis of <5° (Fig. 2.15B). The impeccable chemical durability of the material and its anti-oil-fouling property were mostly due to the existence of extensive covalent cross-linkages (through the 1,4-conjugate addition reaction) in the multilayer of NC.

2.3.3 Substrate-independent underwater superoleophobic coating

The inherent ability of the LbL deposition approach allowed to coat various rigid and flexible objects with multilayer of NC, irrespective of the dimension and geometry of the selected substrates (Fig.

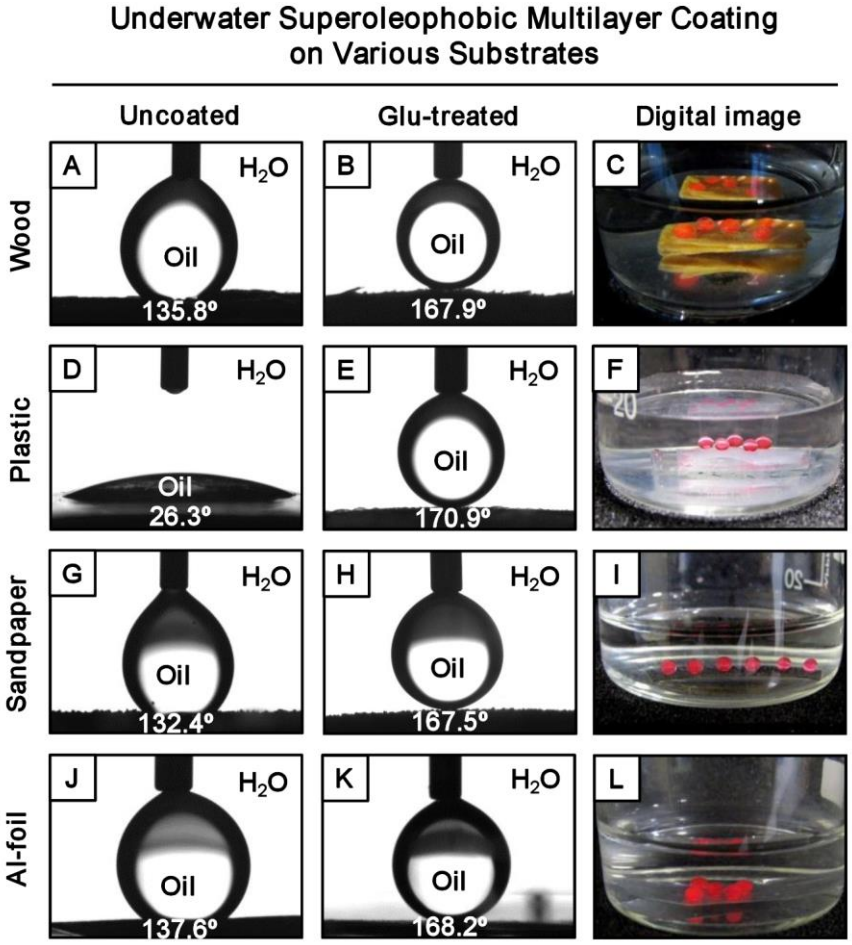

Figure 2.16: (A-L) CA (A-B, D-E, G-H, J-K) and digital (C,F,I,L) images of uncoated (A,D,G,J) and multilayer of NC coated (B,E,H,K; 'Glu-treated') wood (A-C), plastic (D-F), sandpaper (G-I) and Al-foil (J-L), respectively.

2.16A,D,G,J). The amine-'reactive' multilayer (20 bilayers) of NC was deposited on underwater both oleophilic (plastic film, OCA <30°: Fig. 2.16D) and oleophobic (wood, sandpaper and Al-foil, OCA

>130°: Fig. 2.16A, G, J) substrates. The strategic post-functionalization of the multilayer coating with hydrophilic glucamine molecule provided underwater superoleophobicity (Fig. 2.16B-C, E-F, H-I, K-L).

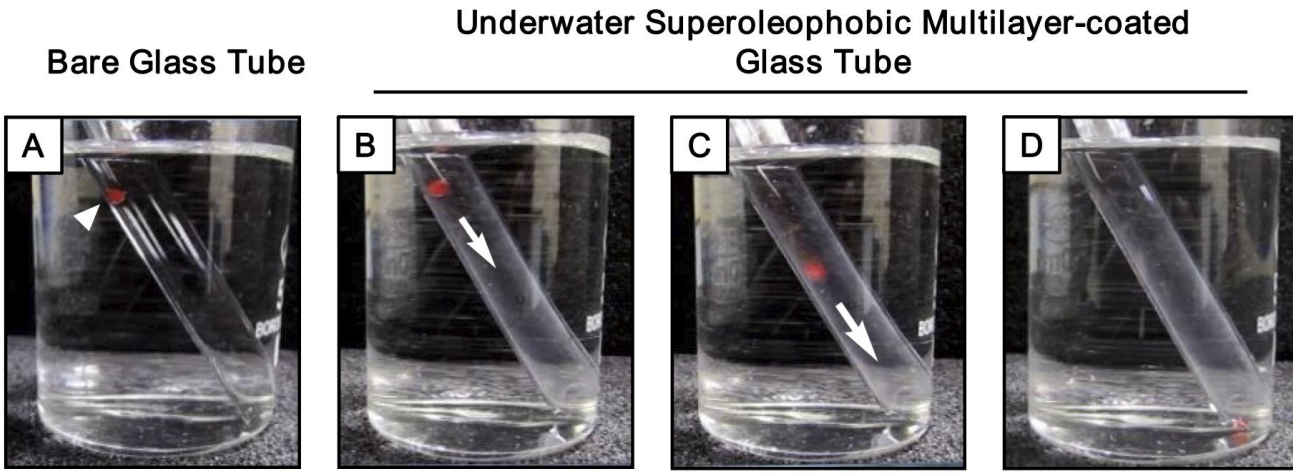

Figure 2.17: (A-D) Digital images illustrating the movement of coloured DCM (model oil) droplets through both the bare glass tube (A) and underwater superoleophobic multilayer-coated (interior part) glass tube (B-D) under water.

The 'Glu-treated' multilayer of NC strongly repelled oil with Advancing OCA >165° and OCA hysteresis <10°. Moreover, the interior of a glass tube (with OCA ~ 124°) could be successfully decorated with underwater superoleophobicity (with OCA ~ 165°), which was further used in demonstration of facile and guided transport of tiny (8 mL) oil droplets under water, without any adhesion or loss of oil during the transportation process (Fig. 2.17B-D), which was impossible to achieve with a bare glass tube (Fig. 2.17A). Thus, this proof-of-concept demonstration revealed the ability of this anti-oil wettability property in preventing unwanted oil contaminations and in providing energy-efficient as well as gravity-driven guided transport of heavy oil or oily substances.

2.4. Conclusion

In conclusion, the design of amine-'reactive' multilayer of NC provided insight into the fundamentals of underwater superoleophobic properties in detail. The 'reactive' multilayer of NC provided a facile avenue to control both the chemistry and topography of the polymeric coating, and this fresh design independently revalidated some key hypotheses that explained the superoleophobicity under water. Moreover, the approach of using covalently cross-linked multilayer of NC resulted in an abrasion-tolerant underwater superoleophobicity, which could withstand various severe both physical and chemical insults. Furthermore, the LbL deposition process allows coating of a wide range of substrates with desired

underwater superoleophobicity for protecting the substrates from unwanted oil-contamination under water.

Such durable underwater superoleophobic coating would be more appropriate for prospective applications in various practically relevant and severe conditions.

2.5. References

(1) Y. Tian, B. Su and L. Jiang, *Adv. Mater.*, 2014, **26**, 6872.

(2) Z. Chu, Y. Feng and S. Seeger, *Angew. Chem. Int. Ed.*, 2015, **54**, 2328.

(3) B. Su, Y. Tian and L. Jiang, *J. Am. Chem. Soc.*, 2016, **138**, 1727.

(4) M. J. Liu, S. T. Wang, Z. X. Wei, Y. L. Song and L. Jiang, *Adv. Mater.*, 2009, **21**, 665.

(5) Y. Wu, B. Su, L. Jiang and A. J. Heeger, *Adv. Mater.*, 2013, **25**, 6526.

(6) Z. Shi, W. Zhang, F. Zhang, X. Liu, D. Wang, J. Jin and L. Jiang, *Adv. Mater.*, 2013, **25**, 2422.

(7) M. Tao, L. Xue, F. Liu and L. Jiang, *Adv. Mater.*, 2014, **26**, 2943.

(8) Y. Cai, Q. Lu, X. Guo, S. Wang, J. Qiao and L. Jiang, *Adv. Mater.*, 2015, **27**, 4162.

(9) K. Chen, S. Zhou and L. Wu, *ACS Nano*, 2016, **10**, 1386.

(10) A. K. Kota, G. Kwon, W. Choi, J. M. Mabry and A. Tuteja, *Nat. Commun.*, 2012, **3**, 1.

(11) A. Tuteja, W. Choi, M. L. Ma, J. M. Mabry, S. A. Mazzella, G. C. Rutledge, G. H. McKinley and R. E. Cohen, *Science*, 2007, **318**, 1618.

(12) H. Bellanger, T. Darmanin, E. T. de Givenchy and F. Guittard, *Chem. Rev.*, 2014, **114**, 2694.

(13) Y. C. Jung and B. Bhushan, *Langmuir*, 2009, **25**, 14165.

(14) X. Liu, J. Zhou, Z. Xue, J. Gao, J. Meng, S. Wang and L. Jiang, *Adv. Mater.*, 2012, **24**, 3401.

(15) Y. Cai, L. Lin, Z. X. Xue, M. J. Liu, S. T. Wang and L. Jiang, *Adv. Funct. Mater.*, 2014, **24**, 809.

(16) U. Manna and D. M. Lynn, *Adv. Funct. Mater.*, 2015, **25**, 1672.

(17) L. P. Xu, J. T. Peng, Y. B. Liu, Y. Q. Wen, X. J. Zhang, L. Jiang and S. T. Wang, *ACS Nano*, 2013, **7**, 5077.

(18) L. Lin, M. J. Liu, L. Chen, P. P. Chen, J. Ma, D. Han and L. Jiang, *Adv. Mater.*, 2010, **22**, 4826.

(19) Z. Xue, S. Wang, L. Lin, L. Chen, M. Liu, L. Feng and L. Jiang, *Adv. Mater.*, 2011, **23**, 4270.

(20) S. Gao, J. Sun, P. Liu, F. Zhang, W. Zhang, S. Yuan, J. Li and J. Jin, *Adv. Mater.*, 2016, **28**, 5307.

(21) F. Zhang, W. B. Zhang, Z. Shi, D. Wang, J. Jin and L. Jiang, *Adv. Mater.*, 2013, **25**, 4192.

(22) Z. Cheng, H. Lai, Y. Du, K. Fu, R. Hou, C. Li, N. Zhang and K. Sun, *ACS Appl. Mater. Interfaces*, 2014, **6**, 636.

(23) J. Yong, F. Chen, Q. Yang, U. Farooq and X. Hou, *J. Mater. Chem. A*, 2015, **3**, 10703.

(24) T. Guo, L. Heng, M. Wang, J. Wang and L. Jiang, *Adv. Mater.*, 2016, **28**, 8505.

(25) R. A. Farrer, C. N. LaFratta, L. Li, J. Praino, M. J. Naughton, B. E. A. Saleh, M. C. Teich and J. T. Fourkas, *J. Am. Chem. Soc.*, 2006, **128**, 1796.

(26) M. R. Weatherspoon, M. B. Dickerson, G. Wang, Y. Cai, S. Shian, S. C. Jones, S. R. Marder and K. H. Sandhage, *Angew. Chem. Int. Ed.*, 2007, **46**, 5724.

(27) J. Ford, S. R. Marder and S. Yang, *Chem. Mater.*, 2009, **21**, 476.

(28) G. Wang, Y. Fang, P. Kim, A. Hayek, M. R. Weatherspoon, J. W. Perry, K. H. Sandhage, S. R. Marder and S. C. Jones, *Adv. Funct. Mater.*, 2009, **19**, 2768.

(29) S. L. Bechler and D. M. Lynn, *Biomacromolecules*, 2012, **13**, 1523.

(30) A. M. Rather and U. Manna, *Chem. Mater.*, 2016, **28**, 8689.

(31) E. Zhang, Z. Cheng, T. Lv, L. Li and Y. Liu, *Nanoscale*, 2015, **7**, 19293.

Title: Synthesis of Stretchable and Durable Underwater Superoleophobic Membrane for Filtration-based Oil/Water Separation*

Synthesis of stretchable biomimicked special wettability—particularly fish scale-inspired superoleophobicity is challenging, but it could be useful in various potential applications in practical scenarios. In general, 'fish-scale'-inspired artificial interfaces were prepared by deposition of polymeric hydrogel, metal oxide and electrostatic multilayer, which are inappropriate for practical relevance due to lack of their durability in various and severe physical/chemical exposures. Thus, developing such interfaces are highly challenging and examples of such interfaces are rare in the literature. In this chapter, a highly stretchable (tolerating 150% strain) and physically/chemically durable underwater superoleophobic membrane has been developed via simple and strategic integration of covalently cross-linked 'reactive' multilayer with a stretchable fibrous substrate. This as-synthesized interface with bio-mimicking wettability owned outstanding stability towards various harsh physical and chemical conditions, like successive (1000 times) tensile deformations, different physical abrasion tests, prolonged exposure (30 days) to both UV radiation and extremes of temperatures (100ºC and 10ºC) and complex chemical environments. Furthermore, the as-synthesized stretchable material was successfully found to be very efficient in the gravity-driven eco-friendly separation of oil/water mixtures, even under severe physical/chemical conditions (e.g., extreme conditions of temperatures, tensile strain, pH (1 and 12), artificial seawater, and river water). Such durable and highly stretchable oil-repellent interface would be very useful in various submarine-related and biomedical applications, including prevention of oil contamination, oil/water separations, and anti-biofouling coating on flexible medically relevant substrates (e.g., catheter balloon).

*D. Parbat and U. Manna, *J. Mater. Chem. A*, 2018, **6**, 22027.

3.1. Introduction

Synthesis of stretchable and smart interfaces is immensely acknowledged for its enormous potential in addressing various biomedical challenges and designing advanced materials for different smart applications.[1–6] Recently, artificially designed bio-mimicked interfaces which have been mostly synthesized through appropriate co-optimization of both topography and chemistry, are being widely recognized owing to their innumerable prospective applications and the potential to revolutionize scientific innovations.[7–12] In general, any significant perturbation in the essential hierarchical topography during tensile deformation of such special interfaces plausibly alter the bio-mimicked wettabilities embedded in those interfaces.[13,14] Such compromise of wettability property eventually affects their highly prospective and eco-friendly applications in practically relevant harsh conditions.[15,16] Nevertheless, 'lotus leaf'-inspired dry and stretchable interfaces that extremely repelled water in air, even after incurring physical deformations above 100% tensile strain, have been successfully synthesized recently with few elegant designs, and such interfaces are strategically being explored for various prospective applications.[17–20] Unlike 'lotus leaf'-inspired wettability, the 'fish-scale'-inspired extreme oil-repellent property performs only under water.[11,14,21–37] Therefore, the synthesis of stretchable biomimicked wet interfaces that remain functional under water even after exposure to various mechanical stresses, is even more difficult, and examples of such stretchable superoleophobic interfaces are rare in the literature. Rather, the synthesis of artificial interfaces with 'fish-scale'- mimicked wettability by using high-mechanical-strength coating have emerged as a common strategy to avoid any large scale perturbation in topography, where the rigid/flexible substrates having restricted tensile deformation were tactfully selected for developing stable artificial underwater superoleophobic coatings.[35–37] Therefore, further progress in designing stretchable 'fish-scale'-mimicked wettability would be highly desirable and important in many relevant and smart applications in real-world scenarios, including fabrication of stretchable and smart anti-oil-fouling textiles, highly durable membranes for oil/water separation and stretchable anti-biofouling coatings on a relevant and flexible medical device. The synthesis of interface with 'fish-scale'-inspired wettability having the ability to sustain various physical manipulations (including winding, twisting, stretching and scratching) which are commonly practiced during packaging, transportation and/or process of oil-repelling performance at the outdoor location of interest, is highly relevant to its prospective applications in realistic scenarios. After the seminal report from Jiang et al.[14] on the 'fish scale'-mimicked artificial interfaces in 2009, the extremely oil-repellent heterogeneous wettability (Cassie–Baxter state)[14] of liquid oil under water has been mostly designed by strategic incorporation of (a) polymeric hydrogels[14,21–27] and (b) metal oxides[28–34] with appropriate hierarchical topography. Both of

these commonly used organic and inorganic coating approaches inherently and severely suffer from various durability issues.[36,37] The polymeric hydrogels are highly susceptible to swelling and deformation in a chemically harsh aqueous phase and under application of external tensile strain. Moreover, the brittle metal oxide coatings are expected to get damaged on prolonged exposure to chemically complex aqueous phases and (or) under applied stress. Thus, the mechanically durable artificial superoleophobic coatings have been mostly studied over the last few years to avoid any major physical deformations of highly water-compatible hierarchical topography.[35–37] As expected, such approaches are inappropriate to design stretchable underwater superoleophobicity. In the Chapter 3, a highly stretchable and robust underwater superoleophobic interface was synthesized by strategic integration of 'reactive' nanocomplex (NC) onto a stretchable and fibrous substrate following a simple and covalent layer-by-layer (LbL) deposition process as followed in the Chapter 2. The as-synthesized material was capable of sustaining its extreme oil-repellence under the applied tensile strain of above 100%. Furthermore, as-synthesized underwater superoleophobic interface was capable of withstanding repetitive physical deformations with 150% tensile strain for 1000 times, which is unprecedented in the literature. Furthermore, the biomimicked wettability was found to be unaltered even after exposure of the polymeric coating to various other severe physical and chemical treatments, including different physical manipulations, abrasions and exposures to extreme conditions of pH and temperature, artificial seawater, river water and prolonged (30 days) ultraviolet (UV) radiation. This robust and stretchable wettability was further exploited in the separation of various forms of oil/water mixtures, which resemble practically relevant scenarios, including extreme conditions of pH and temperature, with a water separation/collection efficiency of 99 wt%. Moreover, the underwater superoleophobic fibrous substrate that was exposed to various manual deformations, including bending, creasing, winding, twisting, and repetitive stretching (for 1000 times), was also successfully extended in selective filtration of the aqueous phase from oil/water mixtures. Further, the synthesized underwater superoleophobic membrane was capable of successive (at least 50 times) oil/ water separation without any alteration in the efficiency of selective filtration of the aqueous phase from oil-in-water emulsions.

3.2. Experimental Section

3.2.1. Materials

Fibrous polyurethane (PU) substrate (fabric), soybean oil (vegetable oil) and kerosene oil were purchased from a local shop in Guwahati city (Assam, India). Motor oil (Castrol Active 20W-40) was purchased from Castrol India Ltd. Detailed descriptions of other materials were already mentioned in the Chapter 2.

3.2.2. General consideration

The oil-in-water emulsion droplets were characterized by Nikon Eclipse Ts2R (Nikon digital sight DS-U3). Other instruments for this piece of study are the same as Chapter 2.

3.2.3. Construction of reactive multilayer on stretchable fibrous substrate and post-covalent modification of multilayer

The 'reactive' multilayer of NC/BPEI was prepared and further post-modified with primary amine-containing hydrophilic small molecule (i.e., glucamine) following the same protocol that is discussed in the Chapter 2. However, insists of using a model glass substrate, the multilayer was embedded on a fibrous substrate (PU).

3.2.4. Physical and chemical durability of the bio-mimicked wettability

3.2.4.1. Sand drop test: The procedure for sand drop test was discussed in the Chapter 2 in detail. The underwater oil wettability was examined by measuring the OCAs and digital images after performing the test.

3.2.4.2. Sandpaper abrasion test: A detailed discussion on the protocol of sandpaper abrasion was discussed in the Chapter 2. Finally, the oil wettability property of the sandpaper abraded material was investigated with CA measurements and digital images.

3.2.4.3. Adhesive tape test: The procedure for adhesive tape test was same as mentioned in the Chapter 2. After performing the test, the underwater oil wettability was re-examined by measuring the OCAs and digital images.

3.2.4.4. Effect of bending, creasing, twisting, and winding on bio-mimicked interface: The synthesized 'fish scale' mimicked wettability was exposed to commonly practised various physical manipulations—including bending, creasing, twisting and winding. The stretchable biomimicked substrate was manually bent, creased, twisted and winded with random preferences for several times. Thereafter, the OCAs were measured under water to examine the impact of these physical manipulations on the embedded bio-mimicked wettability.

3.2.4.5. Chemical durability test: The chemical durability tests were performed on the bio-mimicked interface following the same protocol as in Chapter 2. The property was still unaltered which was confirmed by CA measurements.

3.2.5. Preparation of 2% (v/v) DCE-in-water emulsion solutions

49 mL of deionized water was taken in a clean 100 mL glass beaker and placed it inside the water bath of the sonicator. Now 1 mL of DCE was added slowly using a graduated pipette with

continuous sonication for 30 minutes to prepare a 2% (v/v) oil-in-water emulsion of DCE. Then the emulsion solution was examined by DLS study and bright-field microscopic image analysis.

3.2.6. Calculation of percentage (%) of oil-absorption

Efficiency of oil separation is defined as amount of oil phase is separated from the given oil/water mixture after the filtration process and it was measured by following the given eqn 3.1;

$$\% \text{ Efficiency } of\ oil\ Separation\ = \frac{Weight\ of\ absorbed\ oil}{Weight\ of\ oil\ present\ in\ the\ mixture}\ x\ 100 \ldots\ldots\ldots\ldots\ldots (3.1)$$

3.3. Results and Discussions

3.3.1. Synthesis of stretchable underwater oil-repellent interface

The synthesis of functional polymeric nanomaterials has been recognized as an important avenue for tailoring various physical/chemical properties.[38–44] In the Chapter 2, a chemically reactive

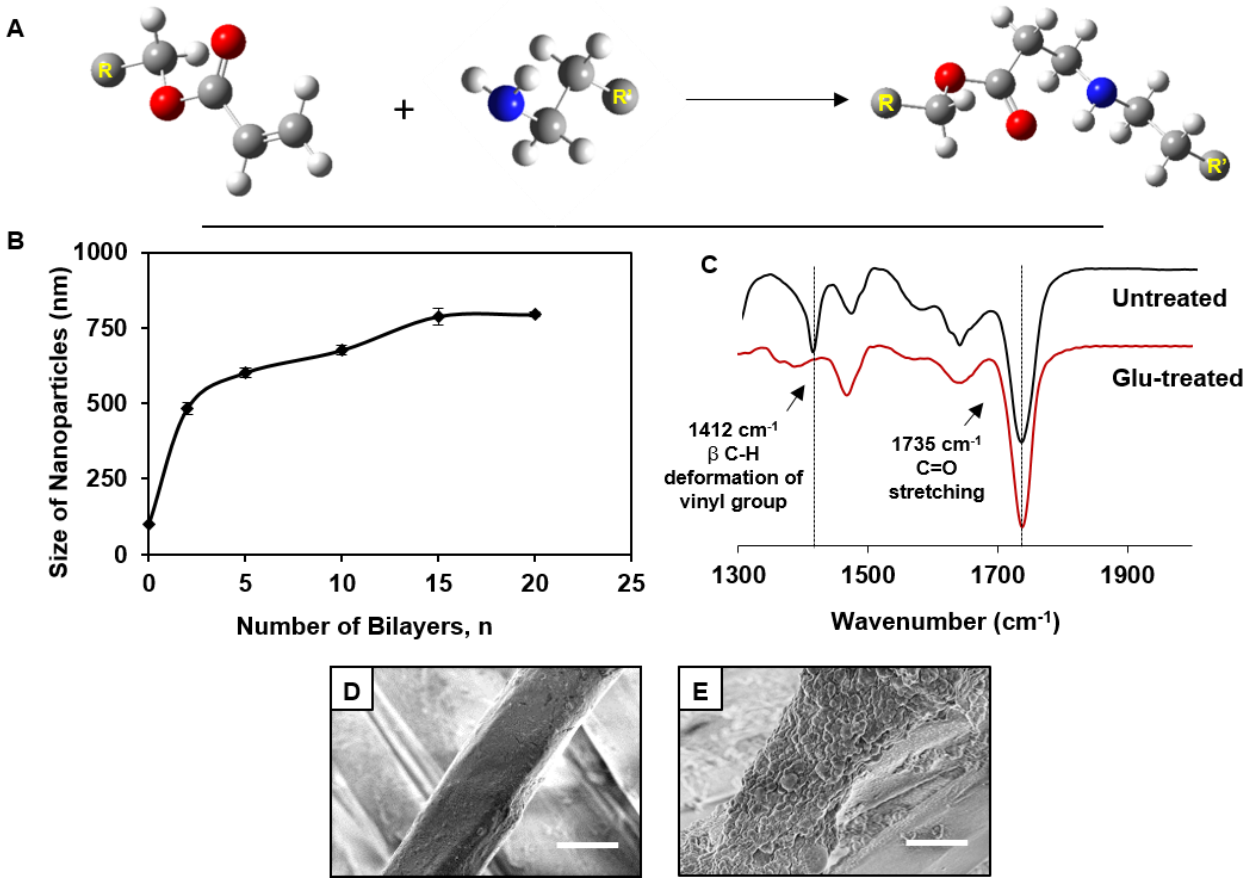

Figure 3.1: (A) Representing the catalyst-free facile 1,4-conjugate addition reaction between acrylate group and primary amine group. (B) The DLS study accounting the growth of the nanocomplex. (C) FTIR spectral analysis of chemically reactive multilayer coating before (black curve) and after (red curve) glucamine modification. (D-E) FESEM images of both the uncoated (C) and coated (D) fibrous substrate (scale bar: 4 µm).

nanocomplex (NC) that prepared using 1,4-conjugate addition reaction (Fig. 3.1A), was deposited following layer-by-layer (LbL) coating process for achieving bio-inspired durable liquid wettability.

In this Chapter 3, the 'reactive' NC was strategically deposited on the stretchable fibrous substrate through LbL deposition of BPEI polymer and NC (for 20 bilayers) for fabricating highly stretchable and robust 'fish-scale'-mimicked membrane. As expected, the size of the polymeric NC gradually increased during the consecutive LbL deposition process (each bilayer consisted of two layers, one of NC and the other one of BPEI), which was confirmed by dynamic light scattering (DLS) study, as shown in Fig. 3.1B. After deposition of 20 bilayers, the available chemical functionalities present in the covalently cross-linked multilayer were investigated by a standard Fourier transform infrared (FTIR) spectroscopy study.[44–46] The appearance of IR peaks at 1412 cm^{-1} and 1735 cm^{-1}, which were attributed to the C–H deformation of the β-carbon of the vinyl groups and carbonyl stretching, respectively (Fig. 3.1C; black curve), revealed the presence of residual acrylate groups in

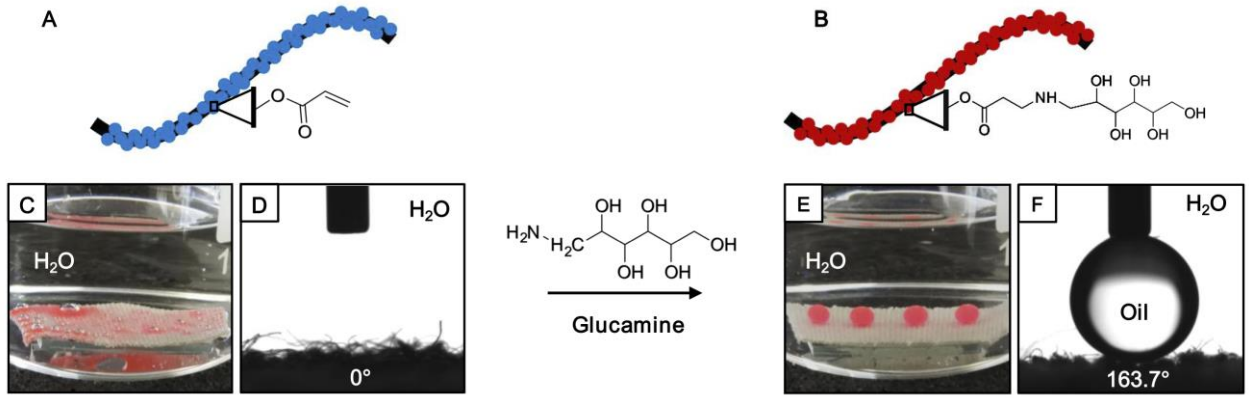

Figure 3.2: (A-B) The scheme illustrating the post-covalent modification of 'reactive' polymeric multilayer coating on fibrous substrate with glucamine. (C-D,E-F) Digital images (C,E) and CA images (D,F) of beaded oil droplets (under water) on the 'reactive' multilayer coated fibrous substrate before (C-D) and after (E-F) covalent modification of with glucamine.

the polymeric coating. Further, these residual acrylate moieties were found to be highly reactive with primary amine-containing small molecules. It was observed that the IR peak intensity at 1412 cm^{-1}, decreased significantly after post-modification of the same multilayer coating with hydrophilic small molecules (i.e., glucamine) via 1,4-conjugate addition reaction (Fig. 3.1C; red curve). Further, the existence of micro/nano featured topography that consisted of randomly aggregated granular polymeric domains on the smooth and native fibrous substrate was confirmed using FESEM imaging, as shown in Fig. 3.1D-E. The LbL deposition of granular NC on the fibrous substrate rendered the essential topography that conferred the 'fish-scale'- mimicked wettability after the chemical modulation of the reactive multilayer-coated substrate (Fig. 3.2B) with glucamine. As a result, the coated fibrous substrate that instantly soaked the beaded oil droplet (red colour aided visual inspection)

under water (Fig. 3.2C-D) became an extremely oil-repellent interface (Fig. 3.2E-F) with advancing OCA of 163.7º (Fig. 3.2F) after the post-modification of the same 'reactive' interface with glucamine (Fig. 3.2E). In the past, the elastomeric property of the selected fibrous substrate was exploited earlier for developing various functional materials.[47] In recent past, polyurethane (PU) based fibrous/porous substrates, decorated with 'lotus leaf'-inspired wettability, displayed a highly selective affinity towards oil/oily phases, and such materials were explored as oil-absorbent materials.[48–50] However, in this chapter, the PU-based substrate was extended in the synthesis of fish-scale-mimicked underwater extreme oil-repellent membrane with impeccable durability. The multilayer-coated stretchable fibrous

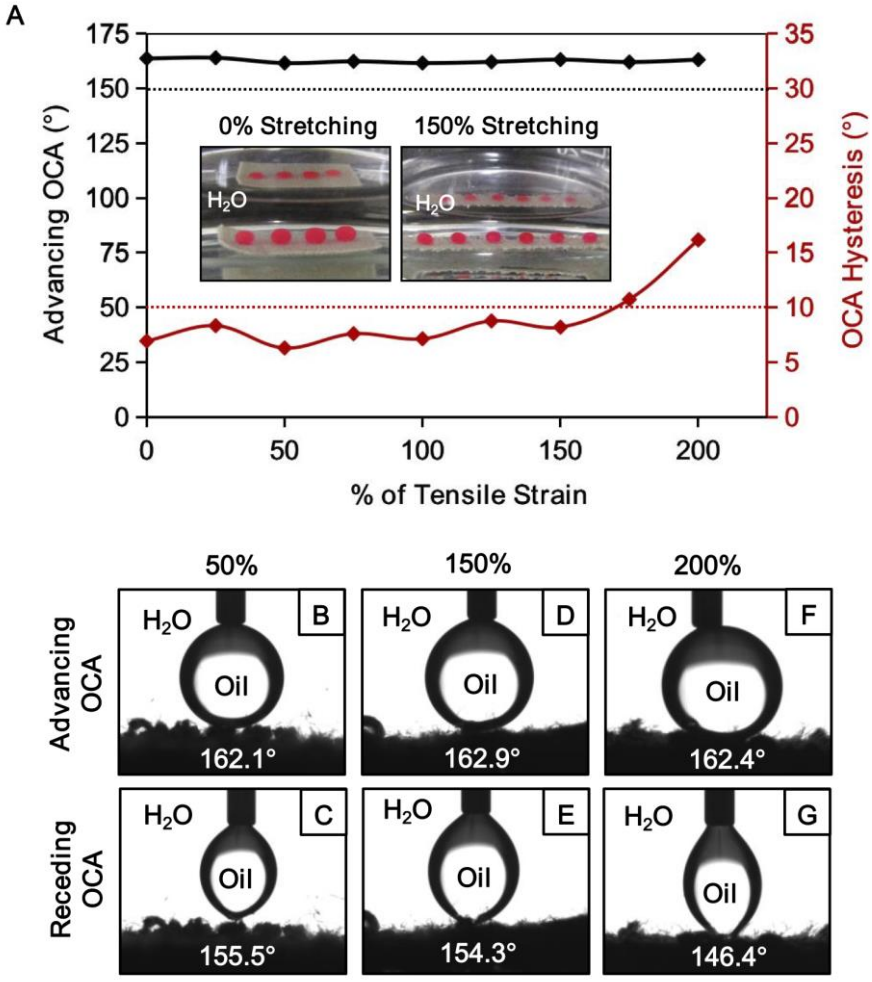

Figure 3.3: (A) Graphical representation of the change in underwater oil wettability on the biomimicked stretchable interface, where the tensile deformation was gradually increased from 0 to 200% under water. (B-G) Advancing (B,D,F) and receding (C,E,G) CA images of beaded (under water) oil droplet on the underwater superoleophobic interface after incurring tensile deformations with applied strains of 50% (B-C), 150% (D-E) and 200% (F-G), respectively.

substrate, which was post-modified with glucamine, was gradually deformed under applied tensile stress. The coated substrate was stretched up to 150% tensile strain without compromising the embedded anti-oil-fouling property under water, as shown in Fig. 3.3A,D-E. Even after such high

tensile deformation, the coated substrate was capable of repelling the beaded oil droplet with advancing OCA above 160º and OCA hysteresis well below 10º. With further increase in the tensile strain from 150% to 175% of the as-synthesized material, a slight change in underwater OCA hysteresis (just above 10º; but the beaded oil droplet still repelled extremely with advancing OCA above 160º) was noticed, as shown in Fig. 3.3A. Upon further deforming the substrate with 200% tensile strain, the coated fibrous substrate became more adhesive with OCA hysteresis of 16° as shown in Fig. 3.3F-G.

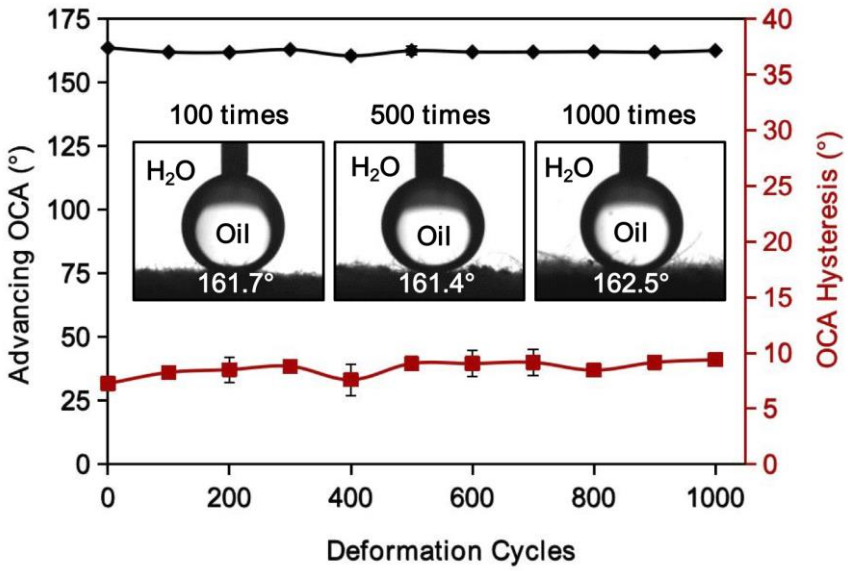

Figure 3.4: The plot illustrating the change in both advancing OCA and OCA hysteresis of beaded oil droplet on the biomimicked super-oil-repellent interface after incurring 1000 times of physical deformation with 150% of tensile strain.

Nevertheless, the stretched interfaces again restored their non-adhesive super-oil-repellence under water with an OCA hysteresis below 10º after releasing the tensile strain. As the bio-mimicked interface was capable of withstanding up to 150% of tensile deformation, so the same interface was manually and repetitively deformed with 150% tensile strain, and the underwater advancing OCA was examined on the stretchable interface after every 100 times of tensile deformations as shown in Fig. 3.4. The synthesized underwater superoleophobic coating continued to display non-adhesive extreme oil-repellence under water with advancing OCA of well above 160º and an OCA hysteresis of below 10º, even after deforming the interfaces with 150% tensile strain for 1000 times, as observed in Fig. 3.4.

3.3.2. Physical and chemical durability of stretchable 'fish-scale'- mimicked interfaces

Furthermore, the stretchable interface, embedded with 'fish-scale'-inspired wettability, was exposed to various other commonly practiced and widely accepted physical insults, including bending, twisting, creasing, and winding. The extreme oil-repellence of the as-synthesized material was found

to be capable of surviving all these practically relevant physical challenges with advancing OCA of above 160º and OCA hysteresis below 10º, as shown in Fig. 3.5. Thereafter, the coated fibrous substrate was exposed to some standard abrasion tests that are highly relevant for outdoor applications of such biomimicked interface.[15,16] This stretchable underwater superoleophobic interface was subjected to abrasive sandpaper test, sand drop test and adhesive tape-peeling test. However, the fish scale-mimicked wettability remained unperturbed, as shown in Fig. 3.6. First, the abrasive sandpaper (2 cm x 1 cm) was rubbed manually over the top surface of the stretchable fibrous substrate with back and forth motion, repetitively (5 times) with a constant applied load of 700 g (equivalent to 34 kPa applied pressure); the applied pressure helped in maintaining the homogeneous and uniform contact between the abrasive sandpaper surface and the surface of biomimicked coating. However, no

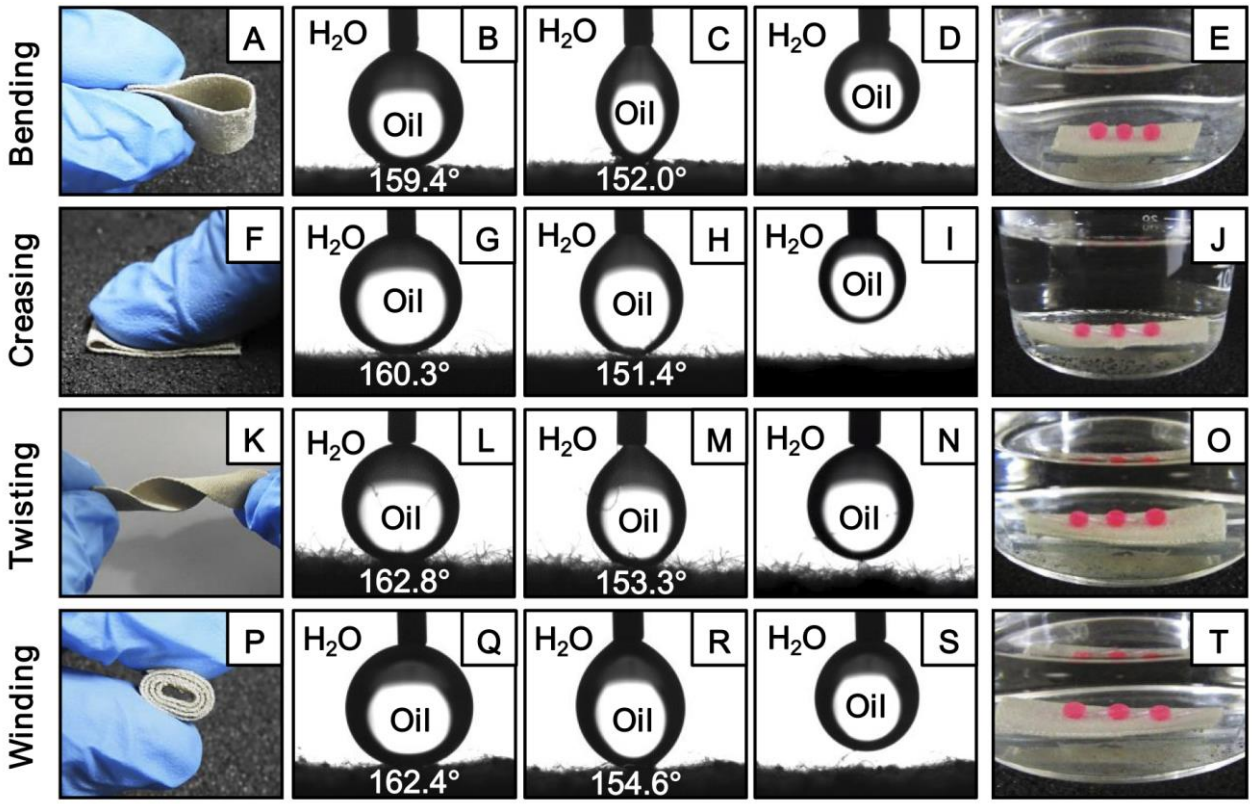

Figure 3.5: (A,F,K,P) Digital images illustrating various physical manipulation on highly stretchable underwater superoleophobic interfaces. (B-D,G-I,L-N,Q-S) Advancing (B,G,L,Q) and receding (C-D,H-I,M-N,R-S) CA images of beaded oil droplet on the physically manipulated (bended: B-D, creased: G-Z, twisted: L-N, winded: Q-S) underwater oil-repellent interface. (E,J,O,T) Digital images of beaded oil droplets on the biomimicked interfaces after performing various physical deformations—including bending (E), creasing (J), twisting (O) and winding (T).

noticeable change in underwater oil wettability was observed; instead, the oil droplets (red colour aided visual inspection) that beaded on the interface with advancing OCA of above 160º completely receded to the oil-dispensing needle without breaking or leaving the droplet on the biomimicked interfaces, as shown in Fig. 3.6B-D. This simple demonstration unambiguously revealed the appropriate coexistence

of hierarchical topography and high surface energy chemistry, which was essential to achieve such robust extreme oil repellency even after performing these severe physical abrasion tests. Next, this 'fish-scale'-inspired artificial interface was exposed to a continuous stream of sand grains (100 g) from a height of 25 cm (Fig. 3.6F) and then, the oil-wettability was examined under water. The red coloured (aids visual inspection) oil droplets were beaded on the sand-treated interfaces with advancing OCA of 161º and an OCA hysteresis below 10º, as shown in Fig. 3.6G–J. Next, the as-synthesized material

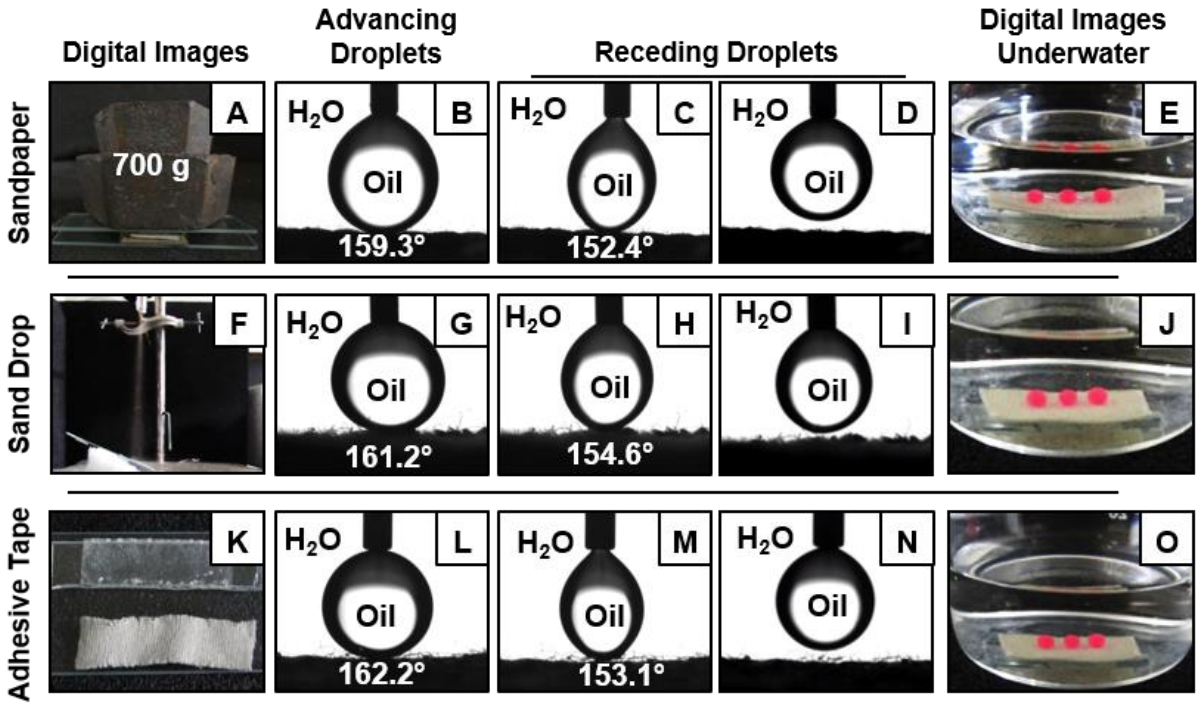

Figure 3.6: (A,F,K) Digital images depicting various physical abrasion tests—including sandpaper abrasion (A), sand drop (F) and adhesive tape peeling (K) tests, on the as-synthesised underwater super-oil-repellent interface. (B-D,G-I,L-N) Advancing (B,G,L) and (C-D,H-I,M-N) receding CA images of beaded oil droplet on the coated fibrous substrates after conducting the sandpaper abrasion (B-D), sand drop (G-I) and adhesive tape peeling (L-N) tests. (E,J,O) Digital images of beaded oil droplets under water on the stretchable biomimicked interface after the performance of various abrasive tests—including sandpaper abrasion test (E), sand drop test (J) and adhesive tape peeling test (O).

was subjected to another severe physical abrasion test, that was, the adhesive tape peeling test (Fig. 3.6K) in order to create a random rupture of the interface, in which the freshly exposed adhesive surface was placed in contact with the biomimicked interface. Then, a 700 g load was applied over 2 cm^2 area of the as-synthesized underwater superoleophobic coating to facilitate the contact between the material and the adhesive surface. The applied pressure (34 kPa) was significantly higher as compared to other reported demonstrations.[15] After peeling off the adhesive tape from the biomimicked interface, some whitish polymeric material was found on the adhesive surface, which was mostly transferred from the edge of the material (Fig. 3.6K). Thus, the edge of the fibrous material was found to be physically distorted, as shown in Fig. 3.6K. However, no change in underwater oil

wettability was noticed on the as-synthesized material, including the distorted edges and other areas of the material. Even after the adhesive tape test, the randomly abraded interface was able to maintain extreme oil repellence with OCA of 162º, as shown in Fig. 3.6L–O and the whole droplet receded to the needle without any fragmentation of the beaded oil droplet on the biomimicked interfaces. Then, the same biomimicked interface was repetitively subjected to adhesive tape-peeling test for multiple

Physical Insults	$\theta_{adv.}$ (°)	$\theta_{hys.}$ (°)
Cold Oil (10°C)	159.3 ± 0.2	5.8 ± 1.0
Hot Oil (100°C)	161.7 ± 0.3	7.5 ± 0.6
Hot water treatment (100°C)	160.2 ± 0.4	7.3 ± 1.1
Cold water treatment (10°C)	159.6 ± 0.4	7.0 ± 0.4

Table 3.1: Accounting advancing OCA ($\theta_{adv.}$) and OCA hysteresis ($\theta_{hys.}$) of the biomimicked wettability in the coated interface after the exposures of extremes of temperature (e.g. cold oil (10°C), hot oil (100°C), treatments of hot (100°C) and cold (100°C) aqueous phase for 6 hours).

times, and the underwater oil wettability was investigated after regular intervals of every 10 times of this test. Even after successive adhesive tape peeling test for 90 times, the non-adhesive underwater superoleophobicity was unperturbed in the as-synthesized fibrous substrate with advancing OCA of above 155º and an OCA hysteresis of below 10º. Generally, the 'lotus leaf'-inspired superhydrophobic interfaces that are well recognized for extremely repelling liquid water droplets in air are found to

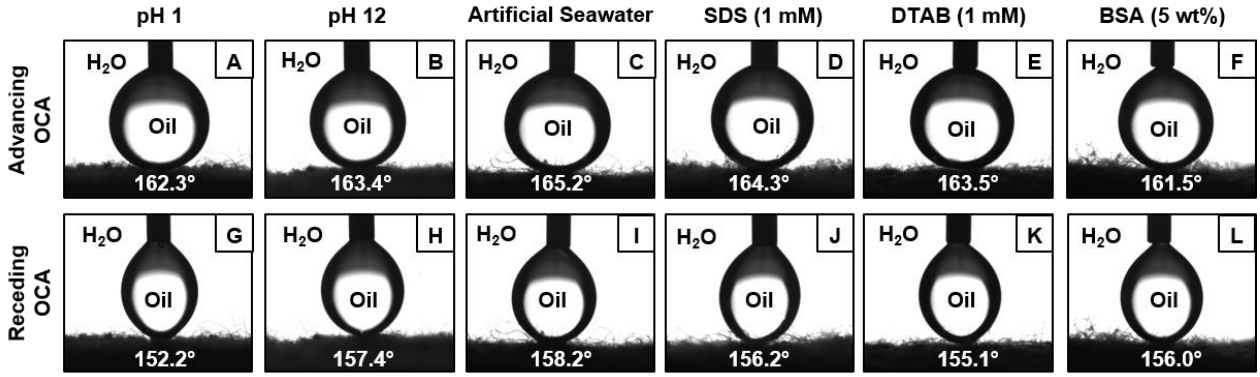

Figure 3.7: (A-L) Advancing (A-F) and receding (G-L) OCA images of beaded oil droplet on the biomimicked super-oil-repellent interface—after treating with different chemically complex harsh environments—including highly acidic (pH 1, A,G) water, highly alkaline (pH 12, B,H) water, artificial seawater (C,I), surfactants (sodium dodecyl sulfate (SDS; D,J) and dodecyltrimethylammonium bromide (DTAB; E,K)) contaminated (1 mM) aqueous phases and bovine serum albumin (BSA; F,L) contaminated water (5 wt%) for continuous 10 days.

compromise its biomimicked wettability at extreme temperatures due to the instability of the meta-stable trapped air present in the hierarchical interface.[51,52] In contrast, the 'fish-scale' mimicked wettability that mainly arises due to confinement of the aqueous phase in appropriately chemically modulated hierarchical topography,[14] was found to be highly stable even after exposure to cold (10ºC)

and hot (100ºC) oils as noted in Table 3.1. The as-synthesized stretchable underwater superoleophobic interfaces were continuously exposed to extremes of temperature for 6 hours, and the embedded underwater superoleophobicity remained intact with advancing OCA of above 160º and OCA hysteresis of below 10º, as shown in Table 3.1. This inherent stability of such biomimicked wettability in the as-synthesized material would be appropriate for prospective applications in outdoor scenarios, including various severe physically/chemically challenging settings. Next, the coated fibrous substrate was submerged into different chemically complex aqueous phases, prior to examining their impact on the underwater super-oil-repellency. The artificially designed biomimicked wettability remained unaffected with advancing OCA of above 160º (as shown in Fig. 3.7A-F) even after continuous and prolonged (10 days) exposure of the as-synthesized underwater superoleophobic interface to various chemically harsh aqueous phases, including highly acidic (pH 1; Fig. 3.7A and G) phase, alkaline (pH 12; Fig. 3.7B and H) phase, artificial seawater (35% salinity, composed of various metal salts; Fig. 3.7C and I) and surfactants (SDS (Fig. 3.7D,J) and DTAB (Fig. 3.7E,K); 1 mM) contaminated aqueous phases. This impeccable chemical durability of the artificial 'fish-scale'-inspired wettability is

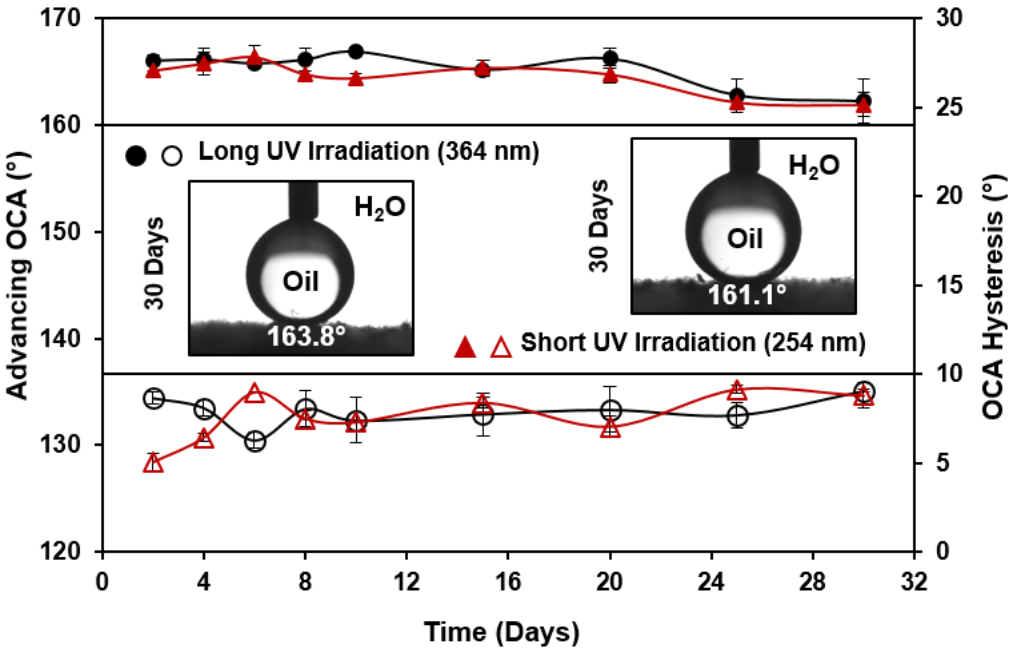

Figure 3.8: Accounting the impact of prolonged (30 days) exposure of both long (wavelength 364 nm) and short (wavelength 254 nm) UV irradiations on the underwater superoleophobic coating.

attributed to the strategic design of the covalently cross-linked hierarchical topography, which was further optimized with essential chemistry via 1,4-conjugate addition reaction. In this particular design, glucamine molecules that have an inherent ability to prevent the adhesion of proteins and microorganisms[53,54] were strategically integrated into the reactive multilayer (a) to make the

hierarchical topography highly water-compatible and (b) to protect such interfaces from any unwanted deposition of chemicals (e.g. proteins, and surfactants). As a result, the underwater anti-oil-fouling property was preserved even after prolonged (10 days) exposure to BSA protein (5 wt%; Fig 3.7F and L) contaminated aqueous phase. The investigation of the effect of UV irradiation on the coated fibrous substrate was another important and relevant durability test with regard to its prospective outdoor applications. The 'fish-scale'-mimicked interface was exposed to both short (254 nm) and long (364 nm)-UV radiation for 30 days, and the advancing OCA and OCA hysteresis were examined at regular intervals. The anti-oil-fouling property remained unaltered with the advancing OCA of above 160º, as

Physical and Chemical Manipulations On Stretchable PU Fibrous Substrate with 150% Strain

Physical Insults	% Strain	$\theta_{adv.}$ (°)	$\theta_{hys.}$ (°)
Bending	150	159.3 ± 0.1	7.8 ± 0.8
Creasing	150	159.6 ± 0.4	8.8 ± 1.1
Twisting	150	160.4 ± 1.2	8.0 ± 0.2
Winding	150	160.3 ± 0.4	6.3 ± 1.5
Sandpaper	150	159.9 ± 0.8	6.1 ± 1.5
Sand Drop	150	159.3 ± 0.1	5.8 ± 0.4
Adhesive Tape	150	160.7 ± 1.1	7.2 ± 0.8
Acidic Water (pH=1)	150	159.4 ± 0.2	8.9 ± 0.9
Basic Water (pH=12)	150	159.2 ± 0.1	6.1 ± 0.4
Artificial Sea Water	150	160.5 ± 0.2	7.3 ± 0.0
SDS Water	150	160.1 ± 0.2	7.0 ± 0.5
DTAB Water	150	159.7 ± 0.6	6.3 ± 0.7
BSA (5 wt%) Water	150	159.2 ± 0.5	7.8 ± 0.1

Table 3.2: Accounting the effect of tensile deformation (150%) on the underwater superoleophobic interface that were pre-treated with various and severe other physical and chemical insults.

shown in Fig. 3.8. Furthermore, the stretchable underwater superoleophobic interfaces, which were pre-treated with various physical abrasions and chemical treatments, were exposed to large (150% tensile strain) physical deformation. However, the embedded 'fish-scale'-inspired wettability remained unperturbed, as noted in Table 3.2. The exemplary physical, chemical and mechanical durability of the as-synthesized interface with 'fish-scale'-mimicked wettability is expected to greatly enhance its performance in practically relevant challenging settings.

3.3.3. Oil/water separation under practically relevant severe conditions

Industrial waste-water discharge with oil/oily contaminants and oil spillage accidents are severely polluting the environment and have raised serious concerns across the world in the recent past. To the best of our knowledge, there are some existing approaches to remove oil contaminants

from the aqueous phase, but most of them are energy-inefficient and/or other causing secondary pollutions in the environment. As an alternative, biomimicked interfaces have emerged as a prospective candidate for energy-efficient and eco-friendly separation of oil/water mixtures. Though the 'lotus leaf'-inspired wettability has been useful in selective filtration and collection of oil from oil/water mixtures, the 'fish-scale'-mimicked wettability has allowed to selectively filtrate aqueous phase from various forms (i.e., floating oil, sediment oil and emulsified oil) of oil/water mixture even at practically relevant extremely challenging conditions.

However, the demonstrations of oil/water separation in practically relevant different severe settings are limited in the literature. In this chapter, the highly durable and stretchable fibrous substrate was used as a membrane for energy-efficient and eco-friendly collection of oil-free aqueous phases in various physically and chemically harsh scenarios. In this demonstration of oil/water separation, a prototype was developed by customizing a falcon tube (50 mL capacity), where the opening of the falcon tube was wrapped with the 'fish-scale'-inspired stretchable membrane for selective filtration of the aqueous phase from various oil/water mixtures, and a side hole was made near the closed end of the tube for both (1) pouring the oil/ water mixture and (2) collecting the residual oil phase, simply by tilting the falcon tube and rotating the side hole of the tube upside down (Fig. 3.9). To facilitate the

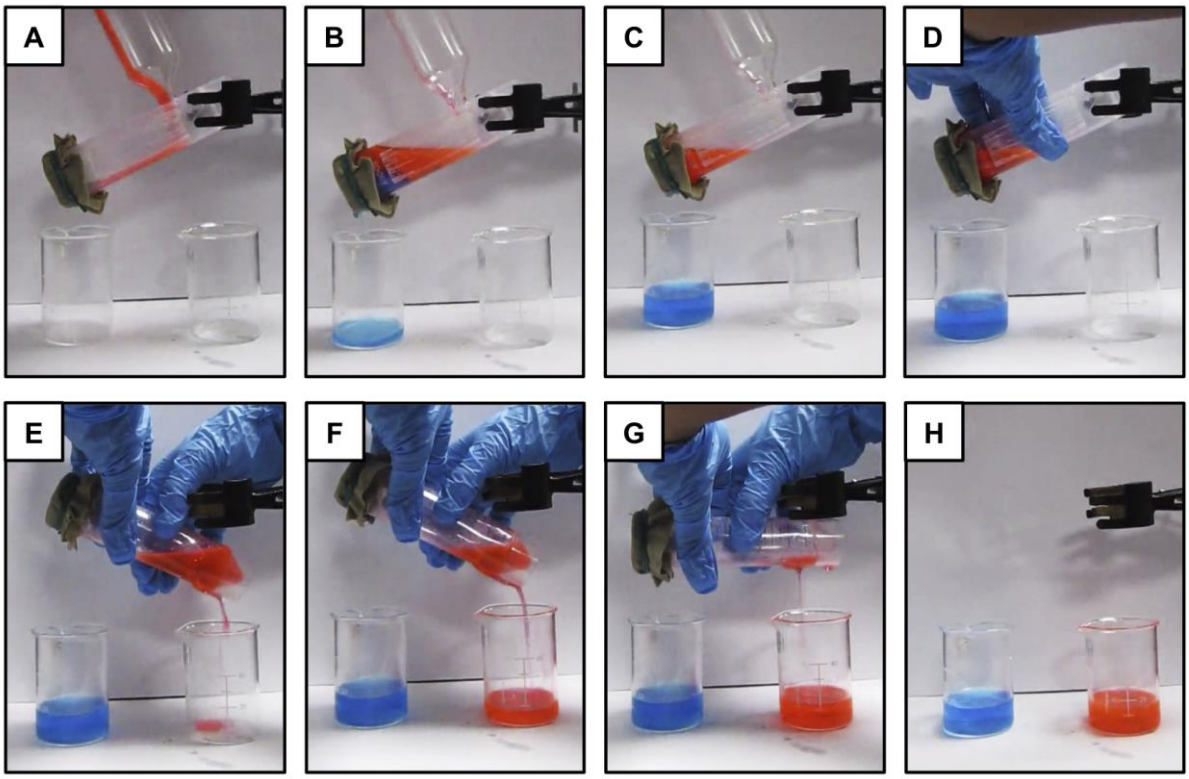

Figure 3.9: (A-H) Digital images depicting the selective filtration/collection (A-C) of aqueous phase (dyed with methylene blue) from oil (soybean oil, dyed with Nile red)/water mixture. (D-H) Digital images illustrating the collection of water-free residual oil phase in a separate container through the side hole of the prototype.

gravity-driven and eco-friendly oil/water separation, the prototype was tilted at 25º angle. Moreover, the end of the tube, which was wrapped with the underwater superoleophobic membrane, was kept at

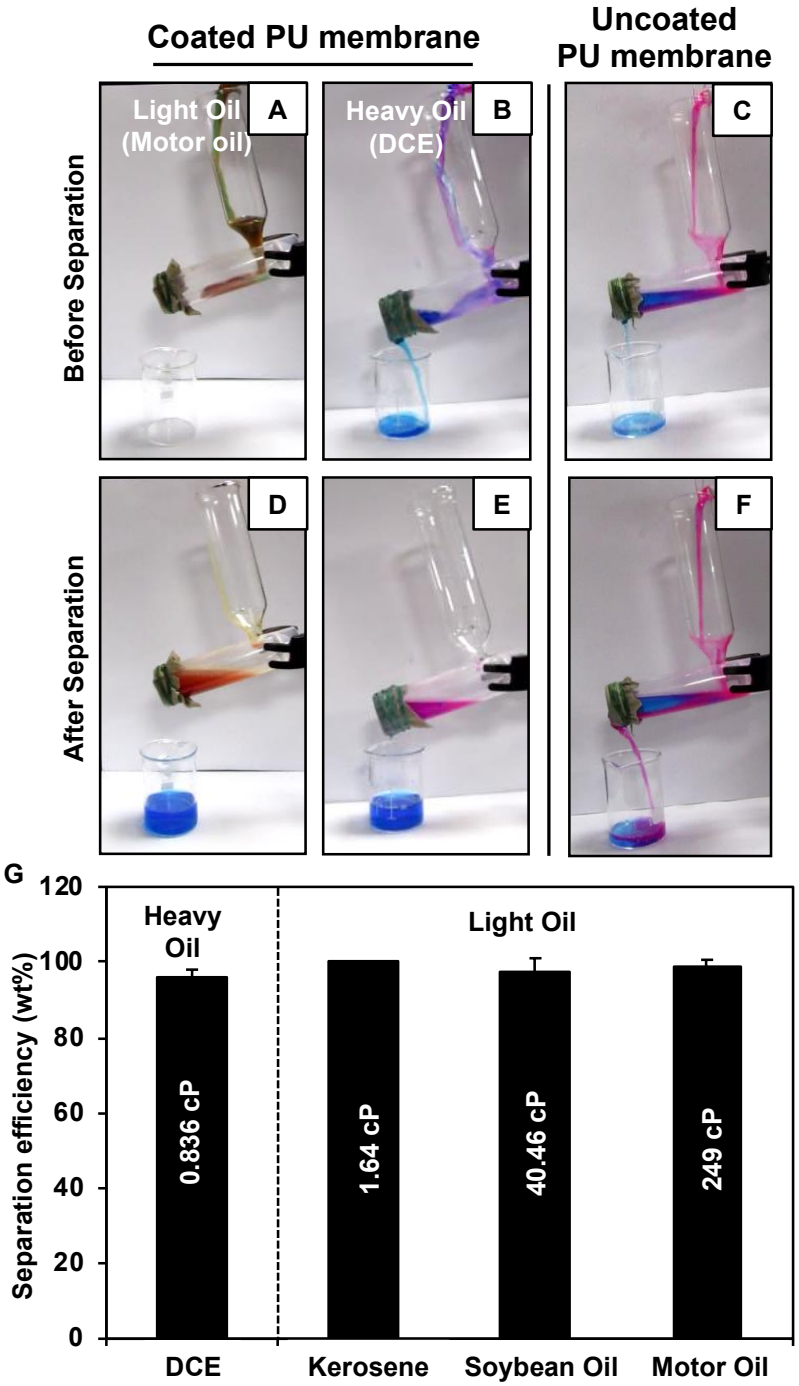

Figure 3.10: (A-B,D-E) Digital images illustrating the gravity-driven selective filtration/collection of aqueous phase (methylene blue dye aided visual inspection) from oil/water mixtures, where both light (A,D) and heavy (B,E) oils (Nile red aids visual inspection) were individually used for preparing respective oil/water mixture. (C,F) However, the uncoated membrane allowed to pass both oil and water phases. (G) Plot accounting the performance of oil/water separation through the biomimicked interface, irrespective of the viscosity of the used oil phases.

a downslope, as shown in Fig. 3.10A. The oil-water mixture consisting of both light and heavy oils was poured from the side hole with the help of a funnel. This resulted in the selective passage of the

aqueous phase through the 'fish-scale'-mimicked stretchable membrane (Fig. 3.10A and B) and the aqueous phase was collected in a separate beaker (placed under the prototype), as shown in Fig. 3.10D and E. The residual oil phase was extremely repelled by the super-oil-repellent membrane and was

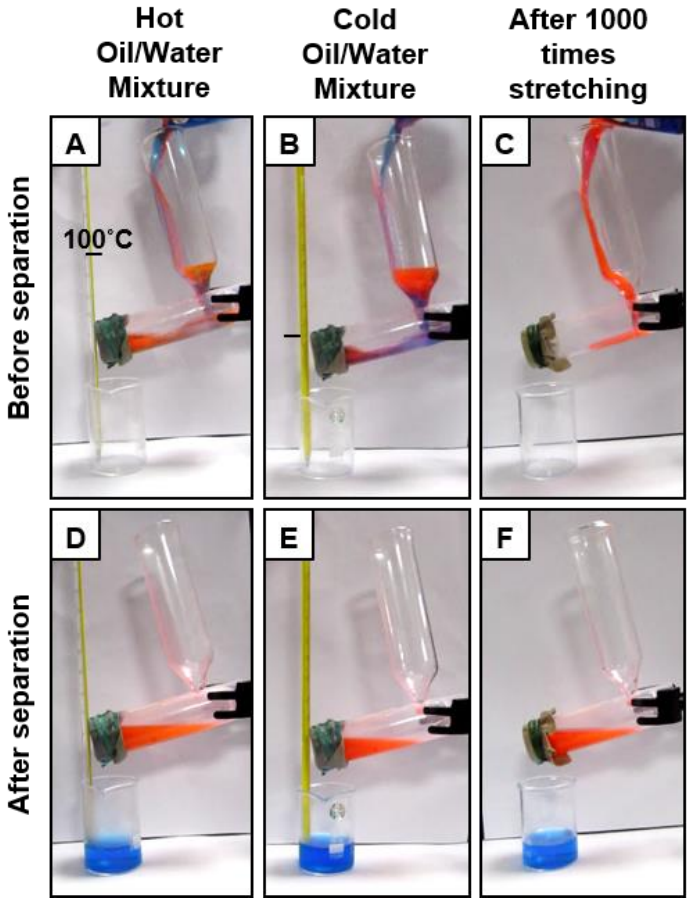

Figure 3.11: (A-B,D-E) Digital images demonstrating the successful oil (dyed with nile red dye) / water (dyed with methylene blue) separation through biomimicked interfaces at high (100°C; A,D) and low (10°C; B,E) temperatures. (C,F) Digital images accounting the oil/water separation performance of the 'fish-scale' mimicked interface—which was repetitively exposed to high (150 %) tensile deformation for 1000 times.

collected in another separate beaker by a downward rotation of the side hole of the prototype, as shown in Fig. 3.9. However, the uncoated fibrous substrate which soaked oil under water (Fig. 3.2C-D), was incapable of separating the oil from the aqueous phase as both the oil and water phases easily passed through the membrane, as shown in Fig. 3.10C,F. The prototype, wrapped with the coated membrane having stretchable 'fish-scale'-mimicked wettability, was found to be highly efficient in separating the oil/water mixture irrespective of the density and viscosity of the oils that were used in the preparation of the oil/water mixtures. The separation efficiency was measured to be above 99 wt% on an average, as shown in Fig. 3.10G. Then, the same prototype was used for the separation of oil/water mixtures under severe physical and chemical conditions to simulate the harshness might be faced during outdoor applications. A variation in the temperature is a practical issue and some of the bioinspired interfaces

are prone to loss of anti-wettability under extreme conditions of temperature.[51,52] However, the as-synthesized underwater superoleophobic coating on fibrous substrate remained highly capable of surviving the exposures of extremes of temperatures, without compromising the anti-oil-fouling property under water. Therefore, oil/water separation at both high and low temperatures was demonstrated with the current prototype, where both the hot (100ºC) and cold (10ºC) aqueous phases (blue colour aided visual inspection of water phase) were selectively and efficiently filtrated through the underwater superoleophobic membrane, as shown in Fig. 3.11A-B,D-E. Then, the underwater superoleophobic membrane, which was manually and repetitively deformed with 150% tensile strain for 1000 times, was used for demonstrating the oil/water separation performance. The membrane was noticed to be efficient in complete separation of the aqueous phase from the oil/water mixtures (red colour aids visual inspection of oil phase) even after incurring successive tensile deformations, as shown in Fig. 3.11C,F. Next, the current prototype was further used to investigate the oil/water separation performance, where the aqueous phases were contaminated with harsh chemicals. Highly acidic (pH 1)/alkaline (pH 12) aqueous phases, artificial seawater and river water were successfully

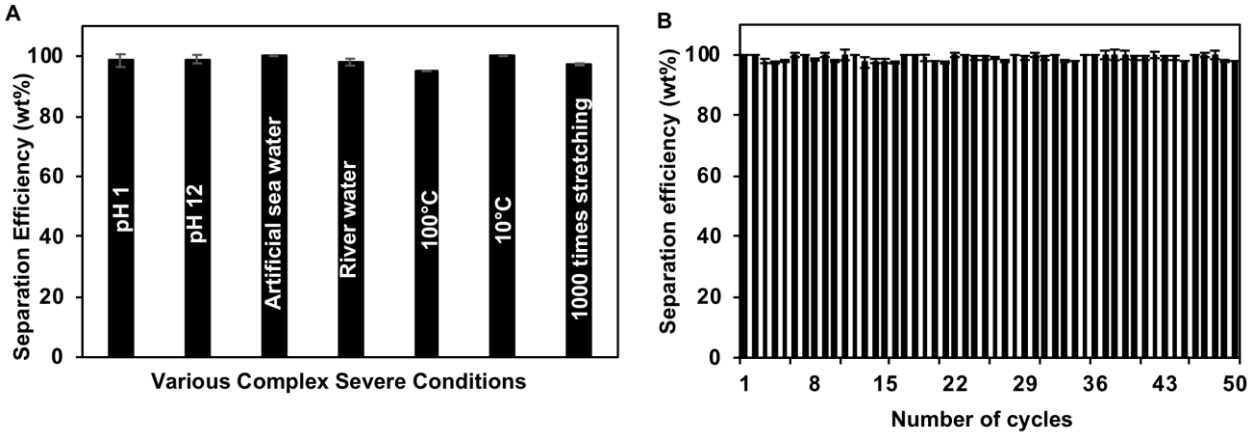

Figure 3.12: (A) The bar graph depicting the water separation efficiency (wt%) from bulk oil/water mixtures under various practically relevant severe conditions. (B) The plot estimating the water separation efficiency (wt%) after repetitive separation of oil/water mixtures using the same biomimicked membrane for consecutive 50 times.

separated from the respective oil contaminated aqueous phases by using the superoleophobic membrane, where the separation efficiency was calculated to be 99%, as shown in 3.12A. Moreover, the current prototype was repetitively used for separating the aqueous phase from the contaminated oil phase for 50 times (Fig. 3.12B). The same stretchable membrane, decorated with 'fish-scale'-mimicked wettability, was repetitively used in oil/water separation processes without washing or application of any additional treatment, and there was barely any change in the selective filtration performance. Thus, the current approach provided a highly prospective biomimicked interface for outdoor applications, and it remained efficient for performing at practically relevant

physically/chemically challenging scenarios. Among other forms of oil contaminations, emulsified

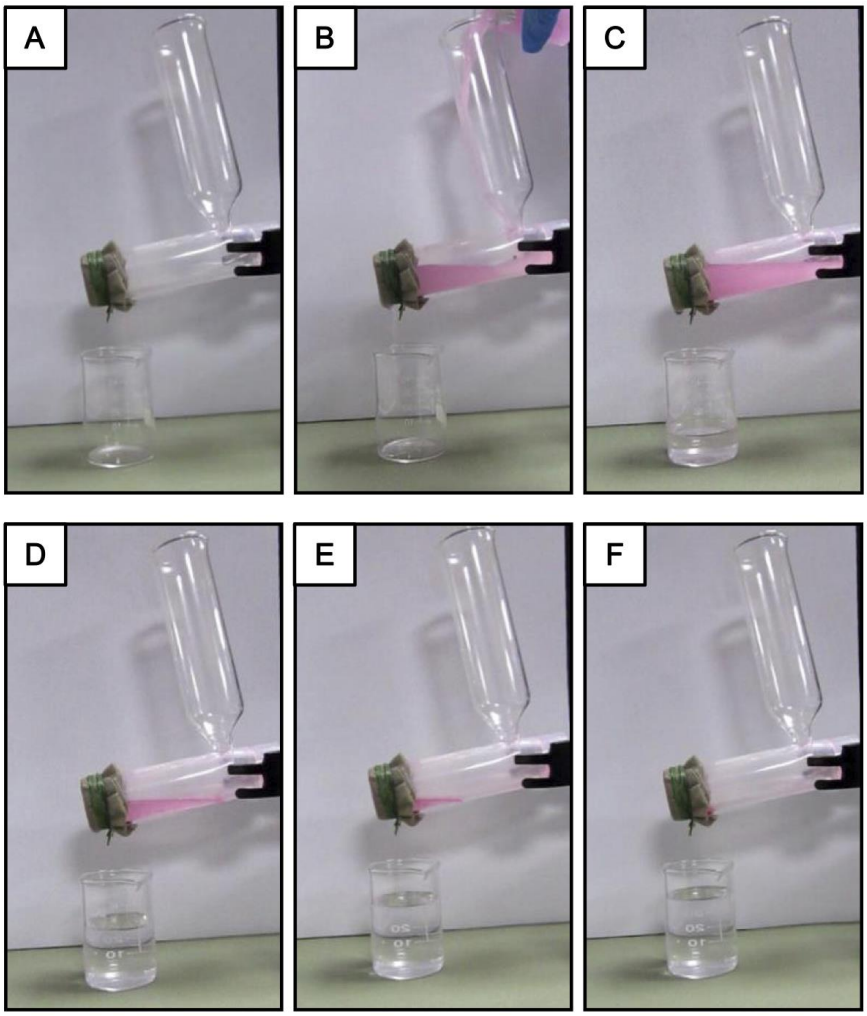

Figure 3.13: (A-F) Digital images demonstrating the ability of the underwater extreme oil-repellent membrane in the oil-in-water emulsion separation, where the emulsion solution consisted of 2% (v/v) of DCE dyed with water-insoluble Nile red.

form is the most difficult to separate. So, the current setup was extended to investigate the performance of this underwater superoleophobic membrane for oil-in-water emulsion separation. While, the 'lotus leaf'-inspired extremely water-repellent interfaces are inherently incapable of separating oil droplets that are dispersed in the aqueous phase, but the 'fish-scale'- inspired wettability has been successfully explored in the separation of oil-in-water emulsion droplets in the recent past.[11,55] As expected, the stretchable underwater superoleophobic interface was observed to be highly efficient in removing oil droplets (with a diameter ranging from 600 nm to 3500 nm, coloured using Nile red for facilitating the visual inspection) that were suspended in the aqueous phase, as shown in Fig. 3.13. Further, the separated aqueous phase was examined using an optical fluorescence microscopy. The oil droplets that were present initially (refereeing before separation process) in the oil-in-water emulsion were completely removed from the separated aqueous phase, which was confirmed using the fluorescence

images (Fig. 3.14A-B) and DLS (Fig. 3.14C) study, where the oil phase was labelled with the water immiscible Nile red dye. Thus, the synthesized underwater superoleophobic membrane has a high

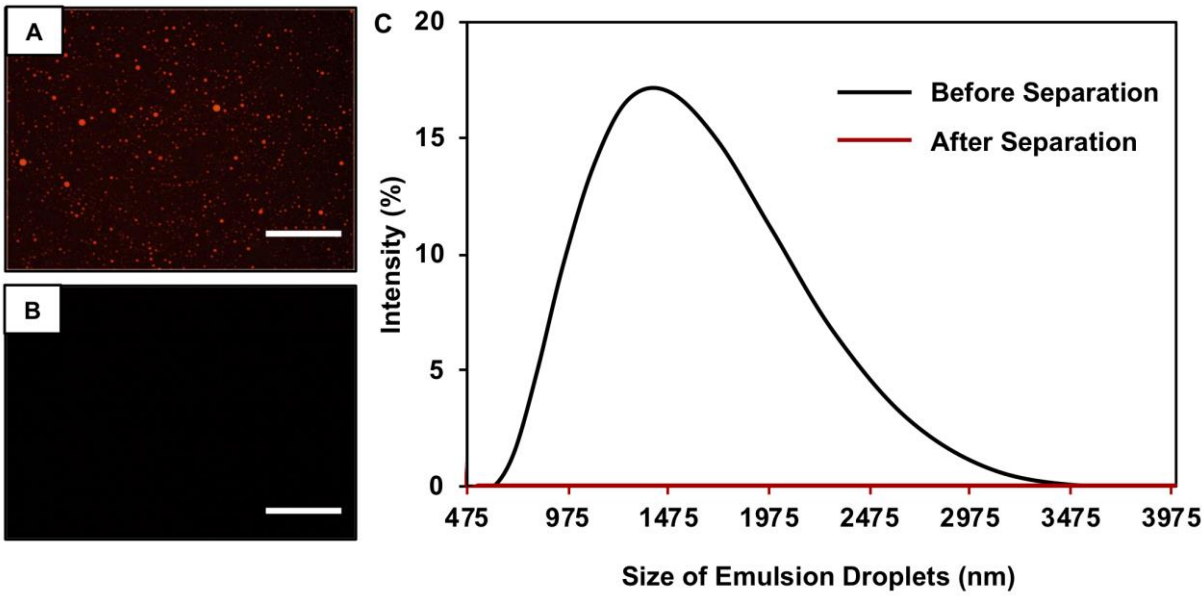

Figure 3.14: (A-B) Fluorescence microscope images (scale bar: 100 μm) of the oil-in-water emulsion before (A) and after (B) performing the filtration through underwater superoleophobic membrane. The model oil phase was labelled with water immiscible Nile red dye. (C) Accounting the DLS study of oil-in-water emulsion before (black curve) and after (red curve) filtration through the as-synthesized biomimicked membrane.

potential for removing oil/oily contaminants from various forms of oil/water mixtures in various severe and challenging scenarios.

3.4. Conclusion

In summary, the Chapter 3 introduced a simple approach to artificially synthesize a highly stretchable and durable 'fish-scale'-mimicked underwater oil-repellent membrane for gravity-driven filtration of oil/water mixtures. In general, the synthesis of a durable and scalable underwater superoleophobic interface is highly challenging by following the commonly used polymer-based hydrogel and metal-oxide-based approaches. In this chapter, a covalently cross-linked multilayer of 'reactive' polymeric NC was strategically constructed onto a fibrous and stretchable substrate through successive and rapid 1,4-conjugate addition reaction between amine groups of the BPEI polymer and residual acrylate groups of the polymeric NC. The acrylate functional groups in the as-synthesized material enabled the integration of desired chemical properties via covalent bond formation and eventually, the fibrous substrate was embedded with chemically/physically robust underwater superoleophobicity. The wet hierarchical interface was capable of surviving 150% tensile strain under water without compromising the extreme oil-repellent property. Moreover, the bioinspired wettability remained unaffected in various other physically/chemically complex scenarios, including bending, twisting, winding,

creasing, exposure to extremes of temperatures (100ºC and 10ºC), pH (1 and 12), artificial seawater, river water, and prolonged exposure to UV radiation. Thus, the current material has immense potential for outdoor applications, and this special interface was successfully employed to separate various forms of oil/water mixtures with high separation efficiency (99%) even under practically relevant severe conditions. This current approach could be promising in designing various other functional and smart materials for prospective outdoor and indoor applications, including design of super-oil-repellent smart textiles and anti-oil/bio-fouling coatings on stretchable substrates for various submarine- and biomedical-related prospective applications.

3.5. References

(1) J. A. Rogers, T. Someya and Y. Huang, *Science*, 2010, **327**, 1603.

(2) J.-Y. Sun, X. Zhao, W. R. K. Illeperuma, O. Chaudhuri, K. H. Oh, D. J. Mooney, J. J. Vlassak and Z. Suo, *Nature*, 2012, **489,** 133.

(3) M. L. Hammock, A. Chortos, B. C.-K. Tee, J. B.-H. Tok and Z. Bao, *Adv. Mater*., 2013, **25**, 5997.

(4) X. Shi, L. Li, S. Ostrovidov, Y. Shu, A. Khademhosseini and H. Wu, *ACS Appl. Mater. Interfaces*, 2014, **6**, 11915.

(5) Z. Pan, T. Wang, S. Sun and B. Zhao, *ACS Appl. Mater. Interfaces*, 2016, **8**, 1795.

(6) Y. Liu, M. Pharr and G. A. Salvatore, *ACS Nano*, 2017, **11**, 9614.

(7) T. Sun, L. Feng, X. Gao and L. Jiang, *Acc. Chem. Res*., 2005, **38,** 644.

(8) X. Zhang, F. Shi, J. Niu, Y. G. Jiang and Z. Q. Wang, *J. Mater. Chem*., 2008, **18**, 621.

(9) K. Liu, X. Yao and L. Jiang, *Chem. Soc. Rev*., 2010, **39**, 3240.

(10) E. Ueda and P. A. Levkin, *Adv. Mater*., 2013, **25**, 1234.

(11) L. Wen, Y. Tian and L. Jiang, *Angew. Chem. Int. Ed*., 2015, **54**, 3387.

(12) K. Chen, S. Zhou and L. Wu, *ACS Nano*, 2016, **10**, 1386.

(13) L. Gao and T. J. McCarthy, *Langmuir*, 2006, **22**, 2966.

(14) M. J. Liu, S. T. Wang, Z. X. Wei, Y. L. Song and L. Jiang, *Adv. Mater.*, 2009, **21**, 665.

(15) T. Verho, C. Bower, P. Andrew, S. Franssila, O. Ikkala, R. H. A. Ras, *Adv. Mater.*, 2011, **23**, 673.

(16) X. Tian, T. Verho, R. H. A. Ras, *Science*, 2016, **352**, 142.

(17) S. J. Cho, H. Nam, H. Ryu and G. Lim, *Adv. Funct. Mater*., 2013, **23,** 5577.

(18) Z. Jianfeng, R. Seunghwa , P. Nicola, W. Qiming, T. Qing, J. B. Markus and Z. Xuanhe, *Nat. Mater.*, 2013, **12**, 321.

(19) D. Wu, S. Wu, Q. Chen, Y. Zhang, J. Yao, X. Yao, L. Niu, J. Wang, L. Jiang and H. Sun, *Adv. Mater.*, 2011, **23,** 545.

(20) E. Joseph. W. Mates, S. I. Bayer, J. M. Palumbo, J. Patrick, C. Carroll and M. Megaridis, *Nat. Comm.*, 2015, **6**, 8874.

(21) L. Lin, M. J. Liu, L. Chen, P. P. Chen, J. Ma, D. Han and L. Jiang, *Adv. Mater.*, 2010, **22**, 4826.

(22) Z. Xue, S. Wang, L. Lin, L. Chen, M. Liu, L. Feng and L. Jiang, *Adv. Mater.*, 2011, **23**, 4270.

(23) Y. Cai, Q. Lu, X. Guo, S. Wang, J. Qiao and L. Jiang, *Adv. Mater.*, 2015, **27**, 4162.

(24) K. Chen, S. Zhou and L. Wu, *ACS Nano*, 2016, **10**, 1386.

(25) S. Gao, J. Sun, P. Liu, F. Zhang, W. Zhang, S. Yuan, J. Li and J. Jin, *Adv. Mater.*, 2016, **28**, 5307.

(26) D. Zang, H. Yi, Z. Gu, L. Chen, D. Han, X. Guo, S. Wang, M. Liu, and L. Jiang, *Adv. Mater.*, 2017, **29**, 1602869.

(27) X. Yuan, W.-C. Nie, C. Xu, X.-H. Wang, Q. Xiao, F. Song, X.-L. Wang, and Y.-Z. Wang, *Adv. Funct. Mater*., 2018, **28,** 1704956.

(28) X. Liu, J. Zhou, Z. Xue, J. Gao, J. Meng, S. Wang and L. Jiang, *Adv. Mater.*, 2012, **24**, 3401.

(29) Z. Cheng, H. Lai, Y. Du, K. Fu, R. Hou, C. Li, N. Zhang and K. Sun, *ACS Appl. Mater. Interfaces*, 2014, **6**, 636.

(30) J. Yong, F. Chen, Q. Yang, U. Farooq and X. Hou, *J. Mater. Chem. A*, 2015, **3**, 10703.

(31) K. Han, L. Heng, and L. Jiang, *ACS Nano*, 2016, **10**, 11087.

(32) X. Meng, and D. Deng, *J. Mater. Chem. A*, 2016, **4,** 6919.

(33) C.-L. Xu and Y.-Z. Wang, *J. Mater. Chem. A*, 2018, **6**, 2935.

(34) S. Zhang, G. Jiang, S. Gao, H. Jin, Y. Zhu, F. Zhang, and J. Jin, *ACS Nano*, 2018, **12**, 795.

(35) L.-P. Xu, J. Peng, Y. Liu, Y. Wen, X. Zhang, L. Jiang, and S. Wang, *ACS Nano*, 2013, **7**, 5077.

(36) T. Guo, L. Heng, M. Wang, J. Wang and L. Jiang, *Adv. Mater*., 2016, **28**, 8505.

(37) X. Meng, M. Wang, L. Heng, and L. Jiang, *Adv Mater*., 2018, **30**, 1706634.

(38) M. Shokeen, E. D. Pressly, A. Hagooly, A. Zheleznyak, N. Ramos, A. L. Fiamengo, M. J. Welch, C. J. Hawker, and C. J. Anderson, *ACS Nano*, 2011, **5**, 738.

(39) C. Feng, X. Pang, Y. He, B. Li and Z. Lin, *Chem. Mater.*, 2014, **26**, 6058.

(40) Y. Chen, Y. J. Yoon, X. Pang, Y. He, J. Jung, C. Feng, G. Zhang and Z. Lin, *Small*, 2016, **12**, 6714.

(41) A. M. Rather, S. Mahato, K. Maji, N. Gogoi and U. Manna, *Nanoscale*, 2017, **9**, 16154.

(42) Y. Chen, D. Yang, Y. J. Yoon, X. Pang, Z. Wang, J. Jung, Y. He, Y. W. Harn, M. He, S. Zhang, G. Zhang and Z. Lin, *J. Am. Chem. Soc*., 2017, **139**, 12956.

(43) A. M. Rather and Uttam Manna, *Chem. Mater*., 2016, **28**, 8689.

(44) A. M. Rather, N. Jana, S. Begum, H. K. Srivastava and U. Manna, *Green Chem*., 2017, **19**, 4527.

(45) D. Parbat and U. Manna, Chem. Sci., 2017, **8**, 6092.

(46) S. L. Bechler and D. M. Lynn, *Biomacromolecules*, 2012, **13**, 1523. H.-W. Engels, H.-G. Pirkl, R. Albers, R. W. Albach, J. Krause, A. Hoffmann, H. Casselmann, and J. Dormis, *Angew. Chem. Int. Ed*., 2013, **52**, 9422.

(48) P. Calcagnile, D. Fragouli, I. S. Bayer, G. C. Anyfantis, L. Martiradonna, P. D. Cozzoli, R. Cingolani, and A. Athanassiou, *ACS Nano*, 2012, **6**, 5413.

(49) Q. Zhu, Y. Chu, Z. Wang, N. Chen, L. Lin, F. Liu and Q. Pan, *J. Mater. Chem. A*, 2013, **1**, 5386.

(50) L. Wu, L. Li, B. Li, J. Zhang, and A. Wang, *ACS Appl. Mater. Interfaces*, 2015, **7**, 4936.

(51) Y. Liu, X. Chen and J. H. Xin, *J. Mater. Chem.*, 2009, **19**, 5602.

(52) P. Papadopoulos, L. Mammen, X. Deng, D. Vollmer, H.-J. Butt, *Proc. Natl. Acad. Sci. U.S.A*, 2013, **110,** 3254.

(53) M. E. Buck, A. S. Breitbach, S. K. Belgrade, H. E. Blackwell and D. M. Lynn, *Biomacromolecules*, 2009, **10**, 1564.

(54) A. H. Broderick, S. M. Azarin, M. E. Buck, S. P. Palecek, and D. M. Lynn, *Biomacromolecules*, 2011, **12**, 1998.

(55) Y. Pengab and Z. Guo, *J. Mater. Chem. A*, 2016, **4**, 15749.

Title: A Single Multilayer Coating for Controlled Tailoring of Different Liquid Wettabilities*

In the recent past, various liquids (oil/water) wettabilities have been successfully extended in various relevant applications, including oil/water separation, anti-corrosive coatings, underwater robotics, protein crystallization, drug delivery, open microfluidics, water harvesting, etc. In general, separate synthetic approaches were adopted to optimize different bio-inspired liquid wettabilities. In this chapter, another 'reactive' and covalently cross-linked multilayer coating has been reported, which is suitable for the controlled and extreme regulation of both water and oil wettabilities in air and under water, respectively. Along with extremes (super-philicity and super-phobicity) of water (in air) and oil (under water) wettabilities, this single multilayer coating was also able to display special liquid wettabilities (i.e., extremely liquid repellent—but with controlled adhesive properties) both in air and under water, after strategic and appropriate post-chemical modifications of the multilayer coating following 1,4-conjugate addition reaction. The super-liquid-wettability in the synthesized interfaces was able to withstand various severe physical and chemical treatments including adhesive tape test, sand drop test, and harsh chemical exposures like extremes of pH (1 and 11), salinity, river water and surfactant-contaminated aqueous media. Moreover, this approach also allowed the decoration of various flexible and rigid substrates (i.e., wood, Al-foil, synthetic fabric, etc.) with various bio-inspired wettabilities including (1) non-adhesive superhydrophobicity (lotus leaf), (2) adhesive superhydrophobicity (rose petal), (3) underwater superoleophobicity (fish scale), etc. Such single polymeric coating that was capable of controlling the modulation of both oil (under water) and water (in air) wettabilites would be useful in developing various functional materials for practical applications.

* D. Parbat, S. Gaffar, A. M. Rather, A. Gupta and U. Manna, *Chem. Sci.*, 2017, **8**, 6542.

4.1. Introduction

Bio-inspired heterogeneous wettability of liquids (oil and water)[1–5] on solid surfaces is instrumental in developing various advanced materials that are useful in widespread applications such as oil/water separation, drug delivery, protein crystallization, underwater robotics, water harvesting, open microfluidics, etc.[6–20] The Cassie–Baxter model (thoroughly discussed in Chapter 1) explains this extreme repellency of liquids (oil and water) on solid surfaces by hypothesizing the presence of an external third phase (either air or water) in the solid surface,[21,22] which is responsible for the heterogeneous wettability of the selected liquid (e.g., oil or water). For instance, the metastable trapped air in the lotus leaf is mainly responsible for the extreme water repellency, where the water droplets bead with an advancing water contact angle (WCA) of above 150º, and readily roll off on tilting the surface below 10º. This anti-fouling property has been widely recognized as superhydrophobicity.[23,24] Several top-down and bottom-up approaches[25,26] have been introduced in the literature to fabricate artificial superhydrophobic surfaces by following a general principle, where (1) hydrophilic building blocks are mainly exploited to adopt the essential hierarchical topography (appropriate combination of micro/nano features)—which is (2) again coated with inert and low surface energy chemicals (either fluorinated molecules or with long hydrocarbon chain-containing molecules), generally through a chemical vapour deposition process. However, due to the lack of a strong interaction between the hydrophilic hierarchical structures and inert low surface energy coating, the materials were inherently fragile and were prone to lose their anti-wetting property on exposure to harsh physical (bending, twisting, scratching, etc.) or chemical (extremes of pH, salt, etc.) treatments.[27–31] Recently, a few approaches have been introduced to develop durable superhydrophobic materials, yet the synthesis of such durable biomimicked surfaces remains a challenging and interesting research topic for fundamental and applied contexts.[32–37] In 2009, a seminal report by Jiang and co-workers revealed the existence of another anti-fouling property that exists in fish scales—which displays extreme oil-repellency under water with an advancing oil contact angle (OCA) of above 150º and a contact angle (CA) hysteresis below 10º.[3] Early demonstrations related to this underwater anti-oil-fouling property revealed its prospective potential in separation of oil/water emulsions, underwater robotics, anti-biofouling coatings, and developing smart microfluidic devices, etc.[7,9–11,14,18] Generally, metal oxides,[38–41] polymeric hydrogels[3,14,18,42–45] and electrostatic multilayer[46,47] have been explored in developing appropriate topography and surface chemistry—which confer the desired heterogeneous oil-wettability under water through the impregnation and confinement of a meta-stable water layer within the hierarchical topography of the coatings. These polymeric hydrogels, electrostatic multilayer and metal oxide coating approaches are useful for understanding the fundamentals of this anti-oil-

fouling property. However, most often, these synthesized interfaces fail to retain the embedded artificial anti-fouling property on exposure to either harsh physical insults and/or complex chemical environments as (1) polymeric hydrogels are highly susceptible to easy deformation under regular physical/chemical manipulations and (2) brittle metal oxide and electrostatic multilayer are prone to corrosion under harsh chemical treatments.[48] Nevertheless, these two completely distinct anti-fouling properties are undifferentiated in terms of the state of wettability—a common heterogeneous (Cassie–Baxter state) liquid wettability is encountered in the respective materials. However, the entrapped third media (either air or water) is unambiguously different as the third phase is (1) air for superhydrophobicity and (2) water for superoleophobicity under water.[2,3,21,22] As a consequence, the general requirements to stabilize the appropriate external trapped phase in the respective materials/coatings are significantly different: (a) a hierarchical topography with a low surface energy is the basis to achieve metastable trapped air for superhydrophobicity,[1,2,23] whereas (b) superhydrophilic materials in air with appropriate micro/nano features are efficient for displaying extreme oil repellency under water.[3–5] In the Chapter 4, a single multilayer coating is introduced that displayed multiple durable extreme/special liquid wettability properties including superhydrophobicity in air and both superoleophobicity and superoleophilicity under water through facile and precise control over the fraction of the solid contact area with beaded liquid phases both in air and under oil. The facile and robust 1,4-conjugate addition reaction between acrylate and amine groups that was discussed earlier, was strategically and differently exploited in this chapter for rapid construction of chemically 'reactive' and thick coatings with the desired topography and chemical functionalities—which are essential for adopting the desired super-liquid wettability in the synthesized material. First, amine-'reactive' nanocomplex (NC) was synthesized by mixing branched polyethyleneimine (BPEI) and dipentaerythritol penta-acrylate (5Acl) in presence of sodium chloride (NaCl). Then, a multilayer coating was developed following a covalent and layer-by-layer (LbL) deposition of the NC and BPEI polymer. In comparison to the synthesized multilayer coating that mentioned in the Chapter 2, an accelerated growth of multilayer coating was achieved in presence of added salt. Then, the essential surface chemistry was adopted in the multilayer coating by strategic post-chemical modification of the residual acrylate moieties of the polymeric coating. Furthermore, the synthesized multilayer (9 bilayers of NC/BPEI) was explored for the tailoring of various water and oil wettabilities both in air and under water through a controlled change in both chemical functionality and topography of the multilayer. Moreover, the multilayer of NC displayed impeccable physical and chemical durability, and was able to withstand various kinds of insults without compromising the super-wetting properties of the coatings. Furthermore, this chemical approach allowed the decoration of various rigid/flexible substrates

including wood, fabric, Al-foil, etc. with desired super-anti-wetting properties. Such an exemplary synthetic approach—that is capable of coating various objects with desired physically/chemically durable super/special-liquid (water and oil) wettability properties both in air and under water, is unprecedented in the literature.

4.2. Experimental Section

4.2.1. Materials

Propylamine, hexylamine, octylamine and decylamine were acquired from Sigma Aldrich, Bangalore, India. n-butylamine was bought from Spectrochem Pvt. Ltd., Mumbai, India. 1-pentylamine and heptylamine were purchased from Alfa-Aesar. Methanol was acquired from Merck Life Science Pvt. Ltd., New Delhi, India. Sources of other chemicals have already been mentioned in previous chapters.

4.2.2. General consideration

All the instrumental details have been provided in the Chapter 2.

4.2.3. Construction of salt-assisted reactive multilayer coating post-covalent modification of multilayer

The solutions of 5Acl (265 mg mL^{-1}) and BPEI (50 mg mL^{-1}) were prepared first in methanol—which was doped with NaCl salt (0.5 mg mL^{-1}), separately in two glass vials. Then, 1250 μL of BPEI was mixed with 5 ml of 5Acl solution in methanol and the mixture was kept for 5 minutes to initiate the formation of 'reactive' polymeric NC. Then, a glass substrate (5.5 cm x 1 cm) was selected for constructing multilayer coatings of NC/BPEI by exploiting a covalent LbL deposition process as mentioned in the Chapter 2. In this chapter, the multilayer coatings of NC/BPEI were achieved both in presence and absence of added salt (NaCl). This whole deposition cycle was repeated for desired times and then either immediately used for other relevant studies or stored in vacuum desiccator. Further, the multilayer of BPEI polymer was synthesized using same protocol, where solution of NC was replaced with solution of 5Acl.

The 'reactive' multilayer coatings that are either consisted of BPEI and NC (in presence/absence of salt) or consisted of BPEI and 5Acl, was chemically post-modified with strategically selected amine-containing small molecules including propylamine (34.23 mg mL^{-1}, in THF), butylamine (35.23 mg mL^{-1}, in THF), pentylamine (35.95 mg mL^{-1}, in THF), hexylamine (36.6 mg mL^{-1}, in THF), heptylamine (37 mg mL^{-1}, in THF), octylamine (37.23 mg mL^{-1}, in THF), decylamine (37.47 mg mL^{-1}, in THF) and other relevant chemical modifications following the previously reported procedures that mentioned in the Chapter 2. Each modified multilayer coating was

thoroughly washed with ethyl alcohol/THF, and finally dried in compressed air, prior to further essential characterization or other relevant proof of concept demonstrations.

4.2.4. Physical and chemical durability of the bio-mimicked wettability

4.2.4.1. Sand drop test: Sand drop test was performed following the same way as described in the Chapter 2. Both the oil wettability (under water) and water wettability (in air) were examined by measuring the OCAs and digital images.

4.2.4.2. Adhesive tape test: The adhesive tape test was performed and both the oil (under water) and water (in air) wettabilities were further confirmed following the same protocol as Chapter 2.

4.2.4.3. Chemical durability test: The multilayer coatings (9 bilayers) of NC/BPEI, which were individually post-functionalized with glucamine and octadecylamine (ODA), were treated with different harsh and chemically complex conditions as in the Chapter 2.

4.3. Results and Discussions

4.3.1. Fabrication and characterization of the salt-assisted multilayer of NC

In the past, the 1,4-conjugate addition reaction was strategically exploited in the chemical modifications (dendritic amplification of functional groups or selective modification of polymeric microstructures)[49,50] as well as the development of complex nanostructures (multilayer coatings, porous and moldable gels).[51-53] In the Chapter 2, a chemically reactive multilayer (20 bilayers) coating of nanocomplex (NC) has been introduced following a covalent LbL deposition process, where the multilayer coating of NC display underwater superoleophobicity after appropriate chemical modification with selected hydrophilic small molecule—that is glucamine. However, such multilayer coating remained inappropriate to display superhydrophobicity, even after hydrophobic modification. In this chapter, a single chemical avenue was designed by exploiting the 1,4-conjugate addition reaction (Fig. 4.1A) between acrylates of 5Acl and amine groups of BPEI (Fig. 4.1B) through LBL deposition (Fig. 4.1C) to develop a multilayer coating (Fig. 4.1D) that is capable of tailoring various special wettabilities including superhydrophobicity (Fig. 4.1E; in air) and superoleophobicity (Fig. 4.1F; under water). In that context, stable dispersions of NC were individually prepared by mixing BPEI/5Acl in methanol (Fig. 4.1B), both in the presence and absence of salt (0.5 mg ml^{-1}). These dispersions of NC were later strategically used in the multilayer constructions (Fig. 4.1D) in association with the amine-containing branched polymer (BPEI). During the LbL deposition process, with increasing number of LbL deposition cycles, an expedited growth in the size of NC was observed in the presence of NaCl (0.5 mg mL^{-1}), as confirmed by a DLS study as shown in Fig. 4.2A. Later, the

growths of multilayer coatings of NC that were prepared both in the presence and absence of salt, were monitored by measuring the thickness of the respective multilayer at regular intervals as shown in Fig. 4.2B. The growth of the multilayer of NC in the presence of salt was noticed to be exponential and yielded a thick (3.15 mm) multilayer coating after 9 bilayers (a pair of NC and BPEI layers are together denoted as a single bilayer) depositions. However, the growth of the multilayer of NC that were prepared in the absence of salt was noticed to be sluggish and the thickness of the coating (9 bilayers of NC/BPEI) was found to be only 830 nm. In comparison, the multilayer of the polymer that was directly constructed by sequential deposition of BPEI and 5Acl, provided a coating with 700 nm

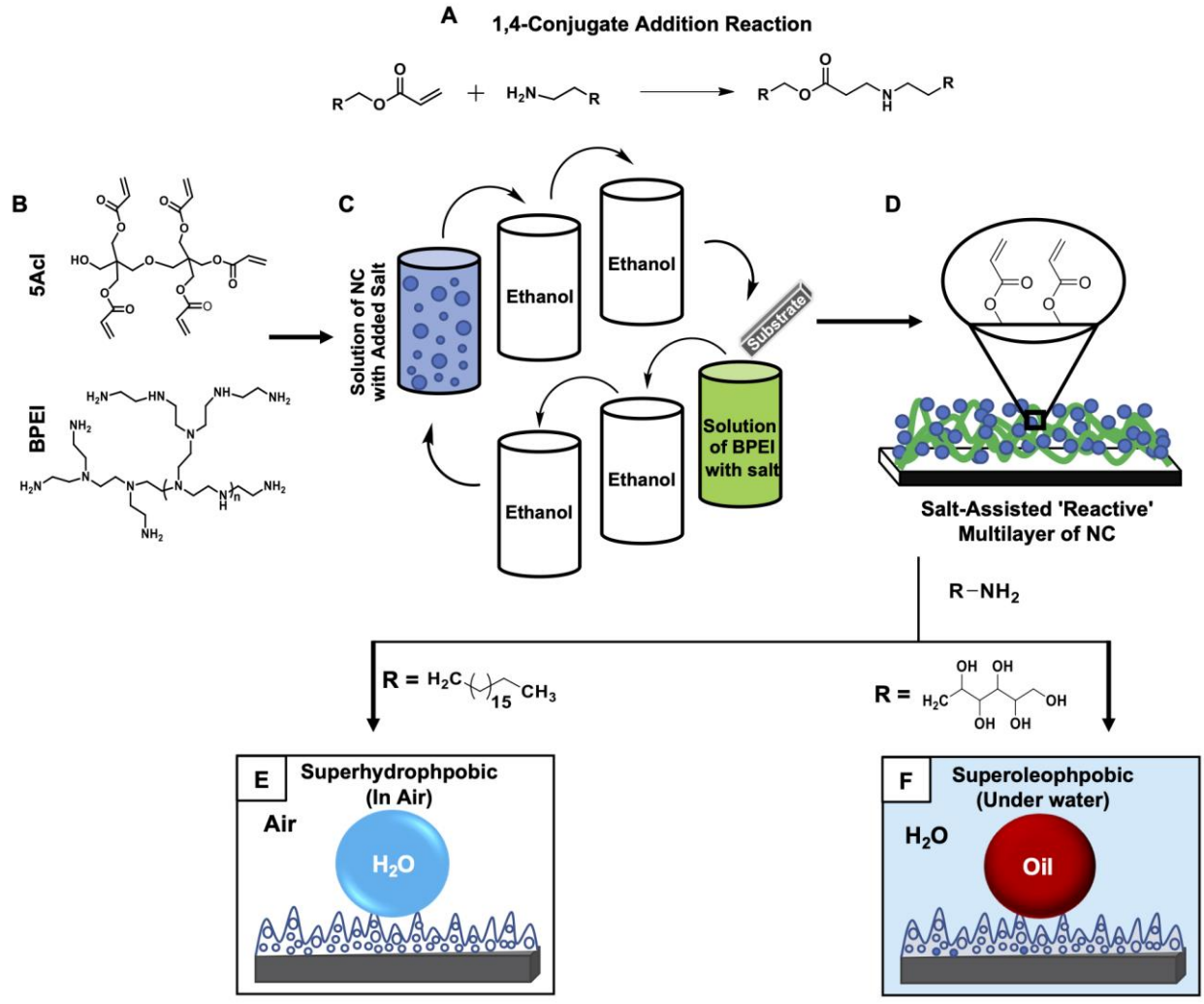

Figure 4.1: (A) Schematic representation of the 1,4-conjugate addition reaction between primary amine and acrylate group. (B) Chemical structural of 5Acl (top panel) and BPEI (bottom panel). (C) Illustrating the formation of 'reactive' polymeric NC (in methanol) in presence of NaCl salt which was further extended for constructing a 'reactive' multilayer coating in combination with BPEI through covalent LbL deposition process. (D) Schematic representation of the salt-assisted multilayer of NC having residual acrylate groups. (E-F) Strategic post-chemical modifications of the multilayer of the NC with appropriate small molecules (ODA and glucamine) provided extremes of liquid wettabilities both in air (superhydrophobicity, (E)) and under water (superoleophobicity, (F)).

thickness after 80 bilayers (each bilayer has been referred as a pair of BPEI and 5Acl deposition) deposition.[50] Thus, the strategic and rapid incorporation of the same components (BPEI and 5Acl) in the form of NC in the covalent multilayer through the 1,4-conjugate addition[47–50] reaction allowed a high throughput synthesis of a thick and reactive polymeric coating. Next, the topography of the coatings was examined by field emission scanning electron microscope (FESEM) imaging. At low magnification, the multilayer coatings of NC that were prepared in the presence of salt, were found to have a prominent and random micro structure throughout the coating as shown in Fig. 4.3A-B. Whereas, in the absence of salt, such dominated micro structures were not observed in the multilayer of NC, rather, comparatively smaller micro-domains appeared as evident from the images in Fig. 4.3D-E. These micro-domains in both of these multilayer coatings (that are prepared in presence and absence of salt) were developed due to random arrangements of granular NC structures as evident from the FESEM images at higher magnification in Fig. 4.3C,F. In contrast, the morphology of the multilayer of BPEI polymer that constructed in the presence of salt, was observed to be mostly featureless under FESEM as shown in Fig. 4.3G-I. As expected, the size of the granules is comparatively smaller in the

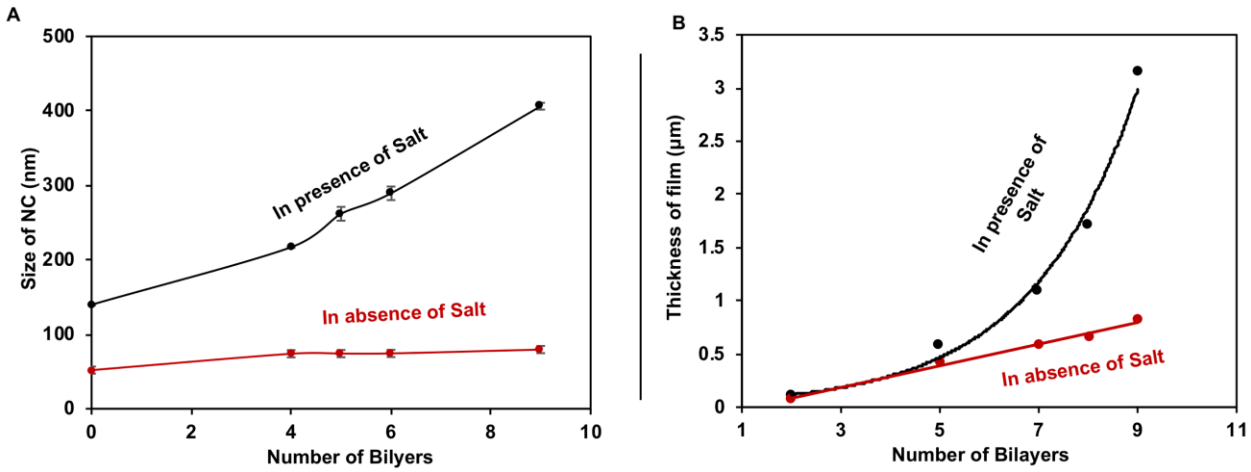

Figure 4.2: (A) Illustrating the growth (size) of the NC in the presence (black line, 0.5 mg ml^{-1}) and absence (red line) of salt (NaCl) in the LbL deposition process. (B) A comparison of the growth (thickness) of the multilayer of NC with LbL deposition cycles both in the presence (black line) and absence (red line) of salt in the NC solution (one of the dipping solutions in the LbL deposition process).

multilayer of NC that are prepared in the absence of salt as shown in Fig. 4.3F, which is consistent with the DLS study in Fig. 4.2A where the growth of NC was observed to be rapid in the presence of salt. However, the exact role of salt behind this expedited growth of NC is not understood yet. This accelerated growth of NC and the difference in the size of the granular structures would have eventually influenced the growth of the micro domains in the respective multilayer. Further, Fourier transform infra-red (FTIR) spectroscopy was used to investigate the residual chemical functionalities

in the synthesized multilayer coatings (prepared in the presence of salt). The appearance of characteristic IR peaks at 1409 cm^{-1} and 1739 cm^{-1} for β C-H deformation of vinyl group and carbonyl stretching, strongly suggested the existence of residual acrylate groups—which eventually made the multilayer coating chemically reactive as shown in Fig. 4.4 (black). A significant depletion in characteristic IR peak (ODA: blue curve and glucamine: red curve in Fig. 4.4) at 1409 cm^{-1} for the symmetric deformation of the C–H bond for the β carbon of the vinyl group with respect to another IR peak at 1739 cm^{-1} which corresponds to ester carbonyl stretching,[49,50] was noticed in the multilayer of NC (in presence of salt) after successful post-chemical modifications of the multilayer coatings of NC with primary amine-containing small molecules (e.g., ODA and glucamine). This simple IR study

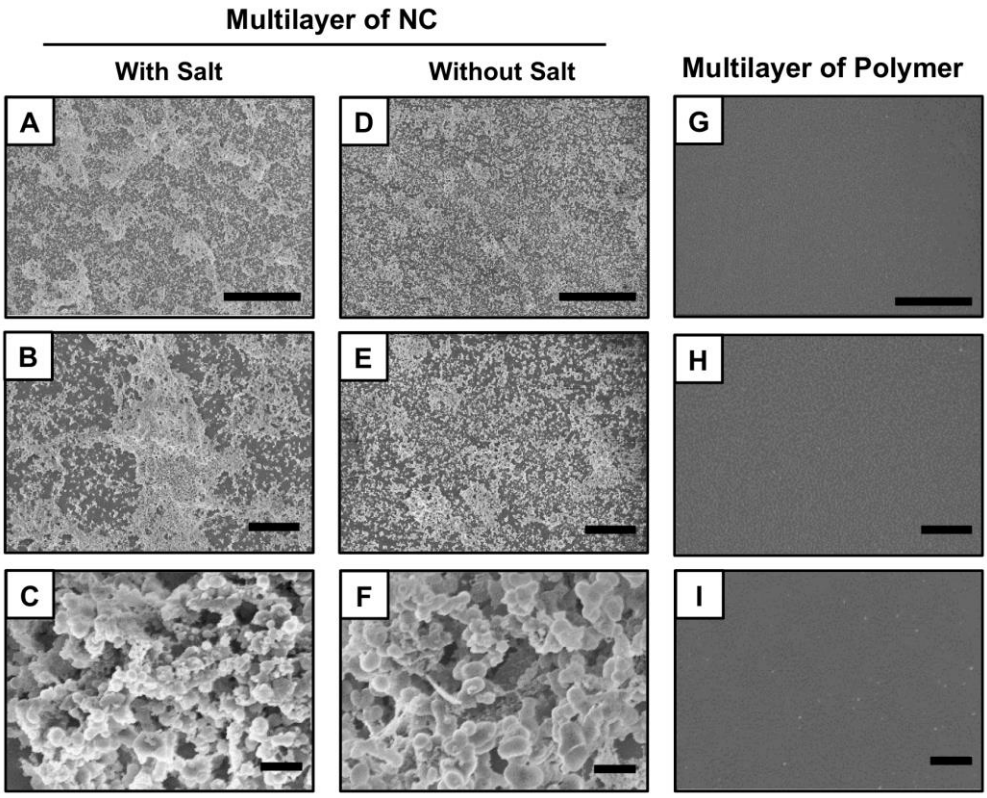

Figure 4.3: (A-F) Field emission scanning electron microscope (FESEM) images of the multilayer (9 bilayers) of the NC/BPEI in low (A,D; scale bar = 20 μm), medium (B,E; scale bar: 15 μm) and high (C,F; scale bar: 500 nm) magnifications, which were constructed in presence (A-C) and absence (D-F) of salt. (G-I) FESEM images of multilayer coating of polymer (multilayer of 5Acl/BPEI prepared in presence of salt) in low (G, scale bar: 20 μm), medium (H; scale bar: 15 μm) and high (I, scale bar: 500 nm) magnifications.

validating that the residual acrylate groups in the multilayer of NC allowed a successful and covalent post-modification with primary amine-containing small molecules (glucamine and ODA) through 1,4-conjugate addition reaction. Based on the past reports on the Michael addition reaction,[47–50] this carbonyl stretching most likely appeared due to amino ester-type cross-linkages in the multilayer

through the repetitive 1,4-conjugate addition reaction between the amine and acrylate from BPEI and 5Acl, respectively. A very similar result was noticed with the multilayer of NC that are prepared in the absence of salt.

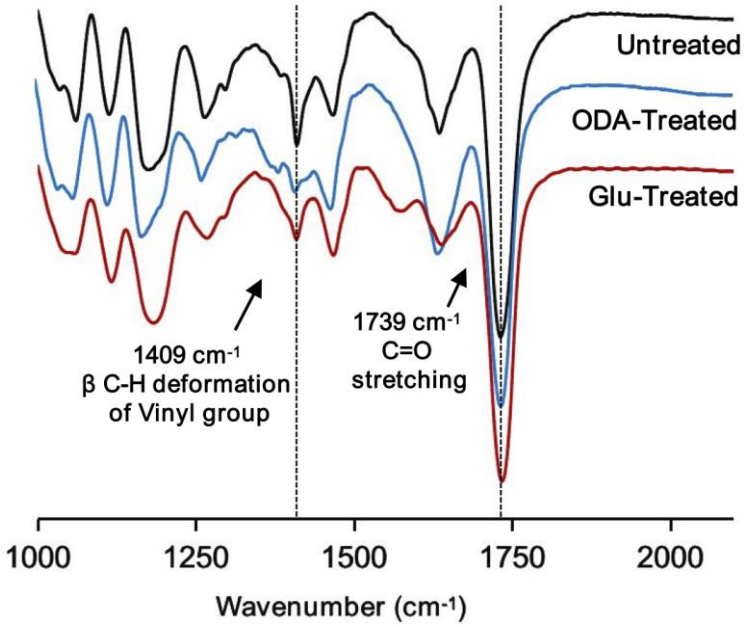

Figure 4.4: FTIR spectra of multilayer coatings of NC, which were synthesized both in presence of salt, before (black) and after post-chemical treatments with small molecules, i.e., ODA (blue) and glucamine (red).

4.3.2. Characterization of extreme liquid wettabilities in the multilayer of NC

The synthesized multilayer (9 bilayers) of NC, which was prepared in the presence and absence of NaCl salt, was noticed to be moderately hydrophobic in air (Fig. 4.5A,D). However, after post-chemical modification with ODA molecules (having a long hydrocarbon tail), the multilayer of NC constructed in the presence of salt, became superhydrophobic with an advancing WCA of 167º (Fig. 4.5B) and with a roll-off angle of 3º (Fig. 4.5H-K). Moreover, a jet of water was noticed to immediately bounce away from the superhydrophobic surface as shown in Fig. 4.5L. In contrast, the hydrophobicity of the multilayer of NC prepared in the absence of salt, was improved slightly and the water droplet beaded with a WCA of 104º after post-chemical modification with the same ODA molecules as shown in Fig. 4.5E. Furthermore, with gradual increase in LbL deposition cycles from 2 to 9 bilayers, the changes in water wettability were examined in detail for the post-modified (ODA) both the multilayer of NC (both in the presence and absence of salt) and multilayer of BPEI. The water repellency of the post-modified (ODA treated) multilayer of NC was gradually increased with the number of LbL deposition cycles, the WCA was increased from 88º (2 bilayers) to 112º (7 bilayers), and suddenly, after 8 bilayer depositions, the hydrophobicity of the multilayer of NC was significantly improved with a static WCA of 148º, and the multilayer of NC was embedded with superhydrophobicity (static WCA

of 153º) after 9 bilayer depositions (black curve in Fig. 4.5G). However, the change in the WCA of the post-modified multilayer of NC that were prepared in the absence of salt was noticed to be completely different, and the WCA was measured to be 104º even after 9 bilayer depositions (red curve in Fig. 4.5G). In another control study, the multilayer (9 bilayers) of BPEI polymer that was prepared in the presence of salt was found to be moderately hydrophobic with a static WCA of 81º after post-chemical modification with ODA molecules as shown in Fig. 4.5G (blue curve). On the other hand, the strategic

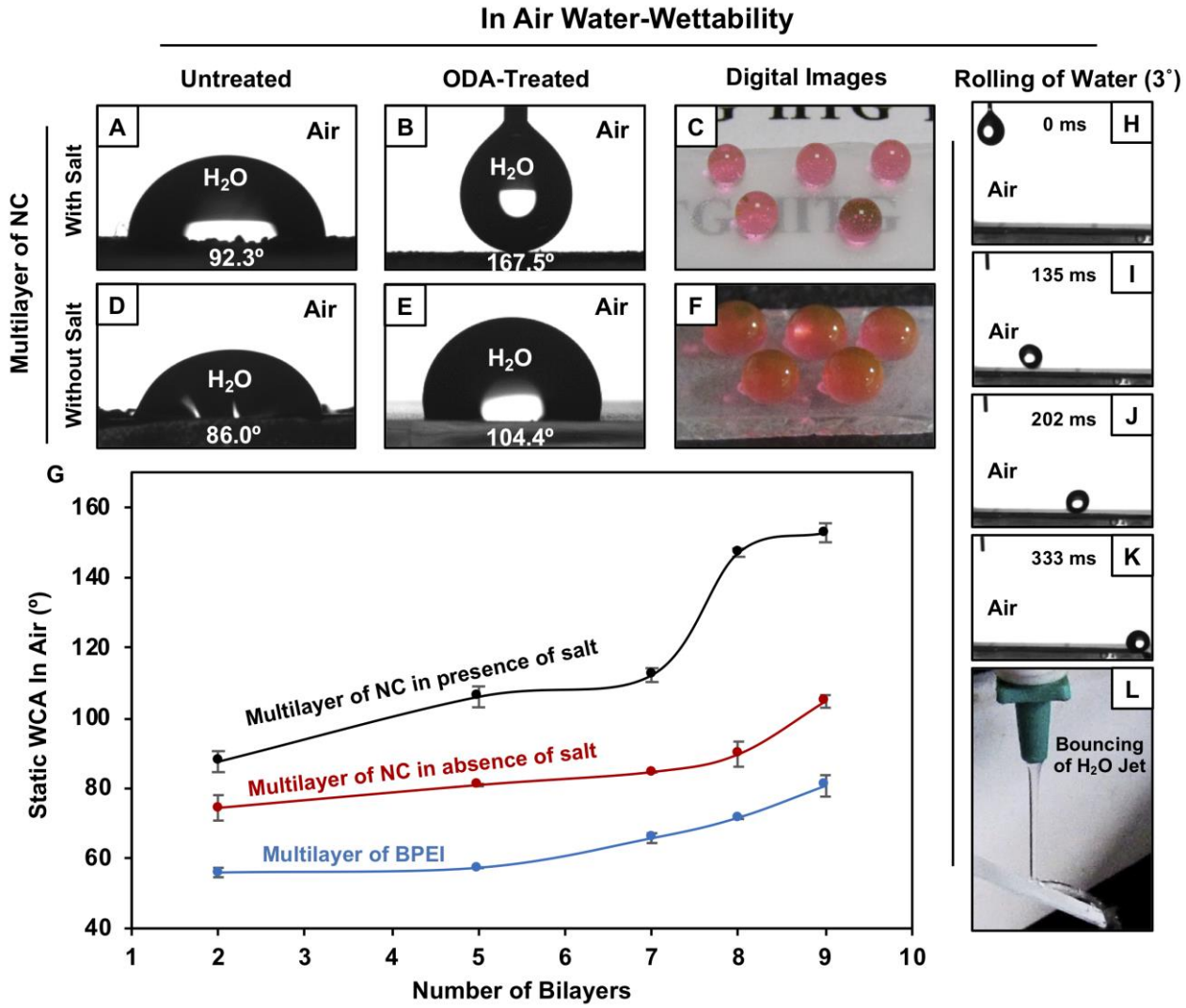

Figure 4.5: (A–F) Contact angle (A-B, D-E) and digital (C,F) images of beaded water droplets (the red colour aided visual inspection) on both the multilayer of NC (that were constructed in the presence (A–C) and absence (D–F) of salt) before (A,D) and after (B-C,E-F) post-chemical modification with ODA molecules. (G) A plot showing the change in the static WCA of the beaded water droplets (4.5 μL) on ODA-treated multilayer of the NC (built in the presence (black line) and absence (red line) of NaCl salt) and BPEI (in the presence of salt, blue line) in air with an increase in the number of bilayer deposition cycles. (H-K) Contact angle images showing the rolling of a water droplet (5 μL) on an ODA-treated multilayer of NC (which was synthesized in presence of salt) that was tilted at 3º angle in air. (L) Digital image of a bounced water jet on the ODA-treated multilayer.

post-modification of the same multilayer (9 bilayers) of NC (that was fabricated in the presence of salt, and having an inherent static OCA of 31º, Fig. 4.6A) with hydrophilic small molecules (i.e., glucamine)

provided a completely different bio-inspired liquid wettability, which has been recognized as underwater superoleophobicity. The oil droplet beaded with an advancing OCA of 169º under water as shown in Fig. 4.6B. In comparison, the multilayer (9 bilayers) of NC (having an inherent static OCA of 36º (Fig. 4.6D)) which was built in the absence of salt, failed to display extreme oil-repellency under water even after post-chemical modification with the same glucamine molecules (Fig. 4.6F). The oil

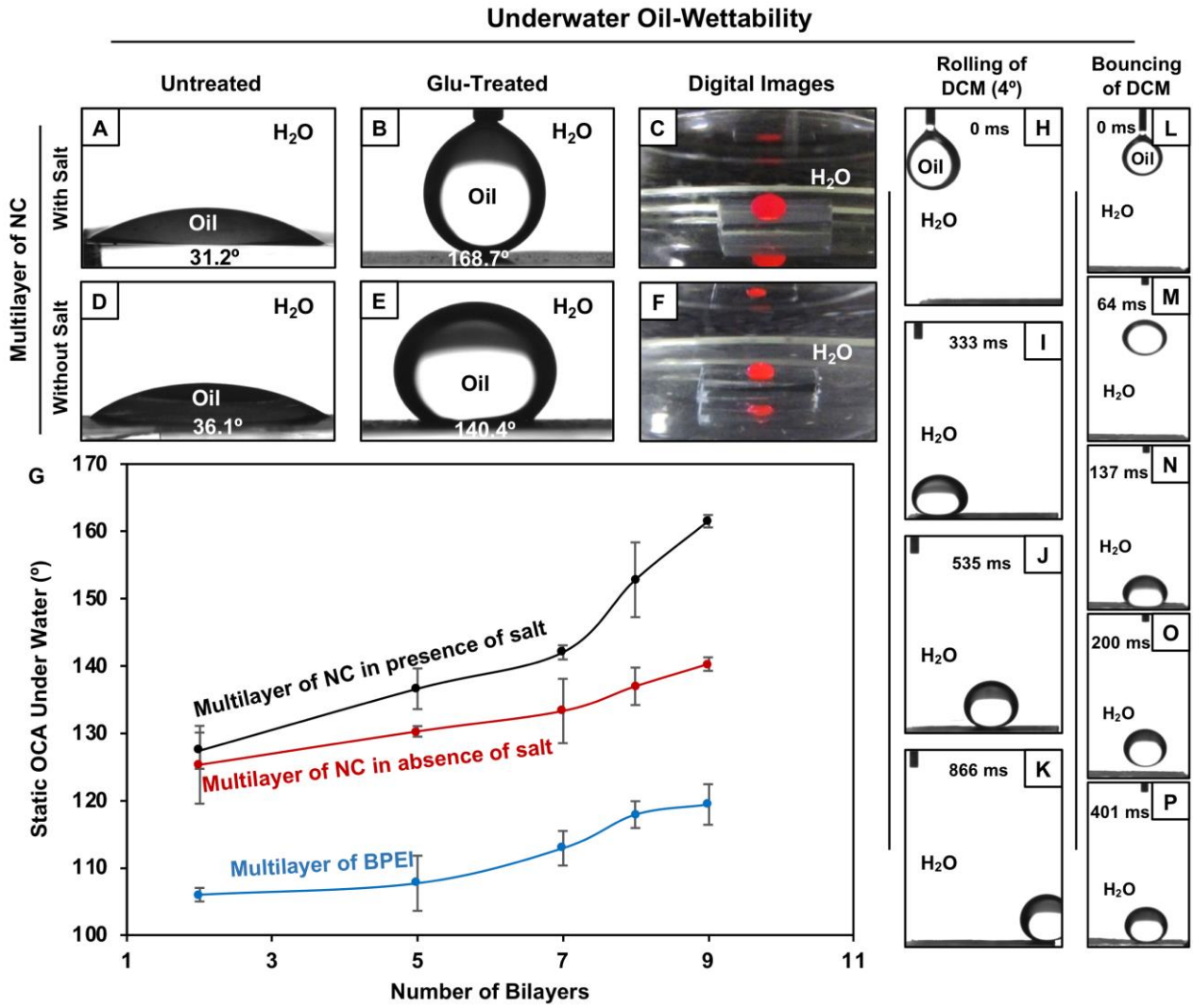

Figure 4.6: (A–F) Contact angle images (A-B,D-E) and digital images (C-F) show the underwater oil (the red colour aided visual inspection) wettability on the multilayer of NC prepared in the presence (A–C) and absence (D–F) of NaCl, before (A,D) and after (B-C,E-F) post-chemical modification with glucamine molecules. (G) The change in static OCA on the glu-treated multilayer of NC (black and red curves represented the multilayer which were prepared in the presence and absence of salt, respectively) and polymer (BPEI, blue curve) with an increase in the number of deposition cycles is shown in the plot. (H-K) Accounting the rolling of an oil droplet (11 μL) under water, on the glu-treated multilayer of NC. (L-P) The bouncing of the oil droplet under water (DCM, 11 μL) on the glu-treated multilayer (9 bilayers) which was built in the presence of salt.

droplet was beaded on the post-modified multilayer with a static OCA of 140º (Fig. 4.6E). Furthermore, the effect of the gradual increase in the number (from 2 to 9 bilayers) of bilayers depositions on the

oil-wettability was examined in the post-modified (glucamine) multilayer of both NC (that are fabricated in the presence/absence of salt) and polymer (BPEI) (Fig. 4.6G). The change in oil-wettability was observed to be more sluggish with increasing the bilayer deposition cycles for the post-modified (glucamine) multilayer of BPEI, where the underwater oil wettability was increased by only 13º (Fig. 4.6G, blue curve) on increasing the bilayers deposition from 2 bilayers (static OCA of 106º) to 9 bilayers (static OCA of 119º; Fig. 4.6G), and the static OCA was similarly increased (by 15º) from 125º (2 bilayers) to 140º (9 bilayers) in the post-modified multilayer of NC that were prepared in the absence of salt. However, the change in oil-wettability was noticed to be completely different in the modified multilayer of NC that were constructed in the presence of salt, and the static OCA was increased significantly from 125º (2 bilayers) to 162º (9 bilayers) as shown in Fig. 4.6G (black curve). These significant changes in the pattern of liquid (water/oil) wettability in air and under water most likely arise from the difference in topography of the multilayer of NC that were fabricated in the presence and absence of NaCl salt. The oil droplet rolled off on tilting the surface at an angle of 4º (Fig. 4.6H-K). Moreover, an 11 mL DCM (model oil) droplet was observed to bounce on the surface as shown in Fig. 4.6L-P.

4.3.3. Controlled and extreme tailoring of liquid wettability

In the recent past, a few approaches have been introduced in the literature to control the liquid wettability through a change in topography[58–62] and chemistry[54–57] of the coatings. However, in most of the designs, either the topography was tailored by adopting a complex fabrication process[59–62] or different chemical modifications was introduced using delicate chemistry[55–57] (e.g., metal–sulfur bond,

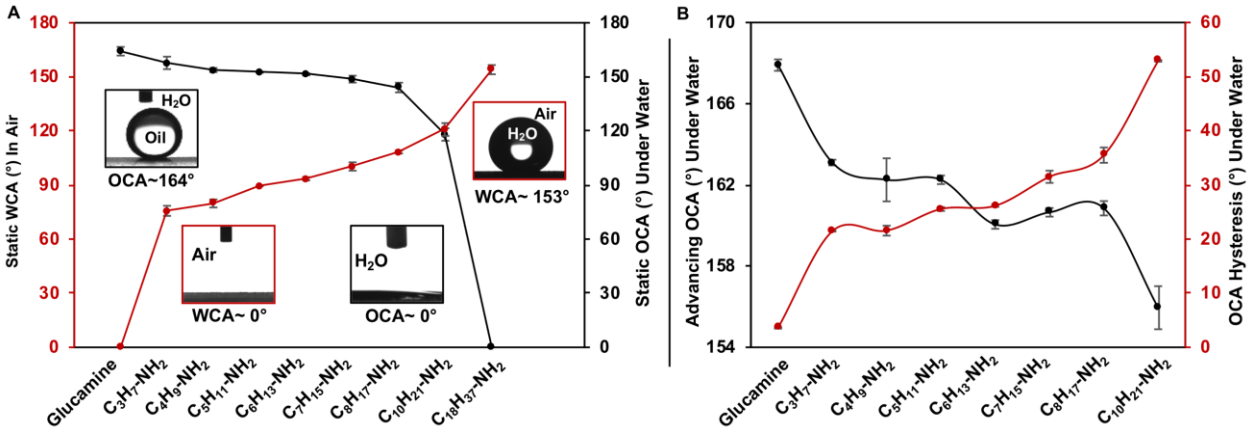

Figure 4.7: (A) The plot is illustrating the controlled and extreme change in both the WCA (red line) in air and the OCA (black line) under water through facile post-chemical modification with strategically selected primary amine-containing small molecules. (B) The plot shows the change in advancing OCA (black) and OCA hysteresis (red) under water after post-chemical treatment of the multilayer with selected alkyl amines.

metal–ion interaction, etc.). In this chapter, (1) the reactive and covalent LbL deposition process

inherently provided a simple avenue to control the topography of the multilayer, and (2) the amine-'reactive' residual acrylate groups in the salt-doped multilayer of NC further allowed the modification of the polymeric coatings with a wide range of chemical functionalities through the facile 1,4-conjugate addition reaction. Hence, the salt-doped multilayer of NC allowed to tailor various oil and water wettabilities. The same multilayer of NC (prepared in presence of salt) was post-modified with different primary amine-containing small molecules, where the hydrocarbon tail length of the reacted small molecules was strategically and progressively increased from $–C_3H_7$ (propyl) to $–C_{18}H_{37}$ (octadecyl). As expected, the WCA (in air) of the beaded water droplet on the post-modified multilayer of NC gradually increased from 75º (propylamine) to 153º (ODA) (Fig. 4.7A, red curve). Simultaneously, the advancing OCA of the beaded oil droplet (under water) on the post-modified multilayer coating continuously depleted from 158º to 0º (Fig. 4.7A, black curve), and eventually, the oil wettability in the multilayer coating was transformed from superoleophobic (extreme repellency to oil) to superoleophilic (extreme attraction to oil) as shown in Fig. 4.7A. To the best of my knowledge, such continuous and extreme regulation of both oil and water wettabilities using a single polymeric multilayer coating is unprecedented in the literature. Furthermore, other special oil-wettabilities (under water) were also achieved in the multilayer coating during these strategic post-chemical modifications of the multilayer of NC (prepared in the presence of salt), where the oil droplets were beaded on the differently post-modified multilayer with advancing OCAs of above 155º as shown in Fig. 4.7B. However, OCA hysteresis gradually enhanced from 21º to 53º with increasing hydrocarbon tail length of the selected small molecules from $–C_3H_7$ (propyl) to $–C_{10}H_{21}$ (decyl) for post-modification as shown in Fig. 4.7B. This unambiguously revealed the gradual increment in adhesive interaction between the beaded oil droplet and multilayer coating. Eventually, more deformations of the beaded oil droplet at the liquid/solid interface were observed during the receding of the beaded oil droplet. However, post-modification of the same multilayer of NC with small molecules having a much longer hydrocarbon tail (ODA, $–C_{18}H_{37}$) provided a completely different super-wettability—called underwater superoleophilicity—which soaked oil with a CA of 0º (as discussed in the previous section of this chapter, Fig. 4.7A). Thus, this current approach provided facile basis for tailoring various liquid (water and oil) wettabilities including extremes of wettabilities and special wettabilities (with controlled adhesiveness) on solid surfaces both in air (for water wettability) and under water (for oil wettability) through the controlled modulation of chemical functionality in the reactive multilayer of NC. The topography of the coating is another important criteria that confers the heterogeneous wettability of liquids (oil and water) on solid surfaces both in air and under water. In the past various different approaches—which were generally either complex designs or require specialized equipment[59–62]—

have been introduced to tailor the topography of the materials for adopting adhesive, but extreme, liquid repellent interfaces both in air and under water. The current approach provided a simple avenue to tune the appropriate topography in the multilayer of NC for adopting desired special wettability of liquids through facile and controlled regulation on the LbL deposition cycles. The ODA-modified multilayer of NC (prepared in presence of salt) displayed extreme water repellency with advancing WCA of >160º and WCA hysteresis of 8º after 8 bilayer depositions (Fig. 4.8C-D). However, after 9 bilayer depositions, the same multilayer coating of NC was observed to be ultra-non-adhesive superhydrophobic with advancing WCA of >160º (Fig. 4.8E) and WCA hysteresis of 3º. Similarly, the oil-wettability under water was modulated in the glucamine-treated (glu-treated) multilayer of NC by changing the LbL deposition cycles. The glu-treated multilayer of NC displayed adhesive superoleophobicity with an advancing OCA of 166º and with a OCA hysteresis of 34º after 7 bilayer depositions, and the shape of the beaded oil droplets was significantly deformed at the oil/solid interface as shown in Fig. 4.8G-H. Whereas, after 8 bilayer depositions, the same multilayer of NC was found to be non-adhesive with an advancing OCA of 167º (Fig. 4.8I) and with a OCA hysteresis of 6º. The non-adhesive superoleophobicity was further improved with an advancing OCA of 168º and a OCA hysteresis of 4º after 9 bilayer depositions (Fig. 4.8K,L) of multilayer of NC (glu-treated) in

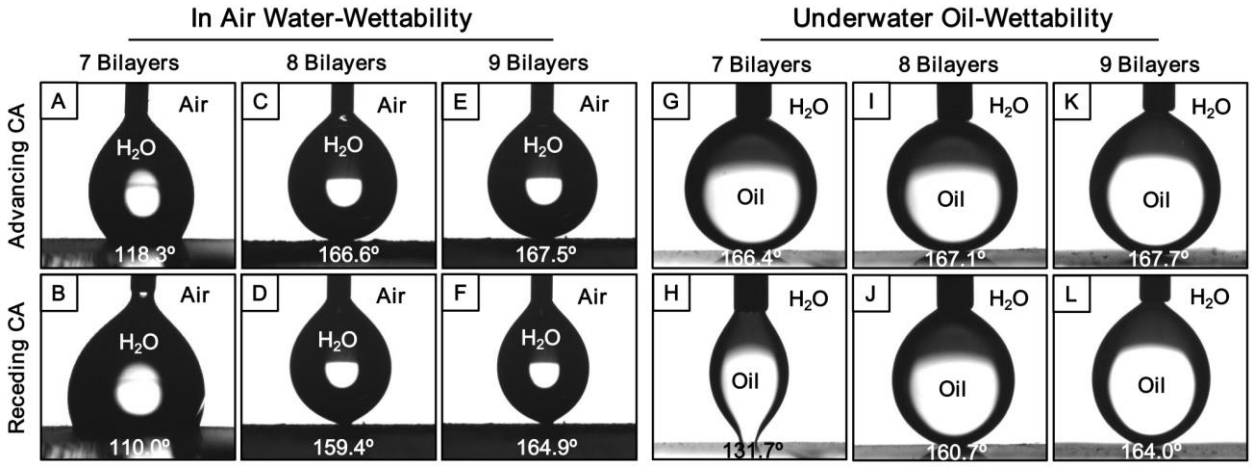

Figure 4.8: (A–L) Advancing (A,C,E,G,I,K) and receding (B,D,F,H,J,L) contact angle images of both the beaded water (A–F, in air) and oil (G–L, under water) droplets on the multilayer (7 bilayers: A-B, and G-H; 8 bilayers: C-D, and I-J; 9 bilayers: E-F, and K-L) of NC that were post-chemically modified with ODA (A–F) and glucamine (G–L).

the presence of salt. The whole amount of beaded oil completely receded without a noticeable deformation of the shape of the beaded oil droplets at the oil/solid interfaces as shown in Fig. 4.8J,L. Thus, the current design of a 'reactive' multilayer construction through covalent LbL deposition allowed us to examine independently the role of the essential parameters— (1) topography and (2)

chemical functionality—which confer the heterogeneous liquid wettability on a solid surface, without perturbing the other parameters at the same time. For example, the effect of the change in chemical functionality could be studied independently without perturbing the topography of the material, and vice versa. The heterogeneous wettability of water and oil in air and under water, respectively has often been described by adopting the Cassie–Baxter model,[4] where either the metastable trapped air (for water wettability in air) or the confined liquid water layer (for oil-wettability under water) within the featured solid surfaces were attributed to the heterogeneous wettability for both water and oil, respectively through limited access to the contact area between the solid surface and respective beaded liquid phases.

$$\cos \theta_r = f_1 \cos \theta - f_2 \quad \text{..... (4.1)}$$

$$f_1 + f_2 = 1 \quad \text{.....(4.2)}$$

The fraction of the contact area between the beaded liquid (water and oil) phase and multilayer of NC (that were either modified with ODA or glucamine) was calculated using eqn (4.1) and (4.2), where θ and θ_r were denoted as the liquid (water/oil) CAs on a multilayer of BPEI/5Acl (smooth surface, 9 bilayers) and multilayer of NC (featured surface prepared in the presence of salt; 9 bilayers), respectively. The fraction of the solid contact area and either the trapped air or confined water contact area with the respective beaded liquid (water and oil) phases were labelled as f_1 and f_2, respectively.

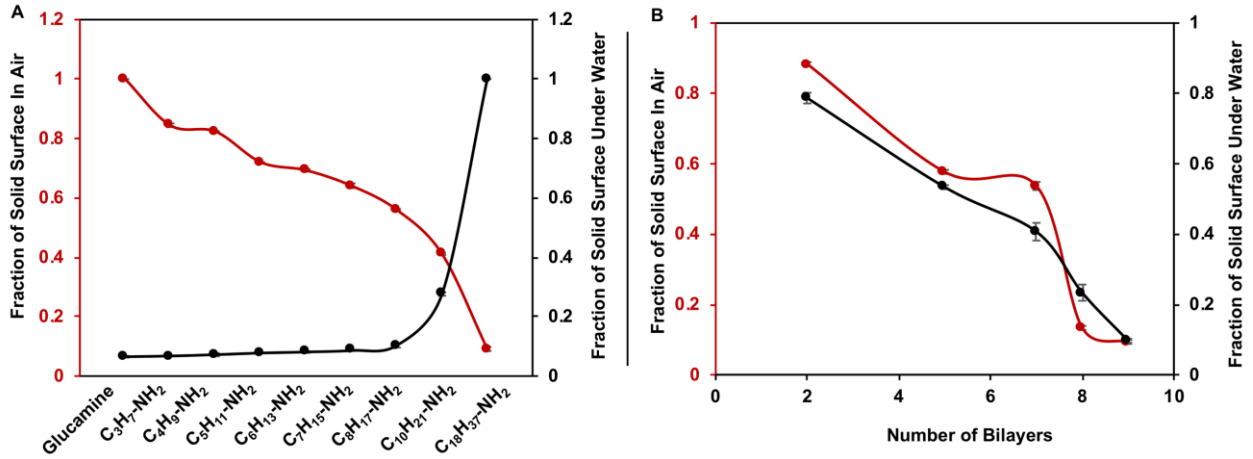

Figure 4.9: (A-B) The plot accounting the change in the fraction of the solid surface area with the beaded water (red line) and oil (black line) phases both in air (red line) and under water (black line), respectively through the modulation of chemical functionality (A) of the multilayer of NC and controlling the deposition cycles (B) during LBL multilayer construction of NC in the presence of salt.

The fraction of the solid contact area with the beaded water droplet on the strategically post-modified multilayer of NC (in the presence of salt) in air was noticed to gradually decrease with the increasing hydrocarbon tail length of the amine-containing small molecules from 0.844 (–C_3H_7: propylamine) to

0.091 ($–C_{18}H_{37}$: ODA) as shown in Fig. 4.9A (red curve). As a consequence, the hydrophobicity in the multilayer of NC was progressively increased, and eventually, the multilayer was embedded with superhydrophobicity in case of ODA treatment. However, on increasing the hydrophobic tail length of the reacted small molecules in the post-modified multilayer of NC from–C_3H_7 (propylamine) to–$C_{10}H_{21}$ (decylamine), the change in the fraction of the solid contact area for the beaded oil phase on the multilayer coatings was comparatively more sluggish under water, and the solid contact area was only increased from 0.067 to 0.276 as shown in Fig. 4.9A (black curve). This controlled and sluggish change in the fraction of the solid contact area with the beaded oil phase effectively controls the adhesive interaction between the multilayer and beaded oil phase—but the multilayer surfaces continued to display underwater extreme oil repellency with an advancing OCA of above 155º as the fraction of the solid contact area with the beaded liquid phase remained low in general, even after post-chemical modification with decylamine molecules. However, the fraction of the solid contact area suddenly increased to 1 on the modification of the multilayer with ODA molecules—which essentially transformed the multilayer to be underwater superoleophilic. Thus, the same multilayer of NC (9 bilayers) with an identical topography controlled the access of contact area between the solid surface (multilayer of NC) and beaded liquid (water/oil) phases both under water (for oil droplets) and in air (for water droplets), depending on the selection of appropriate post-chemical modifications with small molecules. Eventually, the simple chemical modification tailored the liquid (oil/water) wettabilities both in air and under water. However, the trends in the change of the fraction of the solid contact area with beaded liquid phases both in air and under water were considerably different. With increasing the hydrocarbon tail length of the reacted small molecules from $–C_3H_7$ (propyl) to $–C_{10}H_{21}$ (decyl) in the post-modified multilayer of NC, the hydrophobicity (in air) was found to undergo a change of WCA from 76º to 121º. In comparison, the multilayer of NC was proficient in displaying superoleophobicity (with an advancing OCA of above 155º) under water, and the adhesive property increased with increasing hydrocarbon tail length of the reacted small molecules (Fig. 4.7A). Next, the effect of consecutive LbL deposition (or the topography of multilayer) of NC on the fraction of the solid contact area with the respective liquid (either water or oil) phase was examined both in air and under water, where the chemical functionalities (ODA-treatment (Fig. 4.1E) for water wettability in air and glu-treatment (Fig. 4.1F) for oil wettability under water) of the multilayer were kept unaltered during the entire study. The fraction of the solid contact area of the beaded water droplet on the multilayer of NC (which was post-modified with ODA molecules) in air was initially decreased slowly from 0.88 (2 bilayers) to 0.54 (7 bilayers) with increasing the number of LbL deposition cycles, and after 7 bilayers depositions, the fraction of the solid contact area had significantly dropped as shown in Fig. 4.9B (red

curve), and eventually provided superhydrophobicity to the multilayer. However, in the case of the underwater beaded oil droplet on the multilayer of NC that was post-functionalized with glucamine molecules, the fraction of solid contact area decreased following a 'linear-like' trend from 0.78 to 0.09 on increasing the number of consecutive LbL dipping cycles as observed in Fig. 4.9B (black curve). Thus, this study re-established that both the chemical functionality and topography of the material actively contribute to the heterogeneous wettability of both water and oil in air and under water, respectively through the appropriate change in the solid contact area with beaded liquid droplets.

4.3.4. Physical and chemical durability of the anti-fouling properties

In general, several reported anti-fouling materials (having either superhydrophobicity in air or

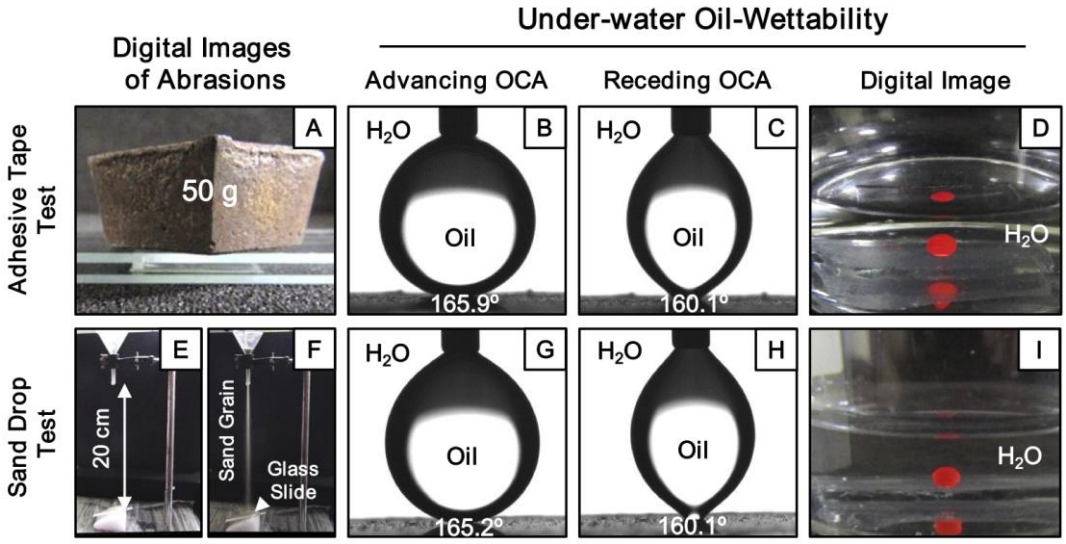

Figure 4.10: (A,E-F) Digital images depicting the adhesive tape test (A) and sand drop test (E-F). (B-D,G-I) Digital images (D,I) and CA images (B-C,G-H) of beaded oil (under water) droplets on the glu-treated multilayer of NC (9 bilayers) after performing the adhesive tape test (B-D) and sand drop test (G-I).

superoleophobicity under water), which were developed from metal oxides,[38–41] polymeric hydro-gels[3,14,18,42–44] or other organic substances,[45–47] are highly delicate and susceptible to perturbation of the chemical functionality and/or the topography that existed in the synthesized interfaces, after exposure to common physical manipulations or harsh chemical environments.[27–31,48] So, the as-synthesized multilayer that were embedded with super-anti-fouling properties, were exposed to various harsh chemical and physical insults to investigate the durability of the embedded anti-liquid-wettability properties in the strategically post-modified multilayer of NC (prepared in presence of salt). First, the adhesive tape test (Fig. 4.10A) was performed, where adhesive tapes were manually and individually placed on both the glucamine and ODA-treated multilayer coatings of NC with an applied load of 50

g to facilitate uniform contact between the adhesive surface and multilayer coating, prior to peeling off the adhesive tapes from both the underwater superoleophobic coating and superhydrophobic

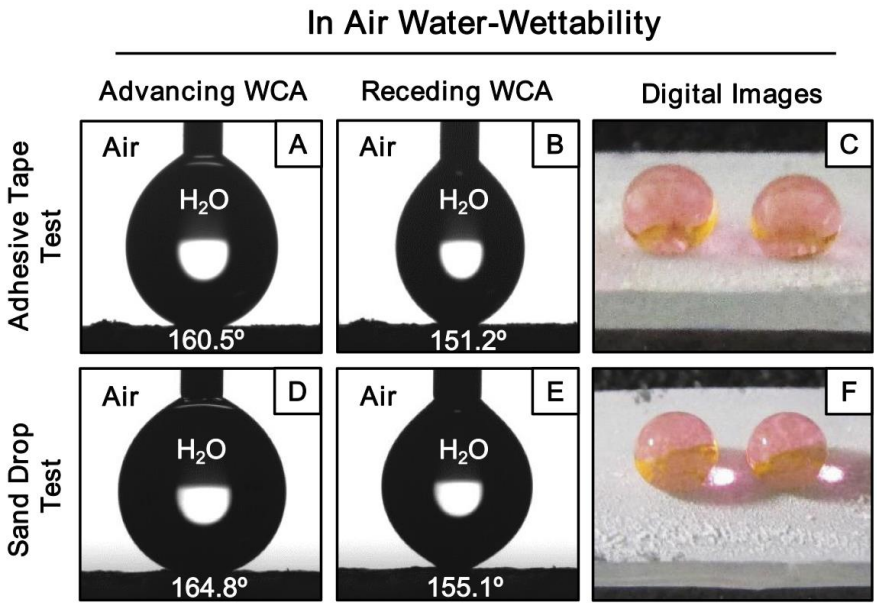

Figure 4.11: (A-F) Contact angle (A-B, D-E) and digital images (C,F) of the beaded water droplets (in air) on the ODA-modified multilayer of NC after carrying out the adhesive tape test (A-C) and sand drop test (D-F).

coating. Both the biomimicked extreme liquid wettabilities under water (Fig. 4.10B-D) and in air (Fig. 4.11A-C) were noticed to be intact even after abrasive exposures. A very similar result was also noticed after performing another conventional physical abrasive test, recognized as sand drop test (Fig. 4.10E-

Chemical Insults	Underwater Superoleophobic		In Air Superhydrophobic	
	Advancing OCA (º)	OCA Hysteresis (º)	Advancing WCA (º)	WCA Hysteresis (º)
pH 1	165.7 ± 0.7	5.3 ± 0.8	164.4 ± 0.4	4.1 ± 0.6
pH 11	165.9 ± 0.7	6.1 ± 2.2	164.9 ± 1.5	5.3 ± 2.1
River Water	166.6 ± 0.3	8.1 ± 0.5	161.0 ± 0.3	2.1 ± 1.3
SDS Water	165.7 ± 0.5	3.0 ± 1.1	165.7 ± 0.6	1.8 ± 1.4
Sea Water	166.3 ± 1.0	2.5 ± 1.4	166.9 ± 0.8	6.0 ± 0.8

Table 4.1: Accounting both the advancing liquid (oil/water) CAs and CA hysteresis both in air and under water after exposing the multilayer to different chemical- (extremes of pH (pH 1, 11), river water, sea water and surfactant (SDS 1 mM)) contaminated aqueous environments.

F), where both superhydrophobic coating and underwater superoleophobic coatings were placed under a continuous flow of sand grains (60 g) that was dropped from a height of 20 cm, (Fig. 4.10E-F). Eventually, both the bio-inspired multilayer coatings were recovered with their respective anti-fouling properties intact. Both the water and the oil droplets were beaded on the respective multilayer coatings

with advancing CAs above 160º and CA hysteresis below 10º both in air (Fig. 4.10G-I) and under water (4.11D-F). Next, the multilayer coatings were exposed to complex and corrosive aqueous solutions including extremes of pH (pH 1 and pH 11), SDS surfactant (as model detergent, 1 mM), artificial sea water and river water (Brahmaputra river, Guwahati, India). However, the multilayer coatings retained the ability to repel both water (in air) and oil (under water) droplets with advancing CAs of >160º and CA hysteresis of <10º as listed in Table 4.1. This impeccable durability of the liquid wettability in the synthesized bio-inspired coatings might arise from the covalent cross-linkages in the multilayer through the 1,4-conjugate addition reaction.

4.3.5. Salt-assisted multilayer coatings on various substrates

There are few reported approaches[47,63–66] in the literature that allow to coat various substrates irrespective of their composition (metallic, polymeric, etc.), wettability (hydrophilic, hydrophobic, etc.) and geometry (rigid, flexible, smooth, fibrous, etc.) of the substrates. In this current chapter, the salt-assisted covalent and 'reactive' multilayer coating can be achieved on various substrates including smooth (glass or Al-foil), rough (synthetic fabric, wood) substrates to decorate those substrates with the desired anti-wettability properties in air and under water through facile and appropriate post-chemical modifications as shown in Fig. 4.12A-R. The uncoated synthetic fabric, which inherently soaked both water in air (Fig. 4.12A) and oil under water (Fig. 4.12J), was observed to display extreme

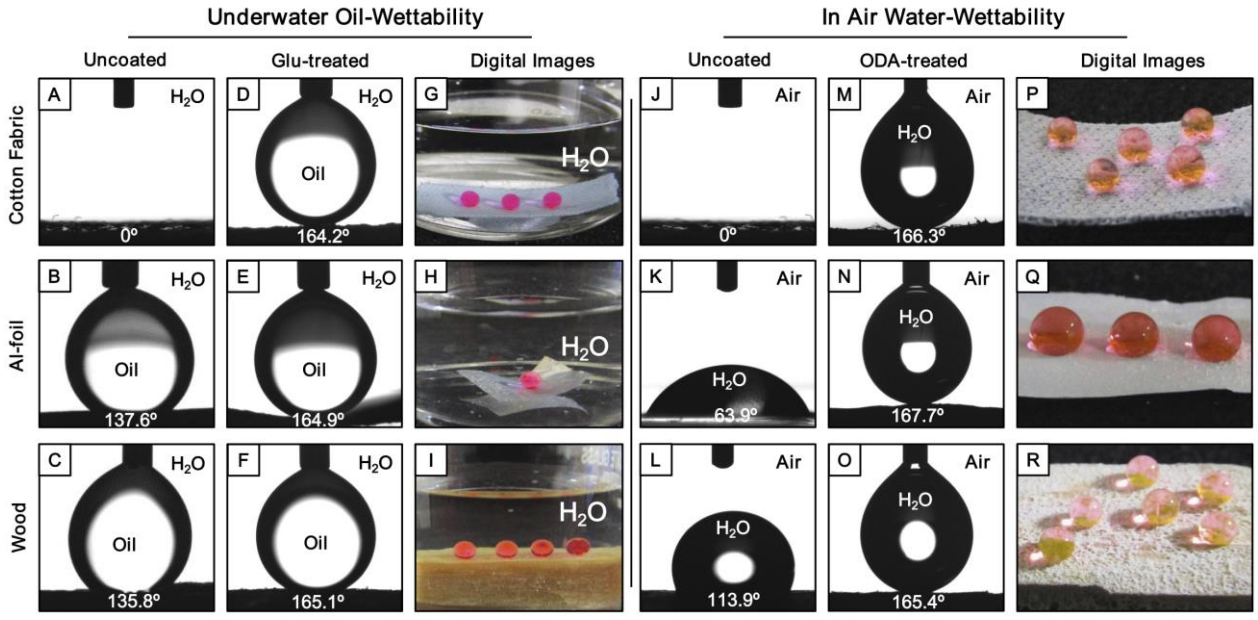

Figure 4.12: (A–R) CA images (A–F, J-O) and digital images (G–I, P-R) of the uncoated (A–C, J-L) glu-treated (D-I) and ODA-treated (M-R) multilayer (9 bilayers, in presence of salt) of NC coated fibrous (cotton fabric; A,D,G,J,M,P), flexible (Al-foil; B,E,H,K,N,Q) and rigid (wood; C,F,I,L,O,R) substrates under water.

liquid (water/oil) repellency both in air and under water with an advancing CA of above 160º (Fig.

4.12D,G,M,P), where the respective liquid droplets (red colour aided visual inspection) were beaded on the appropriately post-functionalized multilayer coatings with spherical shapes (Fig. 4.12G,P). This study revealed the existence of both superhydrophobicity (in air) and super-oleophobicity (under water) in the respective multilayer coatings. Similarly, a smooth metal surface, Al-foil, which is inherently oleophobic (Fig. 4.12B) and hydrophilic (Fig. 4.12K), was decorated with under water superoleophobicity (Fig. 4.12E,H) and superhydrophobicity (Fig. 4.12N,Q) in air by exploiting the current design. Another model substrate—wood—which moderately repels both oil (OCA of 136º under water; Fig. 4.12C) and water (WCA of 114º in air; Fig. 4.12L) became superoleophobic under water and superhydrophobic in air after coating the substrate with the multilayer of NC and followed by post-chemical modifications with appropriate small molecules through the facile Michael addition reaction. The stability of the coating on these substrates was investigated by the adhesive tape peeling test, and the polymeric coating was found to retain their anti-fouling properties even after the adhesive tape peeling test. Thus, this current strategy could be highly useful for marine and other relevant applications including prevention of oil contamination, oil/water separation, protein crystallization, developing smart fabrics, etc. Moreover, this approach would enable the coating of a wide range of other useful substrates with desired anti-fouling properties for a specific or wide variety of applications related to energy, health and the environment.

4.4 Conclusion

In this chapter, a multilayer was constructed by strategically exploiting a robust 1,4-conjugate addition reaction between acrylate and amine groups in presence of salt for the controlled and extreme regulation of both water and oil wettability in air and under water, respectively. The growth of multilayer of NC was comparatively rapid and exponential in the presence of salt, and provided appropriate topography that was capable of displaying extreme liquid wettability properties including superhydrophobicity/superhydrophilicity in air and superoleophobicity/superoleophilicity under water. Moreover, the consecutive LbL deposition allowed a facile control over the topography of the multilayer coatings, to adopt special adhesive anti-fouling properties by controlling the fraction of the contact area of the solid with the beaded liquid droplets. On the other hand, residual acrylate groups in the multilayer provided a convenient basis for the precise control of the fraction of the solid contact area with the beaded liquid phases both under water and in air through suitable and appropriate post-chemical modification of the multilayer of NC with small molecules. As a result, the appropriately post-functionalized multilayer was eventually embedded with various special water (in air) and oil (under water) wettability properties. The current design allowed a comprehensive and comparative

investigation on the homogeneous/heterogeneous wettability of both water and oil in air and under water, respectively. However, the same extent of change in the chemistry and topography in the material has an independent implication on the water (in air) and oil (under water) wettability. Moreover, the synthesized multilayer of NC was able to withstand various physical and chemical insults without compromising the anti-fouling properties of the materials, and the current strategy also provided a facile avenue to decorate a wide variety of substrates with the desired anti-fouling properties. Thus, this material would be useful in various relevant applications including the synthesis of patterned interfaces through site-specific functionalization of the 'reactive' multilayer of NC, and could be useful in various advanced applications.[67]

4.5. References

(1) L. Feng, S. H. Li, Y. S. Li, H. J. Li, L. J. Zhang, J. Zhai,Y. L. Song, B. Q. Liu, L. Jiang and D. B. Zhu, *Adv. Mater.*, 2002, **14**, 1857.

(2) X. M. Li, D. Reinhoudt and M. C.-Calama, *Chem. Soc. Rev.*, 2007, **36**, 1350.

(3) M. J. Liu, S. T. Wang, Z. X. Wei, Y. L. Song and L. Jiang, *Adv.Mater.*, 2009, **21**, 665.

(4) Z. Chu, Y. Feng and S. Seeger, *Angew. Chem. Int. Ed.*, 2015, **54**, 2328.

(5) B. Su, Y. Tian and L. Jiang, *J. Am. Chem. Soc.*, 2016, **138**, 1727.

(6) X. Yao, J. Gao, Y. Song and L. Jiang, *Adv. Funct. Mater.*, 2011, **21**, 4270.

(7) A. K. Kota, G. Kwon, W. Choi, J. M. Mabry and A. Tuteja, *Nat. Commun.*, 2012, **3**, 1.

(8) E. Ueda and P. A. Levkin, *Adv. Mater.*, 2013, **25**, 1234.

(9) Y. Wu, B. Su, L. Jiang and A. J. Heeger, *Adv. Mater.*, 2013, **25,** 6526.

(10) Z. Shi, W. Zhang, F. Zhang, X. Liu, D. Wang, J. Jin and L. Jiang, *Adv. Mater.*, 2013, **25**, 2422.

(11) M. Tao, L. Xue, F. Liu and L. Jiang, *Adv. Mater.*, 2014, **26**, 2943.

(12) L. Wen, Y. Tian and L. Jiang, *Angew. Chem. Int. Ed.*, 2015, **54**, 3387.

(13) Z. Chu, Y. Feng and S. Seeger, *Angew. Chem. Int. Ed.*, 2015, **54**, 2328.

(14) Y. Cai, Q. Lu, X. Guo, S. Wang, J. Qiao and L. Jiang, *Adv. Mater.*, 2015, **27**, 4162.

(15) A. Gao, Q. Wu, D. Wang, Y. Ha, Z. Chen and P. Yang, *Adv. Mater.*, 2016, **28**, 579.

(16) C. Li, M. Boban, S. A. Snyder, S. P. R. Kobaku, G. Kwon, G. Mehta and A. Tuteja, *Adv. Funct. Mater.*, 2016, **26**, 6121.

(17) C. Yu, M. Z. Dong, J. Wang, K. Li and L. Jiang, *Adv. Funct. Mater.*, 2016, **26**, 3236.

(18) K. Chen, S. Zhou and L. Wu, *ACS Nano*, 2016, **10**, 1386.

(19) M. Wu, B. Ma, T. Pan, S. Chen and J. Sun, *Adv. Funct. Mater.*, 2016, **26**, 569.

(20) S. T. Yohe, J. D. Freedman, E. J. Falde, Y. L. Colson and M. W. Grinstaff, *Adv. Funct. Mater.*, 2013, **23**, 3628.

(21) A. B. D. Cassie and S. Baxter, *Trans. Faraday Soc.*, 1944, **40**, 546.

(22) A. B. D. Cassie and S. Baxter, *Nature*, 1945, **155**, 21.

(23) A. Tuteja, W. Choi, M. Ma, J. M. Mabry, S. A. Mazzella, G. C. Rutledge, G. H. Mckinley and R. E. Cohen, *Science*, 2007, **318**, 1618.

(24) V. Zorba, E. Stratakis, M. Barberoglou, E. Spanakis, P. Tzanetakis, S. H. Anastasiadis and C. Fotakis, *Adv. Mater.*, 2008, **20**, 4049.

(25) X. Feng and L. Jiang, *Adv. Mater.*, 2006, **18,** 3063.

(26) Y. Y. Yan, N. Gao and W. Barthlott, *Adv. Colloid Interface Sci*., 2011, **169**, 80.

(27) G. R. J. Artus, S. Jung, J. Zimmermann, H. P. Gautschi, K. Marquardt and S. Seeger, *Adv. Mater.*, 2006, **18**, 2758.

(28) Y. H. Xiu, Y. Liu, D. W. Hess and C. P. Wong, *Nanotechnology*, 2010, **21**, 155705.

(29) T. Verho, C. Bower, P. Andrew, S. Franssila, O. Ikkala and R. H. A. Ras, *Adv. Mater.*, 2011, **23**, 673.

(30) L. Ionov and A. Synytska, *Phys. Chem. Chem. Phys*., 2012, **14**, 10497.

(31) U. Manna and D. M. Lynn, *Adv. Mater.*, 2013, **25**, 5104.

(32) X. Deng, L. Mammen, Y. Zhao, P. Lellig, K. Mullen, C. Li, H. J. Butt and D. Vollmer, *Adv. Mater.*, 2011, **23**, 2962.

(33) X. Deng, L. Mammen, H. J. Butt and D. Vollmer, *Science*, 2012, **335**, 67.

(34) U. Manna, M. C. D. Carter and D. M. Lynn, *Adv. Mater*., 2013, **25**, 3085.

(35) J. E. Mates, I. S. Bayer, J. M. Palumbo, P. J. Carroll and C. M. Megaridis, *Nat. Commun.*, 2015, **6**, 8874.

(36) M. Paven, R. Fuchs, T. Yakabe, D. Vollmer, M. Kappl, A. N. Itakura and H. J. Butt, *Adv. Funct. Mater.*, 2016, **26**, 4914.

(37) X. Tian, T. Verho and R. H. A. Ras, *Science*, 2016, **352**, 142.

(38) X. Liu, J. Zhou, Z. Xue, J. Gao, J. Meng, S. Wang and L. Jiang, *Adv. Mater.*, 2012, **24**, 3401.

(39) F. Zhang, W. B. Zhang, Z. Shi, D. Wang, J. Jian and L. Jiang, *Adv. Mater.*, 2013, **25**, 4192.

(40) Z. Cheng, H. Lai, Y. Du, K. Fu, R. Hou, C. Li, N. Zhang and K. Sun, *ACS Appl. Mater. Interfaces*, 2014, **6**, 636.

(41) J. Yong, F. Chen, Q. Yang, U. Farooq and X. Hou, *J. Mater. Chem. A*, 2015, **3**, 10703.

(42) L. Lin, M. J. Liu, L. Chen, P. P. Chen, J. Ma, D. Han and L. Jiang, *Adv. Mater.*, 2010, **22**, 4826.

(43) Z. Xue, S. Wang, L. Lin, L. Chen, M. Liu, L. Feng and L. Jiang, *Adv. Mater*., 2011, **23**, 4270.

(44) S. Gao, J. Sun, P. Liu, F. Zhang, W. Zhang, S. Yuan, J. Li and J. Jin, *Adv. Mater*., 2016, **28**, 5307.

(45) L. P. Xu, J. Zhao, B. Su, X. Liu, J. Peng, Y. Liu, H. Liu, G. Yang, L. Jiang, Y. Wen, X. Zhang and S. Wang, *Adv. Mater.*, 2013, **28**, 606.

(46) L. P. J. Xu, T. Peng, Y. B. Liu, Y. Q. Wen, X. J. Zhang, L. Jiang and S. T. Wang, *ACS Nano*, 2013, **7**, 5077.

(47) W. Ma, H. Xu and A. Takahara, *Adv. Mater. Interfaces*, 2014, **1**, 1300092.

(48) T. Guo, L. Heng, M. Wang, J. Wang and L. Jiang, Robust, *Adv. Mater*., 2016, **28**, 8505.

(49) R. A. Farrer, C. N. LaFratta, L. Li, J. Praino, M. J. Naughton, B. E. A. Saleh, M. C. Teich and J. T. Fourkas, *J. Am. Chem. Soc*., 2006, **128**, 1796.

(50) G. Wang, Y. Fang, P. Kim, A. Hayek, M. R. Weatherspoon, J. W. Perry, K. H. Sandhage, S. R. Marder and S. C. Jones, *Adv. Funct. Mater.*, 2009, **19**, 2768.

(51) J. Ford, S. R. Marder and S. Yang, *Chem. Mater.*, 2009, **21**, 476.

(52) S. L. Bechler and D. M. Lynn, *Biomacromolecules*, 2012, **13**, 1523.

(53) A. M. Rather and U. Manna, *Chem. Mater*., 2016, **28**, 8689.

(54) H. Zhu, Z. Guo and W. Liu, *Chem. Commun*., 2014, **50**, 3900

(55) C. Tan, P. Cai, L. Xu, N. Yang, Z. Xi and Q. Li, *Appl. Surf. Sci.*, 2015, **349**, 516.

(56) Z. Cheng, H. Lai, Y. Du, K. Fu, R. Hou, N. Zhang and K. Sun, *ACS Appl. Mater. Interfaces*, 2013, **5**, 11363.

(57) Z. Cheng, H. Liu, H. Lai, Y. Du, K. Fu, C. Li, J. Yu, N. Zhang and K. Sun, *ACS Appl. Mater. Interfaces*, 2015, **7**, 20410.

(58) M. J. Nine, T. T. Tung, F. Alotaibi, D. N. H. Tran and D. Losic, *ACS Appl. Mater. Interfaces*, 2017, **9**, 8393.

(59) X. Yang, X. Liu, Y. Lu, S. Zhou, M. Gao, J. Song and W. Xu, *Sci. Rep*., 2016, **6**, 23985.

(60) D. Wu, S. Z. Wu, Q. D. Chen, Y. L. Zhang, J. Yao, X. Yao, L. G. Niu, J. N. Wang and L. Jiang, *Adv. Mater.*, 2011, **23**, 545.

(61) X. Yao, J. Gao, Y. Song and L. Jiang, *Adv. Funct. Mater.*, 2011, **21**, 4270.

(62) Y. Huang, M. Liu, J. Wang, J. Zhou, L. Wang, Y. Song and L. Jiang, *Adv. Funct. Mater.*, 2011, **21**, 4436.

(63) S. M. Kang, I. You, W. K. Cho, H. K. Shon, T. G. Lee, I. S. Choi, J. M. Karp and H. Lee, *Angew. Chem. Int. Ed.*, 2010, **49**, 9401.

(64) S. T. Yohe and M. W. Grinstaff, *Chem. Commun*., 2013, **49**, 804.

(65) H.-Y. Chen, M. Hirtz, X. Deng, T. Laue, H. Fuchs and J. Lahann, *J. Am. Chem. Soc.*, 2010, **132**, 18023.

(66) L. P. Xu, D. Han, X. Wu, Q. Zhang, X. Zhang and S. Wang, *Sci. Rep.*, 2016, **3**, 38016.

(67) J. Li, L. Li, X. Du, W. Feng, A. Welle, O. Trapp, M. Grunze, M. Hirtz and P. A. Levkin, *Nano Lett.*, 2015, **15**, 675.

Title: A Facile Approach for Stabilizing Underwater Superoleophilicity*

Extremely water-repellent, bio-inspired superhydrophobic interfaces having ability to soak oil/oily phase, provide a simple basis for the selective filtration and absorbance based separation of the bulk oil/oily phases from oil/water mixtures. However, the extreme water repellence in such interfaces appears as “Achilles' heel” for the separation of another practically relevant and complex form of oil/water mixture, i.e. oil-in-water emulsion, as the suspended oil droplets in bulk aqueous phase are inaccessible to the selectively oil-absorbent superhydrophobic interface. Moreover, the superhydrophobic interface that inherently embedded with underwater superoleophilicity, is less appropriate for prolonged performance under water and at elevated temperature as the continuous trapped air layer is readily displaced on continuous exposure to aqueous phase and at elevated temperature. In the Chapter 5, a moderately hydrophobic (WCA ≤130º) multilayer coating, designed though the co-optimization of appropriate topography (following the procedure of chapter 2) and low surface energy chemistry by using 1,4-conjugate addition reaction, displayed a highly durable underwater superoleophilicity. The stability of underwater superoleophilicity in hydrophobic multilayer coating was superior than the superhydrophobic multilayer coating due to the existence of discontinuous trapped air in the hydrophobic multilayer coating. Such hydrophobic multilayer coating was further extended for developing a unique super-oil-absorbent, where naturally abundant fibrous cotton used as porous substrate. The super-oil-absorbent possessed a highly selective affinity towards oil phases even in physically and chemically harsh conditions (extremes of temperature (100°C and 10°C), pressure (184.7 mbar), and prolonged (7 days) exposures to extremes of pH (1/12), surfactant-contaminated water, artificial seawater, etc.) with absorption capacity of above 1000 wt%. Further, this super-oil-absorbent having impeccable durability was exploited in demonstrations of comprehensive and facile clean-up of oil spillages from various forms of oil/water mixtures, including bulk-oil/water mixture, oil-in-water emulsions etc. The oil/separation performance remained unaltered in extremes and complex settings that are relevant to practical scenarios following eco-friendly and energy-efficient selective-absorption/active-filtration principles.

*D. Parbat, A. Das, K. Maji and U. Manna, *J. Mater. Chem. A*, 2020, **8**, 97; D. Parbat and U. Manna *ChemSusChem*, 2017, **10**, 4839.

5.1. Introduction

Nature-inspired superhydrophobic interfaces, which are defined in the chapter 1, are artificially synthesized by the appropriate co-optimization of both essential hierarchical topography and appropriate low surface energy chemistry.[1–8] The metastable and continuous trapped air layer in the hierarchical topography is the primary basis for minimizing the contact between the beaded aqueous phase and the biomimicked superhydrophobic interfaces, which results in super-water-repellence with effortless rolling of the beaded water droplet on slight tilting of such interfaces.[9–11] This metastable and continuous trapped air layer is also hypothesized to be the prime criterion for achieving extreme oil-affinity under water which is termed as underwater superoleophilicity, in superhydrophobic interfaces.[12–14] In the past, superhydrophobic interfaces successfully explored in the separation of various forms of oil/ water mixtures (i.e., floating light oil, sedimented heavy oil and emulsified oil) following either selective absorption or filtration principles.[15–22] However, in superhydrophobic interface repels an oil-in-water emulsion, where the oil droplets are dispersed in a continuous aqueous phase. Thus, superhydrophobicity is inherently inappropriate for the separation of an oil-in-water emulsion, which is practically a more relevant and complex form of oil contaminations that has severe and adverse impacts on the environment.[23,24] In recent past, a superhydrophilic porous substrate was used strategically for the separation of oil-in-water emulsions;[25] however, this principle is ineffective for the selective absorption-based removal of oil spillage from vast and open water reservoirs.

The underwater and selective superoleophilicity is an important and emerging oil-wettability. In 2012, Wang and co-workers investigated the reason behind the transition of underwater superoleophilicity to superoleophobicity in superhydrophobic interfaces,[13] where the impact of a continuous layer of metastable trapped air on the spreading and soaking of an oil phase underwater was examined. In an earlier demonstration, the embedded underwater superoleophilicity was compromised within a few hours and gradually switched to underwater superoleophobicity over 48 hours.[13] Furthermore, this continuous trapped air layer in the superhydrophobic interface is known to be highly labile above 50ºC,[26] which makes such biomimicked interfaces inherently inappropriate to perform at elevated temperatures.[26,27] In this current chapter, a very unusual property of a moderately hydrophobic (referred to the interface that displayed water wettability with CAs in the range of 120º to 130º) multilayer coating was compared with that of a superhydrophobic multilayer coating that introduced in the Chapter 4. Unlike, the superhydrophobic interface, the hydrophobic coating can coexist with both ‘discontinuous’ trapped air and infiltrated aqueous phase when submerged under water. However, such interfaces are highly efficient for displaying underwater superoleophilicity, as similar to the freshly exposed superhydrophobic interface under water. Furthermore, the complete

switching between two extreme oil wettabilities under water for hydrophobic coating was significantly delayed to 100 days in comparison to that of the superhydrophobic coating (2 days). Even at a highly elevated temperature (90ºC), the hydrophobic multilayer coating continued to display uninterrupted underwater superoleophilicity, which is extremely difficult to achieve with superhydrophobic interfaces. Further, this approach was extended for synthesizing a sustainable super-oil-absorbent by associating the hydrophobic multi-layered coating on a naturally abundant fibrous cotton. Moreover, similar to that of the superhydrophobic coating, the as-synthesized hydrophobic super-oil-absorbent was highly efficient (1000 wt%) in selective absorption-based bulk oil phase separation from the aqueous phase even at diverse complex scenarios. Unlike superhydrophobic interfaces, this moderately hydrophobic multilayer coating, which was filled with discontinuous trapped air and inherently allowed the selective infiltration of the aqueous phase, was unprecedentedly extended for oil-in-water emulsion separations following the selective absorption principle even under challenging conditions, including extreme pH, temperatures, and salinity etc.

5.2. Experimental Section

5.2.1. Materials

Fibrous cotton was collected from the medical store of IIT-Guwahati hospital. Sources of other chemical/materials were already mentioned in the Chapter 2 and Chapter 4.

5.2.2. General consideration

The digital images were captured using a Nikon COOLPIX B700 digital camera. The oil in water emulsion droplets were characterized with Nikon Eclipse Ts2R (Nikon digital sight DS-U3). 600MHz NMR instrument was used for determining the total organic carbon value of the filtrate after oil-in-water emulsion separation. Other instrumental specifications were already mentioned in the Chapter 2 and Chapter 4.

5.2.3. Preparation of superhydrophobic and hydrophobic multilayer coatings

Superhydrophobic multilayer (9 bilayers) coating was synthesized in the presence of salt, following the procedure mentioned in the Chapter 4. Hydrophobic multilayer (20 bilayers) coating was constructed on glass substrate—in absence of any salt. The chemically reactive multilayer coating that prepared in the Chapter 2, was used to develop hydrophobic coating. The repeated 20 consecutive LbL depositions of ‘reactive’ NC and BPEI polymer in absence of salt provided chemically reactive polymeric coating. Further, the multilayer-consisted of 20 BPEI/NC bilayers were post-modified with different amine containing small molecules i.e. decylamine (DA in THF; 0.055 M), dodecylamine (DDA in THF; 0.054 M) and octadecylamine (ODA in THF; 0.0185 M). Finally, all the multilayer

coatings were washed with THF for 3 to 4 times and dried completely in compressed air prior to further essential characterisation. Further, both the hydrophobic and superhydrophobic multilayer coatings were deposited on selected substrates (fibrous cotton) for comparing the performance of the respective super-oil-absorbents towards oil-in-water emulsion separation.

5.2.4. Physical and chemical abrasions

5.2.4.1. Sand drop test: The sand drop test was performed following the earlier procedure mentioned in the Chapter 2.

5.2.4.2. Adhesive tape test: The experimental procedure for this durability was adopted from chapter 2.

5.2.4.3. Chemical durability test: The ODA-modified hydrophobic multilayer-coated cotton was exposed to various complex and harsh chemical environments including alkaline solution (pH 12), acidic solution (pH 1), SDS solution (1 mM), DTAB solution (1 mM) and artificial sea-water for 7 days to study the chemical durability of the embedded underwater superoleophilicity.

5.2.5. Preparation of 5% (v/v) DCE-in-water emulsion solutions

100 mL of deionized water was taken in a clean 250 mL glass beaker and placed it inside the water bath of the sonicator. Now total 5 mL of DCE was added using a graduated pipette (1 mL in each time) with continuous sonication for 1 hour to prepare a water-in-oil emulsion of DCE 5 (v/v)%. Then the emulsion solution was examined by DLS study and bright-field microscopic image analysis.

5.2.6. Calculation of percentage (%) of oil-absorption

The percentage (wt %) of oil-absorption is defined as the ability of absorbing oil by the given dry materials (both the ODA-treated coated cotton and bare cotton) and the parameter is calculated by following the given equation;

$$\%\ of\ oil\ absorption = \frac{Weight\ of\ absorbed\ oil}{Weight\ of\ oil\ absorbent} \text{ x } 100 \quad \text{..... (eq. 5.1)}$$

5.3. Results and Discussions

5.3.1. Comparative underwater oil wettability study on superhydrophobic and hydrophobic multilayer coatings

The superhydrophobic coating that already introduced in the last chapter has been extended further to understand the underwater superoleophilicity in detail in this chapter. The catalyst-free and facile 1,4-conjugate addition reaction between amine and acrylate groups at ambient conditions was extended

for building chemically reactive multilayer coatings of NC in both the presence and the absence of

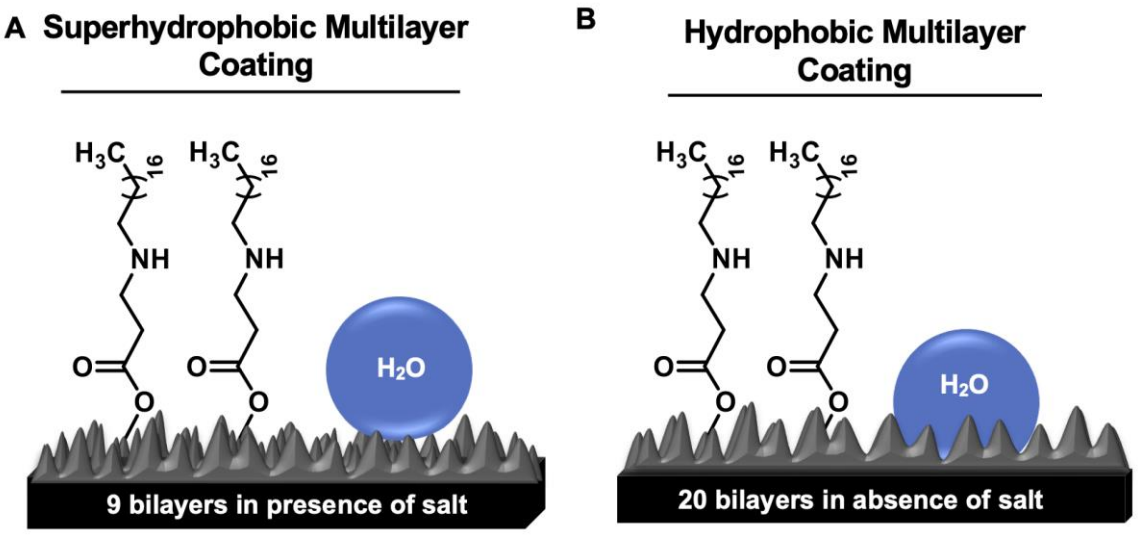

Figure 5.1: (A-B) Schematic illustration of two distinct ODA-modified multilayer coatings that displayed superhydrophobicity (A; 9 bilayers constructed in the presence of NaCl salt) and hydrophobicity (B; 20 bilayers coating fabricated in the absence of salt).

sodium chloride (NaCl, 0.5 mg mL^{-1}) salt[28], following the procedure that discussed in the Chapter 4. The multilayer (9 bilayers) coating that prepared in the presence of the salt, displayed superhydrophobicity, (Fig. 5.1A and Fig. 5.2A), after post modification with selected alkylamine (i.e., octadecylamine (ODA)).[28] However, the multilayer (9 bilayers) coating prepared in absence of the salt displayed low hydrophobicity with a WCA of 104° after identical post-covalent modification as shown

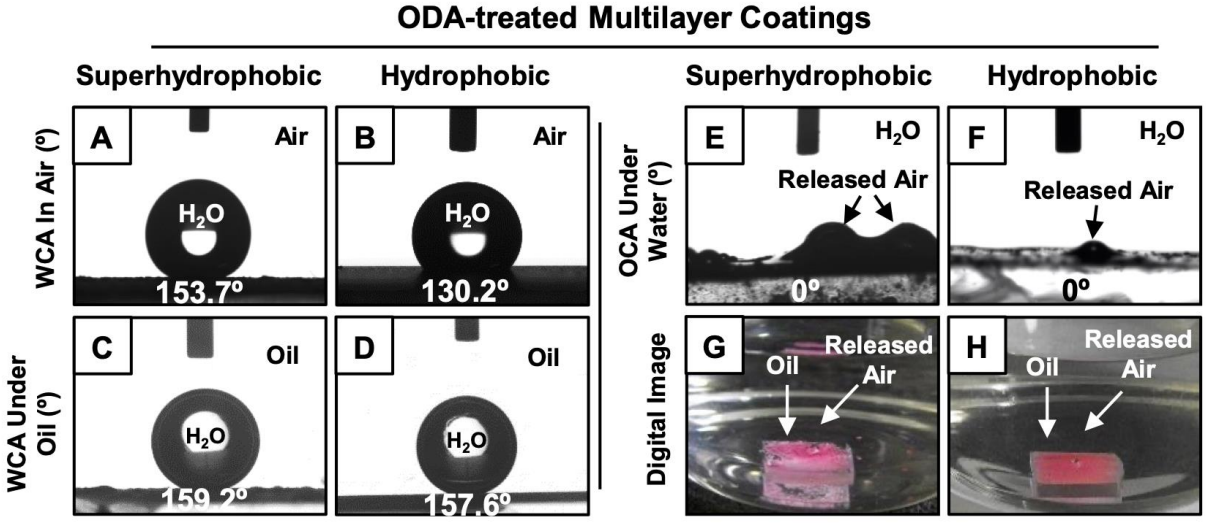

Figure 5.2: (A-D) CAs of beaded water droplets on both superhydrophobic (A,C) and hydrophobic (B,D) multilayer coatings in air (A-B) and under oil (C–D), respectively. (E–H) CA (E-F) and digital images (G-H) depicting the soaking of beaded oil droplet on both superhydrophobic (E,G) and hydrophobic (F,H) multilayer coatings under water followed by the release of continuous and discontinuous trapped air from respective multilayer coatings.

in Fig. 4.5E (in the Chapter 4). Such low hydrophobicity was inappropriate in the relevance to the

design of underwater superoleophilicity in this current chapter. However, another chemically reactive multilayer coating (20 bilayers) that introduced in the Chapter 2, displayed moderate hydrophobicity (Fig. 5.1B) in air with a WCA of 130º (Fig. 5.2B), after post-covalent modification with the same alkylamine (i.e., ODA). Interestingly, the moderately hydrophobic multilayer coating (20 bilayers, ODA treated; prepared in absence of salt) displayed extreme water repellence under oil with WCA of 157º, similar to the superhydrophobic multilayer coating (9 bilayers, ODA treated; prepared in presence of salt) as shown in Fig. 5.2C-D. This heterogeneous water-wettability under oil was likely due to the appropriate confinement of an external oil phase in both the hydrophobic and superhydrophobic multilayer coatings.

On the other hand, both the superhydrophobic and hydrophobic multilayer coatings displayed super-affinity for oil phase with OCA of 0º under water, as shown in Fig. 5.2E-H. Eventually, both the continuous and discontinuous trapped meta-stable air layers, which were present in the

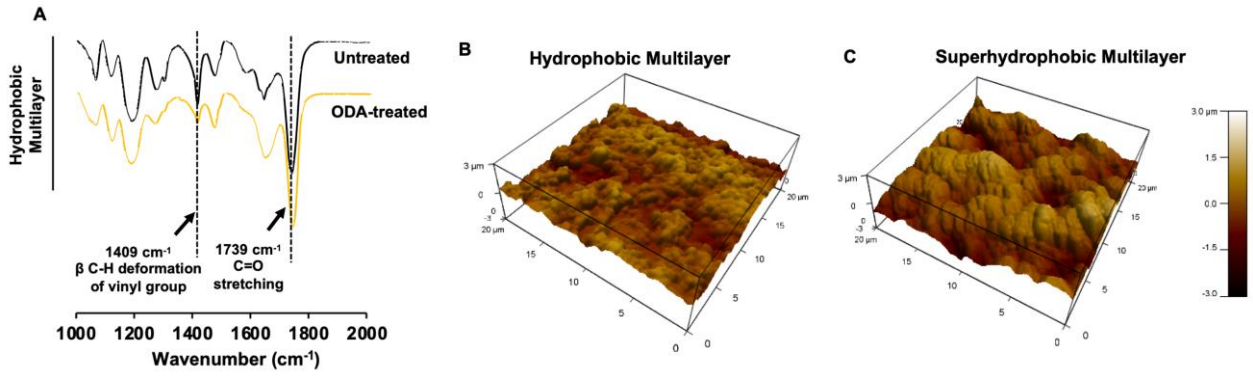

Figure 5.3: A FTIR spectra of the multilayer (20 bilayers) coating before (black) and after post-modification (yellow) with ODA. Three dimensional atomic force microscope (AFM) images of hydrophobic (A) and superhydrophobic (B) multilayer coatings over an area of 20 μm x 20 μm. Both the images are calibrated at the same Z value.

superhydrophobic and hydrophobic interfaces, respectively, were released from the respective multilayer coatings (Fig. 5.2E-H). The characterization of post-chemical modification (with ODA) of multilayer (9 bilayers, prepared in presence of salt) coating that provided superhydrophobicity has been already discussed in the Chapter 4 (Fig. 4.4). However, the same post covalent modification (with ODA) of the multilayer (20 bilayers) coating that prepared in absence of salt was characterized with standard and widely accepted Fourier transform infra-red spectroscopy (FTIR) analysis. After treatment with selected alkylamine (ODA), significant depletion in IR peak intensity at 1409 cm^{-1} (corresponding to the C–H deformation of the β-carbon of vinyl group) with respect to the IR peak intensity for the carbonyl stretching at 1739 cm^{-1} (Fig. 5.3A), which revealed the successful post-covalent reaction between the primary amine groups of ODA and the residual acrylate groups present in the synthesized multilayer coating. Further, atomic force microscopy (AFM) imaging of both the

multilayer (hydrophobic and superhydrophobic) coatings were carried out; it confirmed the existence of completely distinct topography in both the superhydrophobic and hydrophobic multilayer coatings (Fig. 5.3B-C), where both the multilayer (20 bilayers and 9 bilayers) coatings were post modified with ODA. The roughness in both the hydrophobic and superhydrophobic multilayer coating were also calculated to be 423.5 ± 15.7 nm and 735.2 ± 20.8 nm, respectively. This change in the roughness for the hydrophobic and superhydrophobic multilayer has a significant impact on minimizing the contact area between the beaded aqueous phase and the respective multilayer coatings. The fraction of contact area was measured following the modified Cassie–Baxter equation (eqn (5.2)),[1–3,29] where θ and θ_r are the static WCAs of the ODA-treated smooth (80.7º, 2 bilayered coatings) and rough hydrophobic (130.2º) and superhydrophobic (153.7º) multilayer coatings.

$$\cos \theta_r = f_1 \cos \theta + f_2 \quad \ldots\ldots\ldots\ldots\ldots\ldots\ldots\ldots \quad (5.2)$$

The fractions of contact area for the beaded water droplet with both multilayer coatings (hydrophobic and superhydrophobic) and the trapped air were denoted as f_1 and f_2, respectively, and

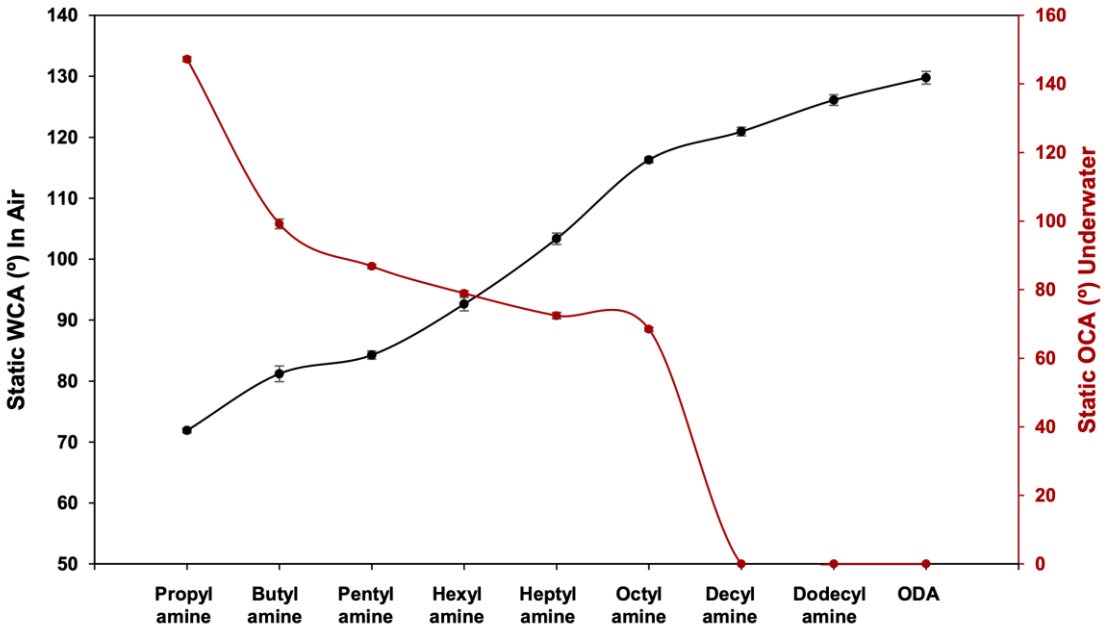

Figure 5.4: The plot shows the change in WCA (in air) and OCA (under water) of beaded water (black) and oil (red) phase on the multilayer (20 bilayers) coatings after post-modification with various alkylamines, including propylamine, butylamine, pentylamine, hexylamine, heptylamine, octylamine, decylamine, dodecylamine and ODA (octadecylamine).

the total fraction of contact area ($f_1 + f_2$) between the beaded water droplet with multilayer coatings and trapped metastable air was considered to be 1.[29] Smooth and featureless multilayer was built from

the same chemical ingredients following the procedure discussed in the Chapter 4. The dominant hierarchical roughness in the superhydrophobic multilayer allowed the trapping of a continuous layer of metastable air, which reduced the fraction of contact area between the aqueous phase and the multilayer coating to 0.089. In contrast, the hydrophobic multilayer that was loaded with discontinuous trapped air allowed the beading of a liquid water droplet with a higher fraction (0.305) of contact area than that of the superhydrophobic coating. Nevertheless, the hydrophobic multilayer displayed underwater superoleophilicity very similar to that of the superhydrophobic interface (Fig. 5.2E-H). Furthermore, experiments were designed to investigate the relation between the water wettability (in air) and oil wettability (under water) of the multilayer coatings depending on the selection of post-

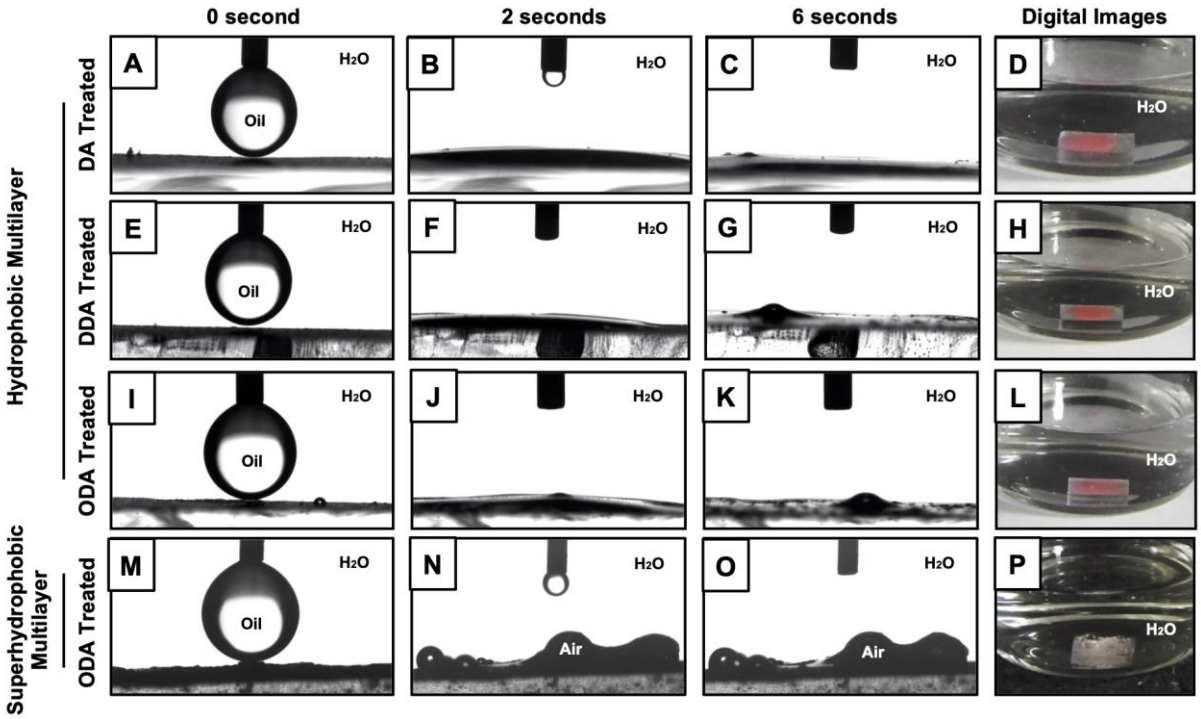

Figure 5.5: (A-L) CA images comparing the extent of release of trapped air on soaking oil droplet on both hydrophobic (DA treated: A-C; DDA treated: D-F and ODA treated: G-I) and superhydrophobic (ODA treated: J-L) multilayer coatings under water.

chemical modifications. The multilayer (20 bilayers, prepared in absence of salt) coatings were individually post-modified with different alkylamines (i.e., propylamine, butylamine, pentylamine, hexylamine, heptylamine, octylamine, decylamine, dodecylamine and octadecylamine) through the 1,4-conjugate addition reaction for tailoring a wide range of water wettabilities in air. A variation in underwater oil wettability was also noted for the multilayer (20 bilayers) coatings having different water wettabilities depending on the post-chemical modifications, as shown in Fig. 5.4. The multilayer coatings having WCA ≥120º displayed underwater superoleophilicity with an OCA of 0º as shown in Fig. 5.4. On exposure of both superhydrophobic and moderately hydrophobic (WCA ≥120º) coatings

to oil phase under water, the release of the continuous trapped air from the superhydrophobic interfaces was observed to be much faster compared to that of the hydrophobic interfaces which were packed with discontinuous trapped air, as evident from Fig. 5.5. In fact, the stability of the underwater superoleophilicity in the hydrophobic multilayer coating was noticed to be exceptionally superior over that of the superhydrophobic interface, as clearly evidenced in Fig. 5.6. The inherent extreme oil

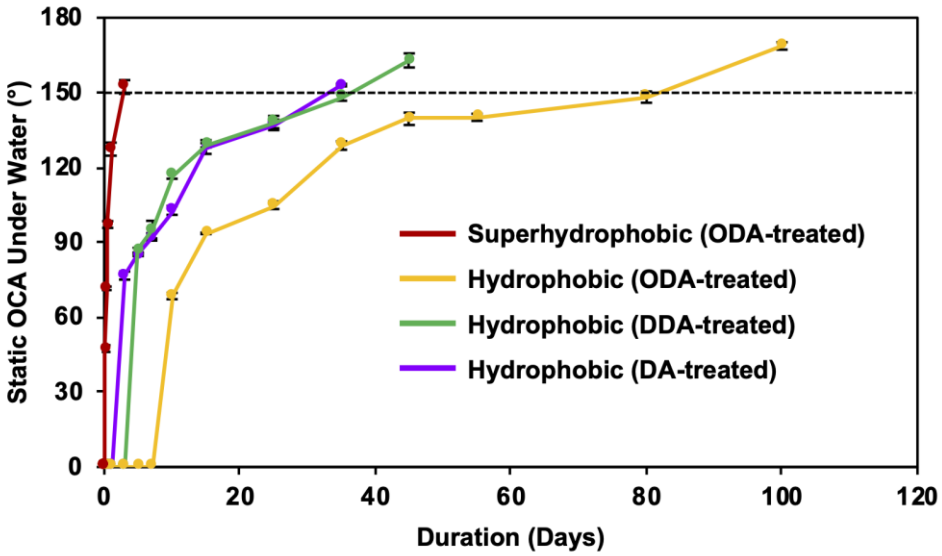

Figure 5.6: The plot accounts the change in underwater oil wettability with time (days) for both the hydrophobic (purple, green and yellow) and the superhydrophobic multilayer (ODA, red) coatings, where the hydrophobic multilayer (20 bilayers) coatings were post-modified with decylamine (DA, purple), dodecylamine (DDA, green), octadecylamine (ODA, yellow).

affinity underwater in the superhydrophobic multilayer coating was noticed to be compromised within a few hours and resulted in altering the superoleophilicity to superoleophobicity of the same multilayer coating under water after continuous exposure to the aqueous phase for 2 days, as shown in Fig. 5.7A. In contrast, moderately hydrophobic multilayer coating, which were loaded with discontinuous trapped air (Fig. 5.7B), remained as underwater superoleophilic with OCA of 0º even after submerging the interface for consecutive 7 days. Moreover, in case of the moderately hydrophobic multilayer coating, the duration for a complete transition between the two extreme oil wettabilities from superoleophilicity to superoleophobicity was significantly delayed to 100 days (Fig. 5.6 and Fig. 5.7B,D), which was remarkably higher than that for the superhydrophobic interface (2 days). However, the hydrophobic multilayer, which were post-chemically optimized with the lower analogues (e.g., DDA and DA) of ODA, displayed less stability of underwater superoleophilicity with respect to the ODA-treated hydrophobic interface, as noted in Fig. 5.6, and the release of trapped air was also slower for such multilayer coatings as shown in Fig. 5.5A-H. Thus, both the chemistry and topography in multilayer coatings played a crucial role in modulating the stability of underwater superoleophilicity.

Furthermore, the continuous trapped air layer in the superhydrophobic interfaces is known to be labile at elevated temperatures and therefore, the superhydrophobic multilayer readily and completely failed to display underwater superoleophilicity at 50 ºC, rather displayed underwater superoleophobicity as shown in Fig. 5.8A-B. In contrast, the ODA-treated hydrophobic multilayer coating remained

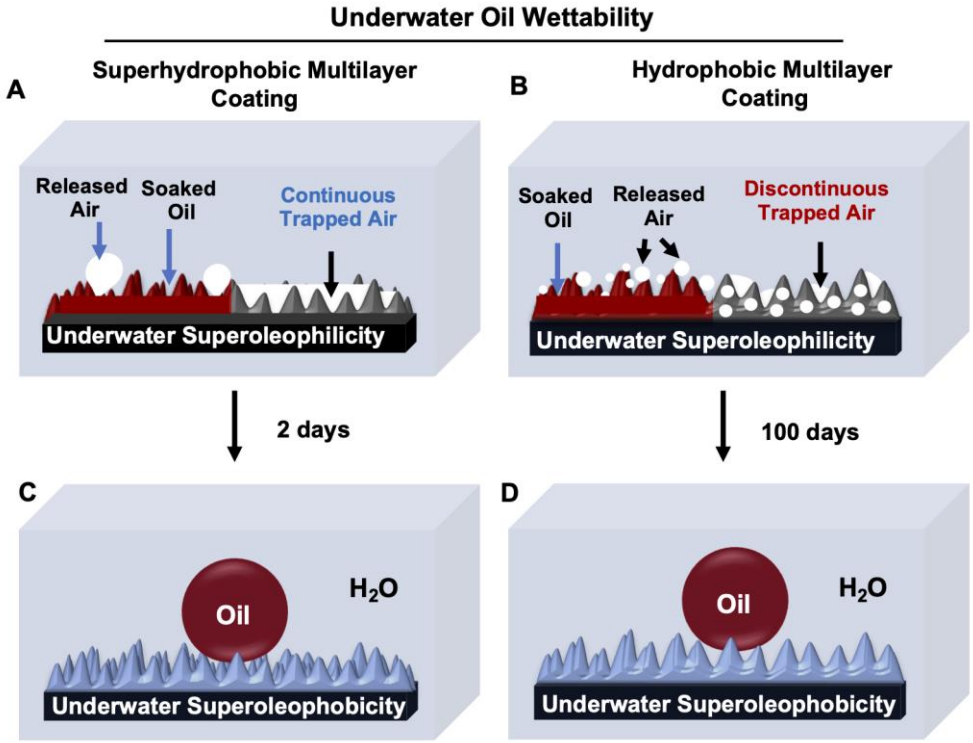

Figure 5.7: (A-B) The underwater oil wettability on both the superhydrophobic (A; having continuous trapped air phase) and hydrophobic (B; having discontinuous trapped air phase) multilayer coatings. (C-D) The complete and extreme switching of underwater oil wettability (from superoleophilic to superoleophobic) in superhydrophobic (C) and hydrophobic (D) multilayer coatings after continuous submersion of the respective multilayer coatings for 2 days and 100 days, respectively.

superoleophilic at 50ºC, and this extreme oil affinity of the hydrophobic multilayer remained unperturbed even at 90ºC, as illustrated in Fig. 5.8C-D. The exact reason for this superior thermal stability of hydrophobic multilayer has yet to be revealed experimentally. The discontinuous trapped air layer (Fig. 5.7B) in the hydrophobic multilayer played a crucial role in such superior thermal stability. In the past, experiments were designed to reveal the reason behind the failure of superhydrophobicity at high temperatures.[30] It was experimentally validated that superhydrophobicity was readily compromised when the temperature of the superhydrophobic surface was lower than that of the beaded aqueous phase due to the condensation process at the interface.[30] In general, at high temperatures, the thermally insulating continuous trapped air layer in the superhydrophobic coating is expected to keep the superhydrophobic surface cooler than the aqueous phase as the continuous metastable trapped air (Fig. 5.7A) prevented the transport of heat across the solid/liquid interface. As a result, the superhydrophobic multilayer coating failed to perform at high temperatures. In contrast,

in hydrophobic multilayer coatings, the discontinuous trapped air layer allowed the infiltration of the aqueous phase into the hydrophobic coating, as evident from Fig. 5.9A–D. Thus, the heat transported across the interface of the hydrophobic multilayer coating and the aqueous phase remained continuous, and this process was likely to prevent any difference in temperature at the solid/liquid interface for the

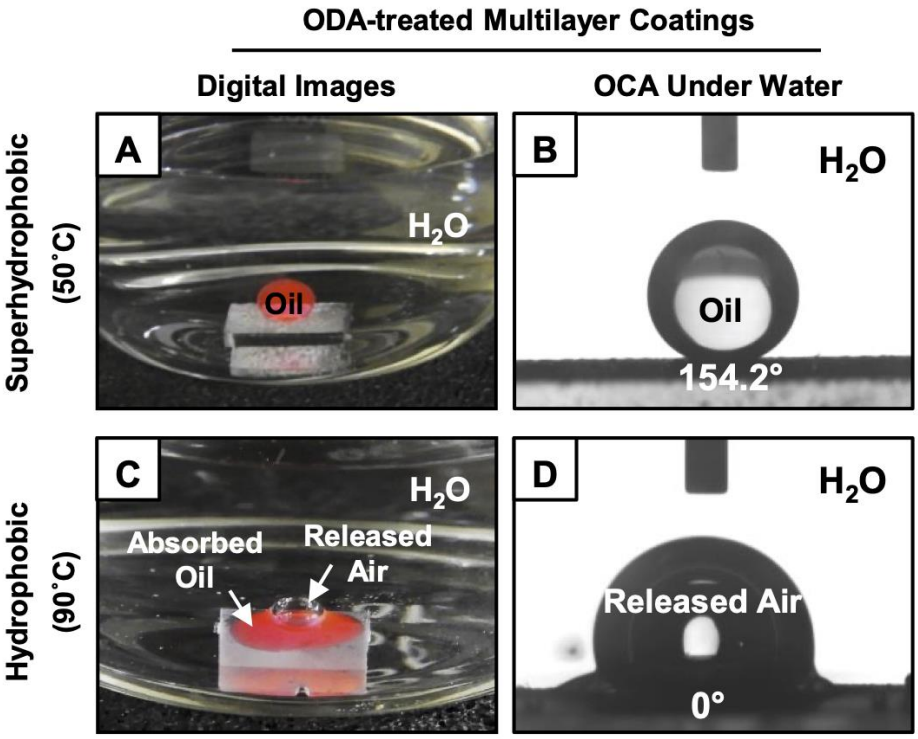

Figure 5.8: (A-D) Digital (A,C) images and underwater OCA images (B,D) of the beaded oil droplets on superhydrophobic (A-B, ODA-modified) and hydrophobic (C-D, ODA-modified) multilayer coatings at elevated temperatures (50°C for superhydrophobic coating and 90°C for hydrophobic coating).

hydrophobic multilayer coating. Eventually, the hydrophobic multilayer coating continued to perform at high temperatures in reality. Thus, the hydrophobic multilayer coating was inherently endowed with superior stability of embedded superoleophilicity under water even at elevated temperatures in comparison to the superhydrophobic multilayer coating.

5.3.2. Investigation on selective underwater oil-affinity for hydrophobic and superhydrophobic multilayer coatings

Furthermore, experiments were designed to investigate the selective affinity of both the superhydrophobic and hydrophobic multilayer (20 bilayers, ODA treated) coatings towards the oil/oily phase under water, where the as-synthesized superhydrophobic and hydrophobic multilayer coatings were submerged in a dye (water soluble fluorescein dye displays green fluorescence) added aqueous phase. In the case of the hydrophobic multilayer, the aqueous phase immediately infiltrated the porous multilayer coating, as evident from the appearance of the green fluorescence signal from the

hydrophobic polymeric coating (Fig. 5.9B). However, no fluorescence signal was observed for the

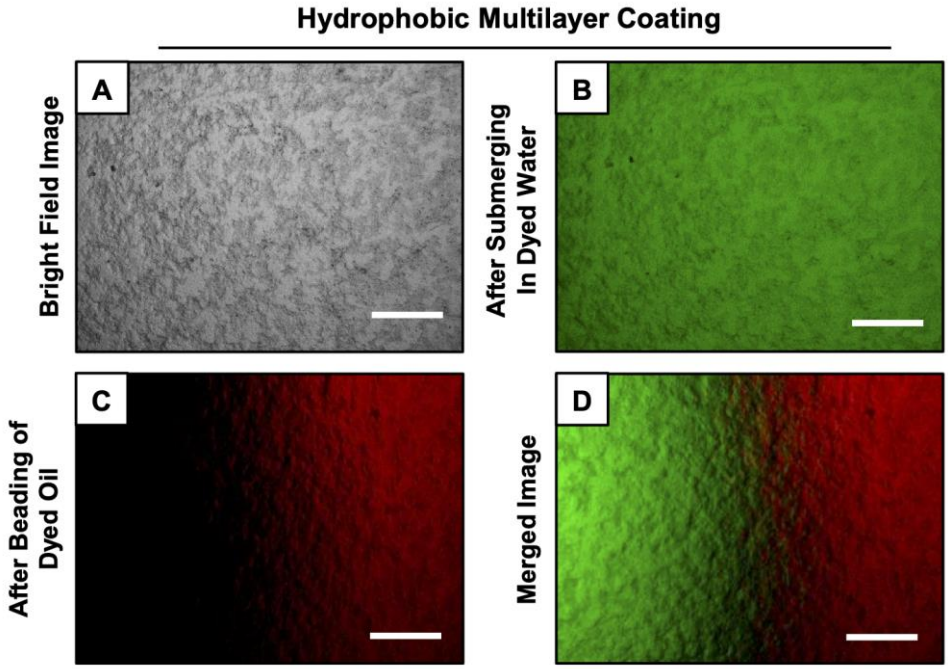

Figure 5.9: (A-D) Bright field (A) and fluorescence (B-D) images of hydrophobic multilayer (20 bilayers and ODA-treated) coating after submerging into aqueous phase (dyed with fluorescein; B), followed by beading of oil phase (dyed with Nile red; C) under water. (D) Merged image of B and C. Scale bar: 200 μm.

superhydrophobic coating as the continuous layer of trapped air in the superhydrophobic multilayer restricted the infiltration of the aqueous phase inside the coating (Fig. 5.10B). After this aqueous (dye

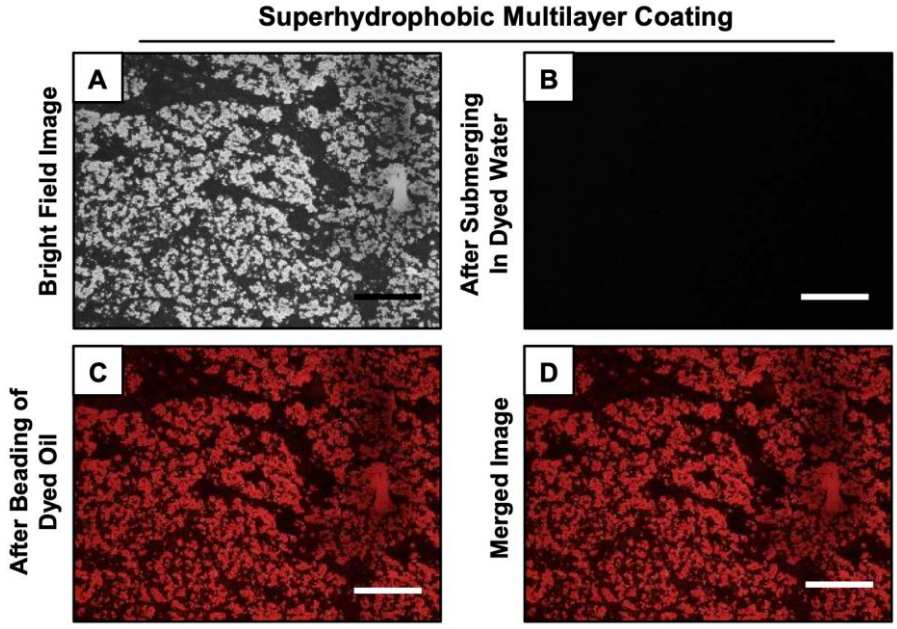

Figure 5.10: (A-D) Bright field (A) and fluorescence (B-D) images of superhydrophobic multilayer (9 bilayers and ODA treated) coating after submerging into aqueous phase (dyed with fluorescein; B), followed by beading of oil phase (dyed with Nile red; C) under water. (D) Merged image of B and C. Scale bar: 200 μm.

added) submersion, immediately, both the hydrophobic and superhydrophobic multilayer coatings

were exposed to the Nile red dye (water immiscible dye provides a red fluorescence signal) contaminated oil phase under water. The dye-added oil phase was immediately soaked by both the multilayer coatings, as evident from the red fluorescence signal from respective hydrophobic (Fig. 5.9C) and superhydrophobic (Fig. 5.10C) polymeric coatings. Interestingly, the infiltrated aqueous phase in the hydrophobic multilayer was completely replaced by the beaded oil phase underwater. The merged image (Fig. 5.9D) of hydrophobic multilayer coating (after consecutive exposures to aqueous phase and followed by oil phase), unambiguously confirmed the gradual replacement of entrapped aqueous phase by beaded oil phase in the hydrophobic multilayer coating. However, such replacement of aqueous phase was not observed in superhydrophobic interface (Fig. 5.10D, merged image) as the continuous trapped air layer prevented the penetration of aqueous phase during short exposure (few minutes) to the dye added aqueous phase. Thus, both hydrophobic and superhydrophobic multilayer coatings have highly selective affinity towards oil phase under water.

5.3.3. Synthesis and characterization of hydrophobic coating based super-oil-absorbent

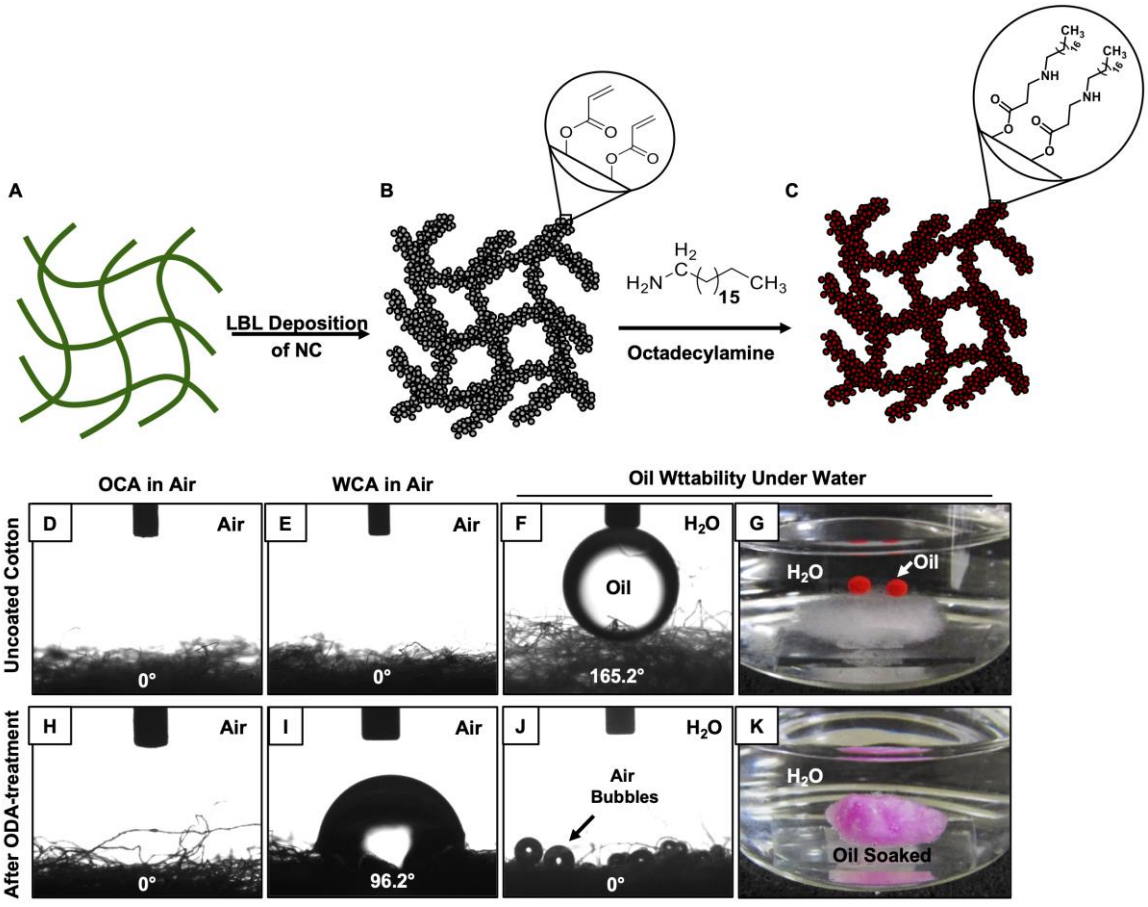

Figure 5.11: (A-C) Schematic illustrating the deposition of chemically reactive multilayer (20 bilayers) coatings on the fibrous cotton (A-B) followed by post-chemical modification of the multilayer coating with ODA (C). (D-K) CA images (D-F, H-J) and digital images (G,K) of beaded oil (D,H; in air and F-G, J-K; under water) and water (E,I; in air) droplets on bare (D-G) and ODA-treated coated cotton (H-K).

Inspired from this robust underwater superoleophilicity in hydrophobic multilayer coating, a sustainable super-oil-absorbent was designed through appropriate association of naturally abundant fibrous substrate and hydrophobic multilayer coating of NC (Fig. 5.11A-C), for facile and environment-friendly removal of different forms of oil spills at practically relevant diverse and severe conditions. In the past, fibrous substrates were strategically used in developing efficient materials for removing the oil-spills.[31-35] In this chapter, the naturally abundant oleophilic and hydrophilic (Fig. 5.11D-E, in air) fibrous cotton—that inherently and extremely repels oil droplets (red colour for visual inspection) under water with Advancing OCA of ~165° (Fig. 5.11F-G) was judiciously chosen as a substrate for constructing durable underwater superoleophilic coating, with a hypothesis that the

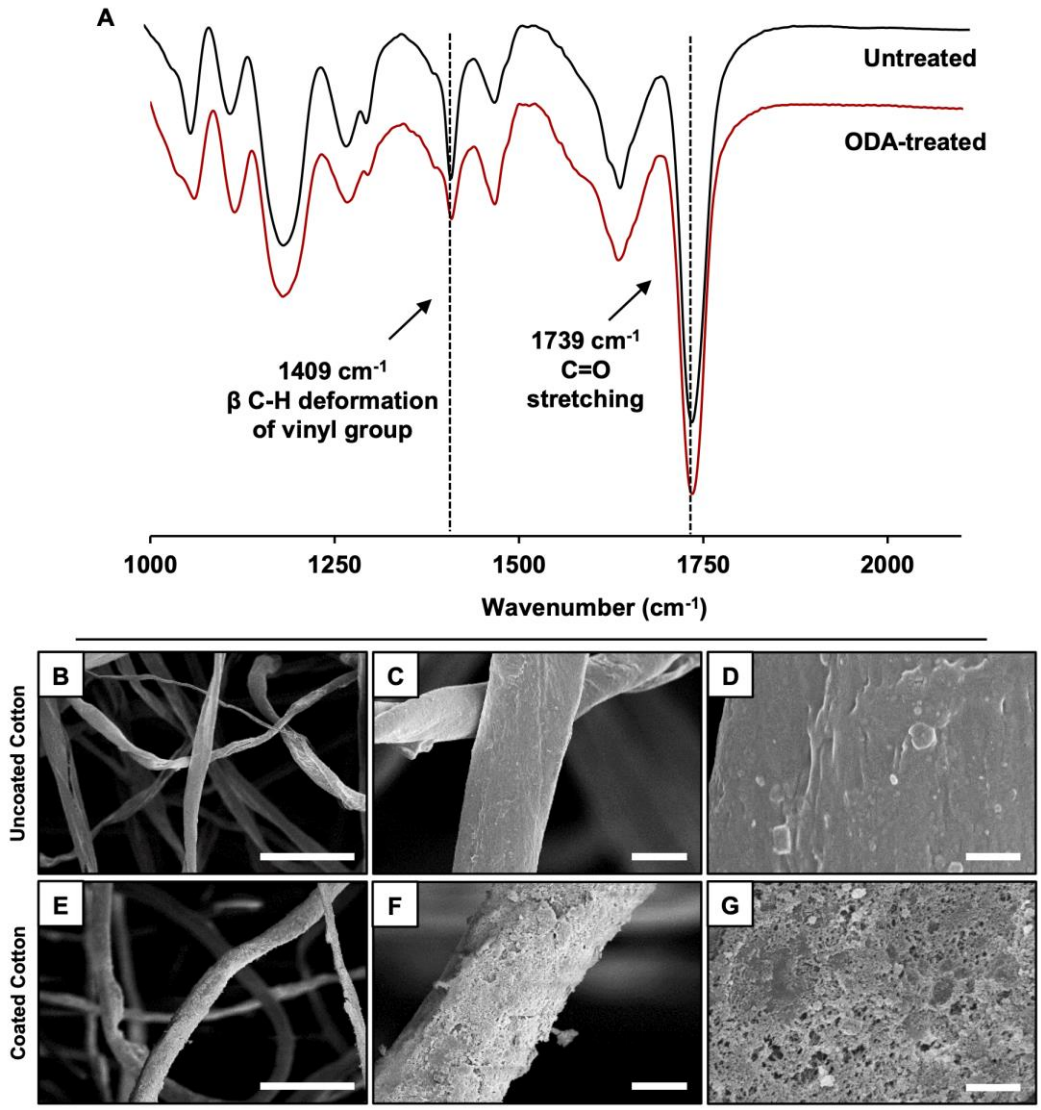

Figure 5.12: (A) FTIR spectra of multilayer (20 bilayer) coated fibrous cotton before (black) and after (red) post-modification with ODA. (B-G) FESEM images of bare (B-D) and hydrophobic multilayer-coated (E-G) cotton in different magnifications. Scale bar: 20 μm (B,E); 10 μm (C,F); 2 μm (D,G).

optimum integration of i) multilayer coatings with essential chemistry/topography and ii) inherent

capillary effect of fibrous substrate would provide the desired extreme oil-absorption property. Further, iii) the squashy cotton allowed distillation free easy recovery of the absorbed oil by applying simple compressive strain on the material. After optimizing the appropriate chemistry and topography in the coated cotton (Fig. 5.11A-C) the underwater oil wettability was drastically changed and the beaded oil droplet was instantly soaked in the material (Fig. 5.11J-K) with concomitant release of some air-bubbles from the interior of the material to the surface (Fig. 5.11J). The release of the trapped air was very rapid after beading the oil droplet on the material under water as similar to the hydrophobic coating on glass substrate that discussed in the earlier section (Fig. 5.2F) in this chapter. Thus, the

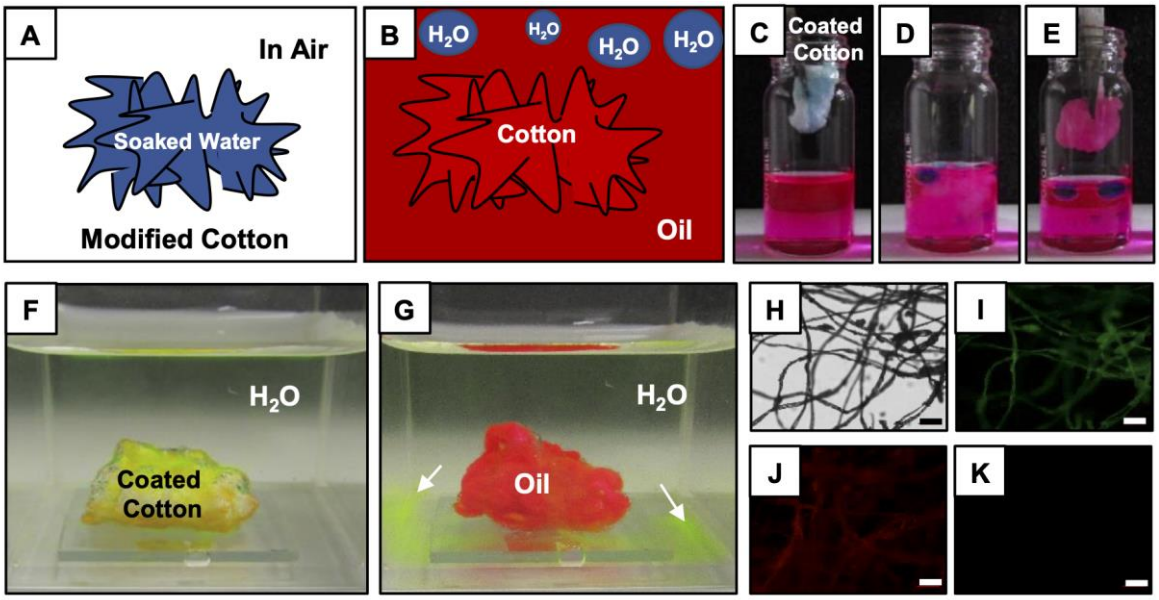

Figure 5.13: (A-B) Demonstration of selective replacement of preloaded aqueous phase (blue coloured) from the super-oil-absorbent by instant influx of oil (red coloured) phase. (C-E) Digital images of super-oil-absorbent that has soaked blue (methylene blue dye) coloured aqueous phase in air (C), after placing under red dyed (Nile red) oil phase (D), and subsequently, after removal of oil phase (E). (F-G) Digital images of super-oil-absorbent (under water) after preloading of green coloured (dyed with fluorescein) aqueous phase (F) and after ejection of water soluble green dye molecules on the exposure to red coloured oil phase (G). The ejected dye was pointed out with white arrows (G). (H-K) Bright-field (H; scale bar: 100 μm) and fluorescence images (I-K; scale bar: 100 μm) of the super-oil-absorbent after soaking the aqueous solution of fluorescein in air and followed by keeping it under water for 5 minutes (H-I), and after exposure to the red coloured oil phase (J-K), (K) No fluorescence signal for fluorescein was noticed in green channel after exposure of super-oil absorbent to the oil phase.

extremely oil repelling cotton became super-oil-absorbent under water. Further, the topography and post covalent modification of the multilayer coating were investigated with FTIR analysis and field emission scanning electron microscope (FESEM) images, respectively. The post-chemical modification of coating on fibrous cotton was examined with FTIR analysis, where the intensity of IR peak at 1409 cm^{-1} was significantly depleted with reference to the carbonyl stretching at 1739 cm^{-1} (Fig. 5.12A), mainly due to the mutual covalent reaction between the residual acrylate groups and primary amine groups from ODA molecules. Moreover, the featureless (Fig. 5.12B-D) fibers of cotton

were uniformly coated with granular polymeric domains as evidenced from Fig. 5.12E-G. Thus, after consecutive multilayer deposition of NC and following covalent modification with ODA molecules, the fibrous cotton was decorated with an appropriate topography and essential chemistry for a) instant absorption of oil and b) even ejection of penetrated water (that was absorbed in air) from the material, under both oil and water. The water droplets beaded on the synthesized material with a temporary WCA of ~ 96° in air and the entire droplet was soaked in the porous coated cotton within few minutes. Interestingly, the material that was wet with aqueous phase in air was proficient in spontaneous absorption of oil by displacing the metastable impregnated aqueous phase from the material once exposed to the oil phase (Fig. 5.13A-B). The blue coloured (due to methylene blue dye) trapped water was instantly released from the synthesized material on placing the wet (by aqueous phase in air) coated cotton in red coloured (Nile red dye) oil (DCM, model oil) phase (Fig. 5.13C), and the blue coloured cotton was completely transformed to red (Fig. 5.13D-E)—due to selective infiltration of oil phase and complete removal of water phase from the synthesized material. Moreover, such excellent super-oil-absorption and the instant release of impregnated water were also observed even under water—which is unprecedented and remarkable. First, the coated and post-modified (with ODA) cotton (denoted as super-oil-absorbent in the rest of the text), which was wetted by green coloured (fluorescein: water soluble dye) aqueous solution in air, was immersed in DI water for 5 minutes, and the super-oil-absorbent appeared green due to the presence of fluorescein dye added aqueous phase in the material (Fig. 5.13F). However, after exposing the material to the red coloured (water insoluble Nile red dye) oil phase, the impregnated green dye (fluorescein—which is only soluble in water) was continuously being ejected out from the material (Fig. 5.13G)—mostly due to removal of the metastable aqueous phase—which was pre-confined in the material prior to exposure of oil phase. Further, the material that soaked aqueous solution of fluorescein in air, was characterized with fluorescence microscope, before and after submerging under water, and even after exposing to red (Nile red dye)-oil phase. As expected, a strong fluorescence signal for fluorescein molecule was noticed from the material that soaked aqueous solution of fluorescence in air, and after the immersion of the same material under water (Fig. 5.13H-I) for 5 minutes. However, after exposing the material to the Nile red (water insoluble dye) added oil phase, only the fluorescence signal for the Nile red dye was observed—and the characteristic signal for fluorescein from the material disappeared completely (Fig. 5.13J-K). Thus, the metastable aqueous phase—which was pre-infused in the synthesized material in air, was readily removed from the material once it get contact with the oil phase. The chemistry and topography in the material provided better interaction with the oil phase over the aqueous phase. Therefore, the current synthesized material soaked water in air and repelled water extremely under oil as shown in Fig. 5.13C-E and Fig. 5.2D. Next, the super-oil-absorbent that was

Physical/Chemical Insults	Oil Absorption Ability
Adhesive Tape Test	Unperturbed
Sand Drop Test	Unperturbed
Alkaline (pH 1) Water	Unperturbed
Acidic (pH 12) Water	Unperturbed
Artificial Seawater	Unperturbed
SDS (1 mM) Water	Unperturbed
DTAB (1 mM) Water	Unperturbed

Table 5.1: Accounted the performance of super-oil-absorption at physically harsh settings like adhesive tape test, sand drop test and chemically diverse and complex scenarios including extremes of pH, artificial seawater and surfactants (SDS, DTAB)-contaminated water.

wetted by water in air, was subsequently exposed to oil/water mixtures—which were kept at extremes of temperatures (100°C and at 10°C), and the oil (red colour aids visual inspection) phase was immediately soaked in the material as accounted in Table 5.1. This interesting and remarkable oil absorption ability of the coated (ODA-treated) cotton under water, remained unaltered, even after physical harsh manipulations (Table 5.1) and prolonged (7 days) exposure of the synthesized super-oil-absorbent to various chemically challenging aqueous media, e.g., extremes of pH, artificial seawater, cationic and anionic surfactant contaminated aqueous media (Table 5.1).

5.3.4. Performance of the super-oil-absorbent in bulk oil/water separation

Further, this material was explored in separation and collection of oil from diverse and complex oil/water mixtures including the floating oil (on water), sediment oil phase (under water) and oil-in-water emulsion, through both the selective absorption and the filtration processes. Moreover, the oil/water separation performance was compared with the bare cotton—which has intrinsic underwater extreme-oil-repellence. As a proof of concept demonstration, the super-oil-absorbent material was brought in contact with a floating oil droplets (i.e. motor oil), and immediately the oil droplet was soaked in the material and the absorbed oil (Fig. 5.14A-C) was collected in a separate place just by manually compressing the oil absorbent. Next, the super-oil-absorbent was strategically exploited in collection of sediment oil phase under water (Fig. 5.14E-G). In contrast, the underwater superoleophobic-cotton (uncoated cotton) was inappropriate for such absorption based oil/water separation as shown in Fig. 5.14D,H. The oil-absorption capacity of the super-oil-absorbent was measured (using eq. 5.1) to be above 1000 wt% for the model heavy oil (DCM) and light oil (silicone

oil) at ambient condition (Fig. 5.15A). Moreover, this super-oil-absorbent separated (with efficiency

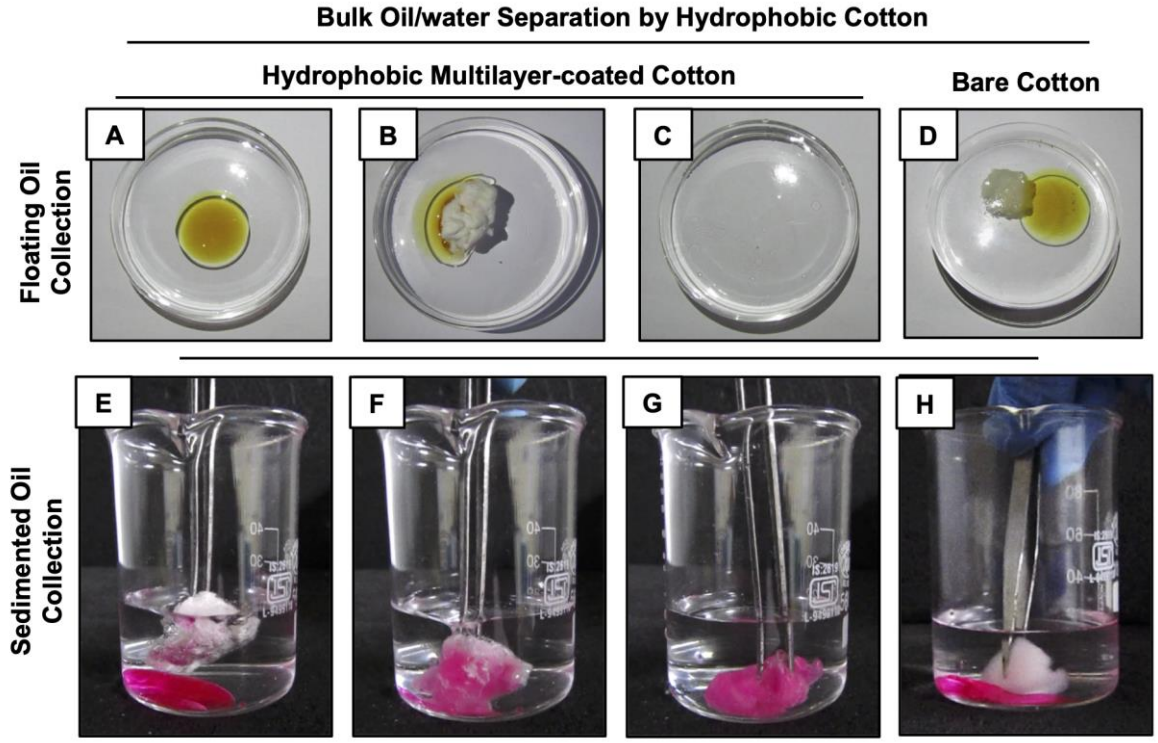

Figure 5.14: (A-H) Digital images demonstrating absorption-based removal of floating light oil (motor-oil; A-D) and sedimented heavy oil (DCM; E-H) by the (A-C, E-G). This oil/water separation performance of the super-oil-absorbent was compared with the bare cotton (D,H).

around 100 wt%, Fig. 5.15B) the bulk oil/water mixture through instant and selective absorption of oil from diverse and chemically-complexed aqueous media including extremes of pH, artificial seawater,

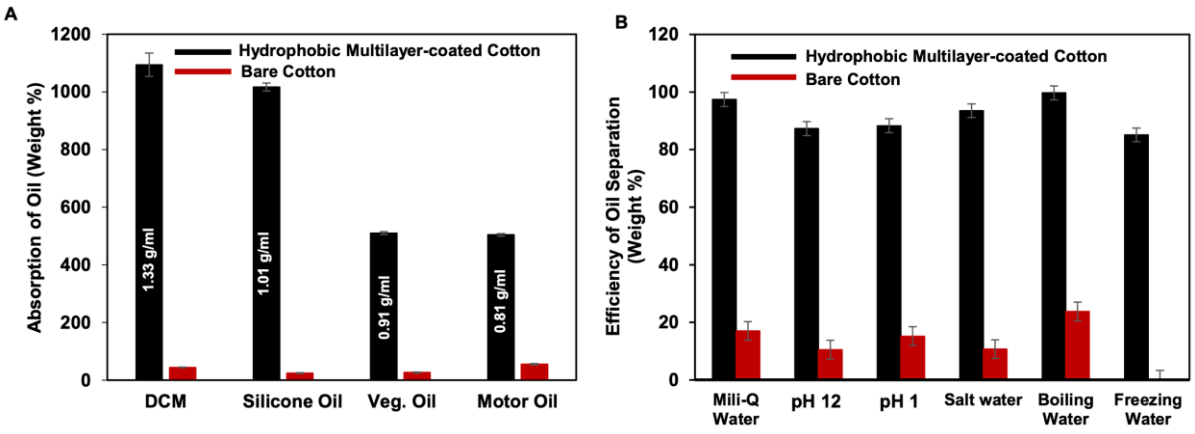

Figure 5.15: (A) Representing the oil (heavy and light) absorption capacity (wt%) of the super-oil-absorbent. (B) Accounting the oil/water separation efficiency by the super-oil-absorbent in diverse and complex practically relevant settings.

boiling water, highly cold (10°C) water (Fig. 5.15B). Such materials would be useful in cleaning of oil-spillages from open and vast water reservoirs at practically relevant settings.

5.3.5. Oil-in-water emulsion separation by the super-oil-absorbent

Next, the performances of the hydrophobic and superhydrophobic multilayer coated fibrous cotton in separating oil-in-water emulsions were compared in detail. In general, the continuous meta-

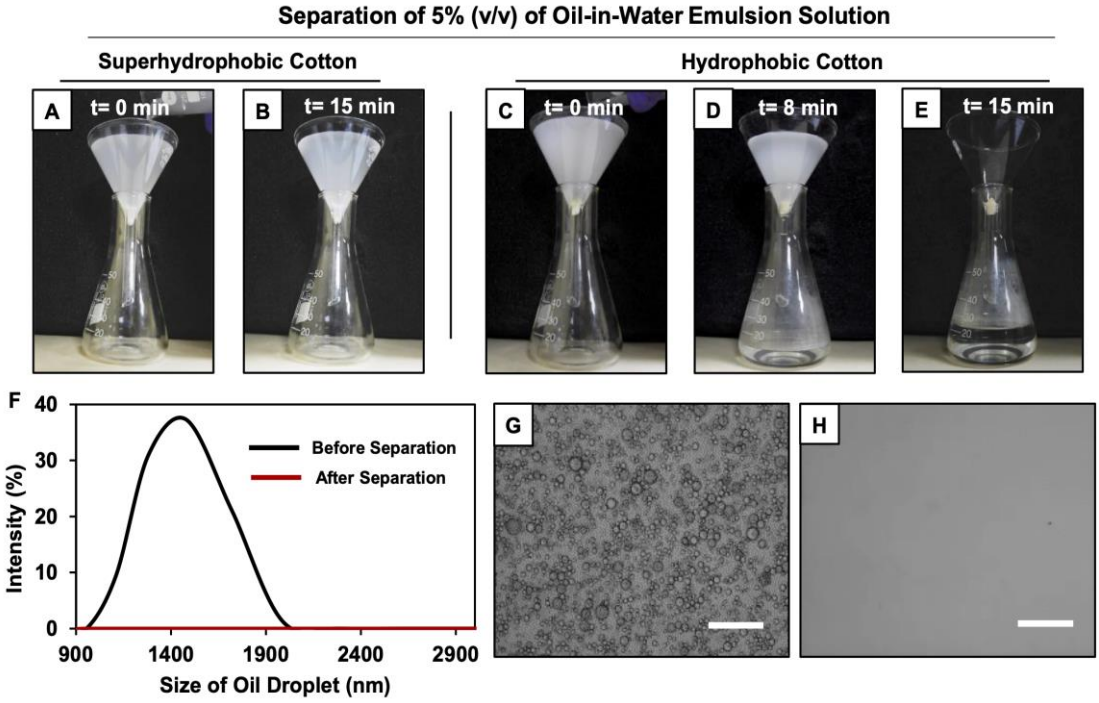

Figure 5.16: (A–E) Comparing the performances of oil-in-water emulsion (5% (v/v) DCE in water) separation with superhydrophobic (A-B) and hydrophobic (C–E) multilayer coated fibrous cottons. (F-H) DLS plot (F) and bright field microscopic images (G-H) accounting the oil-in-water emulsions before (F: black curve, G) and after (F: red curve, H) separation with hydrophobic multilayer-coated cotton; scale bar: 100 µm.

stable trapped air in the superhydrophobic interfaces minimize the physical contact between the beaded water and solid interface. Eventually, the oil-in-water emulsion consisting of tiny oil droplets with the diameter of hundreds/ thousands of nanometers, dispersed in the bulk water phase, was unable to pass through the superhydrophobic coating under the gravitational force, as shown in Fig. 5.16A-B. Eventually, no oil/water separation was observed (Fig. 5.16A-B). However, the hydrophobic interface having a discontinuous trapped air readily allowed the passage of the aqueous oil-in-water emulsion and the embedded underwater superoleophilicity in the hydrophobic multilayer coating readily and selectively absorbed the oil/oily phase as already demonstrated in Fig. 5.9B,D. Eventually, this selective and super oil-affinity of the hydrophobic coating helped in separating the oil-in-water emulsions during the gravity driven filtration process as shown in Fig. 5.16C-E.

Under the gravitational force, the milky oil-in-water emulsion phase (5 (v/v) % 1, 2-dichloroethane (DCE)) passed through the super-oil-absorbent, and the micro oil droplets that were dispersed in the bulk aqueous phase of the oil-in-water emulsion were immediately and selectively

separated by the hydrophobic multilayer coating. Eventually, a clear aqueous phase was selectively filtrated and collected in a separate conical flask/beaker (Fig. 5.16E). The successful separation of oil contamination was further characterized by studying DLS profiles (Fig. 5.16F), optical microscopy

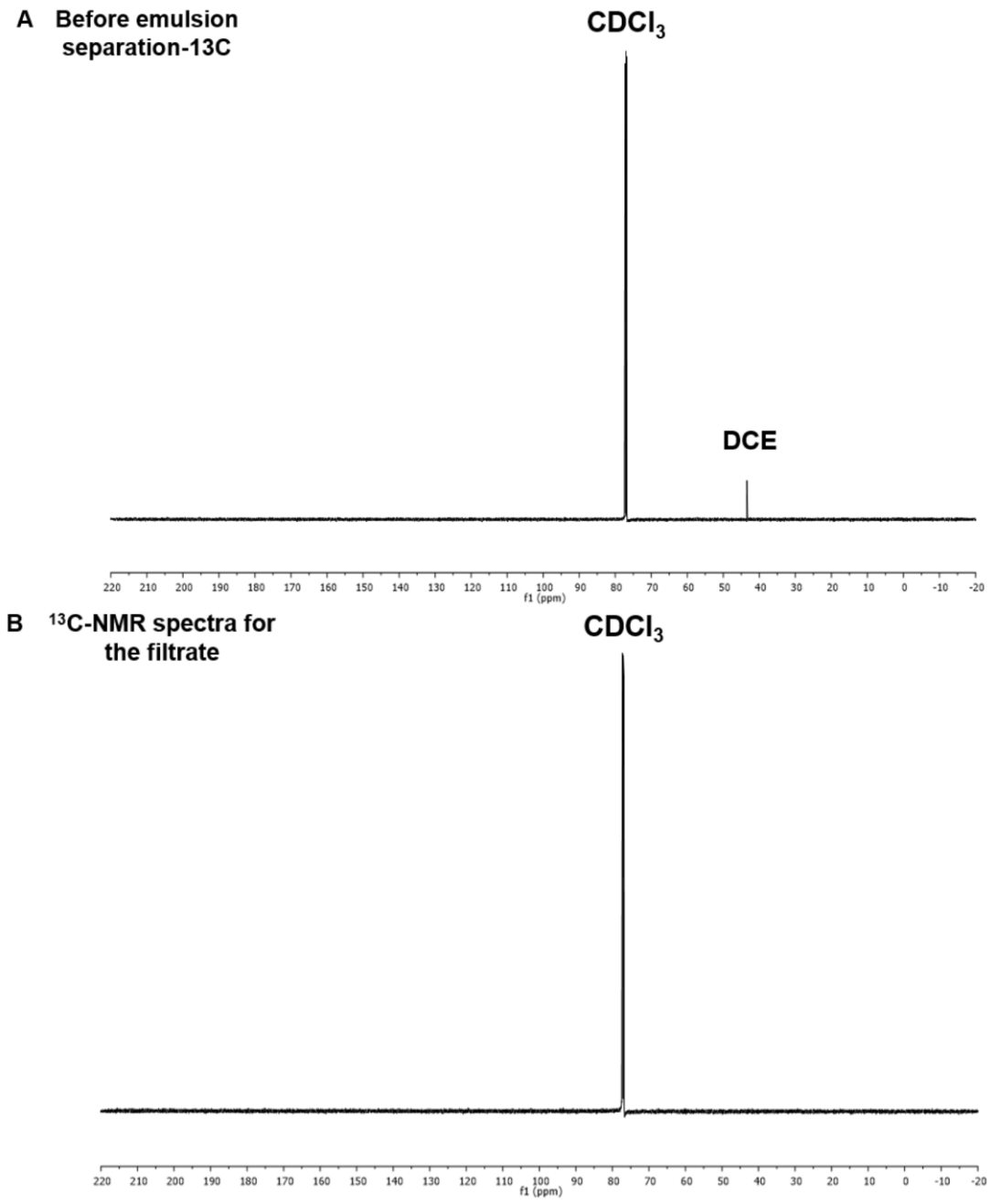

Figure 5.17: (A-B) ^{13}C-NMR analysis of the (5% DCE, model oil) oil-in-water emulsion before (A) and after (B) performing separation using hydrophobic multilayer-coated cotton. In the ^{13}C-NMR spectrum, no carbon peak at 43.46 ppm for DCE was observed for the filtrated aqueous phase (B).

images (Fig. 5.16G-H) and ^{13}C nuclear magnetic resonance (NMR) spectra (Fig. 5.17). No peak for DCE (model oil) was noticed in the of the filtrate after performing the oil-in-water emulsion (5 (v/v) % DCE) separation using the hydrophobic multilayer-coated cotton, as shown in Fig. 5.17A-B. Thus,

the hydrophobic multilayer coated cotton that embedded with super-oil-affinity underwater was efficient for separating both oil-in-water emulsions and bulk oil/water mixtures following both the selective filtration and absorption processes. In this relevance, the hydrophobic multilayer-coated cotton displayed superior performance over the superhydrophobic multilayer coated cotton. Furthermore, this oil/water emulsion separation process was expedited by the application of vacuum, and the separation was successfully carried out with a high flux rate of 238.744 x 10^3 Lm^{-2} $h^{-1}bar^{-1}$, which is more than five times higher than other reported materials.[36-37] Moreover, this oil/water separation was performed under various practically relevant challenging settings including extreme pH, seawater, river water, and extreme temperatures (Fig. 5.18A). Unlike, the superhydrophobic

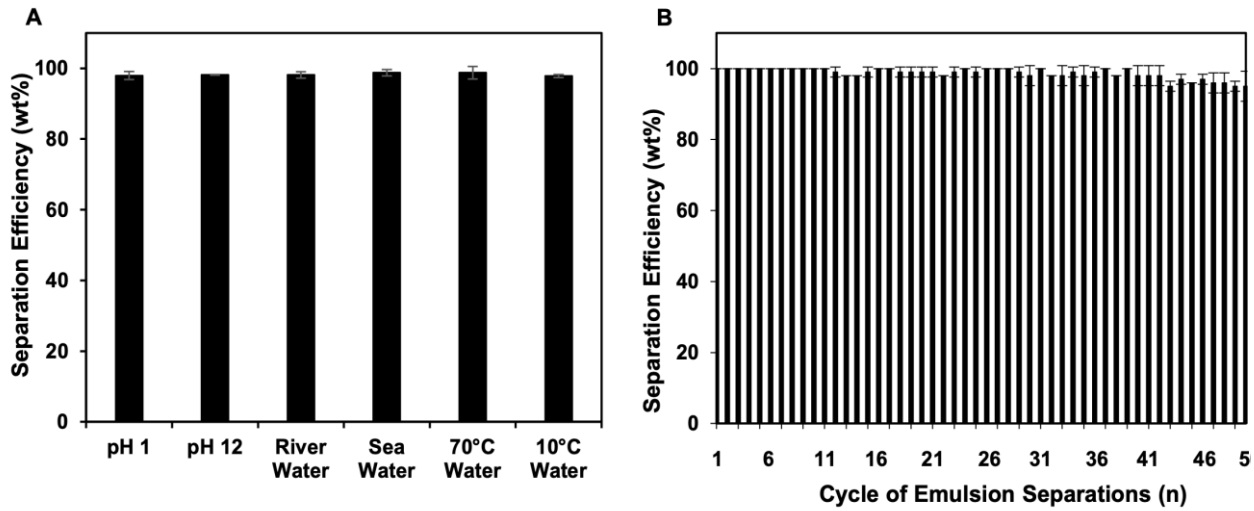

Figure 5.18: (A) Separation efficiency of 5% (v/v) of oil-in-water emulsions in diverse chemically complex environments like pH 1, pH 12, river water, artificial seawater, at elevated temperature (70°C) and at low temperature (10°C). (B) Separation efficiency of oil-in-water emulsion for consecutive 50 times.

interface, the as-synthesized hydrophobic multilayer coating remained very efficient to separate an oil-in-water emulsion repetitively at challenging settings, as shown in Fig. 5.18A-B. Thus, the hydrophobic multilayer coatings were capable of cleaning up different forms of oil spillages including oil-in-water emulsions and bulk oil/water mixtures following both the selective absorption and filtration processes; a report of this demonstration is unprecedented in the literature.

5.4. Conclusion

In conclusion, a simple chemical approach was explored for the very first time to stabilize underwater superoleophilicity by appropriate tailoring of topography and chemistry. Multilayer coatings having moderate hydrophobicity and superhydrophobicty were extended for investigating the stability of underwater superoleophilicity. The synthesized moderately hydrophobic multilayer, comprising discontinuous trapped air, had superior stability of superoleophilicity properties under water over the

superhydrophobic interfaces irrespective of the conditions like a prolonged and continuous exposure to the aqueous phase or elevated temperatures. The interesting findings of this study instigated me to prepare a multilayer-coated fibrous cotton which is moderately hydrophobic in nature and acts as super-oil-absorbent which is a seemingly apt term for this material because of its extreme affinity towards oil. The hydrophobic multilayer-coated cotton, optimized with appropriate alkylamine, were highly efficient in separating both bulk and emulsified oil/oily phases from the aqueous phase following the selective absorption process and the energy-efficient gravity-driven filtration process, respectively. In comparison, the superhydrophobic cotton was not capable of separating an oil-in-water emulsion following the filtration process due to the presence of continuous trapper air layer. In addition to this, covalently cross-linked, hydrophobic cotton was able to perform exceptionally well in oil-in-water emulsion separation in diverse and practically relevant severe settings. Thus, such a simple but unprecedented approach for optimizing durable underwater superoleophilicity and designing super-oil-absorbent is expected to be of great potential for various fundamental studies and practical applications.

5.5. References

(1) X. J. Feng and L. Jiang, *Adv. Mater*., 2006, **18**, 3063.

(2) X. M. Li, D. Reinhoudt and M. Crego-Calama, *Chem. Soc. Rev*., 2007, **36**, 1350.

(3) Y. Y. Yan, N. Gao and W. Barthlott, *Adv. Colloid Interface Sci*., 2011, **169**, 80.

(4) S. Wang, K. Liu, X. Yao and L. Jiang, *Chem. Rev*., 2015, **115**, 8230.

(5) B. Su, Y. Tian and L. Jiang, *J. Am. Chem. Soc*., 2016, **138**, 1727.

(6) Y. Li, X. J. Huang, S. H. Heo, C. C. Li, Y. K. Choi, W. P. Cai and S. O Cho, *Langmuir*, 2007, **23**, 2169.

(7) Y. Li, T. Sasaki, Y. Shimizu and N. Koshizaki, *J. Am. Chem. Soc*., 2008, **130**, 14755.

(8) C. Peng, Z. Chen and M. K. Tiwari, *Nat. Mater*., 2018, **17**, 355.

(9) A. B. D. Cassie and S. Baxter, *Trans. Faraday Soc.*, 1944, **40**, 546.

(10) A. B. D. Cassie and S. Baxter, *Nature*, 1945, **155**, 21.

(11) W. Barthlott and C. Neinhuis, *Planta*, 1997, **202**, 1.

(12) L. Feng, Z. Zhang, Z. Mai, Y. Ma, B. Liu, L. Jiang and D. Zhu, *Angew. Chem. Int. Ed*., 2004, **43**, 2012.

(13) M. Jin, S. Li, J. Wang, Z. Xue, M. Liao and S. Wang, *Chem. Commun*., 2012, **48**, 11745.

(14) M. Hirtz, A. Oikonomou, T. Georgiou, H. Fuchs and A. Vijayaraghavan, *Nat. Commun*., 2013, **4**, 2591.

(15) J. Yong, J. Huo, F. Chen, Q. Yang and X. Houa, *Phys. Chem. Chem. Phys*., 2018, **20**, 25140.

(16) J. Yuan, X. Liu, O. Akbulut, J. Hu, S. L. Suib, J. Kong and F. Stelacci, *Nat. Nanotechnol.*, 2008, **3**, 332.

(17) J. Zhang and S. Seeger, *Adv. Funct. Mater*., 2011, **21**, 4699.

(18) C. R. Crick, J. A. Gibbinsa and I. P. Parkin, *J. Mater. Chem. A*, 2013, **1**, 5943.

(19) Z. Chu, Y. Feng and S. Seeger, *Angew. Chem., Int. Ed*., 2015, **54**, 2328.

(20) J. Ge, H. Y. Zhao, H. W. Zhu, J. Huang, L. A. Shi and S. H. Yu, *Adv. Mater*., 2016, **28**, 10459.

(21) J. Gu, H. Fan, C. Li, J. Caro and H. Meng, *Angew. Chem. Int. Ed*., 2019, **58**, 5297.

(22) J. Jin, X. Zhao, Y.-H. Du, M. Ding, C. Xiang, N. Yan, C. Jia, Z. Han and L. Sun, *iScience*, 2018, **6**, 289.

(23) C. H. Peterson, S. D. Rice, J. W. Short, D. Esler, J. L. Bodkin, B. E. Ballachey and D. B. Irons, *Science*, 2003, **302**, 2082.

(24) C. P. D. Brussaard, L. Peperzak, S. Beggah, L. Y. Wick, B. Wuerz, J. Weber, J. S. Arey, B. Burg, A. Jonas, J. Huisman and J. R. Meer, *Nat. Commun*., 2016, **7**, 11206.

(25) M. J. Liu, S. T. Wang, Z. X. Wei, Y. L. Song and L. Jiang, *Adv. Mater*., 2009, **21**, 665.

(26) Y. Liu, X. Chen and J. H. Xin, *J. Mater. Chem*., 2009, **19**, 5602.

(27) P. Papadopoulos, L. Mammen, X. Deng, D. Vollmer and H.-J. Butt, *Proc. Natl. Acad. Sci. U. S. A*., 2013, **110**, 3254.

(28) D. Parbat, S. Gaffar, A. M. Rather, A. Gupta and U. Manna, *Chem. Sci*., 2017, **8**, 6542.

(29) S. Yang, S. Chen, Y. Tian, C. Feng and L. Chen, *Chem. Mater*., 2008, **20**, 1233.

(30) Z. -J. Yu, J. Yang, F. Wan, Q. Ge, L. -L. Yang, Z. -L. Ding, D. -Q. Yang, E. Sacherc and T. T. Isimj and, *J. Mater. Chem. A*, 2014, **2**, 10639.

(31) Z. Wang, Y. Wang, G. Liu, *Angew. Chem. Int. Ed.* 2016, **55**, 1291.

(32) C. Cao, M. Ge, J. Huang, S. Li, S. Deng, S. Zhang, Z Chen, K Zhang, S. S. Al-Deyab, Y. Lai, *J. Mater. Chem. A*, 2016, **4**, 12179.

(33) J. Y. Huang, S. H. Li, M. Z. Ge, L. N. Wang, T. L. Xing, G. Q. Chen, X. F. Liu, S. S. Al-Deyab, K. Q. Zhang, T. Chen, Y. K. Lai, *J. Mater. Chem. A*, 2015, **3**, 2825.

(34) H. Liu, J. Huang, Z. Chen, G. Chen, K. –Q. Zhang, S. S. Al-Deyab, Y. Lai, *Chem. Eng. J.* 2017, **330**, 26.

(35) S. Gao, X. Dong, J. Huang, S. Li, Y. Li, Z. Chen, Y. Lai, *Chem. Eng. J*. 2018, **333**, 621.

(36) Y. Liu, X. Wang and S. Feng, *Adv. Funct. Mater.* 2019, **29**, 1902488.

(37) H. Guo, J. Yang, T. Xu, W. Zhao, J. Zhang, Y. Zhu, C. Wen, Q. Li, X. Sui and L. Zhang, *ACS Appl. Mater. Interfaces*, 2019, **11**, 13704.

Conclusion and Future Plan

This chapter includes the overview of the current thesis work thoroughly explained in the earlier chapters followed by the future work plan related to this study in various possible directions. The current thesis work comprises a detailed explanation of facile fabrication of two different amine-reactive polymeric multilayer coatings on different flexible and rigid substrates by strategically depositing a branched polymeric amine and reactive-nanocomplex (NC) (of BPEI/5Acl) following LbL deposition. A catalyst-free 1,4-conjugate addition reaction at ambient conditions was adopted for covalent cross-linking of the multilayer coating and its post covalent modification with desired and selected small molecules. The reactive multilayer coating consisting of 20 bilayers displayed a durable and bulk extreme anti-oil wettability, i.e. underwater superoleophobicity, after post-modification of the multilayer coating with selected hydrophilic small molecule—glucamine. This synthetic procedure provides an opportunity to tailor such underwater extreme oil repellency on various substrates irrespective of their physical state or compositions with impeccable durability. The LbL deposition process allowed to develop a substrate-independent coating of chemically reactive multilayer coating that remained capable of displaying extreme oil-repellency property under water. Next, I further extend this work by developing a durable and stretchable underwater superoleophobic membrane by constructing the multilayer coating on a stretchable fibrous substrate. The underwater anti-oil wetting property of the membrane remained unaltered after incurring various physical abrasions like, bending, twisting, winding, adhesive tape test, etc., exposure to various chemically harsh environments (like, pH (1, 12), artificial sea water, river water, etc.) and even after incurring 150% tensile strain repetitively for 1000 times. This membrane was highly capable of separating various oil-water mixtures, including bulk oil, sedimented oil and emulsified oil following gravity driven filtration-based separation process—even under diverse chemically complex conditions, and the efficiency of the oil-water separations was observed to be remained greater than 99 wt%. However, this multilayer coating displayed hydrophobicity after post-modification with hydrophobic octadecylamine (ODA) which has a long hydrocarbon tail that constitutes of 18-carbon atoms. Hence, it was assumed that due to the lack of essential topography, this multilayer coating was incapable of displaying superhydrophobicity even after low surface energy modification. Therefore, another reactive multilayer coating was developed in presence of NaCl salt, where the doping of appropriate amount of salt significantly accelerated the rate of the reaction which led to rapid growth of NC, resulting in formation of a highly porous and durable multilayer coating even after depositing less than half (9 bilayers) of the bilayers, in comparison to the other multilayer (20 bilayers) coating. This multilayer was displaying

superhydrophobicity after successful post-modification with same ODA. Besides, this single multilayer was designed with various wettability properties including, superhydrophobicity, underwater superoleophobicity and also other adhesive wettabilities both in air and underwater by changing the post-chemical modification of the residual acrylate moeity of the coatings with various primary amine-containing small molecules (having different hydrocarbon chain length) through 1,4-conjugate addition reaction. These as-synthesized multilayer coatings can withstand various physical insults, including adhesive tape test, sand drop test, extremes of temperatures (10°C, 100°C), etc. and exposure to various chemically harsh environments (like, pH (1, 12), artificial sea water, river water, etc.) as well as UV radiation. Moreover, the salt-doped ODA-treated multilayer coating was showing an extreme oil-absorption property under water due to the presence of continuous trapped air phase confined in the micro/nano grooves of the multilayer. Interestingly, the hydrophobic multilayer having discontinuous trapped air layer (consisting of 20 bilayers) was also exhibiting the underwater superoleophilicity property similar to the superhydrophobic multilayer. In that context, both these moderately hydrophobic and superhydrophobic multilayer coatings were thoroughly investigated to compare the performance of the embedded underwater superoleophilicity at harsh settings. The detailed studies validated that the hydrophobic multilayer coating having discontinuous trapped air layer was with superior stability than that of the superhydrophobic multilayer coating having continuous trapped air in stabilizing underwater superoleophilicity. The remarkable stability of underwater superoleophilicity of the hydrophobic multilayer led me to extend this work further to develop super-oil-absorbent by coating fibrous cotton substrate. This super-oil-absorbent was demonstrated to be highly efficient (separation efficiency of > 95 wt%) in separating various kind of oil/water mixtures, including floating oil, heavy oil and oil-in-water emulsion following both the selective absorption and the filtration processes, whereas the superhydrophobic multilayer-coated cotton failed to separate oil-in-water emulsion. This study conspicuously suggests that this hydrophobic super-oil-absorbent has more potential than superhyrophobic one as far as oil/water separation in practical scenarios are concerned.

Realizing the importance of this current research work, it can be clearly stated that this work can be further extended in various practically relevant biological and other environmental aspects. For instance, underwater superoleophobicity and superhydrophobicity properties had been explored for applications like anti-platelet adhesion, prevention of biofilm formation, etc. The chemically reactive multilayer coatings developed and explored for this thesis work is believed to have great potential for biologically important applications like blood-compatible materials because wettability plays a crucial role in protein

absorption, platelet activation/adhesion, and blood coagulation. In the future, these multilayer coating can be exploited for controlled prevention and promotion of platelet adhesion on medically relavent substrates.

List of publications

(1) **D. Parbat** and U. Manna, "Synthesis of 'reactive'and covalent polymeric multilayer coatings with durable superoleophobic and superoleophilic properties under water" *Chem. Sci.*, 2017, **8**, 6092.

(2) **D. Parbat**, S. Gaffar, A. M. Rather, A. Gupta and U. Manna, "A general and facile chemical avenue for the controlled and extreme regulation of water wettability in air and oil wettability under water" *Chem. Sci.*, 2017, **8**, 6542.

(3) **D. Parbat** and U. Manna, "Fish-scale-mimicked stretchable and robust oil-wettability that performs in various practically relevant physically/chemically severe scenarios" *J. Mater. Chem. A*, 2018, **6**, 22027.

(4) **D. Parbat** and U. Manna, "Selective Cooperation with Liquids for Environmentally Friendly and Comprehensive Oil–Water Separation" *ChemSusChem*, 2017, **10**, 4839.

(5) **D. Parbat**, A. Das, K. Maji and U. Manna, "Hydrophobicity or superhydrophobicity—which is the right choice for stabilizing underwater superoleophilicity?" *J. Mater. Chem. A*, 2020, **8**, 97.

Other publications

(1) N. Jana, **D. Parbat**, B. Mondal, S. Das and U. Manna, "A biodegradable polymer-based common chemical avenue for optimizing switchable, chemically reactive and tunable adhesive superhydrophobicity" *J. Mater. Chem. A*, 2019, **7**, 9120.

(2) N. Jana, **D. Parbat** and U. Manna, "Rational Use of Dual Chemical Reactivity in a Single Interface for Optimizing Both Superhydrophobicity and Underwater Superoleophobicity" *Chemistry of Materials*, 2019, **31**, 1479-1484.

(3) S. Das, A. Das, **D. Parbat** and U. Manna, "Catalyst-Free and Rapid Chemical Approach for in Situ Growth of "Chemically Reactive" and Porous Polymeric Coating" *ACS Appl. Mater. Interfaces*, 2019, **11**, 34316.

(4) A. Das, **D. Parbat**, A. Shome and U. Manna, "Sustainable Biomimicked Oil/Water Wettability That Performs Under Severe Challenges" *ACS Sustainable Chemistry & Engineering*, **2019**, 7, 11350.

(5) S. Das, R. Kumar, **D. Parbat**, S. Sekula-Neuner, M. Hirtz and U. Manna, "Covalently Modulated and Transiently Visible Writing: Rational Association of Two Extremes of Water Wettabilities" *ACS Appl. Mater. Interfaces*, 2020, **12**, 2935.

Book Chapter

(1) N. Jana, **D. Parbat** and U. Manna, "Superhydrophobic Interfaces for high performance/Advanced

application." 2019, Springer.

Conferences/Seminars Attended

- ♣ Delivered an oral presentation entitled "Bio-inspired Robust Underwater Extreme Oil-wettability; For Both Prevention and Clean-up of the Oil- contamination" in ***'Chemconvene*** **(2017)** organized by Department of Chemistry, IIT Guwahati.
- ♣ Presented poster entitled "A General and Facile Chemical Approach for Controlled and Extreme Regulation of Liquids (Oil/Water) Wettability" in ***'Chemconvene'*** **(2017)** organized by Department of Chemistry, IIT Guwahati.
- ♣ Presented Model based on "Stretchable and Porous Superhydrophobic Fibrous Substrate for Oil Spill Cleanup" in ***'Research Conclave'*** **(2018)** organized by Students' Academic Board (SAB), IIT Guwahati.
- ♣ Presented poster entitled "Bio-inspired Robust Underwater Extreme Oil-wettability: A solution to Aqueous-oil Contamination" in **'*Research Conclave'* (2018)** organized by Students' Academic Board (SAB), IIT Guwahati.
- ♣ Presented poster entitled "Fish scale-mimicked stretchable and robust oil-repellent interface for remediation of oil under severe scenarios" in the international Conference - 'Frontiers in Chemical Sciences **(*FICS 2018*)** organized by Department of Chemistry, IIT Guwahati
- ♣ Delivered a poster entitled "A biodegradable polymer-based chemically reactive switchable superhydrophobicity with Tunable adhesiveness" at Annual Chemical Engineering Festival **Reflux 2019** organized by Department of Chemical Engineering, IIT Guwahati, India.
- ♣ Presented poster entitled "Hydrophobicity or Superhydrophobicity—Which is Right Choice for Stabilizing Underwater Superoleophilicity?" in International Conference on Advanced Nanomaterials and Nanotechnology ***(ICANN-2019)*** conducted by Centre for Nanotechnology, Indian Institute of Technology Guwahati.
- ♣ Presented poster entitled "Selective Cooperation with Liquids for Environmentally Friendly and Comprehensive Oil–Water Separation" in **'*Research Conclave'* (2019)** organized by Students' Academic Board (SAB), IIT Guwahati.

- ♣ Presented poster entitled "A Scalable Synthesis of Highly Tolerant Superhydrophobic material for Remediation of Oil-spills" in Workshop on IITG Society and Northeast India **(ISANI)** organized by IIT Guwahati on the occasion of silver jubilee celebration in **2019**.
- ♣ Delivered an oral presentation entitled "Chemically 'Reactive' Polymeric Multilayers for Tailoring Durable Liquid Wettability" in ***'RSC Roadshow'*** **(2019)** organized by Students' Academic Board (SAB), IIT Guwahati.
- ♣ Presented poster entitled "A biodegradable polymer-based chemically reactive switchable superhydrophobicity with Tunable adhesiveness" in National Conference on 'Recent Advances in Chemistry ***'RAC'*** **(2019)** organized by Department of Chemistry, NIT Meghalaya.

Awards and Achievements

- ♣ Received *Tertiary Prize Award* in ISBE 2017, Bionic Innovation Competition organized by **'Journal of Bionic Engineering & National-Local Joint Engineering Laboratory of Bionic Engineering**, Jilin University' China.
- ♣ Received Best Poster Award in **'Chemconvene 2017'** organized by Department of Chemistry, IIT Guwahati.
- ♣ Received Best Poster Award in **'Research Conclave' (2018)** organized by Students' Academic Board (SAB), IIT Guwahati.